Strength and Hydrodynamic Performance of a Multihull Vessel

Musa Bello Bashir

Submitted for the degree of Doctor of Philosophy

February 2014

School of Marine Science and Technology

Newcastle University

United Kingdom

Acknowledgements

I would like to express my appreciation to my supervisory team which comprised of Professor Mehmet Atlar, Professor Robert – for being my tutors for the past seven years and Professor Longbin Tao. I am deeply indebted to them for their continued assistance and the mentoring that I have enjoyed from them in the last four years. It has been really a great privilege to have worked under your supervision.

I am very grateful to Dr Jonathan Downes and Dr Simon Benson for their assistance on the use of the MAESTRO Program (FEA and Hydrodynamic). I am also grateful to Dr Andrew Smith; Mr Peter Bowes – for pressing the "Green Button"; Mr Robert (Bob) Hindhaugh; Mr Jerry Lambert and Mr Liam Rogerson – for their assistance during the towing tank tests measurement. Special thanks are due to Mr Olgun Hizir for his timely assistance and some collaborative work on the seakeeping validation of this thesis by using the PRECAL program, with the kind permission from Lloyds Register (LR).

I would also like to thank Mr. John F Garside for his invaluable assistance on this work over the last three years. I am also grateful to Professor B Okan; Dr K C Seo; Mr Richard Carter. Miss Victoria Coulson, Ms Carol Bennett and Mrs Sue Vecsey - for the support I enjoyed from them over these years.

I am really greatly indebted to friends and fellow research students whose company I so much enjoyed. I am thankful to Danyal Fard, Nicola Everitt, Hani Al-Hababi, Muhammed Zoolkfakar, Anuar Abu-Bakr, Alfred Emmanuel, Bello Imam, Ali Reza, Hussein Enshaei, Stavros Karamedis, Maryam Haroutunia, David Trodden, Jaime Torres-Lopez, Maria Syrigou, Serena Lim, Ikuobase Emovon, Serkan Turmen, and Batuhan Aktas, I am particularly grateful to Sadiq Lamuwa, Mohammed Mahmud (Graduate), Andriy Wiepandy Ng, Dr Sani Yahaya, Dr. (Cdr) KD Shittu, Dr Umaru M. Ba, Dr Achinike Ibekwe, Dr Aminu Bayawa, Waziri Galadima, Mr Ronye Egborge, Mr Emeka Oti, Sani G. Ibraheem, Sani Shira, Stephen Are, Craig Porter and Norman Craik for their encouragements. I would also express my sincere appreciation to Col MU Wambai for being there for me at all the times.

Lastly, I am grateful to my mum and dad for their love, support and endless patience, my brother and sisters, cousins, nieces and all the people of goodwill - for their support and encouragements. I am particularly grateful to my wife, Fatima, and the kids, Asmat and Alman, for having to endure my absence throughout the duration of my study.

Abstract

The use of catamarans as an alternative to more conventional monohull high speed vessels for transport, naval and offshore applications is on the increase. This uprising trend is a direct consequence of the global demand for commercially and militarily efficient vessels that offer high speed, potential for improved Seakeeping at speed, relatively low hydrodynamic resistance in waves and a more useable deck area. The configuration and hull geometry of catamarans are very critical to achieve improved seakeeping and other hydrodynamic performances.

The Round Bilge hull form is one of the most prominent hull geometries in use for the design of displacement-type multi-hull vessels. An alternative hullform series to the Round Bilge, catamarans, named the Deep-V Catamaran series (DVC), has been developed recently at Newcastle University. Early studies on the DVC concept based on this series indicate that the hull form may have better resistance performance than the Round Bilge. However, other important characteristics of this concept such as the motions and wave-induced load response characteristics are still unknown. There is also a lack of understanding of the general hydrodynamic characteristics of the DVC concept in comparison to the Round Bilge hull form. This study contributes to the understanding of the motions and wave induced load response characteristics of the DVC concept. It is also intended to advance the structural design methodology of the DVC concept and its subsequent application as better alternative to the Round Bilge hull form.

The study involved the experimental and numerical investigations of the motions and wave-induced load response characteristics of the DVC concept by using a prototype model of "The Princess Royal" which is the current research vessel of Newcastle University. The experimental studies involved the motions and wave-induced response measurements in regular waves at both zero and forward speed conditions. The results obtained were validated using alternative potential flow-based numerical codes in frequency domain. The benchmark study indicates that the numerical codes are capable of producing acceptable results.

A comparative study using a representative model of the Round Bilge hull form with the DVC model was conducted in order to establish a direct basis for the comparison of the motion and hydrodynamic load performances. The results obtained from this comparison reveal that the DVC may have better seakeeping characteristics and is less sensitive to wave loads than the Round Bilge hull concept in critical heading conditions. A further comparison of the experimentally validated numerical predicted loads with those obtained using the International Association of Classification Societies (IACS) approach was completed. The study confirms that the IACS approach over predicts the loads by up to 40% in Beam Seas and Quartering Seas when other components of IACS rules are not considered. A simplified structural analysis of the DVC model using the Finite Element Method was also completed to demonstrate the effects of the predicted loads on the strength of the hull structure with emphasis on the cross-deck structure, which is the most sensitive structural element of the vessel.

Overall, the study highlights the promising characteristics of the DVC concept in comparison to the Round Bilge hull form and provides data required for the preliminary design of catamarans using this concept.

Table of Contents

Table of Figures

List of Tables

Nomenclature

g	Acceleration due to gravity (m/s^2)
$\mathbf{m_o}$	Area of root mean square moment due to spectral density (m^2)
$\boldsymbol{\sigma}$	Bending stress (kN/m^2)
B	Breadth of a vessel (m)
Tz	Crossing period (s)
T	Draught Amidships (m)
$\boldsymbol{\omega_e}$	Encounter wave frequency (rad/s)
Fx	Force along the longitudinal axis of a ship (kN)
Fy	Force along the transverse axis of a ship (Side force) (kN)
Fz	Force along the vertical axis of a ship (kN)
$\boldsymbol{V_s}$	Full scale vessel speed (knot)
$\boldsymbol{F_j}$	Hydrodynamic forces on a ship (kN)
$\boldsymbol{F_j^s}$	Hydrostatic forces acting on a ship (kN)
$\boldsymbol{p}$	Hydrodynamic pressure at a point on a ship (kg/m^2)
$\boldsymbol{\zeta_a}$	Incident wave amplitude, (m)
$\boldsymbol{L}$	Length overall of a vessel (m)
S	Mean wetted surface of a ship's hull (m^2)
$\boldsymbol{V_m}$	Model speed (m/s)
$\boldsymbol{I}$	Moment of inertia of a cross section (kg/m^2)
$\boldsymbol{\gamma}$	Partial safety factor
$\boldsymbol{\beta_k}$	Phase angle of motion response with respect to the incoming wave (deg)
Mx	Prying Moment (kNm)
My	Pitch Connecting Moment (kNm)
$\boldsymbol{C_{jk}}$,	Restoring force coefficient matrix (kN)
$\boldsymbol{\lambda}$	Scale factor

Δ	Ship displacement (Tonnes)
Hs	Significant wave height (m)
$S(\omega)$	Spectral density
R	Strength ratio due to the loads acting on a structural member
$\boldsymbol{\sigma_s}$**(Q)**	Steady flow source density
$\boldsymbol{\phi_s}$ **(x, y, z)**	Steady disturbance potential for a ship with forward speed at a given position
ϕ_T	Total velocity potential
$\boldsymbol{-Ux}$	Uniform flow velocity due to forward speed of the ship, U, along x-direction
$\boldsymbol{-Ux}$	Uniform flow velocity due to forward speed of the ship, U, along x-direction
ϕ (x, y, z, t)	Unsteady disturbance potential for a ship at a given position and time
ω	Wave frequency (rad/s)
$\boldsymbol{\rho}$	Water density (kg/m^3)
$\mathbf{A_w}$	Water plane area (m)
$\boldsymbol{v}$	Wave number
$\boldsymbol{\beta}$	Wave angle between the direction of wave propagation and the ship's direction
Mz	Yaw Splitting Moment (kNm)

Abbreviation

DHI	Danish Hydraulic Institute
DOF	Degree of Freedom
DVC	Deep-V Catamaran
DLA	Dynamic Load Analysis
FEA	Finite Element Analysis
Fn	Froude number
LOA	Length overall of a ship
LR	Lloyd's Register
MAESTRO	**M**ethod for **A**nalysis, **E**valuation and **Str**uctural **O**ptimisation
UNEW	Newcastle University
RAO	Response Amplitude Operator
RB	Rigid body model
RBC	Round Bilge Catamaran
M_B	Rule-based maximum transverse bending moment
M_R	Rule-based maximum vertical bending moment
M_T	Rule-based maximum torsional moment
MAST	School of Marine Science and Technology, Newcastle University
SB	Segmented model
SWATH	Small Water plane, Area Twin Hull
SES	Surface Effects Ships

Chapter 1

Introduction

1.1 Introduction`

This chapter presents a brief overview of the research that has been carried out on motion responses and the wave-induced structural loads prediction of a Deep-V catamaran hull form and on the strength assessment of its cross-deck structure. The background and the motivation for the research presented in this thesis are given in Section 1.2. This includes a general introduction to the research that has been undertaken, emphasising on the reasons for the choice of the topic. The specified aims and objectives of the thesis are presented in Section 1.3. A general layout of the thesis is presented in Section 1.4.

1.2 Background and Motivation

The term multihull vessel refers to a group of vessels having configurations such as the catamaran (two demi-hulls), the trimaran (three sub-hulls) and the pentamaran (five sub-hulls). The basic feature of this group of vessel is that it consists of ships having more than one distinctive hull component referred to as demi-hulls – or sometimes called the sub-hulls for vessel having more two hulls. The demi-hulls are connected to each other by a beam that is usually referred to as a cross-structure or simply as a cross-deck. An example of a multihull with two demi-hulls (catamaran) and three sub-hulls (Trimaran) is given in Figure 1.2.

a. RV Princess Royal (Deep-V hull form Catamaran)

b. HMS RV Triton (A Trimaran)

Figure 1.1: Examples of multihull vessels

Multihull vessels are generally known to have the capability for a high speed performance due to slender hulls and to offer a more usable deck area. The vessels are presently used as cargo and passenger ships, as naval operational vessels, and as leisure craft. Of the types of vessels in this group, catamaran is the most widely used. Most recently, the vessel has started making forays into the offshore industry with the recent award for construction of the world's largest catamaran, the Pieter Schelte, as shown in Figure 1.1, as a complex offshore "platform

installation/decommissioning and pipelay vessel" and it was designed by a Swiss company, Allseas in 2010 (Allseas, 2012). The Pieter Schelte vessel has a length overall of 387m and a beam of 117m together with a lift topside capacity of 48,000tonnes.

Figure 1.2: The Pieter Schelte Catamaran, an offshore (multi-purpose) support vessel

From the design perspective, multihull vessels are very challenging because of the presence of a wide beam that connects the two or more otherwise unstable demi-hulls together. On the other hand, commercially, a multihull vessel is considered to be viable when the cargo capacity versus speed is considered in relation to a monohull with similar geometry.

The utilisation of multihull vessels, as an alternative to the more conventional monohull high speed craft for the purpose of cargo and passenger transport and for naval and offshore applications, is on the increase. This increase could be attributed to the global demand for commercially and militarily efficient vessels that offer high speed, improved seakeeping for some types, low wave resistance and a wider deck area. A number of other features, such as the overall size of the vessel, and the shape and the nature of the hull geometry beneath water level, are very critical to achieving better seakeeping and other hydrodynamic performances (Sarioz and Narli, 1998). Amongst these features, the underwater hull form geometry becomes a key factor in the design of a vessel both from the seakeeping and other hydrodynamic performances point of view.

At the present time there are various forms of underwater hull geometries that are used in the design of both mono- and multi-hull vessels. The most distinctive and prominent among them

are the 'Round Bilge' and the 'Deep-V' type hull forms. These designs are intended to improve the speed and seakeeping performances as well as the stability and efficiency of multihull vessels at large displacements.

Multihull vessels achieved their stability by making use of two or more slender otherwise unstable demi- or sub-hulls connected together by a wide beam. This beam is responsible for the presence of a wider deck area in the vessel. However, the problem with the wide beam separating the demi-hulls is that it makes the Metacentric height of a multihull vessel to be relatively high compared with typical monohull vessels, thereby causing stiff vertical and lateral accelerations that could, for example, cause motion sickness to the crew and passengers. Other problems, such as a large wetted area which has a significant impact on the resistance and propulsion of the vessel, have the potential of undercutting the choice of multihull as being an efficient vessel and which could further reduce its potential for large scale use in the maritime industry.

Some considerable numbers of studies have been carried out to address these performance concerns and the concerns due to the effect of hull geometry on the seakeeping performance of a multihull vessel. Other studies have focussed on the development of efficient hull forms with improved seakeeping and resistance properties without, however, compromising the advantageous large deck area. As far as Deep-V catamarans are concerned, notable among these studies was the work of Haslam (1996) on the feasibility of using a Deep-V hull form for a high speed catamaran. This study became the basis for most, and the subsequent, researches that have been carried on Deep-V catamaran hull forms and which led to development of the world's first high speed Deep-V catamaran displacement hull form series by Mantouvalos (2008).

As a direct consequence of these and other studies that were carried on the Deep-V catamarans, a 14m patrol boat with a top speed of 21.5knots was designed for the Port of London Authority (PLA) (Atlar et al, 2009) which was followed by four similar size designs. Following this success, Newcastle University also commissioned the design of an 18m Deep-V hull form having a novel anti-slamming bulb; this became the research vessel, R/V "The Princess Royal", as a replacement for its former vessel R/V "Bernicia". The Deep-V hull form series, that was developed by Mantouvalos (2008), is similar in many ways to the existing National Physical Laboratory's (NPL) high speed Round Bilge displacement hull series developed by Insel and Molland,(1992) on the basis of the work done by Bailey,

(1976), except that the Deep-V hull form combined with the unique anti-slamming bow concept of Serter. These particular form characteristics are claimed for improving the hydrodynamic efficiency of the Deep-V hull form by a considerable amount.

Unlike the Round Bilge hull form, which has already gained prominence in its application to the design of multihull vessels, the use of a Deep-V hull form in the design of multihull vessels is just beginning to evolve. Most of the advantages that this hull form offers are still unknown to many in the marine industry. It is understandable that studies on its seakeeping and other hydrodynamic performances in comparison to that of the Round Bilge hull form are currently very limited. Where available, most of the studies that have been carried out on stability improvement and on seakeeping concerns of multihull vessels were mainly focused on the Round Bilge hull form. The most recent among these studies include the works of Abdul Ghani (2003), who studied an extension of National Physical Laboratory (NPL) database in order to investigate the influence of bulbous bows on high speed displacement hull form catamarans. His work was based on an experimental study of four sets of bulbous bows which were used to create a further understanding of the mechanics of seakeeping, among others, for a catamaran fitted with a bulbous bow that was operating in both deep and shallow water environments.

Davis and Holloway (2003), investigated the influence of hull forms on the motions of high speed vessels using a Green function within a time domain strip theory method. In their study, eight different types of catamaran hull forms were compared to small water plane area twin hulls (SWATH), tri-hulls and monohulls. None of these catamaran hull forms was of a Deep-V hull form type.

Other notable contributions to this area of study include the works of Chan (1993) and Fang et al (1994 and 1996), both of whom studied the motion characteristics of a catamaran in regular waves. In addition, Peng et al, (2006) worked on the effects of wave resistance due to flexibility in the hull form arrangements and varying hull forms for passenger/vehicle transportation. The similarity between most of the above mentioned works is that their researches were largely focused on a Round Bilge hull form. In addition, most of these researches were undertaken using numerical methods albeit validated with some limited experimental results.

From the above, it is evident that studies on the speed performance and motion responses of a Deep-V catamaran hull form are at the infancy stage. It can be seen that it is quite difficult to establish a sound comparative basis under which the hydrodynamic parameters of the Round Bilge and of other types of hull forms can be used in order to estimate the specific parameters that are required for the design of a Deep-V hull form without grossly over estimating these parameters. Even if an estimate of the parameters for the Deep-V form is made under this circumstance, it will still remain an uncertain estimate at best; hence it would not necessarily represent that of the actual characteristics of the real vessel. To this end, there is need to develop the actual monograph of motions and load characteristics of the Deep-V hull form since none exist at the moment.

Since catamarans are very weight sensitive, especially of the cross deck structure, an understanding of the response of this particular structural member to various hydrodynamic loads is particularly important. Several studies have looked at the effects of slamming on the wet deck of a wave-piercing catamaran (Varyani *et al.*, 2000; Ojeda *et al.*, 2004; Davis and Whelan, 2007), however only few a studies have been conducted on the full range of effects of wave induced loads on the cross-deck structure. To date, there is lack of any developed wave-induced loads data for the design of a Deep-V multihull vessel available to ship designers. The current designs rely mostly on data obtained from either Round Bilge hull forms or on other monohull Deep-V vessel.

Another area that merits study is the potential for using non-metallic materials such as glass fibre reinforced plastics, GFRP, and other more advanced composites in the construction of the cross structure of a multihull. Composites are generally relatively light in weight and high in strength, they are weight-strength efficient, and hence they could be useful in solving some aspects of the weight sensitivity of the cross deck structure.

In order to realise the potentials of using Deep-V hull forms in the design of catamaran vessels, the understanding of its motions and load response characteristics and their relationship to the key structural components is highly essential. This important aspect of the Deep-V hull form is currently lacking, hence the reason for this study.

1.3 Aims and Objectives

Based on the above background, the aim of this thesis is to contribute to the understanding of the motion and wave induced load response characteristics of the DVC concept. It is also intended to advance the structural design methodology of the DVC concept and its subsequent application as better alternative to the Round Bilge hull form.

Within the framework of the above aim the specific objectives of this thesis are summarised as follows:

1. To perform a review of the current state of knowledge in the areas of wave-induced load predictions and of the strength assessment of a catamaran vessel designed using a Deep-V hull form.
2. To perform numerical analysis for the load and motions response characteristics of both Deep-V and Round Bilge hull catamaran forms.
3. To conduct experimental model testing using both rigid and segmented scale models of a selected Deep-V hull form with the view to predicting the wave-induced loads and motion responses of a representative full-scale catamaran.
4. To use the loads obtained from the experimental study in order to validate the results from the numerical modelling and calculations.
5. To use the validated loads in performing the strength assessment for the influence of the hull form geometry on the strength of the cross deck structure of a Deep-V catamaran.
6. To perform structural load predictions in order to demonstrate the requirements for the structural design and strength assessment of multihull geometry and cross deck structure of a Deep-V hull form concept.

1.4 Layout of Thesis

In order to achieve the above stated aims and objectives of the research, the work conducted in this thesis are presented in eight chapters which are briefly described as follows:

This chapter, **Chapter One,** provides a general introduction to the thesis and to the aims and objectives of this study. Also included in this chapter is a brief explanation of the overall layout of the thesis and which highlights the procedure that was employed for attaining the specified objectives.

A general review of the available literature on the methodologies for the predictions of **s**tructural loads and their demands on a catamaran vessel is presented in **Chapter Two.** The chapter also contains reviews of motions responses of catamaran vessels in general and more specifically on the Deep-V hull form**.** The review focuses on the various types of hull forms used in the design of catamaran vessels, such as the Round Bilge and the Deep-V forms; on numerical and experimental loads prediction; and on the structural response associated with the effects of loadings and the materials used in construction. A review of the relationships between the strength and the loads on the structural materials was also performed. The chapter concludes with a summary of the review.

In **Chapter Three,** the theoretical background for the motion response and the hydrodynamic loading predictions software, MAESTRO-Wave, is presented. The MAESTRO-Wave code, being a potential flow solver, has the same theoretical background as the PRECAL which is an alternative code used to validate the motion predictions further; hence the method description in this chapter covers background theory for both of these codes. The use of the MAESTRO-Wave numerical program in the prediction of extreme loads is also discussed.

The results of the experimental measurements of the hydrodynamic forces and motion responses, that were performed using a Deep-V hull form model, are presented in **Chapter Four**. The towing tank testing facilities that were used as well as the experimental set-up are described in this chapter. Also, the procedure that was followed in performing the experiments and a description of the model that was used for the experiment are both presented. The chapter also includes a description of the model tests matrices and the results that were obtained.

Chapter Five, presents the results of the benchmark studies which deals with the validation of the results of the MAESTRO-Wave and PRECAL numerical programs using the model test results. Both of these numerical programs are 3D potential flow theory-based numerical codes in frequency domain. The chapter also contains the results and discussion on the effects of the appendages of the Deep-V hull model used.

In **Chapter Six,** the results of the numerical predictions of the hydrodynamic loads and motion responses are presented**.** Also presented in this chapter are the results of the comparative studies that were carried out for the Deep-V hull versus the Round Bilge hull forms in terms of the results of their six degrees of freedom motions and loads effects.

Chapter Seven covers the prediction of the structural loads using the International Association Classification Societies (IACS) approach as obtained in the Lloyds Register Rule for Special Service Craft. The chapter also presents the results of the structural response analyses that were carried out on the hull structure, with emphasis on the cross-deck structure, in order to investigate the influence of material behaviour and the magnitude of the loading on the strength of the vessel.

Chapter Eight concludes the thesis with a presentation of a summary of the findings, and provides recommendations and suggestions for future study.

1.5 Summary

This chapter evaluated the current state of multihull vessels with a specific emphasis on catamaran types and their applications in form of a background to the thesis. Some of the challenges facing the use of this hull form, especially the Deep-V hull form were discussed as part of the motivation for undertaking the research presented in this thesis. The aims and objectives of the research have been presented. Finally, the chapter concludes with a general layout of the thesis and summary of the chapter.

Chapter 2

Background of Multihull Vessel and Literature Review

2.1 Introduction

This chapter presents a survey of the literatures relating to the use of multihull vessels and, more specifically, of the various methods that can be used for predicting the motions responses of and the wave-induced loads on catamarans. In the context of this study, the predicted loads are intended for use as a basis for making comparisons between the responses of a novel Deep-V catamaran hull form design with a more conventional Round Bilge catamaran hull form. In addition, the loads that are determined are to be used for the critical strength assessment of the cross-deck structure of the Deep-V catamaran vessel.

Section 2.1 therefore presents the general introduction of this chapter whilst Section 2.2 presents a review of Deep-V and the Round Bilge hull form as applicable to the design of catamaran vessels. A review of the motions and wave-induced load response characteristics of the vessel is presented in Section 2.3. The section covers topics such as the types of motion responses and of the wave-induced loads measuring techniques that are used in the loads prediction and seakeeping analyses. In Section 2.4, a review of the considerations and procedures for the structural design of catamarans with emphasis on the cross-deck structure and the requirements for the acceptance criteria of such designs is presented. The section also covers the structural loads prediction methodology and strength requirements for the assessment of multihull structures, including the global, transverse (cross-deck) structure and reference to fatigue. Section 2.5 provides the conclusion of the chapter by highlighting a summary of important observations about multihull vessels, in general and for catamaran in particular.

2.2 Review of the Deep-V and the Round Bilge Catamaran Concepts

The catamaran is the most widely used hull configuration in the group of vessels classified as multihulls and it consists of two demi-hulls connected together by a set of cross deck structure. There are various concepts of catamaran and twin-hull vessels presently in existence and some examples of these vessels consist of the Displacement and the Semi-displacement type, wave-piercing, foil-assisted, Small Waterplane, Area Twin Hull (SWATH), Surface Effects Ships (SES) etc. A typical catamaran is symmetrical about the centre line of the main hull about a longitudinal axis but there are others whose geometrical configurations consist of asymmetrical demi-hull arrangement (Dubrovski, 2004).

The displacement-type catamaran is widely used in the design of multihull vessels that need to have an appreciable buoyancy capacity, for cargo purpose, as well as one that operates at a relatively modest speed with Froude numbers of less than 1.0. The geometry of these hulls is very significant in determining the seakeeping performance of, and the dynamic flow characteristics around the, vessel. The effects of this flow behaviour around the vessel and between the demi-hulls are that they can potentially induce a large resistance on the vessel, thereby resulting in reduced efficiency and the under performance of the vessel for a given propulsive power.

There are various forms of the displacement-type demi-hulls around but the most prominent ones amongst them, as referred to above are the Round Bilge hull form and, more recently, the Deep-V hull. These two hull forms offer competing advantages in terms of improvements to the resistance and seakeeping problems that are inherent to multi hull vessels.

2.2.1 The Round Bilge Hull Form Concept

The Round Bilge catamaran concept is a displacement-type vessel having basically "U-Shaped" hull form geometry. The hullform has been extensively used over many years for the design of monohull naval craft and its origin has been generally credited to the works of Nordstrom in the early 1930s that was undertaken on selected models (Nordenstrom *et al.*, 1971). The study involved the testing of Round Bilge models at various vessel draughts for different systematic series. Although Nordstrom's studies did not particularly result in significant contributions, it generated sufficient interest amongst other researchers that eventually led to the further extensive research that was done on the hullform (Sahoo, 2003).

The concept of this hullform, as it is also used in the design of multihull vessels, was developed further by Bailey (1976) in the National Physical Laboratory, NPL. It is widely referred to as the NPL hullform series and it is prominently used in the design of monohull high speed (displacement) craft. This concept was later used by Insel (1990) in developing the NPL series for displacement catamaran. The work was later expanded to include the motions response and resistance characteristics of the hull form by Insel and Molland in (1992). The significance of their benchmark study led to most of the displacement type multihull vessels that are currently in existence being designed using the National Physics Laboratory (NPL) hull form series.

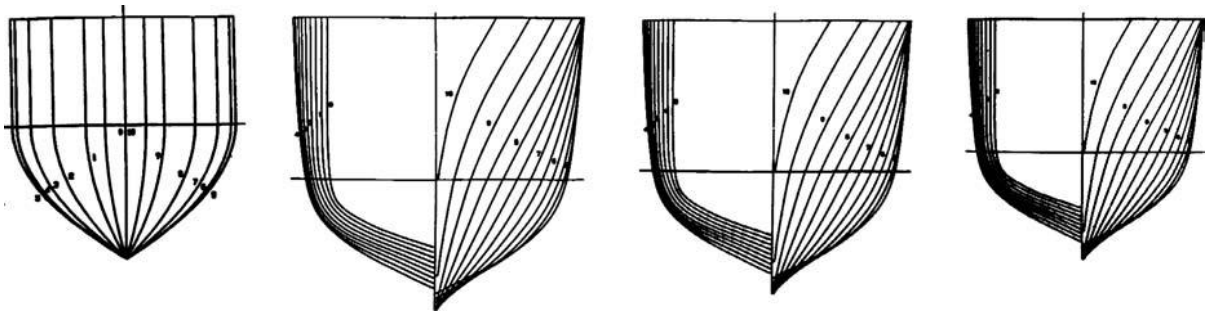

Figure 2.1: Typical body lines of form for a Round Bilge hullform developed by Insel and Molland 1992 (Source:(Sahoo *et al.*, 2007))

The NPL hull form series has been the subject of research for quite some time now, with the model, seakeeping characteristics tested in various speeds and waves (Wellicome *et al.*, 1995; Wellicome *et al.*, 1999); as well as including its geometrical characteristics (Abdul Gani, 2003). The operational speed range of this vessel is between the Froude numbers of $0.25 \leq Fn \leq 1.2$ (Molland and Lee, 1995). A typical geometry body form for this type of hull is given in Figure 2.1

The geometry of the Round Bilge hull form has round-shaped after body sections, straight lines at the buttock and the entrance waterlines. The straight lines at the buttock reduce until they reach the end of the transom (Bailey, 1976). In addition, the approach to studying this geometry and the performance of the Round Bilge hullform in the NPL series has been one of the contributing inspirations to the alternative development of the first Deep-V Catamaran (DVC) series (Mantouvalos, 2009) in the literature.

2.2.2 The Deep-V Hull Form Concept

The Deep-V hull form is one of the emerging concepts of alternative hullform that is being used in the design of multihull vessels. As stated in Chapter 1, there are various parameters that are used in the classification of a vessel's hull form. The inclination angle that the transverse section of the hull form makes from the horizontal plane, or dead rise, angle has a great influence on the seakeeping, resistance and operational performance of any vessel. Hence, a hull form is defined as being a 'Deep-V' if it has a dead rise angle of between 17^o to 22^o at the transom (Serter, 1993a). These parameters, however, are required to be understood before one can properly classify hullform geometry as Deep-V. Out of these various parameters, the most dominant of them are summarised in Table 2.1.

Table 2.1: Key parameters that define a Deep-V hull form

Key Parameters	Characteristics
Dead rise angle at transom	Typically between 17^o-22^o but can increase up to 30^o
Midship section	Could be a Single Chine or a Double Chine
Hull Lines	Could be slightly concave or convex
Length – Beam ratio	Depends on speed and displacement/length
Bow design	Could have an anti-slamming bulb
Bottom keel design	Could be a wedge shaped keel or a slightly rounded keel

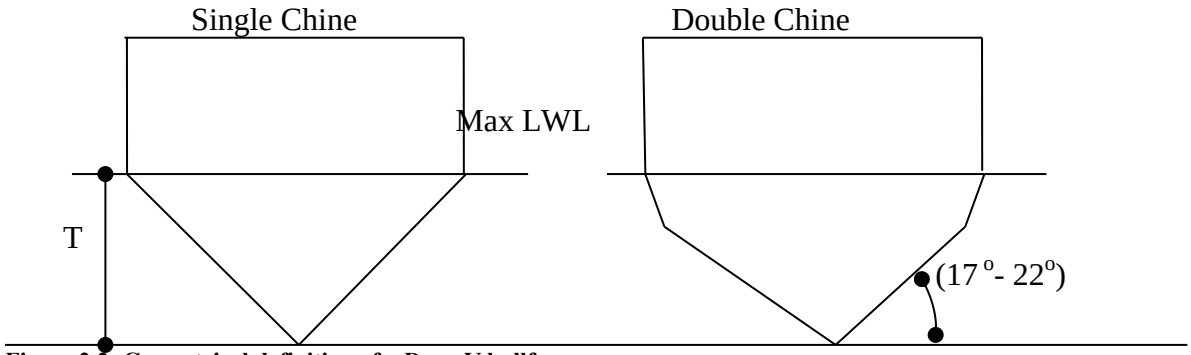

Figure 2.2: Geometrical definition of a Deep-V hullform

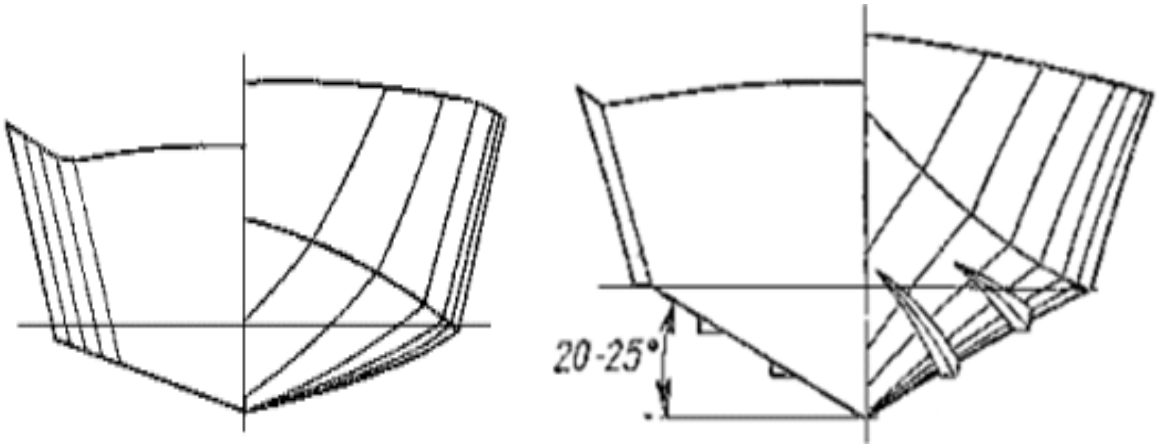

Figure 2.3: The geometry of a typical Deep-V hull forms (Source: (Serter, 1993b)

The Deep-V hullform was initially used mainly in the design of semi- planing or planing monohull vessels until it was discovered that it also possessed some beneficial attributes such as improved speed performance and reduced drag, which are capable of trading-off some of its weakness. Despite the successes recorded by Serter (1993a) in his study on the suitability of using Deep-V hull forms in the design of high displacement vessels, the application was only limited to the design of monohull vessels.

Following the recent growth in the global demand for efficient and the functional vessels that offer better comfort and operating speed in moderate waves, relatively low resistance at a given speed and hence reduced propulsive power requirements and wider usable deck area, the use of the catamaran configuration as being a potential high speed craft started to gain attention. Some of these required features are among the known characteristics that have made catamarans to be more attractive for use as a special cargo transporters, passenger and military ships when compared with other forms of high speed craft. A number of other features, such as the size of the vessel and the nature of the hull form beneath the water level, are very critical factors to accomplishing a better seakeeping performance.

However the superior calm water performance of many multihulls, in particular that of catamarans due to their slender hulls can be adversely affected by their inherently poor seakeeping performance leading to a reduced speed disadvantage when operating in waves. However, in contrast, the superior seakeeping performance of displacement type Deep-V hull forms in waves has been well recognized in monohull applications, as demonstrated e.g. by (Sarioz and Narli, 1998) and there are numerous naval and commercial applications of this hull-form concept already in existence.

The study that was made by Haslam (1996) on the application of the Deep-V hull form to the design of a displacement catamaran followed by a presentation by Atlar (Atlar, 1997a) on a review of the state of application of this hull form to multi hull vessels, has highlighted some of the advantages that could be derived from using this hull form in the design of multihull vessels. Atlar went further in his paper, (Atlar, 1997a), to forecast the growing application of the Deep-V hull form in the emerging multihull vessels industry.

Within this context, it would be only natural to combine the superior seakeeping performance of a displacement type Deep-V monohull with an efficient twin hull form in order to improve the relatively poor seakeeping performance of catamarans thereby reducing their speed loss in a seaway. This hybridisation of two vessel configurations was first proposed at Newcastle University by Atlar (1997b; Atlar *et al.*, 1998) and later on resulted in the development of the first systematic Deep-V catamaran (UNEW-DVC) series that was undertaken by Mantouvalos (Mantouvalos, 2009).

The main features of the UNEW-DVC series are that the demi-hulls are individually symmetric about their longitudinal vertical plane with large dead-rise angles that are constant aft of midship, and that the bow sections have a Serter's trademark anti-slamming bow (Serter, 1993b) which is enhanced by the introduction of a bulbous bow (Atlar *et al.*, 2013).

2.3 Review of Motions and Wave-induced Loads on Catamaran

The study of the motions and wave-induced loads response of multihull vessels has continued to receive tremendous interest from naval architects, ship designers, researchers and classification societies due to the surge in demand for such vessels as well as their relatively complex cross-deck structures. The multihull concept has seen a significant increase in use due to the global demand for efficient, stable and cost-effective means of transportation beside to meet special mission requirements. Improvement in knowledge of the motions response and wave-induced loads characteristics of this hullform thus would further enhance the understanding of its seakeeping and of the structural demands and behaviour as this is critical to the successful utilisation of any hullform concept in general (Ohkusu, 1999).

The motions response and wave-induced loads measurements as well as their assessments are presently being done using some of the following procedures:

i. Experimental model test procedure (Towing tank tests)
ii. Theoretical (and numerical) procedure, either specific or parametric which can be grouped into:
    a. The potential flow-based approaches
    b. Computational Fluid Dynamics (CFD) based approaches - including viscous effects
iii. Sea trials that are suitably instrumented, including recordings of the wave conditions experienced, etc.

The progressive evolution of these procedures has made it possible for the ship designers to more fully comprehend the anticipated environmental challenges that the vessels that they design would encounter during their service years. The insights gained from such studies, plus the operational experiences through the vessel`s in-service records, have been among the reasons that modern ships are safer and generally structurally more efficient than their predecessors.

As the world is now engaged in the quest for design improvements in the marine transport systems, several methodologies for the undertaking of the motions response and wave induced loads measurements or predictions have been developed in the last 50years. These methods are needed in order to improve the efficiency of the design tools used for predicting

the loads and motions which in turn has had a significant impact on the reliability of operations and the safety of the vessel (Clark *et al.*, 2004). With the continuous advent of new hullform concepts for multihull vessels, accurate motions and wave loads data are often not readily available because the existing tools are restricted in the applications of their capabilities to different forms and hence a lot needs to be done in terms of further research in order to overcome these shortcomings. The non-availability of enough validated data on these newer types of vessels, especially on the Deep-V hull form for multihull vessel design, could also be attributed to the fact that, before the recent surge in the use of multihull vessels as efficient transportations system, multihull concepts were mostly used for small-scale services such as leisure and sport vessels, which partially explains the previous near-lack of interest in the entire hullform concept. It is useful to note that small vessels tend to be structurally overdesigned, where scantlings are often based on general robustness considerations. As vessels become larger the demand on the structure need to be examined in a much more rational and calculated manner (Mansour and Fenton, 1973). The Deep-V hull form concept is known to offer a relatively wider beam in the design of multihull vessel, hence the need for careful assessment of its structure.

A firm and clear understanding of the motions and wave-induced loads experienced by a vessel in service is especially important during the preliminary design stage where major decisions are being made because it helps to decide the choice of the hull form and other major design parameters to be subsequently adopted for that designs for further development. The current tools that are available for the prediction of these motions response and wave loads-induced on a group of nominally similar vessels such as the multihull rely on the combinations of empirical formulations and various analyses developed by the class societies and on other data extrapolated from different types of hull configurations including service experience (Heggelund *et al.*, 2002). These design tools, both the experimental and numerical ones, are the product of continuous research in those particular aspects that need benefit from continuous refinements for it to meet the dynamism in the evolution and innovation of the various hullform concepts. Reliance on some of these tools alone, with their limitations, could lead to either an overestimate, or more catastrophically to an underestimate, of the actual contribution of these motions response and loads being an essential component of the overall design parameters (Ohkusu, 1999). The numerical tools mostly assume that the wave conditions in which the model/vessel will operate to be more or less ideal, hence any deviation from that could potentially lead to inaccurate predictions. Although several studies

have been carried on accurately defining the parameters themselves in order to be able to improve the quality of their results, the assumptions of these parameters have continued to limit the total acceptability of the tools. Hence, the applications of these tools have been largely limited to the preliminary stages of the design. Again this is often the stage in the overall design process at which the major decisions that can have significant downstream consequences are usually made.

On the other hand, the experimental measurements of the motions response and wave-induced loads on a vessel involve the use of scaled models in a towing tank or ocean basin. The towing tanks and model basins, in addition to other devices used along with the model for such measurements, constitute the basic facilities that are needed to provide realistic wave conditions with capabilities as required to accurately measure responses due to the behaviour of the ship in different wave conditions (Matsubara, 2011). Knowledge of the behaviour of models in waves offers an insight into what to expect from the actual vessel in real-time situations, while the wave-induced loads, such as the longitudinal, transverse, and vertical, forces and moments and of slamming forces, are very important in the general assessment of the level of structural integrity of a vessel (Dallinga and Tikka, 1986). For the results obtained from both the numerical predictions and the experimental measurements to be relied upon in the design process, one of them has to be used to essentially validate the other by showing some level of agreement between them, unless, in some rare situations, the comprehensive and good quality results of full-scale sea trials of a closely similar vessel are available. For this reason, it is important that when designing a multihull vessel using a new hull form concept, like the Deep-V hull form, that the motions response and wave-induced loads are obtained using both the experimental and numerical approaches.

In most of the situations, the predictions of the motions response and wave-induced loads characteristics of the Round Bilge hullform have been at the forefront in most of the earlier studies that have been carried out on the seakeeping performance and the structural response characteristics of multihull vessels. The Round Bilge hullform is widely used in the design of displacement catamarans, although this could be because the Deep-V form was not so well known to the designers of these types of catamarans. These studies often involved the use of prototype models for testing in towing tanks or model basins. Since the concept of the Deep-V hull form for use in the design of multihull vessels is just beginning to evolve, it is fair to assume that the common knowledge of its seakeeping characteristics and of the wave-induced

loads is almost non-existent. Most naval architects and ship designers, who may wish to use or consider using this hullform, are often constrained to rely on using and extrapolating from the available data and methods on hullforms of other shapes in making their preliminary design assessments.

Early investigations on the experimental prediction of motions and wave-induced loads on catamarans were pioneered by researchers such as (Nordenstrom *et al.*, 1971; Wahab *et al.*, 1971; Lee *et al.*, 1973). The study by Wahab et al (1971), for example, focused on the experimental prediction of motions and loads on catamarans using ASR models with a forward speed in various wave conditions. The results from the above researches were typically validated by both experimental and numerical results that were conducted on other similar model tests data as stated in the papers. These researches have succeeded in setting the pace for other subsequent useful studies on this topic. While there has been some significant progress in terms of model tests for motion predictions of the Round Bilge hullform, further model tests for the wave-induced loads on the hullform still needs more attention due to the ever changing nature of the operating environments and the diverse services that these vessels offer around the world. Most of these studies were conducted on catamaran models. Even though there is sometimes a good basis to extend the use of the data obtained from available studies despite the scarcity of such data, it would have been advantageous if enough studies could had been independently conducted on other hull configurations such as trimaran vessels to provide general trends.

Relatively recent investigations on the motions response characteristics of catamarans in regular waves have been conducted by e.g. (Chan, 1993) and (Fang *et al.*, 1996; Fang *et al.*, 1997). In these studies, (Fang *et al.*, 1996; Fang *et al.*, 1997) presented a comprehensive study on the motion response characteristics of a catamaran in which the results of the predictions based on both the experimental and numerical methods, were carried out in two parts. The numerical method involved the use of a 2-dimensional Green's Function method associated with the cross flow behaviour that takes into account the effects of viscosity and is undertaken in the frequency domain. Some models of the Round Bilge demi-hull of a catamaran having symmetry about the longitudinal vertical centreline plane and with a transom stern were used. The models were assumed to be free running at a forward speed of $Fn = 0.49$**.** The RAO of the heave and pitch motions of the model in 135^{o} vessel headings (bow quarter oblique waves) were compared with the numerical values that were obtained

from the two dimensional methods. These authors used the earlier published experimental results by (Wahab *et al.*, 1971)in order to validate their work on two out of the three models used for the numerical predictions. The study found a good agreement between the set of numerical and experimental results.

In the experimental part of their paper, (Fang *et al.*, 1996; Fang *et al.*, 1997) found "Some discrepancies" in the prediction of pitch motions response at "smaller" wave frequencies. They attributed the source of the variations to the use of the autopilot system (implying a free running model in a basin, etc) and to other experimental errors while trying to ensure that the vessel maintained its directional course during the tests. The significance of this paper is that it has demonstrated that the numerical tools can be relied upon to produce satisfactory results notwithstanding the discrepancies in some of the experimental results whose source of errors were identified.

A similar numerical study by (Wellicome *et al.*, 1995) on the use of a pulsating source distribution method, based on the Green's function, was used to predict the motions response of a catamaran developed from the NPL Round Bilge hullform series. The authors validated their results with others obtained from both numerical (using a different method) and experimental test programmes, showing strong agreements between their findings. The work was later followed by another theoretical study from the authors (Wellicome *et al.*, 1999) on the use of numerical methods based on two different three-dimensional potential flow analysis approaches in order to specifically evaluate the hydrodynamic behaviour of the NPL Round Bilge hullform based catamaran design with a speed effect that was performed. The authors considered the effects of different hull spacing on the hydrodynamic coefficients and the motions response for the catamaran models in three different headings, namely head seas (180^o) and two forward oblique seas (150^o and 120^o) with a fixed forward speed of Fn = 0.65. It was reported in the paper that the results of the numerical predictions agreed with `some` of the experimental results, hence there is still a need for some caution when using these results in certain conditions as it could result in either an over- or an under-estimations of the responses of the models.

In 1999, (Soares and Maron, 1999) conducted an experimental investigation on the motions of a catamaran in waves. Their test programme involved three groups of test regimes with the first two focused on predicting the hydrodynamic added mass and the damping coefficients as well as the wave induced excitation forces and moments on the vessel. The third set of the

tests investigated the motions response of the model in regular waves. They used a radio controlled self-propelled model running at different speeds and vessel orientations relative to a simulated wave environment. Although the instrumentations used for this test is different from those that are available at Newcastle University towing tank, the test programme and the data processing method could be employed in the Deep-V wave-induced loads predictions.

Davis and Holloway (2003) investigated the influence of the hull form on the motions of high speed vessels using the Green`s Function method in a time domain strip theory method. In their study, eight different types of catamaran hull forms were compared to SWATHs, and both tri-hulls and monohulls. The most interesting aspect of these aforementioned studies is that they contained substantial experimental and numerical components within the investigations which provide a useful insight into what is to be expected when comparing the experimental and numerical results of the Deep-V model tests.

Other important studies in this subject area include the work of (Fang and Chen, 2008) on a study of the wave loads on a trimaran having a forward speed and based on a potential flow theory using a three-dimensional panel method. (Matsubara *et al.*, 2011) used a hydroelastic segmented model of a wave-piercing catamaran in order to experimentally investigate the influence of the centre bow, on the under surface of the cross-deck structure, on the vessel on the motions and loads at high speed. A similar study on a large moored catamaran in order to investigate the wave design loads was carried out by (Thomas *et al.*, 2011). Although none of these investigations was carried out using a model representative of a Deep-V catamaran hull form, the procedures that were followed in both the experimental and numerical investigations are very relevant to this study.

Since the concept of the Deep-V hull form for use in the design of multihull vessels is just evolving, it is to be noted that the knowledge of its seakeeping characteristics and of the wave-induced loads is almost non-existent. Most naval architects and ship designers thus have to rely on using and extrapolating information from the available data on hullforms of other shapes in making their preliminary design assessments.

2.4 Review of Structural Modelling and Design Considerations for Multihull Vessels

The structural design process of multihull vessels, just like that for other structures, is intended to provide durable, safe and robust structural configurations capable of resisting the through life-time induced loads on the structures. These loads are comprised of the light weight of the vessel and its components, namely the weight of the equipment, machinery, and the dead weight components, e.g. cargo, passengers, as well as the wave-induced loads due to the vessels motions in its intended operational environment.

For these conditions to be realised, the designer has a principal responsibility of ensuring that accurate predictions of the design loads, the form and scantlings of the structure and of the materials that are needed to withstand the effect of such loads that the vessel would encounter during its service life can be safely achieved. In addition, other contributing loads such as the ones due to the vessel operations inducing cyclic fatigue, green water, and slamming loads etc. must be properly assessed. The structure must also have a general level of robustness for the wear of normal service conditions. Using the knowledge of selected structural materials and effects of fabrication and the relevant design standards and regulations, in combinations with the knowledge of both static and dynamic equations, the structure must be designed to resist all the complex stresses that are induced by the various loads and of the effects of the vessel's operating speed.

In order to predict the loads on the vessel, it is necessary to have an understanding as well as experience in the use of model tests data and of the available numerical tools that can used to determine the applied loads, as outlined in (Bashir *et al.*, 2013). In the event that such an opportunity is not readily available, the design loads can be obtained based on the recommendations of classifications societies as outlined in (ABS, 2011; DNV, 2011; LR, 2012). The maximum global stresses as a result of the application of these loads on the structure can be performed using validated numerical tools e.g. (MAESTRO, 2012). The procedure for doing so must conform to the requirements of the international classification societies, as highlighted above.

Most of these design codes accept the practice of using direct calculations using the equations of quasi - static equilibrium in order to obtain the sea applied loads and the resulting stresses on the structure. For instance, (ABS, 2011) allows for direct analysis to be used but only in the preliminary design or for the assessment of structural strength of the high speed craft. The

code does not accept the use of other criteria for classification acceptance purposes of the design other than that promulgated by the design code itself.

2.4.1 Considerations for Materials Behaviour

The marine-grade aluminum alloys, and more recently the fiber reinforced composites materials, are increasingly being used in the design of the hull girder of the multi hull and high speed vessels in order to achieve the desired weight reduction. The lightweight structure, as used in the design of these groups of vessels, helps it to achieve a higher allowable deadweight fraction and this is a critical requirement during the design stages.

There are two distinct groups of marine grade aluminium alloys that are widely used in the ship fabrications. These groups are referred to as the **5000** and **6000** series and the selected properties of these materials are given in **Table 2.2**. Of the groups, the most commonly used types of materials are the **5083-H116** – for plates and **6082-T6 -** for extruded section. The **5083-H116** material comes in various forms typically as aluminium sheets with plate thickness range of up to 50mm thick (DNV, 2009). The **6082-T6** material, on the other hand, comes in extruded forms as aluminium sections with section thickness range of up to 12.5mm thick (DNV, 2009).

Table 2.2: Properties of Marine-Grade Aluminum Alloy Materials

Aluminium Alloys		Yield Strength (MPa)	Ultimate Tensile Strength	Ultimate Tensile Strength(After welding)	Elongation	Fracture toughness
Type	Temper	MPa	MPa	MPa	%	MPa$\sqrt{m}$
5083	H116/H321	215	305	125/275	10	43
5383	H116/H321	220	305	145/290	10	
5383NG	H116/H321	220	305	160/290	12	
5456	H116/H321	255	350			
5059 "Aluster"	H116/H321	270	370	160/330	10	
5086	H116	207	290		12	49
6082	T6	260	310	115/205	8-10	
6005A	T6	225	270		8	

The strength characteristics of these materials with respect to the design of the hull girder structure for this group of high-speed craft have seen some appreciable increase in interest among researchers recently. Several aspects of the strength characteristics of the hull structure constructed using various configurations of both the aluminium and composite materials have been carried out. The most prominent of these characteristics that affect the strength of the hull structure which are normally given priority are the following:

a. Young's Modulus of Elasticity

The elastic modulus of marine-grade aluminium alloys varies appreciably with the heat resistance characteristics of the material. The heat resistance characteristic is largely determined by the alloys chemical composition. As a result of this, the elastic modulus of the marine-grade material is generally given as 70GPa. Owing to the relatively low modulus of elasticity of this material, it is useful to check for the possible occurrence of buckling, fatigue, etc.

b. Material Density

The density of the marine-grade aluminium alloy material is typically given as 2660kg/m^3. This is essentially the same for all of the aluminium materials. This density is just about one-third of that of ship building steel, which has a density of 7850kg/m^3. This property is thus potentially quite significant in reducing the structural weight of the vessel, hence making it possible to attain the lightweight status of the material. However, partly because of the reduced density of this material, a vessel designed with these structural materials may require some level of passive fire protection systems. The thermal property of the marine-grades aluminium alloy plays an important role in dissipating of heat conducted by the materials in the events of fire. However in extreme situations aluminium alloy can actually melt, hence allowing the material to cool very fast, thereby makes the fire exposure potential a less worrisome issue because of the fact that its resulting effects will only have a localised consequence on the affected member instead of the entire structure.

c. Yield Strength

The yield and ultimate strength value along with other physical/mechanical properties of the marine-grades aluminium materials for both the plates and stiffened panels that have been used in this study are presented **Table 2.2**. The localised characteristics of the strength of the

materials depend on the heat exposure incurred and in terms of its weldability. This strength is significantly influenced by how the materials perform in its weakest state or of how a very localised part of it performs under the welding process of the plates or to produce the stiffened panels (Zha and Moan, 2001; Paik *et al.*, 2005). These areas of weakness, termed the Heat Affected Zones, HAZ, reduces the strength of the plates and the stiffened panels from 10% to up to 50% depending on the composition of the materials and the type and direction of the loading pattern (Dow *et al.*, 2009), and also involves creating patterns of self-equilibrating residual stress systems of tensile and compressive stresses.

2.4.2 The Structural Design Methodology

The choice of the appropriate methods for the structural design of vessels to be employed is generally depended on, among others, the needs of the client, the type and size of hull arrangement, stability considerations, service environment, operational profile of the vessel, and the cost of building the structures. The requirements often dictate the type acceptance criteria to be used in the course of the design e.g. stress levels, as well as minimum required safety factors. The requirements for the design of lightweight structures, as an example, demands that in addition to meeting the strength requirements the vessel must be designed for other failure conditions that must satisfy the requirements of serviceability limit state, accidental limit state (progressive collapse). The avoidance of fatigue damage is another important consideration and the owner may specify a minimum acceptable life, etc.

In most of the modern structural design computer programs, the considerations for the design development have been built in the forms of interactive modules. This allows for one design criteria to be met at a given time before performing combined checks of the various structural components in order to systematically satisfy the acceptance requirements for the respective codes. The use of a unified approach for a rational-based structural design process has been implemented in the MAESTRO program (Dow *et al.*, 1997). The unified approach requires six criteria to be satisfied for a vessel to meet the design requirements based on first-principles. Figure 2.4 presents a schematic diagram of a rationally based design process.

This approach can be used in the global (longitudinal) and transverse (cross-deck structure) as well as the local member strength assessment of the vessel. The overall process that should be followed in order to establish minimum acceptable scantling throughout a vessel has five basic stages (i) to (v). These are reflected within classification activities, and should be

reflected within any structural optimisation process (and which often does not consider the implications of fatigue involving stiffness and/or vibration aspects of the structure).

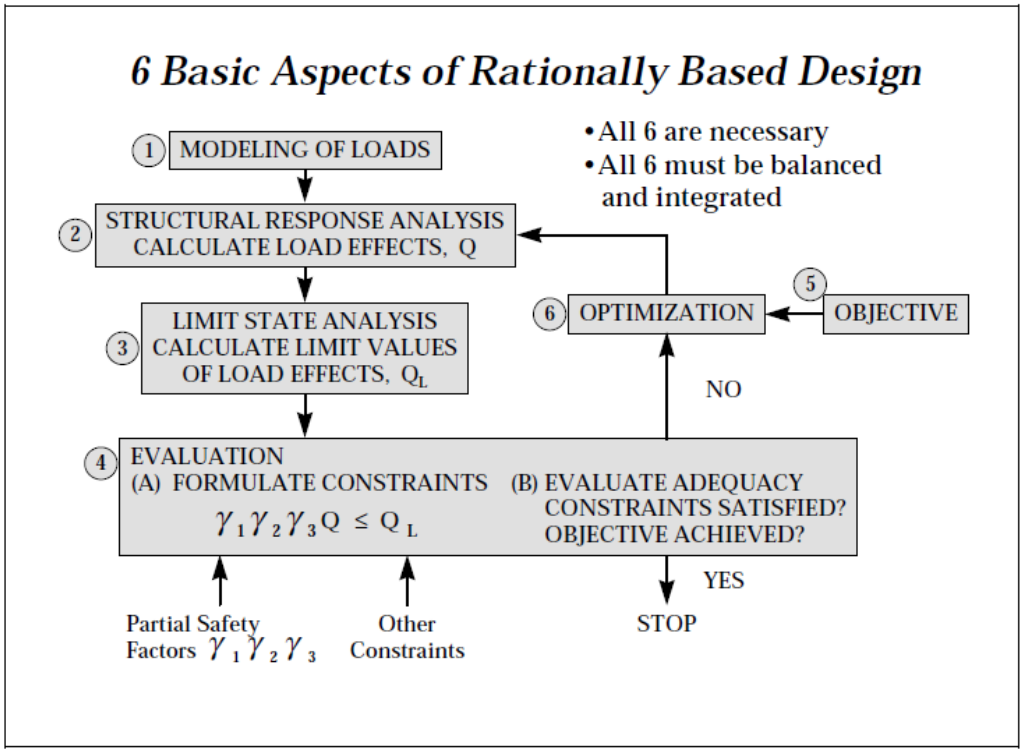

Figure 2.4: Unified approach for the iterative structural design of a ship using MAESTRO (Dow *et al.*, 1997)

Stage (i): Robustness.

Design for general robustness will establish the absolute minimum scantlings that will be allowed. These are often based on general experience and are defined in order to resist the wear and tear of normal operations often from a difficult to define and would reflect general handling small accident events, general deck and work traffic. *Stage(ii): Maximum Localised Loading.*

The structure will need to be designed to allow for the maximum possible levels of local forces that may be imposed on the vessel at some time during its operations. Some of these forces may be part of a global analysis but at an appreciably lower magnitude and phase.

These local loads will include static and quasi-static forces and the transient equivalents of dynamic forces, for example:-

i. Green sea on the weather deck surfaces
ii. Slamming on the wet deck & local surfaces
iii. Extreme wave pressures on hull components
iv. Bow slamming
v. Quasi-static tank pressures with heeled vessel
vi. Patch loads for moving vehicles & equipment
vii. Inertial forces from heavy components/equipment

These will be considered using local structural analyses and may/may not result in an increase in local absolute minimum scantlings. These analyses will probably be based on allowable response criteria that allow for in some indirect manner the other stresses within the structure.

Stage (iii): Global Analyses

The responses of the full scale structure due to the effects of the comprehensive sets of still water/wave-induced/inertial response forces need to be analysed. Typically the employment of a finite element model (or models) of the full structure is widely used in performing the global analysis and it is based on the assumption of linear elastic small deflection behaviours. The quality of the calculated results will depend on the fineness of the model definition (mesh sizes) element types and the stresses that are calculated (from the primary secondary and tertiary levers, e.g. Plate bending stresses between framing and related to applied surface pressures)

A range of load conditions will need to be considered in order to find the combinations that are critical for various regions with the structure.

From the above it is clear that any attempts at structural optimisation must cater for several load combination sets and not a single load case. (It will be similar with same extensions; to ABS's dynamic load analysis, DLA approach). Criteria for optimisation studies will be similar to that assumed in MAESTRO (Figure 2.4) with the minimum limiting scantling being defined by stages (i) and (ii) above.

A full range of stress and buckling criteria will be applied. However a rationale will need to be developed in order to decide upon an appropriate set off partial safe factors. The optimisation process will become more complex if changes in the framing arrangement are to be considered as this will also affect stages (ii) above.

Stage (iv): Fatigue Considerations.

To ensure that the structure will have a fatigue life that is equal to or exceeds the design operational life time.

It is probable that this analysis activity will have only a small effect on the basic scantling. However there is the possibility that a change may need to be made to the material grade that was originally selected and thus merits consideration before the next stage is contemplated.

Stage (v): Ultimate Strength

Assuming that an ultimate strength determination process exists for the various article demand conditions (in addition to that of the pure bending modes, whether uni- or bi-directional there will need to be methods appropriate to pure torsion and combined bending and shear conditions, etc.) there will need to be some criteria for comparison purposes, etc . Some of the above combined loading conditions only exist in some form of simple interaction curve form and will need to be developed. A possible approach could be the use of Finite Element software, albeit useful mainly for final design qualification purposes, given some criteria to compare against.

In some cases the classification societies have adopted a safety factors type of approach relating ultimate strength capability with the maximum through- life demand, with the factors allowing for such as, corrosion margins and a simple partial safety factors based largely on general experience and a statistically unquantified value judgement. This has been the approach for general hull girder vertical bending behaviour. It will be unlikely that similar simplistic approaches are found for the complex loading of the cross deck structure of a catamaran. Hence, for essentially one – off designs, their best probable approach is to undertake several Finite Element Analysis studies of the cross- deck structure (as developed through the first four stages) with fixed combinations of applied forces.

As a general note, and as an example, the thickness of an individual plate element on say, the weather deck or the bottom surface of the cross-deck structure will be progressively developed, for a given framing /stiffening arrangement, such that:

$t_{(v)} \geq t_{(iv)} \geq t_{(iii)} \geq t_{(ii)} \geq t_{(i).}$ Where ***t*** is the plate thickness for the successive stages mentioned above

The overall design philosophy that is employed in the structural strength and integrity assessment of a vessel is based on the consideration of the following sub-headings:

1. Ultimate limit state method

Traditionally, the Working Stress Design method, WSD, which is a concept of the load factor method of design, has historically been the method of choice in the design of ship structures (ABS, 2005). The method is entirely based on the linear elastic behaviour of the materials and it was widely employed in the design of steel ship structures. The allowable stress design offers some advantages such as compatibility between the loads and the material behaviour as well as its familiarity by a generation of ship designers and builders alike. The main drawbacks to the method are that it lacked rationality and clarity in the use of design factors for materials and loads; the unpredictable nature of the larger scale failure mechanism of structures design with it extending beyond the elastic conditions potentially leading to catastrophic failure at times and the possibility of over-designing structures based on overestimated loads.

In order to address some of these identified weaknesses inherent to the WSD method, a more rational method for the design and assessment of strength of structure, called the limit state design was introduced (Paik and Kim, 2002). A limit state is a specified condition beyond which a structure, or its components, is considered as being not fit for the service for which it was designed for. This concept consists of four different key assessment criteria levels, these are the ultimate limit state (ULS), the serviceability limit state (SLS), fatigue limit state (FLS) and the accidental limit state (ALS) (Paik and Thayamballi, 2007).

In the ULS concept, the strength capacity of a structure is assessed based on the maximum loads it can withstand without resulting in a complete collapse, a rapid unloading of the capability of the structure or that of any of its main components. The basis for this assessment is such that the strength of the materials that are used in the design of the structural members is assumed to be capable of withstanding the worst loading conditions by incorporating some design factors to account for statistical uncertainties in the scantlings and the material behaviour.

As shown in Figure 2.5, normally most structural materials behave nonlinearly beyond the elastic limit (**A**) with further increases in applied loads leading to the occurrence of some

degree of permanent deformation. The structure will normally still be able carry significant amount of loads beyond its elastic limit until it begins to deform significantly (**B**). In some zones upon attaining its maximum deformation, sometimes called the plastic limit, the structure is expected to fail. The point (**C**), at which this failure is said to occur is what is usually referred to as the ultimate limit strength of that structural element. Figure 2.5 basically presents the relationship between loads and deformation which defines the ultimate strength behaviour of a typical metallic material (Paik and Kim, 2002). However, depending on the structural element concerned its failure, or partial failure, often may lead to load shedding, or redistribution, to adjacent elements that may not have reached their individual ultimate limit strength. Thus there is some further `overall` capacity owing to the general redundancy within the overall structure. This is observed in for example, ultimate strength studies on hull girder sections etc.

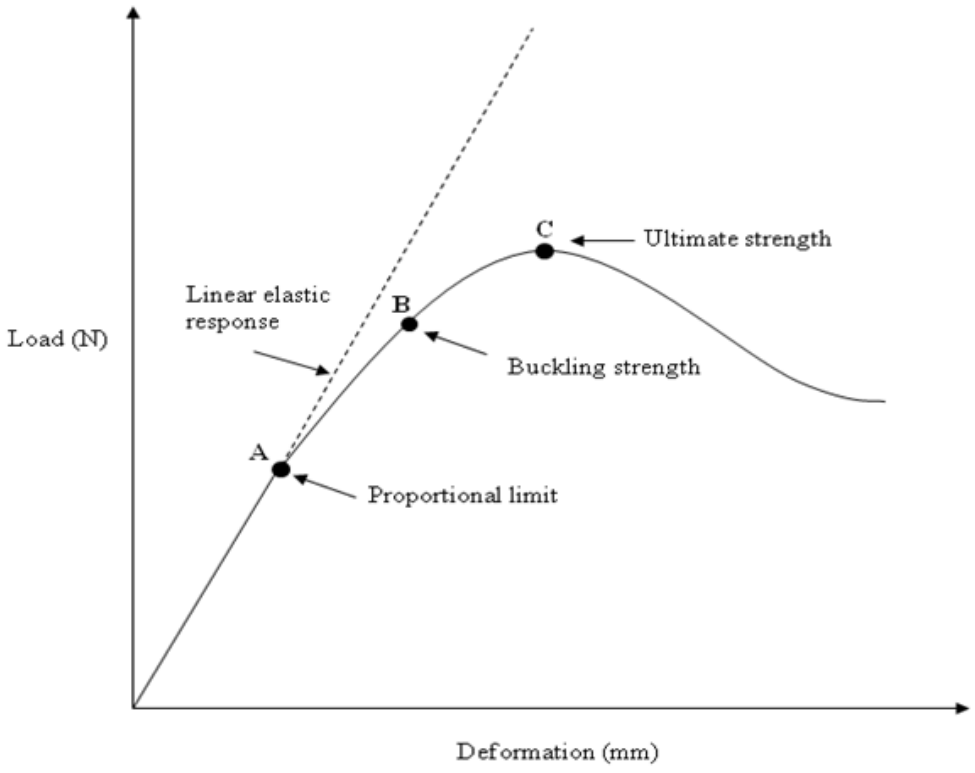

Figure 2.5: Ultimate strength behavior for component typical metallic structure (Paik and Kim, 2002)

The global bending strength of the hull structure of a ship is normally assessed based on ultimate strength principles. The hull itself consists of a combination of many various structural elements such as the frames, girder stiffeners and plating to form a unit structure called the hull girder. In multihull vessel design, most of these hull girders are designed largely with stiffened plates, partly in order to achieve the desired strength of the vessel.

Due to increasingly significant needs for proper understanding of the strength behavior of ships, and of multihull vessels in particular, a number of recent studies have focused on investigating the strength of both the entire hull structure and of the local members made using various metallic materials and geometric configurations. A simple methodology for the prediction of the ultimate strength of ships was presented by Paik and Mansour(1995). Although the focus of the paper was on predicting the strength of ships made of single and double hull structures, the principles are basically useful in the assessing the strength of the individual demi-hulls of the twin- or tri-hulls vessels. In 2002, (Paik and Kim, 2002) presented a more elaborate method of designing ships based on the ultimate strength concept by extending their study to consider other limit state approach requirements such as the SLS, FLS and the ALS. This work was followed by several other similar studies such as (Yao, 2003) who reviewed the approaches for determining the hull girder strength of a ship; Naar et al., (2005) on the ultimate strength of passenger ships using and FEM calculations; Paik (2007) on the development of an empirical formulations for predicting the ultimate compressive strength of welded aluminium stiffened panels; (Chen and Guedes Soares, 2007b; Chen and Guedes Soares, 2007a) studied both the Longitudinal strength analysis of ship hulls as well as the reliability assessment for ultimate longitudinal strength for ship made with composite materials.

2. Serviceability limit state method

The serviceability limit state design method (SLS) is considered to be the state at which the structure cannot perform the service for which it is designed for without reaching its ultimate strength, i.e. before collapse. When a structure is under this condition, the durability of the structure and other components are adjudged to be unsafe for use due to the unacceptable level of deformations.

Generally, the considerations for serviceability assessment are never done in isolation of other limit state design requirements such as the ultimate strength. Most of the studies on the serviceability of ship structures were actually focussed on the materials and structural elements rather than on the entire structural unit. The SLS considers structural failure such as buckling, torsional failure, etc, that is capable of impairing the aesthetics of the structure whose effects are considered to be local to particular structural elements.

Several studies have been performed on the buckling and post-buckling behaviour of the structural plates used in the construction of ships and other marine structures. Zha and Moan (2001) studied the ultimate strength behaviour of aluminium plates stiffened with flat bar under a torsional buckling or tripping failure mode. The study depicts the kind of failure that is commonly expected in the operations of a multihull vessel when experiencing the effects of nonlinear loading conditions. For ship structures with very large length overall beam to ratio, the deformations due to torsion around the hatch openings are normally assessed as part of the structures (Paik *et al.*, 2001). However such openings are nowadays found on the cross deck of the multihull vessel; and because the effect of torsion could cause significant amount of buckling, especially on the cross-deck structure, there is the need for understanding of how this affects the overall design methodology of a multihull vessels.

Another important consideration in design of vessels for serviceability limit state considerations is the effect of vibration due to slamming and green water on the deck (Iijima *et al.*, 2008; Thomas *et al.*, 2008). For any vessel operating in extreme conditions, the vibratory effects on the vessel could results in several forms of deformations such as fatigue, local buckling on the elements in the area of impacts. Such type of failures needs to be understood as well as properly evaluated. Amin et al.,(2013), recently published the results of their study on the development of wavelet tools for use in the analyses of the wave-induced hull vibrations. The tool was experimented on a wave-piercing catamaran yielding reasonable results. Other researchers such as (Ojeda *et al.*, 2004; Qin and Batra, 2009) have previously studied the effects of slamming on the strength of a vessels made using composite materials.

3. Fatigue limit state method

The fatigue design of a vessel such as the multihull is very critical to the assessment of the overall structural strength and integrity of the vessel. Multihull and high speed vessels are normally designed with aluminium or composite materials which are known for their sensitivity to fatigue, especially in their detailed design, than the steel structure. The most common cause of fatigue on a vessel is the effect of nonlinearity of loads due to cyclic loading (Heggelund *et al.*, 1998). This behaviour could be caused by loads such as the wave-induced loads, internal and external variation of pressures due to impact from slamming, green water effects etc, vibration of the vessel due to operational loads and other loads effects from cargo, equipment and machinery.

Most of the classifications societies have developed stand-alone code and guidance or incorporated some recommendations on the means of assessing the fatigue behaviour of a vessel in their respective rules and standards on the strength assessment of such vessels. The method used by the DNV in particular, followed the work of Cramer et al., (1995) on the assessment of fatigue in ship structures. Their study considered the expected accumulated damage of the vessel based on the S-N curves for both the welded and unwelded structures of various geometries. They also investigated fatigue on the basis of areas with high fatigue potentials such joint detail, corroded members and weldment. The study also considered the long term stress range distribution acting on such detail with reference to their stress level using the DNV's rules.

The structural components where the effects of fatigue failure normally occur are the joints detail for both welded and unwelded joints as well as on the corroded members. The Ship Structures Committee (SSC), developed a guide on the 'Fatigue Resistant Detail Design Guide for Ship Structures' (Krammer *et al.*, 2000), following its symposium in 1995. This was followed by another study on the Fatigue of Aluminium Weldments in which the effects of speed and displacement increase on a high speed aluminium craft on the fatigue failure of the vessel were considered (Krammer *et al.*, 2000).

As highlighted earlier, most of the fatigue studies are treated as a localised problem on the structural elements that are deemed to have the potentials of fatigue failure. However, (Heggelund *et al.*, 1998) studied the fatigue analysis of high speed catamarans made using aluminium materials in which he evaluated the contributions of various loads on the vessel to the overall fatigue life of the vessel. In this study, they identified three key areas within the midship section of the vessel where fatigue induces high stress concentrations. These areas were (1) the bottom of the hull; (2) the wheel house structure and; (3) the transverse girder. These areas are all related to the cross-deck structure of the vessel, which again, emphasised the need for the understanding of the strength behaviour of the cross-deck structure of multihull vessel in general. They established a procedure for calculating the long term distribution of nominal stress due to fatigue on a high speed vessel. Other notable study on this subject include the works of (Maddox, 2003) on a review of fatigue assessment procedure for welded aluminium structures.

2.5 Conclusions

In this chapter, it has been demonstrated that the concept of the Deep-V hull form, as used in the design of catamarans and other multihull vessels, in general is just evolving. The catamaran concept combines the superior seakeeping performance of a displacement type Deep-V monohull with an efficient speed and stability performance of twin hull forms in order to improve the relatively poor seakeeping performance of catamarans at speed. Preliminary investigations conducted on some seakeeping aspect of this concept revealed a significant reduction of their speed loss in a seaway, hence giving it the ability to have better resistance than that the commonly used Round Bilge geometry. In spite of this acknowledged advantages, the use of the Deep-V hull form concept in the design of multihull vessel is still faced with challenges due to lack of information about its seakeeping performance, motions response and wave-induced load characteristics of the hull form. At present, naval architects and ship designers rely on the use of available data from other configurations of hull form in other to approximate these design parameters in the preliminary design stage. This act comes with great risk of under- or over- estimating loads on the structure.

This review carried out here demonstrates that there are quite a lot at stake from the perspective of the structural requirements in order to have a holistic design using this hull form concept. This includes the sensitive of the cross-deck structure to weight, fatigue problem at the connections of the cross-deck structure and the demi-hulls and the requirement for transverse strength of vessel. The recommendation of the International Association of Classification Societies (IACS) on the motions and design loads is based on empirical formulations which is difficult to ascertain. Almost all of the IACS rules allows for direction calculations to perform and to be validated with acceptable towing tank results. But such results are equally non-existent for the Deep-V hull concept at present.

It is therefore very difficult to achieve a wholesome structural design of a catamaran vessel using this hull form concept without the understanding of the motions and wave-induced loads response characteristics of the hull form. Hence there is the need for data on the motions and wave-induced load characteristics of the hull form to use in the structural design and analyses in order to expand the use of this hull form concept.

Chapter 3

Theoretical Background of Numerical Prediction of Motion Response and Wave-Induced Loads

3.1 Introduction

The main objective of this chapter is to present the theoretical background behind the numerical codes that have been used to predict and analyse the motion and wave-induced loads responses on catamarans investigated in this study.

Within the above framework, Section 3.1 provides a brief introduction to this chapter while Section 3.2 describes the numerical tools used for the predictions of the motion responses and the wave-induced loads. Section 3.3 presents the frequently employed three-dimensional coordinate systems and the basic assumptions that are used in the formulation of the motion and load problems using 3D potential flow theory. Section 3.4 to 3.6 describes the general equations for the prediction of hydrodynamic forces, hydrostatic forces and the generalised mass matrix for a rigid body as employed in the linear potential theory on which the relevant hydrodynamic coefficients of the equations of motion and wave induced loads is formulated.. Section 3.6 describes the steady flow problem of the linear potential theory whilst Section 3.7 through 3.9 present the formulation of the unsteady velocity potentials and induced due to Radiation, Incident and Diffraction waves, respectively. Section 3.10 presents the equations and solutions of ship motion equations whilst Section 3.11 describes the general application of the hydrodynamic pressures. Section 3.12 presents the wave-induced loads across the cross-section of the vessel and Section 3.13 then discusses the predictions of the extreme design loads using the predicted responses and wave-induced loads measurements. Finally Section 3.14 concludes the chapter with a summary of the background formulations presented.

3.2 Description of the Numerical Predictions Software

In line with the broader objectives of this study, two numerical codes were used for the prediction of motion and load responses of various catamaran concepts investigated in the thesis. These codes are the MAESTRO-Wave and the PRECAL, both of which are specialised numerical codes for solving hydrodynamic problems of marine vehicles. Whilst the former code has been used as the main tool in this study the latter one has been brought at the later stages of the research to study further details of the hydrodynamic analysis as well as to provide further confidence in the predictions of the motion responses. The other reason for validating the experimental data with multiple codes is to combine the strength of these two codes together in order to have more credible validations. A brief overview of these codes is given in the next sub-section while the theoretical background behind the main code MAESTRO is presented in the remaining parts of Chapter 3.

3.2.1 The MAESTRO-Wave

The MAESTRO-Wave is a hydrodynamic software developed by Dr. Zhao and DRS Defense Solutions, LLC for MAESTRO Marine Inc and it has been integrated into the MAESTRO Global Structural Analysis software. The code has been developed based on the potential flow theory using the 3D panel method that makes use of the zero speed Green function with a forward speed correction in the frequency domain as used in this investigation, (MAESTRO, 2012). The 3D panel method is implemented by using quadrilateral panels which has a constant source strength applied to each panel. The wave free surface and hull boundary conditions have been linearised to the calm water condition and mean position of the vessel, respectively. The total velocity potential of the boundary value problem is represented by the summation of the double-body potential for the steady flow disturbance, the incident wave potential, the diffracted wave potential and the radiated wave potential due the ship motion as later defined in this chapter.

The code is used for the predictions of motions and wave-induced load response characteristics of marine vehicles and installations in deepwater and shallow water conditions including catamarans. The main attraction for using this software is that it does not require the use of Finite Element (FE) mesh separate from the hydrodynamic mesh when performing the structural analysis of the same hull geometry. This process therefore ensures that there is equilibrium between the hydrodynamic and the FE mesh; hence it reduces the difficulty of

convergence between the two different meshes which is commonly experienced when importing hydrodynamic mesh into an FE program.

3.2.2 The PRECAL

The PRECAL program has been developed by the members of the PRECAL Working Group of the Co-operative Research Ships (CRS) led by MARIN under a collaborative research. It is also a three dimensional panel method program based on the linear potential flow theory in frequency domain. The PRECAL code has been specifically developed to predict the ship motions and wave-induced loads for monohull and multihull vessels and it is capable of performing other relevant seakeeping attributes including accelerations, relative motions, added wave resistance etc (Huijsmans *et al.*, 1999; Van't Veer, 2009). The basic version of the PRECAL follows the same theoretical formulation of the MAESTRO-Wave whilst there are additional options to handle the treatments of the various types of Green's Functions, speed effects and hydrodynamic interference between the demi-hulls etc. The program consists of four specialist packages, these are: 1. HYDMES – which is used to generate surface of the hull geometries based on the 3D quadrilateral panels; 2. HYDCAL – This is used for the calculation of the hydrodynamic coefficients on the body in fluid; 3. RESCAL – is required for the calculation of the response of the ship in waves and 4. FINMES – This is used for defining the finite element loads.

The other need for using PRECAL in this study arise from the desire to utilise some of its important hydrodynamic outputs such as the added mass and damping coefficient as well as the wave excitation forces that may not be readily available in the MAESTRO-Wave in order to investigate the trends of the motion peaks due to various phenomena. In addition, the program is one of the software that have been used in the validation of the entire MAESTRO-Wave program (Ma *et al.*, 2012).

3.3 Description of General Ship Motion and Potential Flow Problems

3.3.1 Basic Assumptions

The following are the fundamental assumptions made in the formulations:

1. The fluid is assumed to be ideal, (inviscid, incompressible and irrotational).
2. The body maintains its mean position and its oscillatory amplitude are assumed to be small.
3. The double-body steady flow assumption neglects the wave-making of the vessel.

4. Incoming waves are assumed to be sinusoidal with small amplitudes and hence linear free-surface conditions apply.

3.3.2 The Coordinate Systems

The prediction methodology for the motion responses and the corresponding hydrodynamic loads on the multihull vessel in MAESTRO –Wave is based on a linear potential theory in which the following three interrelated coordinate systems are used in order to describe aspects of the spatial orientation of the vessel in its environment.

1. A global coordinate system that is fixed in space (O-XYZ) such that the O-XZ plane coincides with the undisturbed still water surface as shown in Figure 3.1
2. A steady-moving rigid body coordinate system o-xyz which is used to describe the motions of the catamaran as it is travelling in waves at various headings and with a forward speed, U. The horizontal plane, o-xz, is assumed to coincide with the still water surface as shown in Figure 3.1.
3. A local coordinate system that is fixed on the vessel body (o_v-$x_v y_v z_v$), with a forward speed, such that line o-x_y points in the forward direction along the longitudinal centreline axis of the vessel as shown in Figure 3.1.

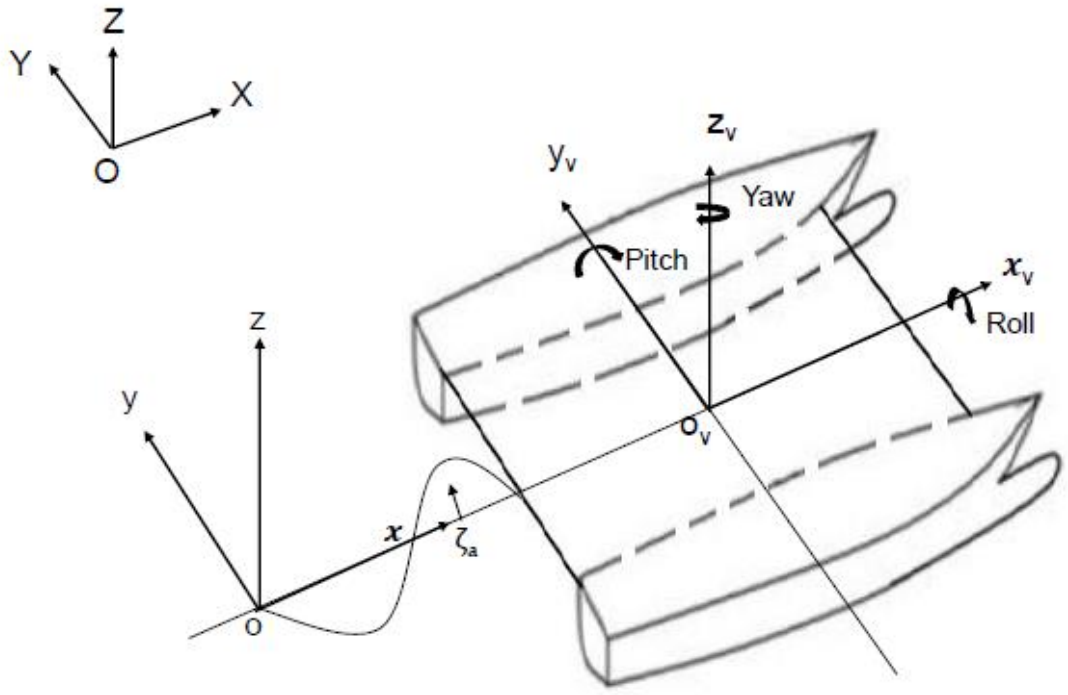

Figure 3.1: Vessel orientation coordinate systems

The x-axis is pointing upstream in the direction of travel within the vertical-longitudinal centreline plane of the body and the y-axis is pointing vertically upward through the centre of gravity of the body with the three origins, O, o and o_v being in the plane of the mean still water free surface. The origins of all the three coordinate axes are thus related to the positions of the still water condition, and with the longitudinal and vertical directions passing through the centre of gravity of the vessel, as shown in Figure 3.1.

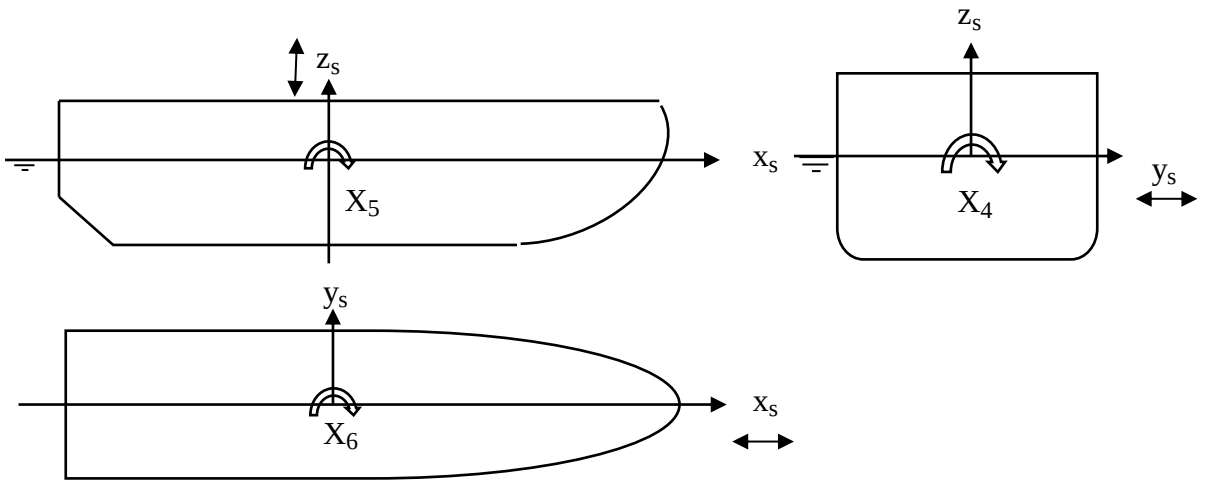

Figure 3.2: Ship motions(Martec, 2006)

Translations of the body along each of the coordinate directions represents the conventional six degrees of freedom of motion of a vessel, with translational motions of the vessel i.e. j=1, 2, 3 (where j = 1 is the surge, j = 2 is the sway, and j = 3 is the heave). The rotations of the vessel about each of these coordinate axes represents the conventional rotational oscillatory motions i.e. j=4, 5, 6 (where j = 4 is the roll, j = 5 is the pitch, and j = 6 is the yaw). As stated earlier the ship motions are measured in the o-xyz system. The static and hydrodynamic moments and ship inertial moments are described about the COG of the vessel. Figure 3.2 shows the orientation of the vessel in the various motions modes.

3.3.3 The Velocity Potentials

Within the framework of the potential flow theory the total velocity potential of the problem can be described as follows (Qiu *et al.*, 1999):

$$\boldsymbol{\phi_T(x,y,z;t) = -Ux + \phi_s(x,y,z) + \Phi(x,y,z;t)} \qquad \textbf{Eq 31}$$

Where,

$-Ux$ is the uniform flow velocity potential due to forward speed of the ship, U but without the disturbance of the ship

ϕ_s **(x, y, z)** is the steady disturbance potential of the ship with its forward speed, U.

ϕ **(x, y, z, t)** is the unsteady disturbance potential of the ship due to the incident wave and vessel's response to it. This can be expressed in the following form as described in (Qiu *et al.*, 1999)

$$\Phi(x, y, z, t) = [\phi_I(x, y, z) + \phi_D(x, y, z) + \phi_R(x, y, z)]e^{-i\omega_e t} \qquad \textbf{Eq 32}$$

Where: ϕ_I**(x,y,z)** is the incident wave potential, which will produce the Froude-Krylov force on the rigidly held body and it is further defined in equation **(Eq 3-41)**

ϕ_D**(x,y,z)** is the diffracted wave potential which will induce diffraction forces/moments on the rigidly held body and described further in **(Eq 3-45).**

ϕ_R**(x,y,z)** is the radiation wave potential due to the six degrees of freedom of the body oscillations in calm water and described further in **(Eq 3-25).**

ω_e is the encounter wave frequency

3.4 Hydrodynamic Forces

General expression for the hydrodynamic forces acting on the vessel can be given by equation (**Eq 3-3) (Newman, 1978; Qiu *et al.*, 1999)**.

$$F_j = \iint_S p n_j \, ds \qquad \textbf{Eq 33}$$

For **j = 1, 6**

Where **S** is the mean wetted surface of the hull, and $\mathbf{n_j}$ is the generalized unit normal vector on the body defined for the different modes of motion as follows:

$$n = \begin{cases} \vec{n} & for\ j = 1, 2, 3 \\ (\vec{r} - \vec{r}_g) & for\ j = 4, 5, 6 \end{cases}, \qquad \textbf{Eq 34}$$

Where $\vec{n}$ the unit is normal pointing towards the ship hull surface, $\vec{r}$, is a position vector at a given point which is normal to the mean surface of the vessel's wetted body. $\vec{r}_g$ is the position vector at a given point from the centre of gravity of the vessel.

General expression for the hydrodynamic pressure $\boldsymbol{p}$ at a point on the body can be derived from the Bernoulli Equation **(Eq 3-5).**

$$\boldsymbol{p = -\rho\left(\frac{\partial \Phi}{\partial t} + \mathbf{W}\,.\,\nabla\Phi\right)} \qquad \textbf{Eq 35}$$

Where $\boldsymbol{\rho}$ is the water density and $\boldsymbol{W}$ is the steady flow velocity vector given as:

$\boldsymbol{W = \nabla(-Ux + \phi_s)}$ Substituting equation **(Eq 3-5)** into **(Eq 3-3)**, gives the general expression for the hydrodynamic forces acting on the vessel as follows (Newman, 1978):

$$\boldsymbol{F_j = -\rho \iint_S n_j\left(\frac{\partial \Phi}{\partial t} + \nabla(-Ux + \phi_s)\,.\nabla\Phi\right)ds \quad for\ \mathbf{j = 1, 6}} \qquad \textbf{Eq 36}$$

3.5 Hydrostatic Forces

The total hydrostatic forces acting on the vessel can be represented using equation (**Eq 3-7**).

$$\boldsymbol{F_j^s = -C_{jk}x_k} \ \textbf{ for j=1, 6} \qquad \textbf{Eq 3-7}$$

Where $\mathbf{x_k}$, for k=1,2,..6 are the generalised ship motions defined as follows:

$$\mathbf{x_k = Re[\bar{x}_k e^{-i\omega_e t}] = Re\left|\bar{x}_k e^{-i(\omega_e t+\beta_k)}\right|} \ \textbf{ for k = 1, 6} \qquad \textbf{Eq 3-8}$$

Where $|\bar{\mathbf{x}}_\mathbf{k}|$ is complex motion amplitude while $\boldsymbol{\beta_k}$ is the phase angle of the motion response with respect to the incoming wave.

$\boldsymbol{C_{jk}}$, is the restoring force coefficient matrix and defined as follows:

$$[\mathbf{C_{jk}}]=\begin{bmatrix} 0 & 0 & 0 & 0 & 0 & 0 \\ 0 & 0 & 0 & 0 & 0 & 0 \\ 0 & 0 & \rho g A_W & 0 & \rho g A_W \bar{x}_f & 0 \\ 0 & 0 & 0 & \rho g(A_W R_1^2 + z_B \Delta) & 0 & 0 \\ 0 & 0 & \rho g A_W \bar{x}_f & 0 & \rho g(A_W R_2^2 + z_B \Delta) & 0 \\ 0 & 0 & 0 & 0 & 0 & 0 \end{bmatrix} \qquad \textbf{Eq 3-9}$$

Where: Aw = Waterplane area (m)

$\bar{\mathbf{x}}_\mathbf{k}$ = x co-ordinate of centre of flotation

$\boldsymbol{\Delta}$ = Ship displacement

R_1 and R_2 are the radii of gyration of the water plane area of the vessel about ox and oy axes.

Z_B is the z-coordinate of the Centre of Buoyancy of the ship

3.6 Generalised Mass Matrix

Since it is assumed that the ship is a rigid body the motions can be expressed by Newton's second law as:

$$\boldsymbol{M_{jk}\ddot{x}_{jk} = F_j + F_j^S} \qquad \text{j=1,2,…6} \qquad \textbf{Eq 3-10}$$

M_{jk} in the equation (**Eq 3-10**) is the generalized mass matrix, and defined as:

$$M_{jk}=\begin{bmatrix} M & 0 & 0 & 0 & 0 & 0 \\ 0 & M & 0 & 0 & 0 & 0 \\ 0 & 0 & M & 0 & 0 & 0 \\ 0 & 0 & 0 & I_{11} & I_{12} & I_{13} \\ 0 & 0 & 0 & I_{21} & I_{22} & I_{23} \\ 0 & 0 & 0 & I_{31} & I_{32} & I_{33} \end{bmatrix} \qquad \textbf{Eq 3-11}$$

Where **M** is the mass and $\mathbf{I_{nm}}$ (1, 2, 3) are the moment of Inertia of the vessel

3.7 Solution of Ship Motions

Solution of the ship motion problem requires the hydrostatic force $\boldsymbol{F_j^S}$ which is given in **Eq (3 -10)** and the hydrodynamic force, $\boldsymbol{F_{j,}}$ which will be presented in the following sections - in more details.

The oscillation of point **(x,y,z)** of the rigid ship can also be expressed in the form of the equation below:

$$\Delta\mathbf{x_k} = \mathbf{Re}[\Delta\bar{\mathbf{x}}_\mathbf{k}\mathbf{e}^{-\mathbf{i}\omega_\mathbf{e}\mathbf{t}}] \;\; \boldsymbol{i} = \mathbf{1, 2, 3} \qquad \textbf{Eq 3-12}$$

And it can be determined by the ship motion, $\mathbf{x_k}$**,** given in **Eq 3-13** as follows

$$\begin{aligned} \Delta\mathbf{x} &= \mathbf{x_1} + (\mathbf{z} - \mathbf{z_g})\mathbf{x_5} - (\mathbf{y} - \mathbf{y_g})\mathbf{x_6} \\ \Delta\mathbf{y} &= \mathbf{x_2} + (\mathbf{x} - \mathbf{x_g})\mathbf{x_6} - (\mathbf{z} - \mathbf{z_g})\mathbf{x_4} \\ \Delta\mathbf{z} &= \mathbf{x_3} + (\mathbf{y} - \mathbf{y_g})\mathbf{x_4} - (\mathbf{x} - \mathbf{x_g})\mathbf{x_5} \end{aligned} \qquad \textbf{Eq 3-13}$$

3.8 Steady Flow Potential due to Forward Speed

3.8.1 Double-Body Potential

The concept of the double-body in the potential flow theory was introduced to address the steady state flow effects due to the forward speed of the ship.

The steady state flow velocity potential is defined as follows (Newman, 1978):

$$\boldsymbol{\Phi_s(x,y,z) = -Ux + \phi_s(x,y,z)} \qquad \textbf{Eq 314}$$

This disturbance potential, $\boldsymbol{\phi_s}$, in equation **(Eq 3-14)** must satisfy the following boundary condition:

$$\begin{cases} \boldsymbol{\nabla^2 \phi_s = 0} \\ \boldsymbol{\dfrac{\partial \phi_s}{\partial z} = 0 \; on \; z = 0} \\ \boldsymbol{\dfrac{\partial \phi_s}{\partial n_1} = U.n_1} \\ \boldsymbol{\nabla \phi_s = 0 \; at \; \infty} \end{cases} \qquad \textbf{Eq 3-15}$$

The disturbance potential can be expressed as follows by using the Green function method

$$\boldsymbol{\phi_s(P) = \iint_S \sigma_s \; (Q)\widehat{G}(P,Q)dS(Q)} \qquad \textbf{Eq 3-16}$$

Where: **P** = P(x, y, z), is the field point

Q = Q(x, y, z), is the source point

$\boldsymbol{\sigma_s}$**(Q) =** is the steady flow source density

$\boldsymbol{\widehat{G}}$ **(P, Q) =** Q(x, y, z), is a unit Rankine source given by

$$\boldsymbol{\widehat{G}(P,Q) = \frac{1}{r_1} + \frac{1}{r_2}} \qquad \textbf{Eq 3-17}$$

Where: $\boldsymbol{r_1 = \sqrt{(x-\zeta)^2 + (y-\eta)^2 + (z-\xi)^2}}$ **Eq 3-18**

$\boldsymbol{r_2 = \sqrt{(x-\zeta)^2 + (y-\eta)^2 + (z+\xi)^2}}$

$\boldsymbol{(\zeta, \eta, \xi)}$, are the coordinates of the point source location positions **x**, **y** and **z**

Applying the body boundary conditions in equation **(3-15),** the source density $\boldsymbol{\sigma_s}$ can be calculated from equation **(3-19)** and this is substituted in **Eq (3-16)** in order to solve the disturbance potential $\boldsymbol{\phi_s(P)}$

$$2\pi\sigma_s(P) + \iint_S \sigma_s(q)\frac{\partial \hat{G}(p;q)}{\partial n_p} dS(q) = U.n_1(P) \qquad \textbf{Eq 3-19}$$

3.8.2 Steady Flow Effect – *m*-terms

The ***m*-terms** are used to represent the steady flow effect on the radiation body boundary condition on the wetted surface of the vessel. The ***m-terms*** are defined as follows (Schmitke, 1978):

$$(m_1, m_2, m_3) = -(\vec{n}.\nabla)\vec{W} = -(\vec{n}.\nabla)\Phi_s \qquad \textbf{Eq 3-20}$$

$$= \left(n_1.\Phi_{sxx} + n_2.\Phi_{sxy} + n_3.\Phi_{sxz}, n_1.\Phi_{syx} + n_2.\Phi_{syy} + n_3.\Phi_{syz}, n_1.\Phi_{szx} + n_2.\Phi_{szy} + n_3.\Phi_{szz}\right)$$

$$(m_4, m_5, m_6) = \vec{r}_g \times (m_1, m_2, m_3) - \vec{n} \times \nabla\Phi_s \qquad \textbf{Eq 3-21}$$

$$= \vec{r}_g \times (m_1, m_2, m_3) + \left(n_3.\Phi_{sy} - n_2.\Phi_{sz}, n_1.\Phi_{sz} - n_3.\Phi_{sx}, n_2.\Phi_{sx} - n_1.\Phi_{sy}\right)$$

Where $\vec{r}_g = (x - x_g, y - y_g, z - z_g)$ is the position vector from the CoG of the vessel to a point (x,y,z) on the body surface..

The simplified form of the ***m-terms,*** for considering uniform flow only, can be given as follows:

$$m_k = 0, \qquad k = 1, 2, 3, 4 \qquad \textbf{Eq 3-22}$$

$$m_5 = -U.n_3, \qquad \textbf{Eq 3-23}$$

$$m_6 = U.n_2, \qquad \textbf{Eq 3-24}$$

The m-terms can be derived from the integral equation as described in details by (Huang and Hsuing, 1993; Qiu *et al.*, 1999)

3.9 Radiated Wave Potential – Added mass and Damping Coefficient

The radiated wave potential, ϕ_R **(x,y,z),** which represents the disturbance of the ship due to the 6 DOF of motions in calm water can be expressed as shown in equation **(Eq 3-25).**

$$\boldsymbol{\Phi_R(x,y,z;t) = Re(\phi_R e^{-i\omega_e t})} \qquad \textbf{Eq 3-25}$$

The boundary conditions that are required to solve the velocity potential due to radiation are given as:

$$\begin{cases} \boldsymbol{\nabla^2 \phi_K = 0} \\ \boldsymbol{\left(g\dfrac{\partial}{\partial z} + U^2\dfrac{\partial^2}{\partial x^2} + 2i\omega U\dfrac{\partial}{\partial x} - \omega_e^2\right)\phi_k = 0 \ \ on\ z = 0} \\ \boldsymbol{\left.\dfrac{\partial \phi_k}{\partial n}\right|_S = n_k - \dfrac{m_k}{i\omega_e}} \\ \boldsymbol{\left.\dfrac{\partial \phi_k}{\partial n}\right|_{z\to\infty} = 0} \\ \boldsymbol{Radiation\ Condition: Outgoing\ waves} \end{cases} \qquad \textbf{Eq 3-26}$$

For interaction between hulls (multihull) or individual vessels (muti-ships), there will be 6M degrees of freedoms where M is the number of unit hulls of the vessel. The radiated wave potential per unit amplitude motion of the $\mathbf{k^{th}}$ mode of freedom on the hull surface **S** of the vessel, **T**, can be expressed as follows:

$$\left.\frac{\partial \phi_k^T}{\partial n}\right|_{Sz} = \begin{cases} 0 & T \neq S \\ n_k^T - \dfrac{m_k^T}{i\omega_e} & T = S \end{cases} \qquad \textbf{Eq 3-27}$$

The radiated wave potential can be written as in **Eq (3-28)** by using Green's function method in combination with the relevant boundary conditions in **Eq (3-26).** i.e

$$\boldsymbol{\phi_k(P) = \iint_S \sigma_k\ (Q)\widehat{G}(P,Q)dS(Q)} \qquad \textbf{Eq 3-28}$$

$\boldsymbol{\sigma_k}$= is the source density

$\boldsymbol{\widehat{G}}$ **(P, Q)** is a Green's Function with zero speed

$$\boldsymbol{\widehat{G}(P,Q) = \frac{1}{r_1} + \frac{1}{r_2} + 2v\int_0^\infty \frac{e^{k(z+\zeta)}}{k-v}J_o(vR)dk + i2\pi v e^{v(z+\zeta)}J_o(vR)} \quad \textbf{Eq 3-29}$$

Where: $\boldsymbol{v} = \frac{\omega_e^2}{g}, =$ Wave number

$\boldsymbol{J_o}$ = First kind Bessel function of zero order

$$\boldsymbol{R} = \sqrt{(\boldsymbol{x}-\boldsymbol{\zeta})^2 + (\boldsymbol{y}-\boldsymbol{\eta})^2} \qquad \textbf{Eq 3-30}$$

Applying the boundary conditions in equation **(Eq 3-26)** yields equation (**Eq 3-32),** which can be used to calculate the source density. $\boldsymbol{\sigma_k}(Q)$

$$2\pi\boldsymbol{\sigma_k}(\boldsymbol{P}) + \iint_{\boldsymbol{S}} \boldsymbol{\sigma_k}(\boldsymbol{Q}) \frac{\boldsymbol{\partial \widehat{G}}(\boldsymbol{P};\boldsymbol{Q})}{\boldsymbol{\partial n_p}} \boldsymbol{dS}(\boldsymbol{Q}) = \frac{\boldsymbol{\partial \phi_k}}{\boldsymbol{\partial n_p}} = \boldsymbol{n_k} - \frac{\boldsymbol{m_k}}{\boldsymbol{i\omega_e}} \qquad \textbf{Eq 3-32}$$

The radiated potential $\boldsymbol{\phi_k}(\boldsymbol{P})$, can be computed using **(Eq 3-28)** once the source density is known.

The associated radiated wave forces due to the **j**$^{\textbf{th}}$ mode of motion can be expressed as:

$$\boldsymbol{F_j^R}(\mathbf{x},\mathbf{y},\mathbf{z};\mathbf{t}) = \boldsymbol{Re}\left[\boldsymbol{f_j^R}(\mathbf{x},\mathbf{y},\mathbf{z})\boldsymbol{e^{-i\omega_e t}}\right] \qquad \textbf{Eq 333}$$

Where $\boldsymbol{f_j^R}(\mathbf{x},\mathbf{y},\mathbf{z})$ is the time independent spatial radiated wave force

By substituting the calculated radiation potential into equation **(Eq 3-6)** and using **(Eq 3-33) t**he time-independent spatial wave-induced force acting on the vessel due to radiation can be calculated from equation **(Eq 3-34).**

$$\begin{aligned}\boldsymbol{f_j^R} = \boldsymbol{\rho\omega_e^2} \sum_{\boldsymbol{k=1}}^{\boldsymbol{6}} \boldsymbol{\bar{x}_k} \Bigg\{ \iint_{\boldsymbol{s}} \boldsymbol{Re}[\boldsymbol{\phi_k}]\, \boldsymbol{n_j dS} \frac{\boldsymbol{U}}{\boldsymbol{\omega_e}} \iint_{\boldsymbol{s}} \boldsymbol{Im}\left[\frac{\boldsymbol{\partial \phi_k}}{\boldsymbol{\partial x}}\right] \boldsymbol{n_j dS} - \frac{\mathbf{1}}{\boldsymbol{\omega_e}} \iint_{\boldsymbol{s}} \boldsymbol{Im}\left[\boldsymbol{\nabla \phi_k} \,.\, \boldsymbol{\nabla \phi_S}\right] \boldsymbol{n_j dS} \Bigg\} \\ + \boldsymbol{i} \Bigg\{ \boldsymbol{\rho\omega_e} \sum_{\boldsymbol{k=1}}^{\boldsymbol{6}} \boldsymbol{\bar{x}_k} \Bigg\{ \iint_{\boldsymbol{s}} \boldsymbol{Im}[\boldsymbol{\phi_k}]\, \boldsymbol{n_j dS} - \boldsymbol{U} \iint_{\boldsymbol{s}} \boldsymbol{Re}\left[\frac{\boldsymbol{\partial \phi_k}}{\boldsymbol{\partial x}}\right] \boldsymbol{n_j dS} \\ + \iint_{\boldsymbol{s}} \boldsymbol{Re}\left[\boldsymbol{\nabla \phi_k} \,.\, \boldsymbol{\nabla \phi_S}\right] \boldsymbol{n_j dS} \Bigg\}\end{aligned} \qquad \textbf{Eq 334}$$

Where $\boldsymbol{\bar{x}_k}$, is the amplitude at the associated reference point on the body of the k$^{\text{th}}$ mode of motion given as:

$$\boldsymbol{\bar{x}_k} = \boldsymbol{Re}(\boldsymbol{\bar{x}_k e^{-i\omega_e t}}) \qquad \textbf{Eq 335}$$

3.9.1 Added Mass and Damping Coefficient

The reactive forces will be proportional with the velocity and acceleration of the body motion responses, which are given in **Eq (3-36)** and **Eq (3-37)** respectively.,

$$\dot{x}_k = Re[-i\omega_e \bar{x}_k e^{-i\omega_e t}] \qquad \textbf{Eq 336}$$

$$\ddot{x}_k = Re[-i\omega_e^2 \bar{x}_k e^{-i\omega_e t}] \qquad \textbf{Eq 337}$$

The radiated wave force on the vessel can be obtained by substituting **Eq (3-36)** and **Eq (3-37)** into equation **Eq (3-34)** which would give **Eq (3-38)**

$$f_j^R(\mathbf{x}, \mathbf{y}, \mathbf{z}; \mathbf{t}) = -\ddot{x}_k \mu_{jk} - \dot{x}_k \lambda_{jk} \qquad \textbf{Eq 338}$$

Where:

μ_{jk} = Added mass and it is defined as:

$$\mu_{jk} = \rho \left\{ \iint_s Re[\phi_k]\, n_j dS + \frac{U}{\omega_e} \iint_s Im\left[\frac{\partial \phi_k}{\partial x}\right] n_j dS - \frac{1}{\omega_e} \iint_s Im[\nabla \phi_k \,.\, \nabla \phi_S\,] n_j dS \right\}$$

Eq 3-39

λ_{jk} = Damping coefficient and it is defined as:

$$\lambda_{jk} = \rho \left\{ \begin{array}{c} \omega_e \sum_{k=1}^{6} \bar{x}_k \left\{ \iint_s Im[\phi_k]\, n_j dS - U \iint_s Re\left[\frac{\partial \phi_k}{\partial x}\right] n_j dS \right. \\ \left. + \iint_s Re[\nabla \phi_k \,.\, \nabla \phi_S\,] n_j dS \right. \end{array} \right\}$$

Eq 3-40

3.10 Incident Wave potential - Froude-Krylov Force

The incident wave potential is expressed as shown in equation **(3-41).**

$$\Phi_I(x, y, z; t) = Re[\phi_I(x, y, z) e^{-i\omega_e t}] \qquad \textbf{Eq 341}$$

Where:

$\boldsymbol{\phi_I(x,y,z)}$ is the spatial velocity potential function of the incident that is independent of time **t** and expressed as:

$$\boldsymbol{\phi_I = \frac{g\zeta_a}{i\omega} e^{vz+iv(x\cos\beta+y\sin\beta)}} \qquad \textbf{Eq 342}$$

Where =

$\boldsymbol{\zeta_a}$ is the incident wave amplitude,

$\boldsymbol{\omega_e} = |\omega - v U \cos\beta|$ is the wave encounter frequency

$\boldsymbol{\omega} = is\ wave\ frequency$

$\boldsymbol{v} = \frac{\omega^2}{g}, =$ Wave number

g is the acceleration due to gravity

$\boldsymbol{\beta}$ is the wave angle between the wave propagation direction and the axis "os-axis direction" as shown in Figure 3.1

In flow conditions where the components due the effects of diffracted and radiated waves on the total pressure on the vessel can be neglected in determining the unsteady state pressure, the resulting force from this situation is defined as the Froude-Krylov force and which is expressed as (Martec, 2006):

$$\boldsymbol{F_j^I(x,y,z;t) = Re\left[f_j^I e^{-i\omega_e t}\right]} \qquad \textbf{Eq 343}$$

Where the time-independent spatial wave-induced force acting on the vessel due to incident wave, $\boldsymbol{f_j^I}$, is given as follows:

$$\begin{aligned} \boldsymbol{f_j^I} = -\boldsymbol{\rho\omega_e} \iint_s \boldsymbol{Im[\phi_I]\, n_j dS} \\ + \boldsymbol{\rho U} \iint_s \boldsymbol{Re\left[\frac{\partial \phi_I}{\partial x}\right] n_j dS} - \boldsymbol{\rho} \iint_s \boldsymbol{Re[\nabla\phi_I . \nabla\phi_S]\, n_j dS} \\ + \boldsymbol{i}\left\{-\boldsymbol{\rho\omega_e} \iint_s \boldsymbol{Re[\phi_I]\, n_j dS} + \boldsymbol{\rho U} \iint_s \boldsymbol{Im\left[\frac{\partial \phi_I}{\partial x}\right] n_j dS}\right. \\ \left. + \boldsymbol{\rho} \iint_s \boldsymbol{Im[\nabla\phi_I . \nabla\phi_S]\, n_j dS}\right\} \end{aligned} \qquad \textbf{Eq 3-44}$$

3.11 The Diffracted Wave Potential – Diffracted Wave Force

The diffracted wave potential ϕ_D **(x,y,z;t)** due to the presence of the body in waves is obtained as a result of the incident waves effects on encountering the rigidly held body and being diffracted by it as described in equation **(3-45)**.

$$\boldsymbol{\Phi_D(x,y,z;t) = Re(\phi_D e^{-i\omega_e t})} \qquad \textbf{Eq 345}$$

This is derived from the incident wave potential by the application of the body boundary conditions given in **(Eq 3-46)**

$$\begin{cases} \boldsymbol{\nabla^2 \phi_D = 0} \\ \boldsymbol{\left(g\dfrac{\partial}{\partial z} + U^2\dfrac{\partial^2}{\partial x^2} + 2i\omega U\dfrac{\partial}{\partial z} - \omega_e^2\right)\phi_D = 0 \; on \; z = 0} \\ \boldsymbol{\left.\dfrac{\partial \phi_D}{\partial n}\right|_S = \left.\dfrac{\partial \phi_I}{\partial n}\right|_S} \\ \boldsymbol{\left.\dfrac{\partial \phi_k}{\partial n}\right|_{z\to\infty} = 0} \end{cases} \qquad \textbf{Eq 3-46}$$

The diffraction velocity wave potential can be expressed as follows by using Green's function method:

$$\boldsymbol{\Phi_D(P) = \iint_S \sigma_D\ (Q)\widehat{G}(P,Q)dS(Q)} \qquad \textbf{Eq 3-47}$$

Where: $\boldsymbol{\sigma_D}$ is the source density

Applying the body boundary conditions in **(Eq 3-46)** to equation **(Eq 3-47),** the source densities can be calculated from equation **(Eq 3-48)**

$$\boldsymbol{2\pi\sigma_D(P) + \iint_S \sigma_D(q)\frac{\partial(p;q)}{\partial n_p}dS(q) = \left.\frac{\partial \phi_D}{\partial n}\right|_P (P)} \qquad \textbf{Eq 3-48}$$

The diffracted wave force being imposed on the body due to the diffracted wave potential in the $\mathbf{j^{th}}$ mode of motion is shown in equation **(Eq 3-49).**

$$\boldsymbol{F_j^D(x,y,z;t) = Re\left[f_j^D(x,y,z;t)e^{-i\omega_e t}\right]} \qquad \textbf{Eq 349}$$

By substituting the calculated velocity potentials obtained by using equation **(Eq 3-47)** into equation **(Eq 3-6)** and using **(Eq 3-49)** the time-independent spatial wave-induced force acting on the vessel due to diffraction can be represented as follows:

$$f_j^D = -\rho\omega \iint_s Im[\phi_D]\, n_j dS + \rho U \iint_s Re\left[\frac{\partial \phi_D}{\partial x}\right] n_j dS - \rho \iint_s Re[\nabla\phi_D . \nabla\phi_S]\, n_j dS + i\left\{-\rho\omega_e \iint_s Re[\phi_D]\, n_j dS + \rho U \iint_s Im\left[\frac{\partial \phi_D}{\partial x}\right] n_j dS + \rho \iint_s Im[\nabla\phi_D . \nabla\phi_S]\, n_j dS\right\} \quad \textbf{Eq 350}$$

3.12 Ship Motion Equations

The ship motion equation can be expressed as (Qiu *et al.*, 1999):

$$\sum_{k=1}^{6}\left[-\omega_e^2(\bar{m}_{jk} + \mu_{jk}) + (-i\omega_e\lambda_{jk}) + C_{jk}\right]\bar{x}_k = f_j \quad \textbf{Eq 3-51}$$

$$f_j = f_j^I + f_j^D, \quad j = 1, 2, .. 6 \quad \textbf{Eq 3-52}$$

Where: $\bar{m}_{jk}$ = The mass matrix

μ_{jk} = Added mass matrix

λ_{jk} = Damping matrix

$\mathbf{C_{jk}}$ = The restoring force coefficient matrix

f_i = Wave Excitation Force/Moments (kN/kNm)

3.13 Hydrodynamic Pressures

The hydrodynamic pressures due to the given wave conditions are then calculated using the velocity potentials of the mean wetted body and which are then applied into the Bernoulli equation. The total hydrodynamic pressure at any given point on the vessel induced by the effects of the incident, diffraction and radiated waves is given as (Qiu *et al.*, 1999):

$$p_{ht} = \rho\left[i\omega(\phi_I + \phi_D) + \vec{W}.\nabla(\phi_I + \phi_D)\omega_e^2 \sum_{k=1}^{6} \bar{x}_k \phi_k - i\omega \sum_{k=1}^{6} \bar{x}_k \left(\vec{W}.\nabla\phi_k\right)\right] \quad \textbf{Eq 353}$$

This equation allows for the hydrodynamic forces and moments on the individual wetted panels that collectively make-up the wetted body of the vessel to be calculated and then by integrating to determine the hydrodynamic loading over the whole wetted surface.

However, the oscillatory motions of the vessel cause fluctuating hydrostatic pressures, hence the complex amplitude of these pressure fluctuations can be expressed as:

$$\Delta \boldsymbol{p_{st}} = -\boldsymbol{\rho g}(\bar{\boldsymbol{x}}_{\boldsymbol{3}} - \boldsymbol{x}\bar{\boldsymbol{x}}_{\boldsymbol{5}} + \boldsymbol{z}\bar{\boldsymbol{x}}_{\boldsymbol{4}}) \qquad \textbf{Eq 3-54}$$

3.14 Total Wave-induced Loads on Cross-Section

For a ship advancing waves, the wave loads acting on the ship are induced by the incident waves, diffracted waves and radiated waves. Other components are the inertia force of ship mass, and the forces due to the hydrostatic and hydrodynamic pressure increment caused by the ship motions. The six components of the wave loads on a specified cross-section, X_c, can be obtained by direct integration of the inertial force of ship mass forward of X_c plus the hydrodynamic pressure and hydrostatic pressure increment over the wetted hull surface forward of X_c (Martec, 2006).

$$\boldsymbol{F_j^W} = \boldsymbol{Re}\left[\boldsymbol{f_j^{WLD}} \boldsymbol{e^{-i\omega_e t}}\right] \quad \textbf{j = 2, 3…6} \qquad \textbf{Eq 3-55}$$

Where:

$$\boldsymbol{f_j^{WLD}} = \boldsymbol{I_j} - \iint_{\boldsymbol{S_x}} (\boldsymbol{p_{ht}} + \Delta \boldsymbol{p_{st}})\, \boldsymbol{N_j dS} \qquad \textbf{Eq 3-56}$$

$\mathbf{S_x}$ is the mean wetted surface of the transverse section

$\boldsymbol{N_j}$ = $\boldsymbol{n_j}$ for j = 1, 2, 3, 4 **Eq 3-57**

$\boldsymbol{N_5}$ = -$x n_3$ **Eq 3-58**

$\boldsymbol{N_6}$ = $x n_2$ **Eq 3-59**

$I_2 = -\omega_e^2(A_1\bar{x}_2 + A_2\bar{x}_6 - A_4\bar{x}_4)$ **Eq 3-60**

$I_3 = -\omega_e^2(A_1\bar{x}_3 - A_2\bar{x}_5)$ **Eq 3-61**

$I_4 = -\omega_e^2(I_{fx}\,\bar{x}_2 + A_4\bar{x}_2 - A_5\bar{x}_6)$ **Eq 3-62**

$I_5 = (x - s_s)I_3$ **Eq 3-63**

$I_6 = (x - s_s)I_2$ **Eq 3-64**

With

$$I_{fx} = \int_{Lx} di_x \quad \textbf{Eq 3-65}$$

$$A_1 = \int_{Lx} dm' \quad \textbf{Eq 3-66}$$

$$A_2 = \int_{Lx} (x - x_g) dm' \quad \textbf{Eq 3-67}$$

$$A_4 = \int_{Lx} (z - z_g) dm' \quad \textbf{Eq 3-68}$$

$$A_5 = \int_{Lx} (x - x_g)(z - z_g) dm' \quad \textbf{Eq 3-69}$$

Where $\boldsymbol{m'}$ is the sectional mass distribution along the ship length; $\boldsymbol{x_s}$ is the longitudinal coordinate of the section; $\boldsymbol{i_x}$ is the sectional mass moment of inertia about $\boldsymbol{x}$- axis; and $\boldsymbol{L_x}$ is the length between ***Xc;*** and the forward perpendicular of the ship

.

3.15 The Design Loads Analysis

The calculation of the design loads in MAESTRO-Wave is done using the Extreme Load Analysis (ELA) module which allows for the hydrodynamic analysis to be performed using the wave load data obtained from the numerically predicted wave-induced load responses (MAESTRO, 2012). The process involves the use of wave scatter diagram which gives the probability that the significant wave heights and their corresponding peak periods (or zero crossing periods) would not exceed certain value for a given sea state condition. The wave scatter data is used in combination with the vessel operational profile, which defines the performance of the vessel in a given sea state with respect to speed; and the wave spectrum in order to calculate the maximum loads on the hull girder structure (Liu *et al.*, 1981). The RAOs used for this calculation are those obtained from the dominant load parameters acting on the vessel. The results are then used in order to perform the short term and long term statistical analyses for the purpose of determining the most extreme design loads on the vessel.

The short term statistics is useful in calculating the wave-induced loads on the hull structure of the vessel for a given seas state. The long term statistics, on the other hand, is used to calculate the extreme loads that the vessel is expected to encounter during its life time operations. Details of the theoretical formulations for both the short term and long term analyses as applicable in the calculations of extreme design loads on a vessel can be found in these references: (Liu *et al.*, 1981; Ochi, 1981; Brown *et al.*, 1991; Heggelund *et al.*, 2002)

The North Atlantic spectrum, which follows the Rayleigh distribution, was used to obtain a probability density function of the maximum and minimum values of the waves and the responses. The equation for the response is given as follows:

$$S(\omega) = \frac{\alpha g^2}{\omega^5} \exp\left[-\beta \left(\frac{g}{U\omega} \right)^4 \right] \qquad \textbf{Eq 3-57}$$

Where: α and β are non-dimensional parameters defining the spectrum given as

$\alpha = 8.1 \text{ X } 10^{-3}$

$\beta = 0.74$

ω= wave frequency, (rad/secs)

U is the wind speed at standard height of 19.5m (m/s)

g is the acceleration due to gravity, 9.81m/s^2

With this function, the probabilities of exceeding threshold values by the ship motions were calculated. The probable design extreme value of wave amplitudes in N waves is given as:

$$A = \left(2m_0 \log \frac{N}{0.01} \right)^{\frac{1}{2}} \qquad \textbf{Eq 3-58}$$

Where:

$\mathbf{m_o}$ is the root mean square moment

N number of wave cycles

The design extreme value of the wave induced loads is given as:

$$Design = \sqrt{\left(\frac{E}{2} \log \frac{N}{0.01} \right)} \qquad \textbf{Eq 3-59}$$

Where: E is the significant wave amplitude.

The long term extreme loads for the DVC hull structure will be predicted based on the methodology described above later in Chapter Seven. The total bending moment values (Stillwater plus wave-induced bending moment) with different return period will be predicted by both the numerical method and the rule based calculations in Chapter Seven.

3.16 Summary

In this Chapter, following a brief review of the two computer codes used in this study, which are MAESTRO-Wave and PRECAL, the theoretical background behind the former code is presented in more details.

MAESTRO-Wave is used to predict the ship motions, hydrodynamic pressure distributions over the ship hull and wave-induced loads for the vessel with a steady forward speed. The program is based on the 3D zero-speed Green function with a forward speed correction in the frequency domain. The 3D panel method is implemented by using quadrilateral panels which has a constant source strength applied to each panel.

The chapter presents the basic assumptions and descriptions of the general motions and velocity potential problems to formulate the hydrodynamic pressures and then to solve the 6 DOF ship motions. The free-surface and hull boundary conditions are linearised and total velocity potential is formulated by a summation of the double-body potential for the steady flow, the incoming wave, the diffracted wave and radiated wave potentials. This is followed by the review of the formulations for the total hydrodynamic, hydrostatic and inertial forces to predict the total wave-induced loads on a cross-section of the vessel.

The chapter finalizes with a brief review of the theory behind the extreme design loads prediction using the linear wave-induced loads previously described.

Chapter 4

Experimental Studies

4.1 Introduction

This chapter presents and discusses the experimental procedures that were followed in the measurements of the motions and wave loads on both the rigid and the segmented scaled models of "The Princess Royal" research vessel. The focus of the experiments was to measure the wave-induced forces on the cross-deck structure of the model for the purpose of developing loading monograph required for performing strength assessments.

Section 4.2 describes the experimental facilities that were used in the study. This comprised of various motions and wave load measuring devices, the towing tank and the models. A description of the experimental set-up and of the tests matrices for the rigid and segmented models, in both the zero and forward speed conditions, is presented in Section 4.3. Section 4.4 presents a description of the testing procedures for the measurement of the motions and of the wave-induced loads for both the zero and forward speed conditions and for both the rigid and the segmented models. The method used in processing the model tests data is presented in Section 4.5. This section also presents the analysis of the effect of the demi-hull wave interference for the purpose of interpretation of the test results. Section 4.5 presents the results that were obtained from the experimental studies and their discussions, whilst Section 4.6 presents the conclusions obtained from the discussion of the results.

4.2 The Experimental Test Facilities

4.2.1 The Towing Tank

The experiments to measure the motion responses and wave-induced loads on the model of the RV Princess Royal were carried out at the Newcastle University's towing tank. The tank has dimensions of 37m in effective length, a width of 3.7m and 1.25m in depth (water depth). Incidence waves were generated by a displacement-type wave maker which had been designed and installed by the Edinburgh Designs Ltd. The wave maker is located at far end of the tank and the resulting waves are then absorbed after travelling the length of the tank, by vertical wedge-type beaches located at the opposite end of the tank.

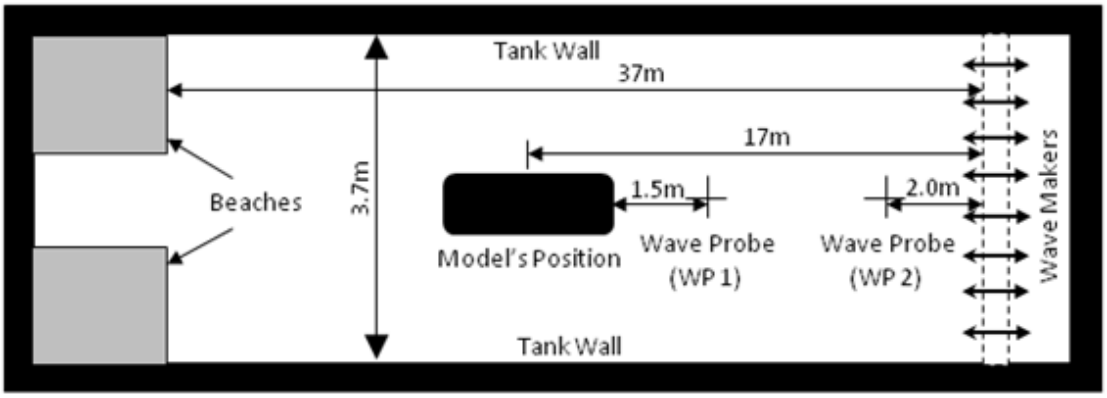

Figure 4.1: MAST Towing Tank testing facilities showing the moored position of the model for the zero speed tests

4.2.2 Motions and Wave Loads Measuring Devices

The wave maker is capable of generating a wide range of both regular waves and long crested irregular waves that can have various described spectra, including the JONSWAP spectrum. The wave heights were measured using Churchill resistance probes and the results were recorded in real time using a numerical code that was developed in-house with the aid of a LabVIEW computer program. A Visual Display Unit (VDU Monitor) was used in monitoring the physical form of the generated wave heights and of the corresponding motions responses of the model to the incidence waves. A simplified schematic diagram of the towing tank is shown in Figure 4.1. A more comprehensive recent documentation of the School of the Marine Science and Technology (MAST) Hydrodynamic Towing Tank testing facilities including the wave tank and the motion measurement devices can be found in (Atlar, 2011)

The measurement of the responses allowing for the six degree of freedom, 6 DOF, motions and of the wave-induced loads on the model of the Princess Royal vessel were measured using a combination of the Qualisys Motions Capture System, Churchill wave probes, Load

cells and a Gifford dynamometer. The measured responses in the 6 DOF are the Surge, Sway, Heave, Roll, Pitch and Yaw responses, whilst the corresponding forces and moments that were measured were the **Fx** (Longitudinal force), **Fy** (Side Force), **Fz** (Vertical Force), **Mx** (Prying Moment) – the induced moment resulting from the rotational effect of loads on the cross-deck structure along the x-axis. This moment induces stresses on the demi-hulls as a result of the rotational effects from the cross-deck structure, **My** (Pitch Connecting Moment) – the induced moment due to the rotation of loads along the longitudinal axis of the cross-deck structure that could cause the individual demi-hull to fail by moving relative to the other and **Mz** (Yaw Splitting Moment) – the induced moment due to the rotation of loads resulting from the cross-deck structures on the individual demi-hull along the yaw-axis (vertical plane) of the cross-deck structure.

4.2.2.1 The QUALISYS Motions Capture System

The QUALISYS Motions Capture System (Qualisys, 2010) is an advanced infrared camera based system whose components is comprised of two sets of high speed optical motion sensors, a monitoring device and an assembly of four tracker balls (Markers). The components are strategically attached to the vessel by a specially constructed plate whose centre of area is positioned coincide with the centre of gravity of the vessel (that is the centreline of the cross-deck structure in the case of the rigid body model tests, or on the centre of gravity of each of the demi-hulls in the case of the segmented model tests). The optical tracker calculates the instantaneous motions of the vessel based on the relative movements of the markers and transfers the results of the 6 DOF motions in a real-time situation with near zero measurement delay time, to the connecting terminal for recording.

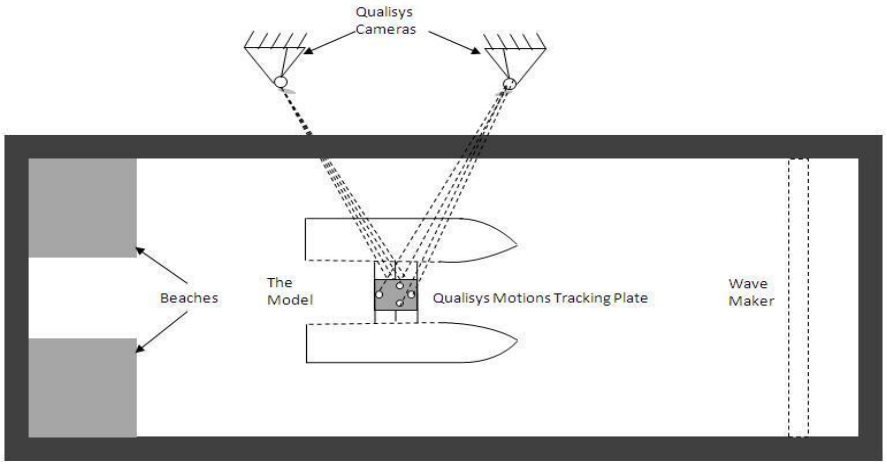

Figure 4.2: Schematic diagram of the Qualisys System set-up on the cross-deck structure at the centerline for the rigid body model motions response measurements

These measurements are achieved based on the relative translational and rotational movements that are induced by the effects of the incoming waves, as generated by the wave maker, on the model. The readings for the experiments were taken and recorded using the LabVIEW program for a continuous period of 30seconds for each test and at a data rate of 200 samples per second. Schematic diagrams showing the locations of the optical tracking markers on the rigid model and on the segmented model that is fitted with two sets of the optical tracking markers are presented in Figure 4.2 and Figure 4.3 respectively.

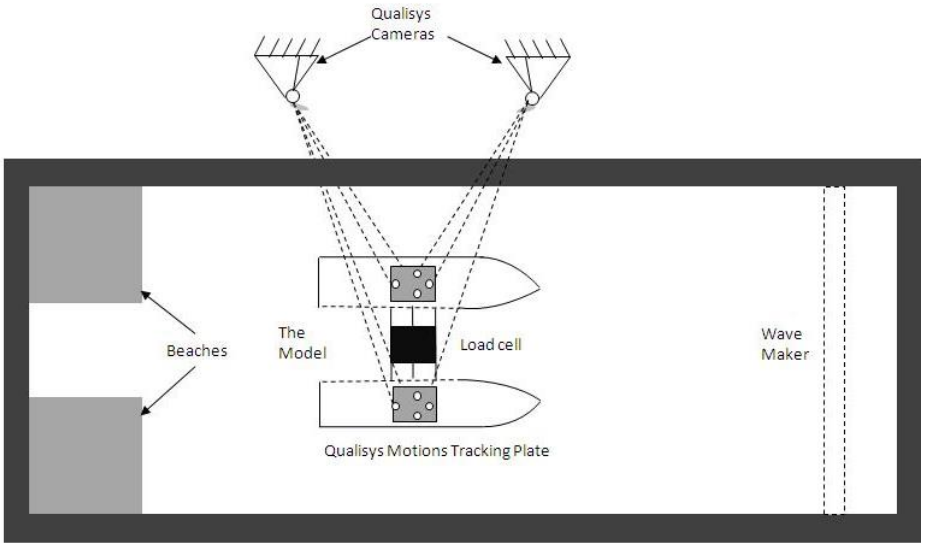

Figure 4.3: Schematic diagram of the Qualisys System set-up for the motions response measurements on the individual demi-hulls of the segmented model

4.2.2.2 Load Cell

The load cell that was used in this experiment was a 5-component force transducer, type 206/5c, manufactured by the Danish Hydraulic Institute (DHI), Denmark, as shown on in Figure 4.4. It consists of four vertical specially shaped and gauged struts connected by stiff plates at each end of the struts.

The load cell was positioned at the centre of gravity (COG) position of the segmented model at 0.637m from the AP towards the forward perpendicular (FP). This coincides with the intersection of the longitudinal and vertical centres of gravity of the overall model at the centreline of the vessel corresponding thus to the middle of the cross-deck structure as illustrated in Figure 4.3. Readings from the gauge were obtained through the output terminals connected to a visual display unit processed using a LabVIEW program.

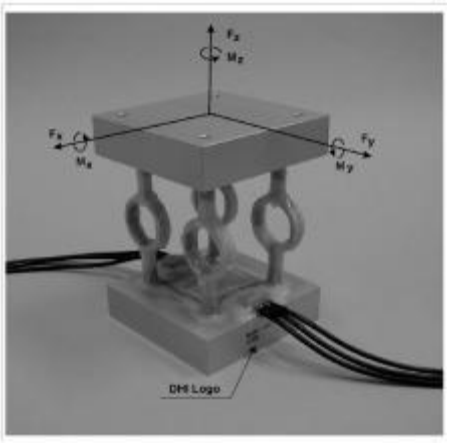

Figure 4.4: DHI Type 206/6c Load Cell

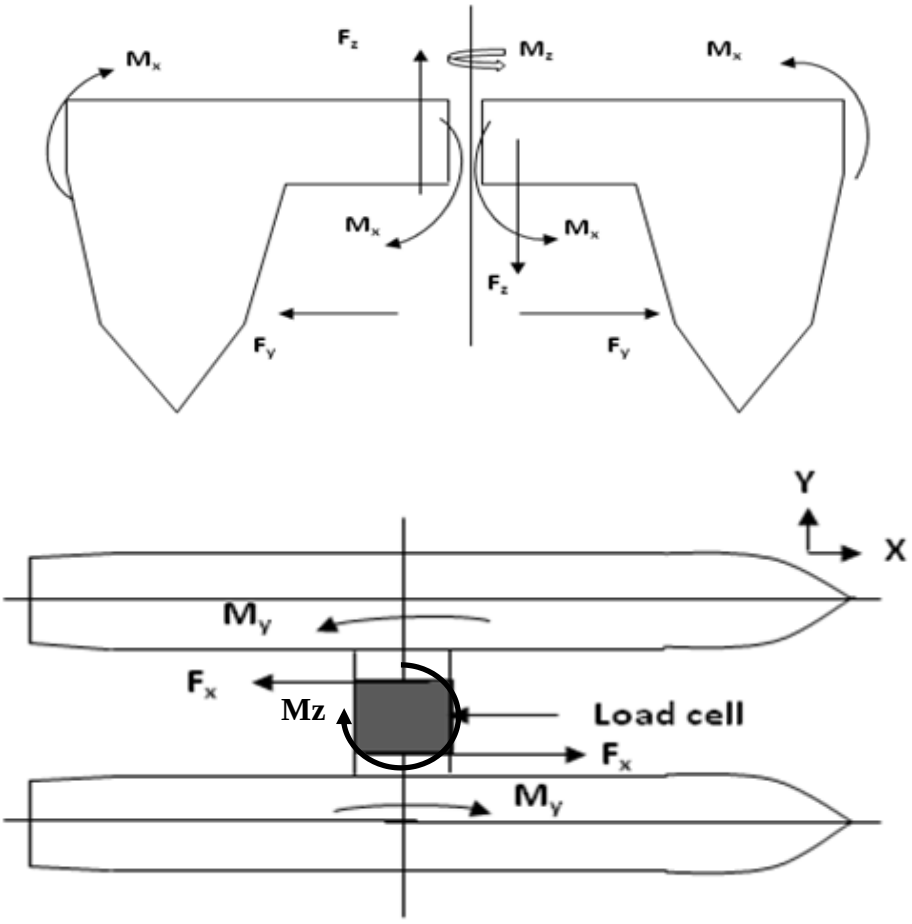

Figure 4.5: Representation of the wave-induced forces and moments acting on the model

The load cell had been calibrated to measure the forces that are caused due to incident waves on the model as they occur at the installed position. These forces and moments are comprised of Fx (Longitudinal force), Fy (Side Force), Fz (Vertical Force), Mx (Prying Moment), My (Pitch Connecting Moment) and Mz (Yaw Splitting Moment), corresponding to the resolution of the measured strains induced on the gauges due to the effect of the waves on the model as

illustrated in Figure 4.5. The rated capacity of this gauge is given in the following specification:

i. The force capacity: $F_x = F_y = F_z = 350N$

ii. The moment capacity: $M_x = 125Nm$; $M_z = 50Nm$ & $M_y = 0Nm$,

Hence the reason it is called the '5-axis' gauge.

4.2.2.3 The Towing Carriage

The towing carriage used for the forward speed tests, is fitted with the Gifford Dynamometer, which is mounted on a monorail carriage to measure the forces developed on the model. The nominal top speed of monorail carriage together with the Gifford Dynamometer attached is 3 m/s and it can be adjusted in order to suit the required corresponding Froude number due to encountered waves of up to a top speed of 4.0m/s for small size models.

The Dynamometer was connected to the model (rigid and segmented)using a towing post that consists of strain gauges that are capable of measuring up to a 50N model towing force. The towing carriage, as used in these experiments, was mainly used for the overall motions response and the wave-induced loads measurements due to encountered waves on the model, which will be either rigid body or the segmented body, with a given forward speed and in two vessel heading orientations. The vessel's orientations considered in these experiments were the full Head Seas (180^O) and the Following Seas (0^O). The model's motions response was only measured in two of the possible six degrees of freedom; these were for the heave and the pitch motions. For full head seas and the following seas the vessel's motions to Sway, Roll and Yaw were restricted while the effect of Surge motion was neglected due to slender hulls. **Figure 4.6** shows the model fitted with the Gifford dynamometer in the towing position and at the tank's 'dock' station.

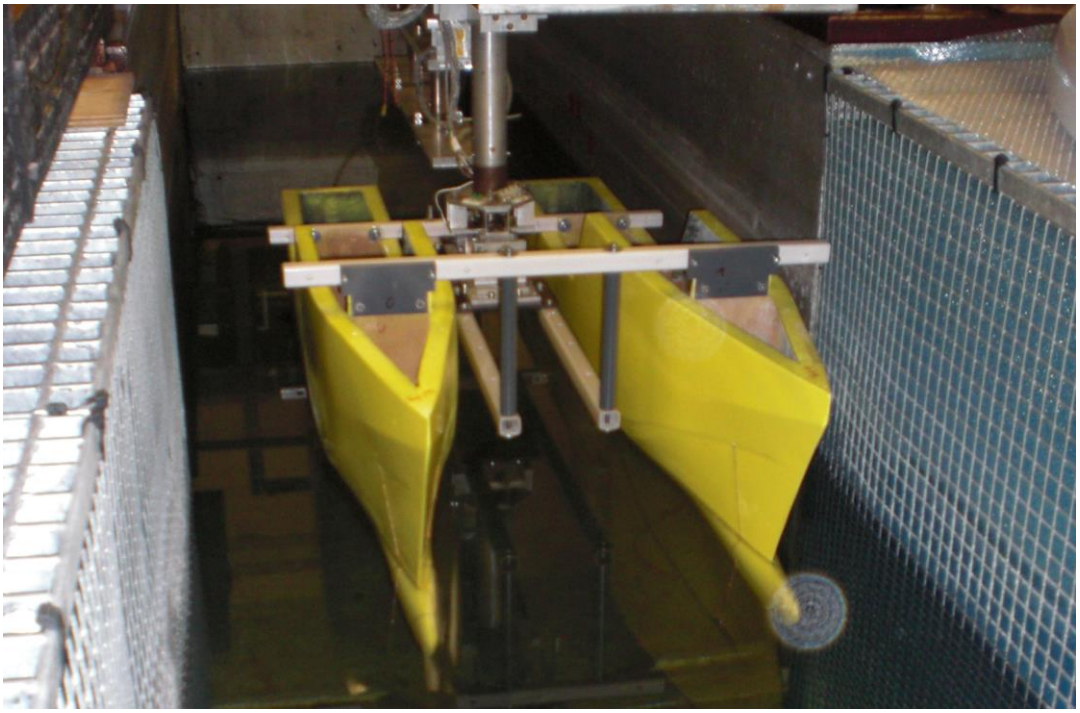

Figure 4.6: Towing carriage assembly showing the rigid body model in the 'dock' station connected to the towing post

The results from each of the experiments, repeated on both models, were obtained from the outputs of the Dynamometer recorded and processed through a LabVIEW program that was connected to the towing carriage assembly. The towing systems only allows for the measurements of the heave and pitch motions of the vessel in addition to the resistance and side forces for starboard and portsides of the model in the forward speed conditions.

4.2.3 The Model Description

As stated earlier, the basic model that was used for this experiment is a prototype of Newcastle University's new research vessel, the RV Princess Royal with slight difference in the details of the bulb. It consists of two demi-hulls which were constructed using 3mm thick Glass Fibre Reinforced Plastic (GRP) plate and a cross deck-structures. Each of the demi-hulls has a length overall (LOA) of 1.500m and a Beam (B) of 0.167m. Table 4.1 presents the particulars of both the model and of the prototype vessel.

The design of the final vessel is the product of a programme of continuous in-house research on the development of a hydrodynamically efficient hull form for a high speed craft (Atlar *et al.*, 2010). The ratio of the model to the prototype vessel is λ=12, and which was, in part, determined by the dimensions of the towing tank and on other relevant testing equipment as required by ITTC (2010).

Table 4.1: Particulars of both the basic model and the prototype vessel.

Particulars	**Units**	**Research Vessel (Full Scale)**	**Model (1:12)**
Length Overall (LOA)	m	18.8	1.5700
Beam (Demi-hull)	m	2.004	0.167
Beam Overall (B)	m	7.34	0.612
Draught Amidships (T)	m	1.748	0.146
Displacement	Tonne	36.707	0.0212
Max Speed	Kn	20.0	3.00*
Cruising Speed	Kn	15.0	1.373*
Block coefficient (C_b)	m	0.333	0.333
LCG location from AP	m	7.764	0.647
LCF location from AP	m	7.084	0.590
Izz		0.35LOA	

*Speed in m/s

In the segmented model tests, the demi-hulls were separated apart by two hollow cross-deck rectangle box sections and connected at the centreline by the load cell, as described earlier, with a fore and aft length equal to 0.284m. This dimension thus represents the length of the cross-deck structure. The model arrangement for the rigid body version is slightly different from the segmented model that the cross-deck structure is represented hollow rectangular sections connecting the two demi-hulls. However, the rigid model was only used to measure the two motions responses of the model, hence wave-induced loads measurement were not possible due the arrangement. Hence the repeated tests with the segmented model were used to determine these.

4.3 Description of the Model Set-up and Tests Matrix

Prior to commencing the model tests, the self-weight of the model was measured in order to determine the necessary contribution to its overall weight of ballasting. The total masses needed for the ballasting of the model to reach the required draught were obtained from the stability calculations of the prototype vessel and taken to be in the load departure condition.

Using one of the small tanks that is dedicated for model ballasting in the hydrodynamic laboratory, the model was thus ballasted using some scaled masses in order to represent the vessel's required displacement condition (load departure condition). Once the ballasting was completed, the masses were securely held in position and the model was transferred to the main towing tank for subsequent testing.

4.3.1 Model Set-up for the Zero Speed Tests

The model set-up for the zero speed experiments was prepared according to the procedure followed by (Korkut *et al.*, 2004). The set-up for both the rigid and the segmented models are similar due to the fact that their test matrix is the same. However, the only difference between individual model set-up can be attributed to the fact that only the model response due to the wave-induced motions was measured in the rigid body set of experiments as different to the both the motions and the wave-induced loads being measured on the segmented model set of tests. Again in both sets of tests the same wave conditions were applied.

Generally, in the zero speed experiments, the models were held at the centre of the tank using four sets of nylon lines each individually connected to a low stiffness tension spring and which were used as the mooring lines. The lines were connected to the stern and bow ends of each demi-hull and to the ends of four vertical columns. These columns were fastened to the walls of the towing tank in order for them to serve as the fixed end connecting points for the mooring lines. The low tension springs, which played a vital role in keeping the model on station, and were held in the required orientations relative to the incoming waves, were attached as an interface between the mooring lines and the columns. The flexible springs thus allowed the model to achieve a small degree of movement but sufficiently small that allows for an accurate prediction of the body motions to be made.

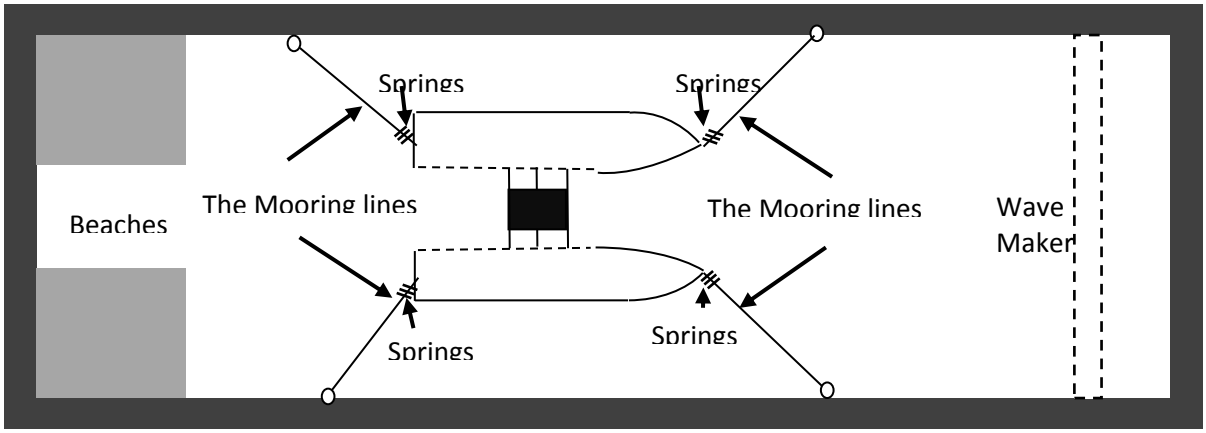

Figure 4.7: Schematic of the mooring arrangement of the segmentedfor the model in zero speed tests head seas position

Nevertheless, at certain range of frequencies and wavelengths the springs tended to prevent excessive relatively large movements due to the effects of the forces generated by the waves. The effect of this restraining movement was neglected since there was no realistic way of preventing it without removing the mooring lines which could thus allow the model to move freely in the tank both in drifting and changing its orientation.

Two wave probes were used for measuring the wave heights as well as in ensuring the accuracy of the planned incidence waves to be generated by the wave makers and experienced by the model. The wave probes were positioned further towards the location of the wave maker. One of them was placed at a position approximately 1.5m away from the model and the other at about 2m from the front of the wave maker.

4.3.2 The Zero Speed Tests Matrix

The heading conditions that were tested during the zero speed experiments were the Head Seas (180^o), Following Seas (0^o), Beam Seas (90^o), Stern Quartering Seas (45^o) and the Bow Quartering Seas (135^o). These orientations are summarised in Table 4.2.

Table 4.2: Vessel heading (orientations) conditions

S/N	Heading	Angle (^{o})
1	Head Seas	180
2	Bow Quartering	135
3	Beam Seas	90
4	Stern Quartering	45
5	Following Seas	0

For this study, there were a total of 220 runs of individual tests per model and that comprised of 11 wave frequencies x 4 wave heights x 5 vessel heading orientations and which were performed in full on each of the two models (rigid and segmented bodies). Details of the tests that were carried out are presented in Table 4.3. For each set of these runs, 3 sets of results were recorded at an interval of 30seconds.

Table 4.3: Zero speed tests incidence waves matrix

	Model scale	**Full scale**
Wave Amplitude	10mm	0.120m
	20mm	0.240m
	30mm	0.360m
	40mm	0.480m
Wave Frequency	0.5Hz	1.00 rad/s
	0.6 Hz	1.17 rad/s
	0.7 Hz	1.74 rad/s
	0.8 Hz	2.32 rad/s
	0.9 Hz	3.49 rad/s
	1.0Hz	1.00 rad/s
	1.1 Hz	1.17 rad/s
	1.2 Hz	1.74 rad/s
	1.3 Hz	2.32 rad/s
	1.4 Hz	2.32 rad/s
	1.5 Hz	3.49 rad/s
No of Runs per model	220 runs (= 4 Amplitudes x 11 Frequencies x 5 Headings)	

4.3.3 Model Set-up for the Forward Speed Tests

In the forward speed experiments, the model was set-up in a slightly different fashion than for the moored rigid and segmented body's model testing activities. The rigid body set up was purely intended to measure the overall motions response in head and following seas only, that is, no provision was made to determine cross-deck forces. In this set-up, the two demi hulls were rigidly connected to each other using the same rectangular hollow section that was previously used as a connecting beam, representing the cross deck structure in the zero speed

measurement. The towing post was connected to the model at the centreline position of the intersection between the model's longitudinal and vertical centres of gravity. The motions response measurement was carried out using the existing devices on the dynamometer.

However, since the segmented model tests involved the measurement of the wave-induced loads in the cross-structure in addition to the overall motions response, the model set up in these tests required the fabrication of a special structure which represents the complete cross-structure that can allow motions response measures at the same time as the wave-induced loads. This special structure, although it was needed in order to rigidly connect the demi-hulls, it restricted the use of the existing motions response measuring device on the dynamometer, hence there was the need for the installations of a new mounting concept for the device.

The two demi-hulls were connected at the position of their respective centre of gravity by a specially fabricated beam which allowed for the placement of the load cell in the middle of the beam as well as serving as a connection terminal for the towing post. The load cell was included as part of the connecting beam using the fabricated structure and it was positioned at the vessel's centre of gravity. The towing of the model was done, as normally, with the fixed monorail and at the desired Froude number. Two sets of accelerometers were fitted on each of the demi-hulls in order to measure the vessel's accelerations, and which were later used in calculating the wave-induced heave and pitch motions. These accelerometers were common to both models

4.3.4 The Forward Speed Tests Matrix

The forward speed tests involved the testing of the model at different forward speeds in regular waves and with two heading conditions, namely the head seas (180^o) and the Following Seas (0^o) conditions. These orientations are summarised in Table 4.4 along with the wave amplitudes and the frequencies.

In determining the parameters of the incidence wave to be generated for these test conditions, the encountered wave frequency ($\boldsymbol{\omega_e}$) was calculated based on the following equations and which takes into account the wave frequency ($\boldsymbol{\omega}$) in Hz, the model speed ($\mathbf{U_x}$) in m/s, and the heading of the vessel (μ) relative to direction of propagation of the waves, in degrees.

$$\omega_e = \omega_o - \frac{\omega_o^2}{g} U_x \cos\mu \qquad \textbf{Eqn 4.1}$$

The dynamic speed of the model was scaled using the Froude scaling laws as shown in **Eqn 4.2** below in which V_m represents the model speed while V_s is the vessel speed at full scale condition. The scale factor is λ.

$$V_s = \sqrt{\lambda}.V_m \qquad \textbf{Eqn 4.2}$$

The procedure adopted for collecting the results from these tests condition was similar to that used in the zero speed condition. The model tests data were obtained from the LabVIEW program which was recorded for a period of 10 seconds at data rate of 100 samples per second. The programs only measured the heave and pitch motions of the vessel in addition to the resistance (drag) and side forces for starboard and port sides of the model.

Table 4.4: Forward speed condition tests matrix

	Model scale		**Full scale**
	Head seas	**Following seas**	
Wave Amplitude	10mm	10mm	0.480m
	20mm	-	0.480m
Wave Frequency	0.5Hz	0.5Hz	1.00 rad/s
	0.7 Hz	0.7 Hz	1.17 rad/s
	1.0 Hz	1.0 Hz	1.74 rad/s
	1.3 Hz	1.3 Hz	2.32 rad/s
	1.5 Hz	1.5 Hz	3.49 rad/s
Speed	0.742 & 2.226m/s	0.742m/s	5kn & 15kn
No of Runs per model	20 runs (= 2 Amplitudes x 5 Frequencies x 2 Headings)		

4.4 The Experimental Test Procedures

All of the experimental measurements were carried out in regular wave conditions. In the zero speed tests, the model was held in position, according to the specific vessel heading being tested, by the mooring lines as described earlier. The towed forward speeds tests were performed using the Gifford dynamometer as explained before. Further descriptions of the test programme are given in the following sections. The motions responses were measured along with the corresponding set of wave loads on the particular model and directly related to the test wave conditions.

Figure 4.8: Rigid model in position during zero speed motions response measurements

4.4.1 The Zero Speed Tests Procedures

The experiments for the zero speed conditions were carried out at the middle of the length of the towing tank. The model was held in position by using the mooring lines that were described earlier in Section 4.3.1. The water level in the towing tank ranged between the depths of 0.85m - 0.90m.

The waves were generated by the piston displacement paddle type wave maker which is located at the rear end of the tank and they were being absorbed, to avoid reflection, by wedge type wave absorbing beaches which are located at the far end of the tank as illustrated in Figure 4.1 and Figure 4.3.

The generated wave heights were measured using Churchill resistance probes and the output results were recorded through a LabVIEW program that was developed in-house. A Visual Display Unit (VDU Monitor) was used for simultaneously monitoring the generated wave heights and the motions response of the model. When a steady wave system had been generated, the resulting 6 DOF motions of the models were measured using a Qualisys Motion Capture System (Qualisys, 2010). Using the high speed motion sensors and the four tracker balls (Markers) located on the model, the motions of the model are recorded.

In order to avoid the occurrence and subsequent spurious measurement of results in the presence of any reflected waves and residual decaying, a waiting period between the respective tests of 15mins - 30mins (depending on the wave amplitude and frequency) was allowed.

Table 4.5: 6 DOF motions and wave-induced loads measured on the cross-deck structure of segmented model.

DOF	Motion	Wave Load
1	Surge	F_x (Longitudinal Force)
2	Sway	F_y (Side Force)
3	Heave	F_z (Vertical Force)
4	Roll	M_x (Prying Moment)
5	Pitch	M_y (Pitch Connecting Moment)
6	Yaw	M_z (Yaw Splitting Moment)

As described earlier in the segmented model, the wave-induced loads were measured using the load cell attached to the cross-deck in the model. The components of the wave loads that were measured were the longitudinal, side and vertical forces along with the prying and yaw splitting moments on the cross-deck structure. Table presents a summary of motions and wave loads that were measured. The system transmits the motion responses of the vessel, based on the movements of the markers calculated in real-time to the VDU. Data from the model tests was collected, using the LabVIEW program, for a recoding elapsed time period, for each test, of 120seconds and at a rate of 200 samples per second.

4.4.2 The Forward Speed Tests Procedures

The model tests for the forward speed conditions were carried out using the Gifford Dynamometer, which was mounted on the monorail towing carriage. The speed of the towing carriage was adjusted in order to reflect the required Froude number based on the full size vessel speed.

All of the experiments were carried out in a regular wave conditions. Incidence waves were generated by the waver maker up to the wave height required for each individual test condition. The model was held in the docking station and it was only released from it once it was determined that the generated wave system had reached down to at least 75% of the length of the tank from the wave maker. This was to ensure that the measurements were correctly taken in constant wave conditions which otherwise would have been done in a reduced wave or even still water condition.

The motions response on the segmented model was measured using two accelerometers mounted on each of the demi-hulls. One of these accelerometers was positioned at centre of gravity of the demi-hull while the remaining accelerometer was placed at the tip of the bow of the demi-hull. Each accelerometer measured the vessel's vertical acceleration at its installed position, hence this arrangement allowed for the relative motions between the two devices to be used in calculating the pitch motions of the model. In addition to the pitch, the vertical component of the accelerations was used in calculating the heave motions.

The choice of this method of measurement was necessitated by the physical restrictions imposed by the presence of the load cell at the location of the vessel's centre of gravity (CoG) of the cross-deck structure of the model. The Head Seas (180^o) Condition

The wave-induced loads in the segmented model were measured using the load cell attached to the model. The position of the load cell was similar to that used in the zero speed measurements. Again, the wave-induced loads that were measured are presented in Table 4.5.

The number of runs that were undertaken, for each model, for this test condition was 40 (Table 4.4), and which comprised of 10 wave frequencies x 2 wave heights x 2 heading conditions. The forward speed heading conditions were the Head Seas (180^o) and the Following Seas (0^o). The speeds for which these models were tested are given in Table 4.4**.**

4.4.3 The Natural Frequency Tests Procedures

Experiments to measure the natural frequencies of the models in various modes in Stillwater were carried out. The purpose of these experiments was to provide a proper means of interpretation and reference of the wave-induced behaviour of the models in various degrees of freedom. The tests were carried out for the heave, pitch and roll natural frequencies of the models. The model was placed at a similar position in the tank to that used in the zero speed experiments.

In the heave natural frequency experiment, two of the mooring lines that were used for ensuring the station-keeping of the model were loosely connected alternately to the bow and stern of the respective demi-hull. The reason for this arrangement was to eliminate the potential effects of potential interference of the low stiffness tension springs that formed part of the mooring lines and at the same time to use the remaining two lines in order to prevent any unwanted movements of the model during testing.

In order to stabilise the model prior to testing, the model was manually held in position up till the time at which it was adjudged to have reached a steady motionless state. To initiate heave actions a specified amount of force was applied vertically downwards at the position of the centre of gravity of the model and then quickly removed in order to achieve the desired transient excitation level for the model. A similar procedure was adopted for the remaining test conditions namely for Pitch and Roll except that the mooring arrangements and the position of the applied exciting forces differed for each test condition.

The results obtained from these experiments were collected and recorded using the Qualisys Motion Capture System and the LabVIEW Program.

.

4.5 The Experimental Results and Discussions

4.5.1 The Natural Frequency Test Results

Several repeated sets of free decay tests, thus representing natural hydrodynamic damping, were carried out in order to determine the heave, roll and pitch natural frequencies of the model. These tests were performed using the Qualisys and was additionally validated using the Gifford dynamometer. The results obtained for the model were extrapolated based on the model scale in order to obtain the equivalent full scale ship natural frequencies and they are presented in Table 4.6.

Table 4.6: Results of the natural frequency tests for rigid (RB) and segmented (SB) models

	Heave		**Pitch**		**Roll**	
	RB	**SB**	**RB**	**SB**	**RB**	**SB**
Model Period (seconds)	0.57	0.60	0.67	0.65	0.88	0.83
Model Nat. Freq. (rad/s)	11.02	10.46	9.38	9.70	7.14	7.55
Ship Nat. Freq. (rad/s)	3.18	3.02	2.71	2.80	2.06	2.18
Non-dimensional Nat Freq. $\omega(L/g)^{1/2}$	4.32	4.10	3.73	3.71	2.83	2.96
Wavelength/Ship Length (λ/ L)	0.34	0.38	0.45	0.44	0.78	0.72

4.5.2 Demi-hull Interference (Standing wave) Phenomenon

Vessel motion responses are magnified at appropriate modes of the natural frequencies and this can be shown in theory as well as experienced in practice. Beside these frequencies, it is theoretically proven and occasionally confirmed by the model tests with twin hull vessels that there is other set of critical frequencies, which are called “interference” or “standing wave” frequencies, where the vessel motions may be affected particularly in the Beam Seas at zero speed. These frequencies may be more effective for twin-hulls like SWATHs with long vertical sided struts where the development of the standing wave can be easier. The standing waves can be formed in transverse as well as in longitudinal direction. At the corresponding frequencies of the standing waves the added mass and the damping characteristics of the vessel may have dramatic oscillations and zero values for the latter which may result in deviations of the motions responses as reported in the open literature e g (Atlar *et al.*, 1985).

The expressions for these critical frequencies can be obtained by equating the length of the standing wave (**λ**) to the clearance between the demi-hulls (**Ss**) in the transverse direction and to the waterline length of the hull (**Ls**) in the longitudinal direction by taking into account the appropriate mode of the motion (**n**) as shown below:

$$n\lambda = Ss \text{ for transverse standing wave}$$
$$n\lambda = Ls \text{ for longitudinal standing wave}$$

where: n = 1, 2, 3...for symmetric modes of motions (i.e. heave, pitch)

n = 0.5, 1.5, 2.5...for asymmetric modes of motions (sway, roll, yaw)

The phenomenon is shown in the following sketches:

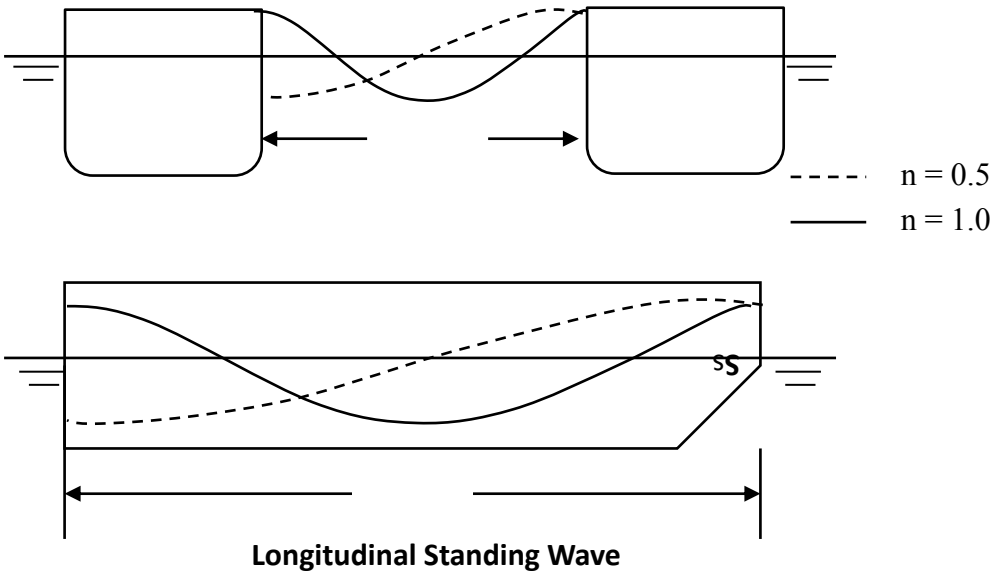

Figure 4.9: Schematic diagram illustrating the development of standing wave phenomenon

The above prediction of the standing waves is based on 2D theory which assumes infinite boundaries (of the underwater hull). In reality this is not the case for actual ships with finite boundaries and the forward speed effects will play important role to weaken the effects and development of these waves.

Based on 2D theory, the critical frequencies of these interference waves can be expressed as follows by using the wave dispersion relationship:

$\omega_T = \sqrt{n * \frac{2\pi g}{S_s}}$ Transverse standing wave frequency

$\omega_L = \sqrt{n * \frac{2\pi g}{L_s}}$ Longitudinal standing wave frequency

Based on the above formulae, the associated critical frequencies are predicted and given in Table 4.7 for the symmetric and asymmetric modes of the motions for Ss = 3.10m and Ls = 18.45m

Table 4.7: Non-dimensional (ND) critical frequencies of standing waves

		Symmetric			**Asymmetric**		
Mode	n	1.0	2.0	3.0	0.5	1.5	2.5
Transverse	$\omega_T\ (ND)$	4.46	6.31	7.72	3.15	5.46	7.05
Longitudinal	$\omega_L(ND)$	1.83	2.59	3.17	1.29	2.24	2.89

4.5.3 The Zero Speed Motions Responses Results and Discussions

The results of the motions responses at zero speed condition for the five wave heading directions that were tested are presented in Section 4.5.3.1, Section 4.5.3.2 and Section 4.5.3.3 for heave, roll and pitch motions, respectively. In each case the plots contain the results for each of the four wave amplitudes that were simulated in the tests. The y-axis of each plots represents the non-dimensional response amplitude operator, RAO, for the selected degree of freedom motions while the x-axis represents the non-dimensional wave frequency, $\omega\ (L/g)^{1/2}$. Where: ω is the angular wave frequency in radians per second (rad/s); L represents the length overall of the vessel in metres (m); while g is the acceleration due to gravity (m/s^2).

In these experiments, all of the six degrees of freedom motion responses for the rigid body (**RB)** and the (**SB)** segmented models were actually measured. However, only the results of the heave; roll and pitch motion responses are presented and discussed in this section. This is because of the more significant influence that these selected motions have on the seakeeping

behaviour of the vessel and their resulting impacts on the structural responses of the vessel to the wave-induced loads.

The results of the motion response at low frequency have been omitted from the various plots for both the rigid body (RB) and the segmented (SB) models. This was done with the sole aim of enhancing the level of confidence in the data and to fully account for the model tank limitation and other instrumentation error could possibly affect the results at such frequencies since it was not possible to estimate the uncertainty due to equipment error which could cause nonlinearity within this range at this stage.

4.5.3.1 Heave Motions Response Amplitude Operator (RAO)

The results of the measurement of the heave motion responses for the **RB** and **SB** models are presented in Figures.4.10 - 4.14 and Figures.4.15 -4.19 respectively. The peak values of the motion responses for all the degree of freedoms measured are summarised in Table 4.8.

In the **Head Seas (180^o)** for the **RB** (Figure 4.10), the trends of the plots for the constituent wave amplitudes are similar and contained three prominent "kinks" having peak magnitudes at non-dimensional frequencies of 1.76; 2.26 and 3.10 respectively. The frequency (1.76) of the first "kink" is consistent with the peak heave response while the second "kink" (frequency 2.26) indicates the physical coupling between the heave motion responses and pitch response in Head Seas.

The trends of the motion response plots for the **SB** model (Figure 4.15) in the Head Seas show a nonlinear behaviour at lower frequency range. The degree of the nonlinearity reduces as the incident wave frequency increases. At higher frequencies, the responses then became linear as the magnitudes begin to decline to zero value. A relatively modest "kink" on the plot was observed at non-dimensional frequency of 3.27. This frequency is within the range of the demi-hull interference frequencies (W_T = 3.15 and W_L = 3.17) due to the asymmetric (mode = 0.5) and symmetric mode 3 in the transverse and longitudinal directions respectively.

The plots of the heave motion response magnitudes for the **RB** and the **SB** models of the vessel show an appreciable difference in their peak magnitudes and the frequencies of occurrence of the two models. The difference is understandably due to the consequence of the rigid body stiffness. The **RB** models responds very rapidly to the motions at resonant frequencies than the segmented model; hence the flexibility offered by the **SB** model as a

result of its hydroelasticity is the one of the reasons for this reduced motion responses in the **SB** model.

The responses in the **Bow Quartering Seas (135^{o})** are presented in Figure 4.11 - for the **RB** model and Figure 4.18 –for the **SB** model respectively. The physical trend of the plots for the **RB** model is reasonably linear but with certain degree of nonlinearity at higher frequencies. The **RB** model responses plots contained two modest "kinks" at non-dimensional frequencies of 2.26 and 2.76; - the first of these "kinks" is consistent with the pitch motions response while the other "kink" occurs at the roll resonant frequency (2.83) of the model. Unlike in the **RB** model response plots, the "kink" in the responses for the **RB** model was observed at non-dimensional of 3.27.

The general trends of the heave responses for the two models (**RB** and **SB**), are somewhat similar with their response magnitudes occurring at the same frequencies but with different values. This coupling is very mild compared to those that were observed in the Head Seas condition (**180^{o}**) at the same frequency. Hydroelasticity of the models plays an important role in the variation of the magnitudes due to the differences in the models stiffness even though they all have exactly the same parameters.

The **RB** and **SB** models heave motion response plots in the **Beam Seas** (**90^{o}**) condition are presented in Figure 4.12 and Figure 4.16 respectively. The plots for the **RB** model increase linearly with increase in frequency at lower range of the frequencies. This behaviour suddenly changed when the responses approached a non-dimensional frequency of 2.75 (resonance range). This condition explains the reason for such a high value of the response magnitude in this otherwise relatively heave-insensitive degree of freedom. It is possible that the standing wave phenomenon due to the effects of demi-hulls separation is contributing to this behaviour but this assertion needs to be further investigated.

The trend of the **SB** model response plot was initially linear but it gradually became nonlinear as the frequency increases. The plots contained two distinctive "kinks" at non-dimensional wave frequencies of 2.26 and 3.01. The first of these two "kinks" suggest a dynamic amplification of the heave motion response possibly due to entrapment of waves (standing waves) between demi-hulls. The second "kink" reveals the coupling of the heave response and the roll motions response in this heading condition.

The flexibility (low stiffness) of the representative cross-deck structure of the **SB** model allows for high movement of the demi-hulls during model test. This explains presence of the phase shift between the plots of the responses for the two models.

In the **Stern Quartering Seas (45^o),** the plots for the responses are presented in Figure 4.13 and Figure 4.19 for the **RB** and **SB** models respectively. Comparison of heave motions response for the two models shows that their trends are significantly different but their magnitudes are similar. There is a clear shift in the frequencies of the peak magnitudes in the **SB** model relative to that of the **RB** model results.

The plots are essentially similar to the responses for the Bow Quartering Seas except for the distinct separation between the plots of the **RB** model responses that have been reported earlier.

The plots of the heave motion responses in the ***Following Seas (0^o)*** are presented in Figure 4.14 and Figure 4.17 for the **RB** and **SB** models respectively. The response plots for the **RB** model display a high degree of nonlinearity which increases with increase in the frequency. The physical behaviour of the response plots for the **SB** model is similar to those observed in the Head Seas. The plots show that the heave motions response is nonlinear at both ends of the frequencies. The severity of the nonlinearity reduces within the mid-range frequencies (1.57 – 2.75). The plots also contained two small "kinks" at non-dimensional frequencies of 3.27 and 3.52. These frequencies confirmed the coupling of the heave motions with the pitch resonant frequency.

A summary of the non-dimensional peak magnitudes of the heave motion response amplitudes for the rigid body **(RB)** and the segmented **(SB)** models in zero speed is presented in Table 4.8.

Table 4.8: Summary of the peak heave motions responses for the RB and the SB models

S/N	***Heading (Deg)***	***Rigid Body RAO***		***Segmented Body RAO***	
		Heave (m/m)	***$\omega(L/g)^{1/2}$)***	***Heave (m/m)***	***$\omega(L/g)^{1/2}$)***
1	Head seas (180^o)	1.30	2.26	0.87	2.01
2	Bow Quartering	0.77	2.01	0.78	1.71
3	Beam Seas	2.94	3.01	2.72	2.26
4	Stern Quartering	0.75	1.51	0.78	1.51
5	Following Seas	1.53	2.26	1.58	2.26

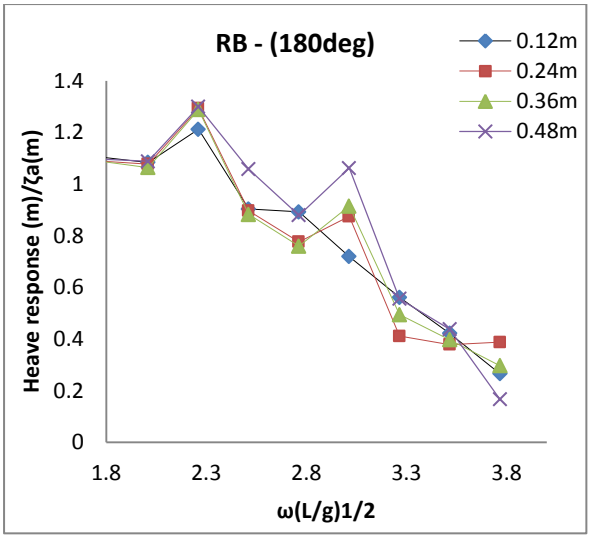

Figure 4.10: Rigid body model heave response in Head Seas (180°) at zero speed

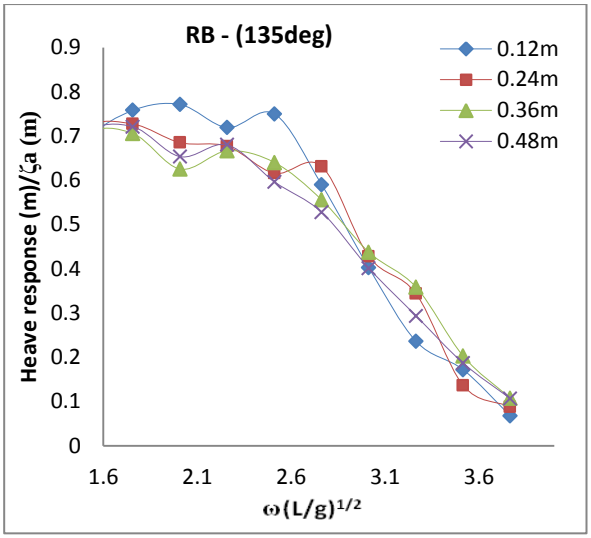

Figure 4.11: Rigid body model heave response in Bow Quartering Seas (135°) at zero speed

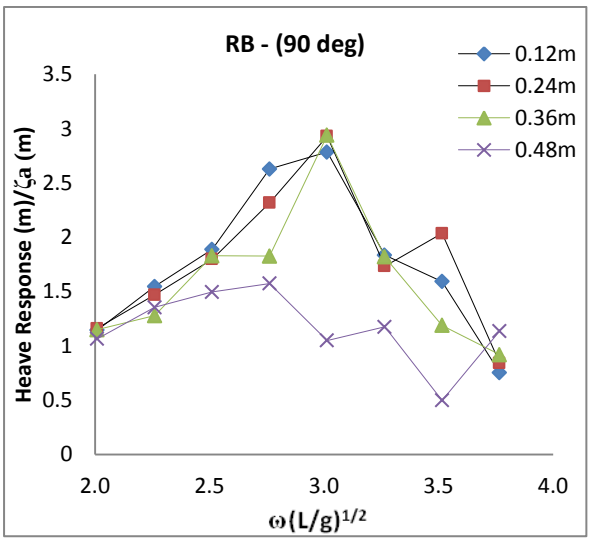

Figure 4.12: Rigid body model heave response in Beam Seas (90°) at zero speed

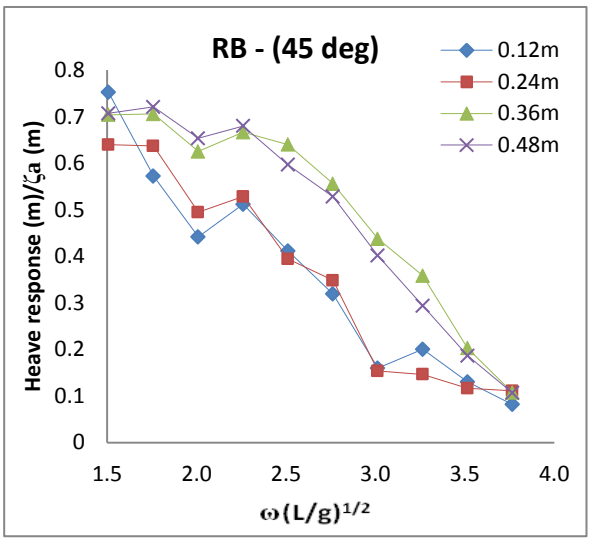

Figure 4.13: Rigid body model heave response in Stern Quartering Seas (45°) at zero speed

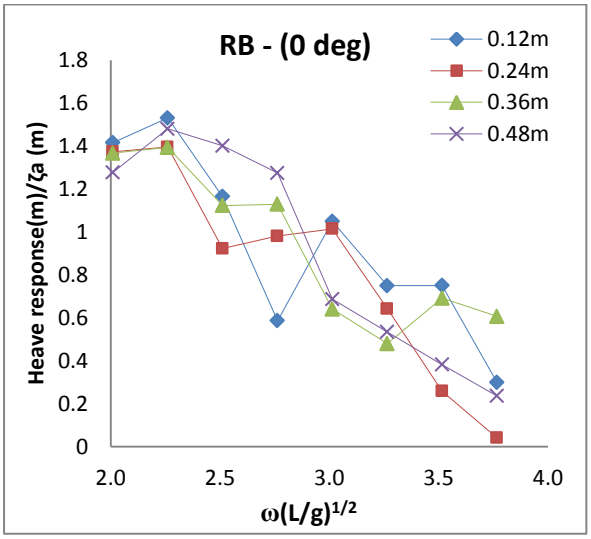

Figure 4.14: Rigid body model heave response in Following Seas (0°) at zero speed

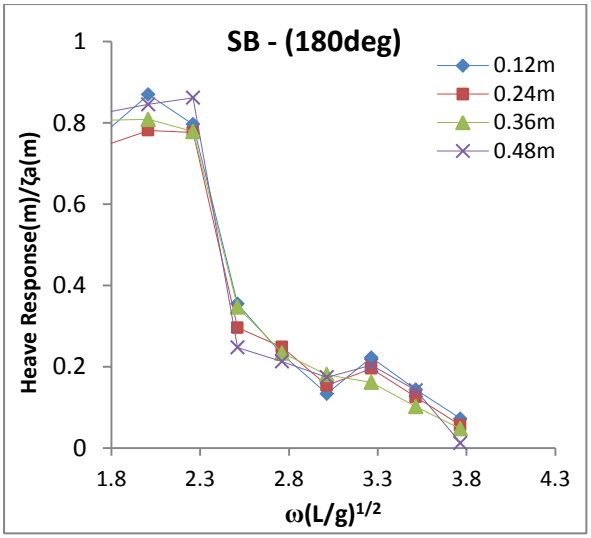

Figure 4.15: Segmented model heave response in Head Seas (180°) at zero speed

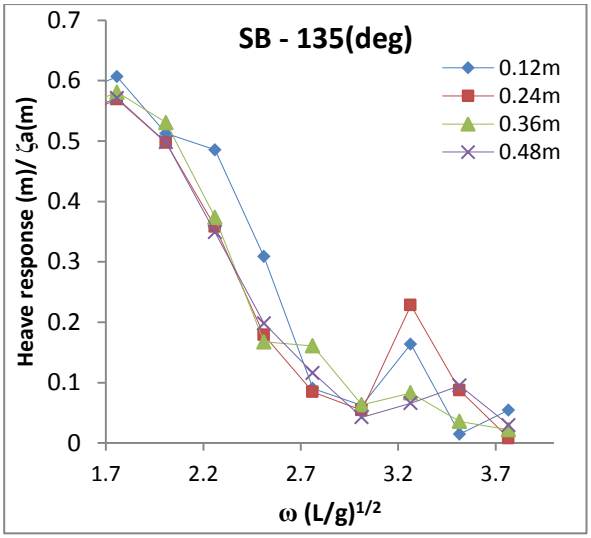

Figure 4.18: Segmented model heave response in Bow Quartering Seas (135°) at zero speed

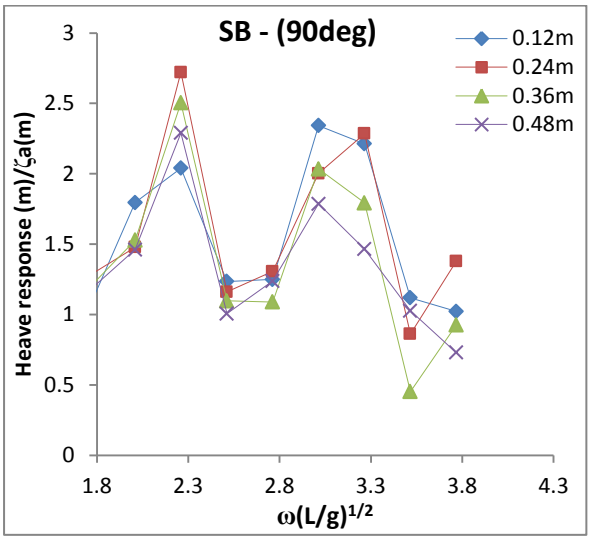

Figure 4.16: Segmented model heave response in Beam Seas (90°) at zero speed

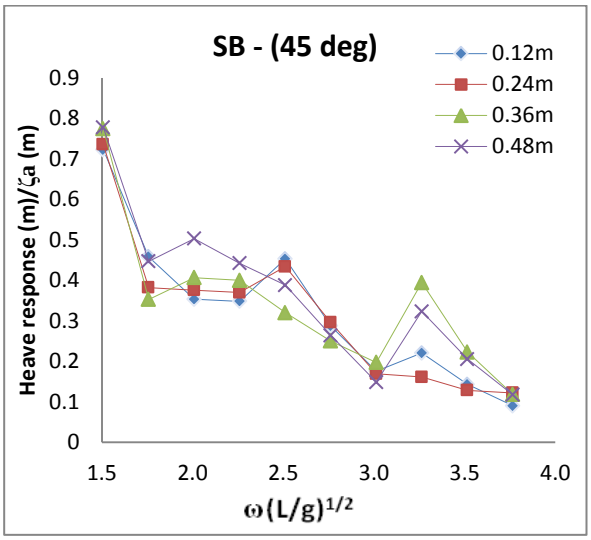

Figure 4.19: Rigid body model heave response in Stern Quartering Seas (45°) at zero speed

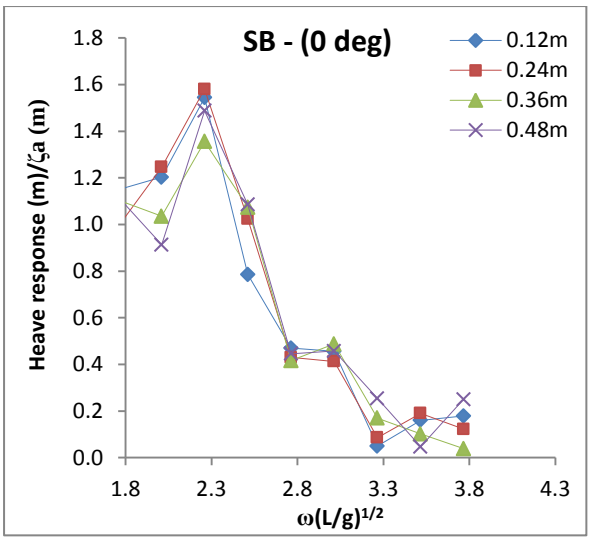

Figure 4.17: Rigid body model heave response in Following Seas (0°) at zero speed

4.5.3.2 Roll Motions Response Amplitude Operator (RAO)

The results of the roll motion responses for the **RB** and the **SB** models at zero speed for three wave heading conditions are presented in Figures 4.20, 4.22 and 4.23 for the rigid body and Figures 4.21, 4.24 and 4.25 – for the segmented model. The left side figures presents the plots of the roll responses for the **RB** model and the right side figures presents the **SB** model responses in degree per unit wave amplitude (deg/m) against a non-dimensional wave frequency ($\omega\ (L/g)^{1/2}$) The peak values of the roll motion responses for the degree of freedoms measured are summarised in Table 4.9.

The roll motion response results for the **RB** and the **SB** models in the ***Bow Quartering Seas*** (135^o) are presented in Figure 4.20 and Figure 4.21 respectively. The physical trends of these response plots are partially linear with respect to the wave amplitudes. A comparison of the plot for the responses of these models reveals a significant variation between the magnitude of the roll angles for the **RB** and the **SB** models.

The plots have their peak magnitudes at different frequencies, which may be attributed to the system of model station keeping (mooring arrangement), used in the experiment than the responses of the model in waves. The difference between the response peak magnitudes for the **RB** and the **SB** model is over 50% with the **SB** model having the highest magnitude.

In the ***Beam Seas*** (90^o)**,** the roll motions response plots are presented in Figure 4.22 and Figure 4.24 for the **RB** and the **SB** models respectively. The plots of motions response for the **RB** model initially behaves linearly with respect to the wave frequency up to its peak magnitude at non-dimensional frequency of 2.51 but then became nonlinear after this frequency. This nonlinearity occurs at higher frequency and it is located within the range of the roll resonant frequency of the model. The implication of having such a high roll angle in beam seas condition further raises the fundamental concern about its potential effects on strength of the cross-deck structure, especially its fatigue strength.

The two models recorded high peak magnitudes of roll motion response in the **SB** model in Beam Seas (**90^o**). The trend of these plots share certain similarity to the heave motion responses in the Beam Seas (**90^o**), which points to the coupling of their respective motion responses. A further comparison of the plots of these responses highlights the difficulty in relating these two plots to each other. While the plots of the motion responses for the **SB** model contained two "kinks" at non-dimensional wave frequencies of 2.26 and 3.01; the plots

of the responses for the **RB** model seem to have a relatively smooth curve with the peak magnitude of frequency occurring at 3.1. The rigidity/flexibility of the models cross-deck structure needs be taken into account when comparing the roll responses of the two models otherwise interpretation of the roll angles could give misleading severity.

The plots of the roll motion responses for the **RB** and the **SB** models in the ***Stern Quartering Seas (45^o)*** are presented in Figure 4.23 and Figure 4.25 respectively. The plots are similar in magnitude and physical trends to the responses for the Bow Quartering Seas (**135^o**). The behaviour of motion responses for this heading is generally nonlinear as their frequencies increase.

As stated earlier, these results are very much a reflection of the responses for the Bow Quartering (13**5^o**) Seas both in terms of their magnitude and physical behaviour. The physical trend of these plots is mostly linear with intermittent presence of nonlinearity.

A summary of the non-dimensional peak magnitudes for the roll motion response amplitudes for both the rigid body **(RB)** and the segmented **(SB)** models in zero speed is presented in Table 4.9.

Table 4.9: Summary of the peak responses for roll motion response amplitudes

S/N	***Heading (Deg)***	***Roll motions responses***			
		Rigid Body		***Segmented Body***	
		Roll (deg/m)	***$\omega(L/g)^{1/2}$***	***Roll (deg/m)***	***$\omega(L/g)^{1/2}$***
1	Bow Quartering	7.34	2.86	2.90	2.24
2	Beam Seas	29.3	3.01	25.5	2.26
3	Stern Quartering	8.0	2.76	6.86	2.04

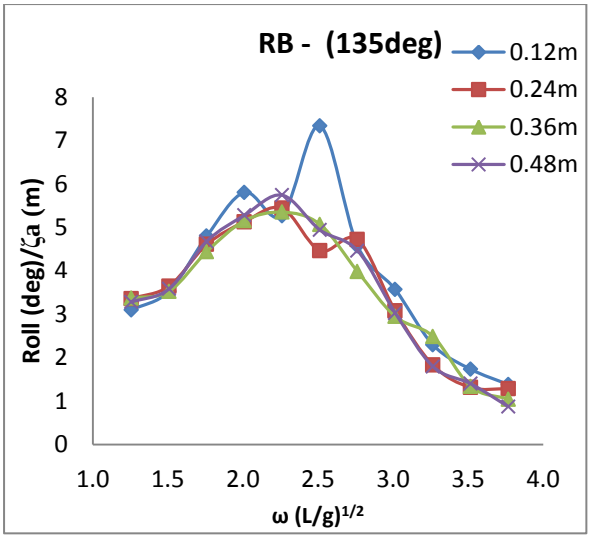

Figure 4.20: Rigid model roll motions RAO in Bow Quartering Seas (135°) at zero speed

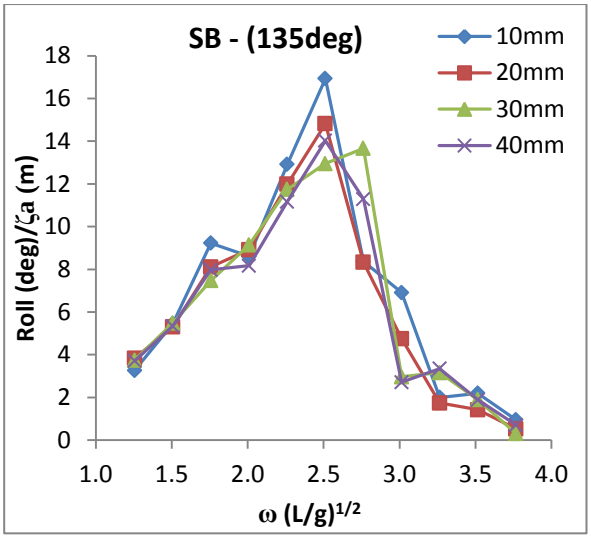

Figure 4.21: Segmented model roll motions RAO in Bow Quartering Seas (135°) at zero speed

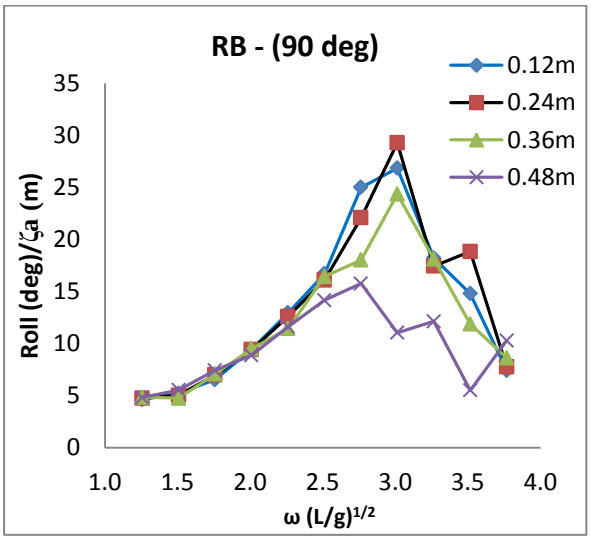

Figure 4.22: Rigid model roll motions RAO in Beam Seas (90°) at zero speed

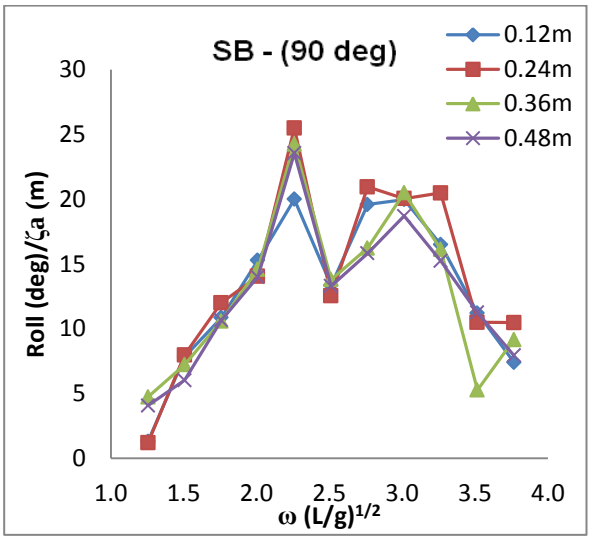

Figure 4.24: Segmented model roll motions RAO in Beam Seas (90°) at zero speed

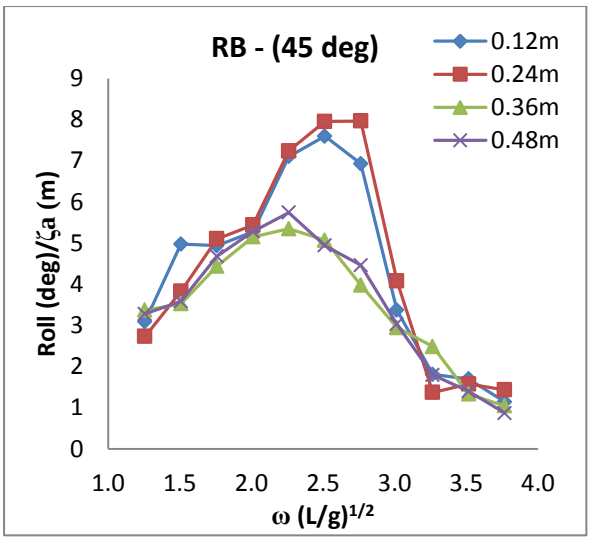

Figure 4.23: Rigid model roll motions RAO in Stern Quartering Seas (45°) at zero speed

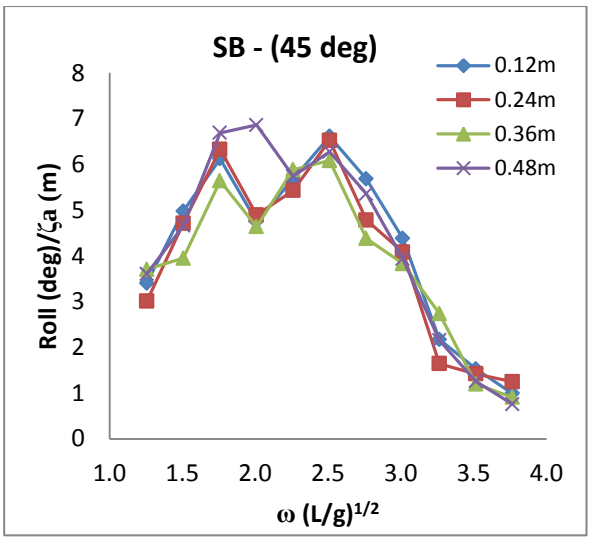

Figure 4.25: Segmented model roll motions RAO in Stern Quartering Seas (45°) at zero speed

4.5.3.3 Pitch Motions Response Amplitude Operator (RAO)

The results of the pitch motion responses for the **RB** and the **SB** models for five wave heading conditions measured are presented in Figures 4.26 – 4.30 and Figures 4.31 – 4.35 respectively. Each of these plots shows the pitch responses in degree per unit wave amplitude (deg/m) against a non-dimensional wave frequency ($\omega (L/g)^{1/2}$) The peak values of the pitch motion responses for the degree of freedoms measured are summarised in Table 4.10.

The plots for the pitch motion response for the **RB** and the **SB** models in the ***Head Seas*** (**180^o**) conditions are presented in Figure 4.26 and Figure 4.31 respectively. The pitch motion responses appear to be largely linear with respect to wave amplitudes even though some slight trace of nonlinearity were observed at non-dimensional frequency range of 2.51 - 3.77. This nonlinearity occurs well within the range of the natural pitch frequency range of the model. The physical trend for the **SB** model response plots is generally linear. This implies that the motion response amplitudes for this vessel orientation vary linearly with the wave amplitudes at given frequency.

Theoretically, the peak magnitude of the pitch motion RAO occurs at non-dimensional frequency of 2.24, which corresponds to a wavelength of 0.5L of the vessel's length. This confirms that the peaks response of the model was rightly measured at the correct frequencies.

A comparison between the magnitudes of response the plots show a significant difference between the pitch angles for the **RB** and the **SB** models. The vessel pitches more in the segmented body model and tends to over predict the responses due to the high flexibility of their cross-deck structure.

The plots of the pitch responses for the **RB** and the **SB** models in the ***Bow Quartering Seas*** **(135^o**) are presented in Figure 4.27 and Figure 4.34: Segmented model pitch motions RAO in Bow Quartering Seas (135^o) respectively**.** The trends of the responses for this heading are fairly nonlinear with some mild kinks on the plots around the natural frequencies range of the vessel. Despite the relatively linear outlook of the **RB** plots, there was no any visible sign of the coupling effect of the motion responses with other motions (roll and heave) observed. However, absence of the coupling effects of the responses with other motions is not enough a

reason to rule out the presence of nonlinearity in the results, hence the need for caution in the interpretation of this phenomenon.

The physical trend of response plots for the **SB** model is mixed because of the presence of some degree of nonlinearity at frequency range of 1.76 to 2.51. The nonlinearity is not really very strong but its occurrence within the range of the maximum recorded pitch angle means it should further be investigated.

In the ***Beam Seas (90^o),*** Figure 4.28 and Figure 4.32 for the **RB** and the **SB** models respectively, the plots are nonlinear and the nonlinearity occurs about the frequencies where coupling effects of the pitch and roll responses were observed. This scenario is similar to conditions that normally occur in parametric rolling of a vessel.

Unlike in the Head Seas condition, the plot of the pitch response for the **SB** model in this wave heading is higher than those for the **RB** model but the overall magnitudes of the responses are generally very small. The peak magnitudes of these pitch angle for the two models appeared to occur at different frequencies. The reason for such occurrence is because of the effects of nonlinearity which appears to be more severe on the segmented model than on the rigid model.

The plots for the pitch motion responses ***Stern Quartering Seas (45^o)*** for both the **RB** (Figure 4.30) and the **SB** (Figure 4.35) models are very similar to those obtained in the ***Bow Quartering Seas (135^o).*** The peak magnitude of the pitch motion responses is approximately 6.85deg/m at a non-dimensional frequency of 2.52.

A close look at these response plots highlight the similarity in both magnitude and trends behaviour, hence discussion on these results is based on the pitch angles of the constituents responses. The peak magnitude of the pitch angle for the **SB** model is measured as 3.54degrees at non-dimensional wave frequency of 2.21 while in the **RB** model; the peak magnitude is 3.24degrees at the same non-dimensional frequency of 2.21. Unlike in the Bow Quartering Seas condition, the plots of the pitch angles for the **SB** model are just slightly higher than those for the **RB** model.

In the ***Following Seas (0^o),*** the plots of the motions response for both the **RB** model (Figure 4.29) is nonlinear with respect to wave amplitude as the frequency increases while in the **SB** model (Figure 4.33), the nonlinearity reduces as the frequency increases The nonlinearity

could be attributed to the changes in the wetted surface of the vessel due to the V-shape nature of the hull geometry.

The response plots for both of these models show the variation in the trends of their magnitudes. The plot of the responses for the **SB** model in this wave heading is higher than those for the **RB** model. The hydroelasticity of the **SB** model itself contributes significantly to the nonlinearity of its responses due to the flexibility of the cross-deck structure of the model.

A summary of the peak motion response angles for the pitch motions in zero speed, stationary condition, is presented in Table 4.10.

Table 4.10: Summary of the peak responses for pitch motions response

S/N	***Heading (Deg)***	***Pitch motions response***			
		Pitch	$\omega(L/g)^{1/2}$	***Pitch (deg/m)***	$\omega(L/g)^{1/2}$
1	Head seas (180^o)	9.05	2.26	15.2	2.26
2	Bow Quartering	6.82	2.51	12.2	2.51
3	Beam Seas	2.83	3.26	2.96	3.52
4	Stern Quartering	6.85	2.51	6.86	2.51
5	Following Seas	8.11	2.26	15.0	2.52

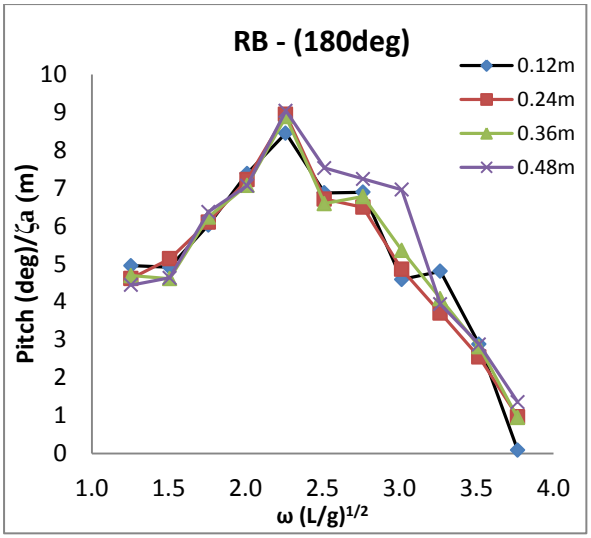

Figure 4.26: Rigid model pitch motions RAO in Head Seas (180°) at zero speed

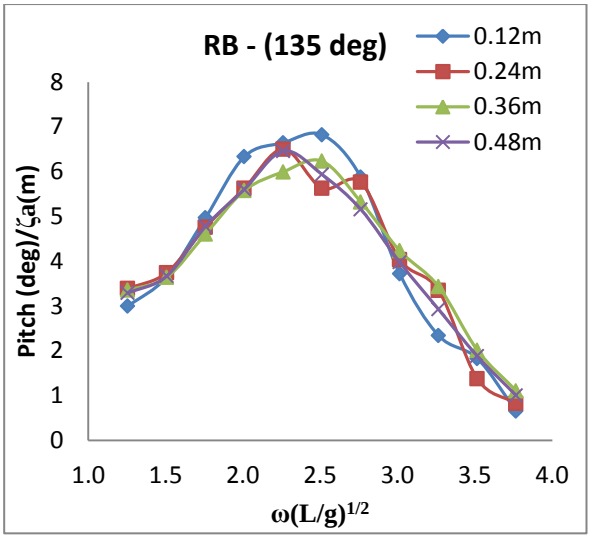

Figure 4.27: Rigid model pitch motions RAO in Bow Quartering Seas (135°) at zero speed

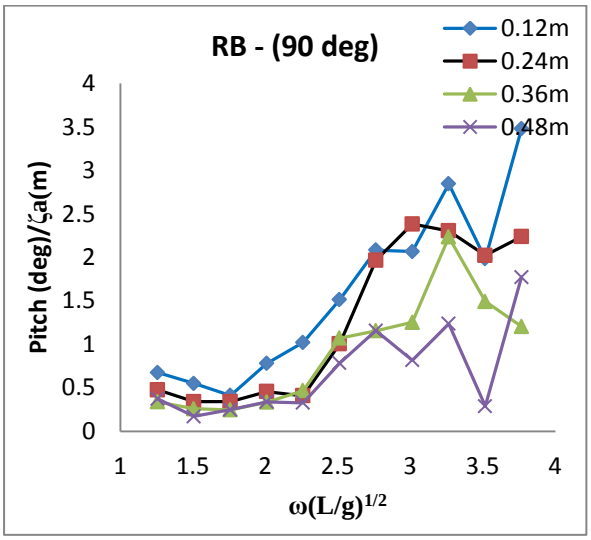

Figure 4.28: Rigid model pitch motions RAO in Beam Seas (90°) at zero speed

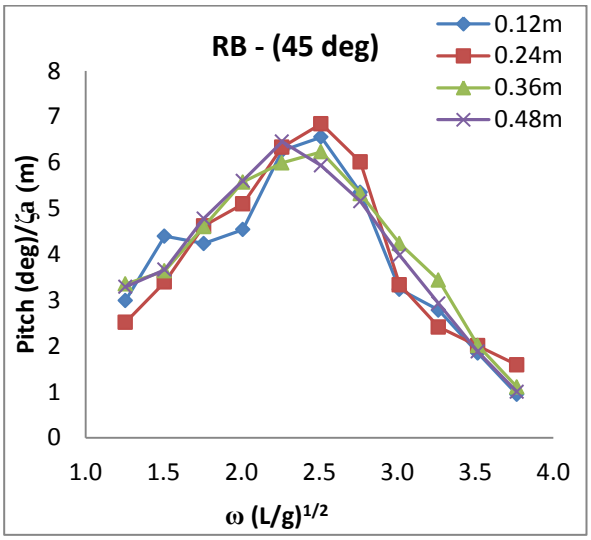

Figure 4.30: Rigid model pitch motions RAO in Stern Quartering Seas (45°) at zero speed

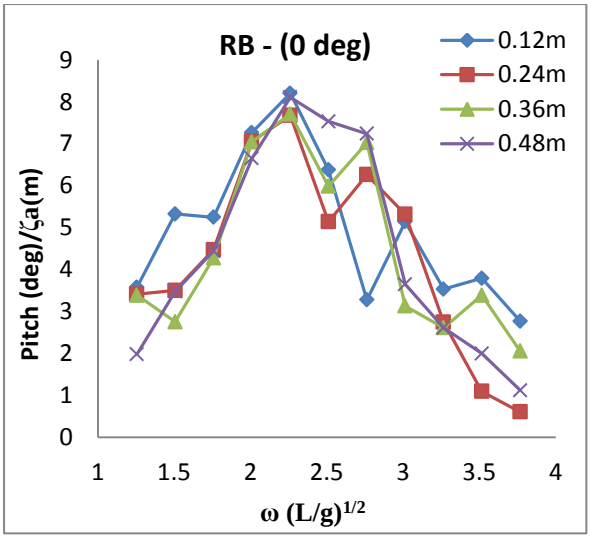

Figure 4.29: Rigid model pitch motions RAO in Following Seas (0°) at zero speed

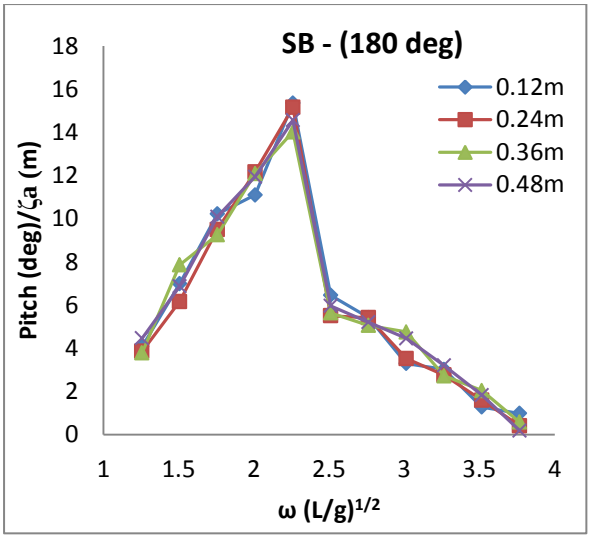

Figure 4.31: Segmented model pitch motions RAO in Head Seas (180°) at zero speed

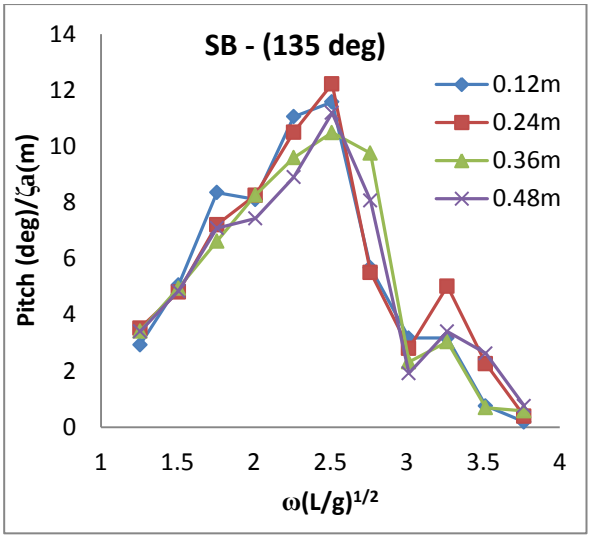

Figure 4.34: Segmented model pitch motions RAO in Bow Quartering Seas (135°) at zero speed

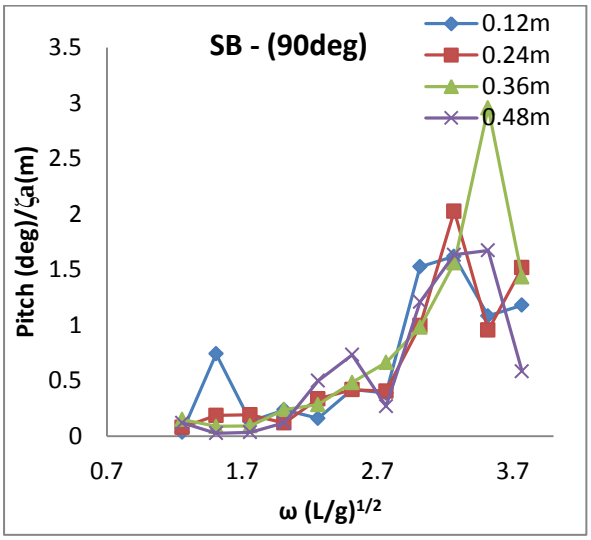

Figure 4.32: Segmented model pitch motions RAO in Beam Seas (90°) at zero speed

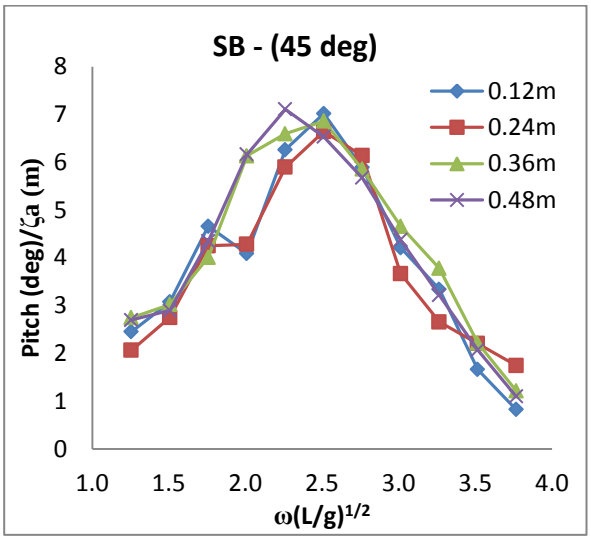

Figure 4.35: Segmented model pitch motions RAO in Stern Quartering Seas (45°) at zero speed

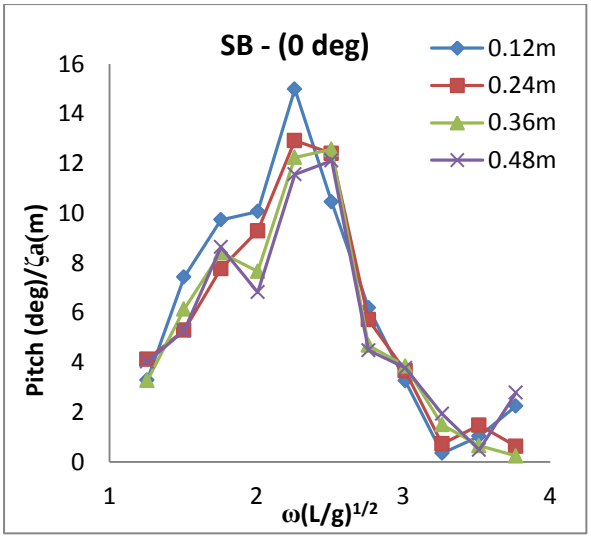

Figure 4.33: Segmented model pitch motions RAO in Following Seas (0°) at zero speed

4.5.4 The Forward Speed Rigid Body Motions Test Results

The experimental results of the heave and pitch motion responses (RAO) for the **RB** and the **SB** models in the forward speed condition corresponding to Froude numbers Fn = 0.2, and 0.6 are presented in Section 4.5.4.1 and Section 4.5.4.2. The towing tank tests were carried out in a wave condition of 10mm amplitude in the model scale (0.12m in the full scale) of various frequencies. The motions response results are plotted against the incident frequency in a non-dimensional form ($\boldsymbol{\omega\ (L/g)^{1/2}}$).

4.5.4.1 Heave Motions Response Amplitude Operator (RAO)

The heave motion responses for the models with forward speeds in the **Head Seas** (**180^o**) condition were measured in wave amplitude of 0.12m and at an equivalent vessel speed of Fn = 0.2 and 0.6, which corresponds to 5kn and 15kn in full size vessel. The trends of the response plots for the **RB** model (Figure 4.36) are fairly linear with respect to speed, especially at the low frequencies. The linearity improves as the incident wave frequency increases. This situation was slightly different in the **SB** model (Figure 4.38) with the responses showing certain degree of nonlinearity as the frequency increases. The effect of speeds on the **RB** model responses was barely registered as the plots look quite similar to each other except for the slight change in their magnitudes. The scenario in **Head Seas** (**180^o**)is quite the opposite of what has been observed in the **Following Seas** (**0^o**), which shows significant reduction in the magnitude of heave at Fn = 0.2 (Figure 4.37). The heave response of the **SB** model is coupled with the pitch at a non-dimensional frequency of 2.0. There was relatively no other noticeable presence of physical interference or coupling effect on the Following Seas plots. However this does not necessarily means that such condition does not exist in **DVC** since the experiment was only carried out in limited wave conditions.

4.5.4.2 Pitch Motions Response Amplitude Operator (RAO)

The plots of the responses for the **RB** model (Figure 4.39) in Head Seas (**180^o**) are nonlinear with both speed and frequency. The plots contain mild "kink" at non-dimensional frequency of 1.76 and 2.8 (at Fn = 0.2 only). In the SB model (Figure 4.41), the "kink" occurs at non-dimensional frequency of 3.23. In the **Following Seas (0^o)** - Figure 4.40, it was quite difficult to conclude whether there was any occurrence of nonlinearity in the result because of the limited number of tests that were carried out for this condition. However, vessel headings and speeds appear to have little effects on trends and magnitudes of the responses measured.

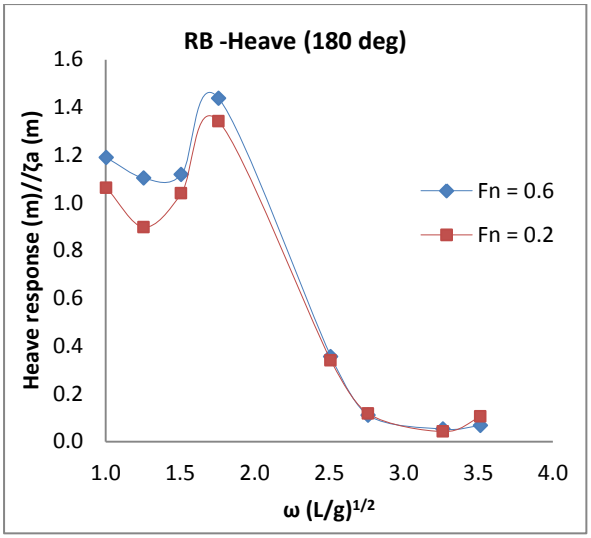

Figure 4.36: Rigid model heave response in Head Seas (180°) at forward speed.

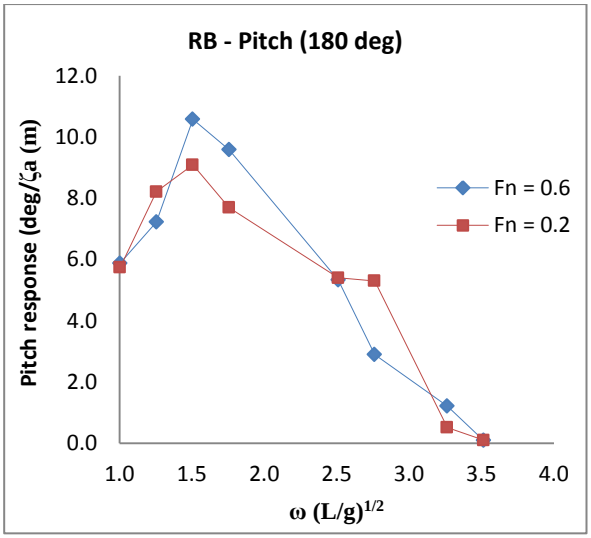

Figure 4.39: Rigid model Pitch response in Head Seas (180°) at forward speed.

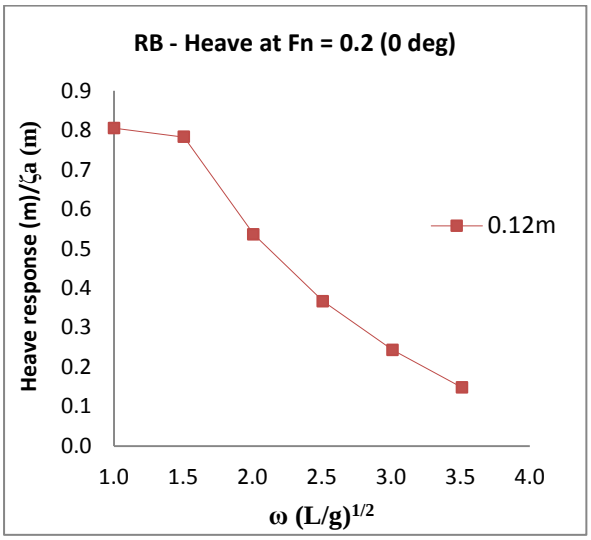

Figure 4.37: Rigid model heave response in Following Seas (0°) at forward speed.

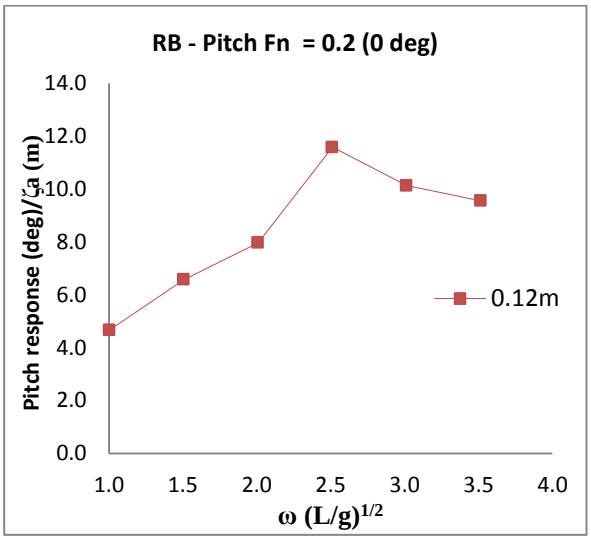

Figure 4.40: Rigid model Pitch response in Following Seas (0°) at forward speed.

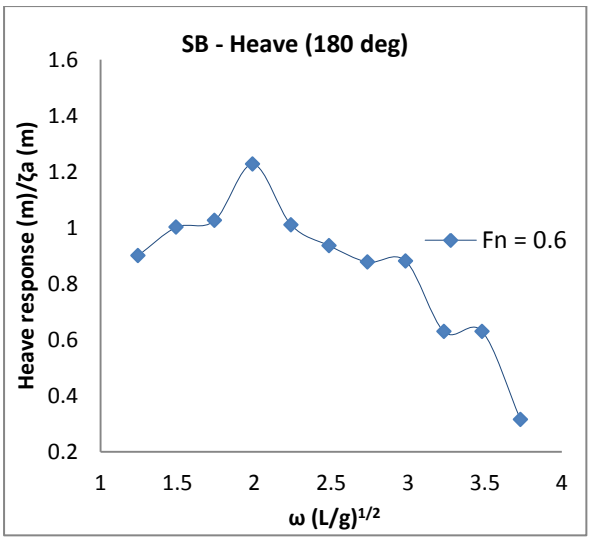

Figure 4.38: Segmented model heave response in Head Seas (180°) at forward speed.

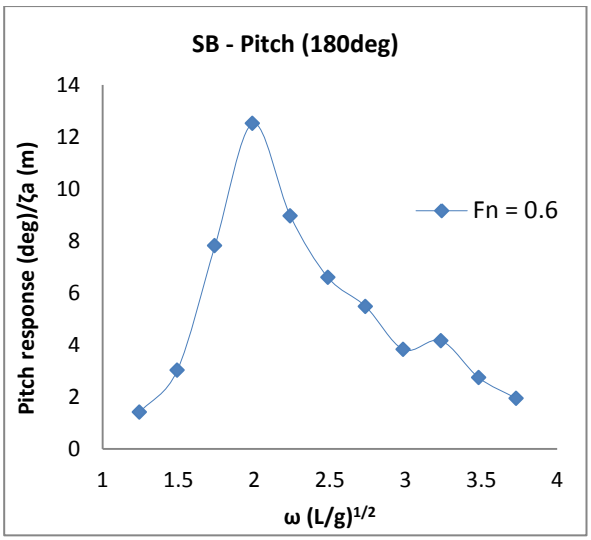

Figure 4.41: Segmented model pitch response in Head Seas (180°) at forward speed.

4.5.5 The Zero Speed Wave-induced Loads Test Results

The results from the experimental measurements of the wave-induced forces and moments acting on cross-deck structure of the vessel are presented in non-dimensional forms in the figures that follow. The vertical axis of these plots represents the non-dimensional wave-induced force response (N) while the vertical axis for the wave-induced moment plots equally represents the non-dimensional wave-induced moment response (Nm). Both the forces ($\boldsymbol{F_i}$) and the moments ($\boldsymbol{M_i}$) were measured along the longitudinal centre line of the model and in the cross-deck structure.

The non-dimensional force response is represented as $\boldsymbol{F_i/k_a}$ while the non-dimensional moment response is represented by $\boldsymbol{M_i/k_b}$. with $\boldsymbol{K_a}$ and $\boldsymbol{K_b}$ defined as follows:.

$\boldsymbol{k_a}$ = The force factor and it is defined as $\mathbf{½\rho g\zeta_a LB}$

$\boldsymbol{k_b}$ = The moment factor and it is defined as $\mathbf{½\rho g\zeta_a L^2 B}$

The horizontal axes of all of the plots for the forces and the moments are equally presented in the non-dimensional frequency form as $\boldsymbol{\omega\ (L/g)^{1/2}}$.

The discussion on the results that were obtained from the measurements of the wave-induced load responses is based on the following principal characteristics of the responses themselves. This approach is similar to that which had been taken in discussing the motion response results. The basis for the discussion is:

i. The physical behaviour and interpretation of the collective/individual plots of the response amplitude operators such as the effect of headings.
ii. The magnitudes of the various wave-induced load responses and their relationship with the concurrent wave heights and frequencies
iii. Interactions between the response amplitude operators of the individual wave amplitudes of the vessel.
iv. Other important observations that are made about the results.

4.5.5.1 The Longitudinal Shear Force (Fx)

The results of the wave-induced longitudinal shear forces acting on the cross-deck structure of the segmented model are presented in Figures 4-42 to 4-46. A summary of the peak magnitudes of these loads for each of the five wave heading conditions that were measured is presented in Table 4.11.

The plots of the longitudinal shear force responses in the **Head Seas** (**180^o**) are presented in Figure 4.42. The trend of these plots shows the presence of nonlinearity due to the effects of wave amplitudes on the results. The cause of this nonlinearity could possibly be attributed to the effects of unsteady wave amplitudes on the wave-induced loads in this axis. The plots also contain two distinct "Kinks" at non-dimensional frequencies of 2.26 and 3.10 which corresponds to the positions of the peak pitch motions.

In the **Bow Quartering Seas** (**135^o**) - Figure 4.43, the plot of the responses initially started as being fairly linear with frequency up until a non-dimensional frequency of 2.76 when it becomes fully nonlinear. At the higher non-dimensional frequencies, the RAO plots exhibited some degree of nonlinearity coupled with a separation between the plots of the higher wave amplitudes from those of the lower amplitudes. The nonlinearity is not as severe as those observed in the **Head Seas** (**180^o**) but it could also be attributed to the effects of unsteady wave amplitudes on the wave-induced loads especially when one takes into consideration that such a response is occurring at a high frequency.

The trend of the responses in the **Beam Seas** (**90^o**) - Figure 4.44, changes as the frequency increases from the mid-range up to the highest non-dimensional frequency. Its characteristics can be described in three frequency range categories. These are the stage one, which comprised of the non-dimensional frequency range of 1.25 - 2.10 in which the RAO is purely nonlinear. In stage two, which is comprised of the non-dimensional frequency range of 2.10 – 3.27, the RAO plots behave in more linear manner but with increased separation between the plots of the higher wave amplitudes response from the lower amplitudes. The cause of this separation within the mid-range frequencies needs to be further investigated. Finally stage three, which is comprised of non-dimensional frequency range of 3.27 – 3.77, the plot is nonlinear as it was the case in the first stage. The magnitude of the response is similar to that which was recorded in the second "Kink" in the Head Seas condition. It appears that the roll response have significant influence on the force in this axis.

In the **Stern Quartering Seas (45^o)** - Figure 4.45, the trend of the plots is very similar to those observed in the **Bow Quartering Seas (135^o)**. The load response changes with the increase in frequency from being linear at the beginning to nonlinear at the mid-range frequency and then exhibiting nonlinearity thereafter. The linearity started at a non-dimensional frequency of 1.25 up until a non-dimensional frequency of 2.10; and at this point it becomes nonlinear. The nonlinear portion of the RAO plots is also coupled with the detachment of the individual response plots for the wave response at the higher and the lower amplitudes which is similar to that which has been described in the **Bow Quartering Seas (135^o)**.

The trend of the longitudinal shear force response in the **Following Seas (0^o)** - Figure 4.46, is somewhat similar to that which has been observed in the **Head Seas (180^o)** in terms of both their magnitude and physical behaviour. The plot was linear from the beginning albeit it became nonlinear as the frequency increases. Again, as observed in the **Head Seas (180^o)**, the plots contain two distinct "Kinks" (and an additionally less pronounced "Kink") at non-dimensional frequencies of 2.26 and 3.10 whose position is the same as the peak pitch motion response and the resonant pitch frequencies measured in the rigid model. The magnitudes of these responses are very small in the region of lower frequencies and they are higher in the high frequency region. This implies that those higher frequencies responses, in addition to the natural frequencies, could potentially be influencing the response to wave-induced loads behaviour of the vessel in this wave heading.

A summary of the peak non-dimensional responses for all the headings for the longitudinal shear force is presented in Table 4.11. This table shows that the most dominant longitudinal shear force acting on the model is found to occur in the **Bow Quartering Seas (135^o)**.

Table 4.11: A Summary of the Longitudinal Shear Force (Fx)

S/N	***Heading (Deg)***	***Longitudinal Shear Force***	
		Fx	$\omega(L/g)^{1/2}$
1	Head Seas (180^o)	0.010	3.10
2	Bow Quartering	0.051	3.10
3	Beam Seas	0.027	3.10
4	Stern Quartering	0.037	2.76
5	Following Seas	0.011	3.10

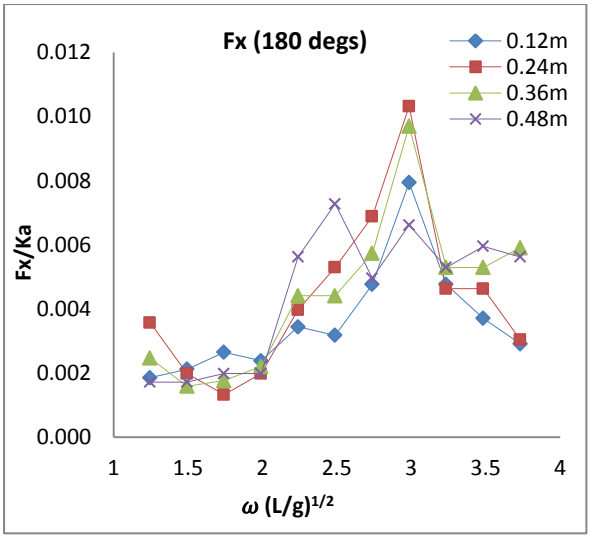

Figure 4.42: Longitudinal Shear Force (Fx) in Head Seas (180°) at zero speed

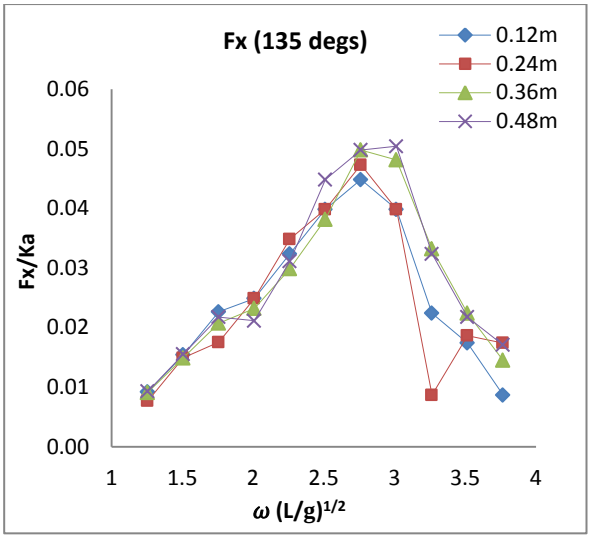

Figure 4.43: Longitudinal Shear Force (Fx) in Bow Quartering Seas (135°) at zero speed

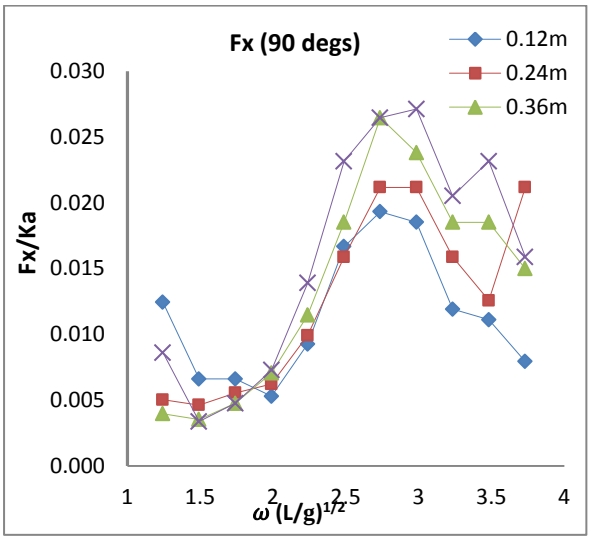

Figure 4.44: Longitudinal Shear Force (Fx) in Beam Seas (90°) at zero speed

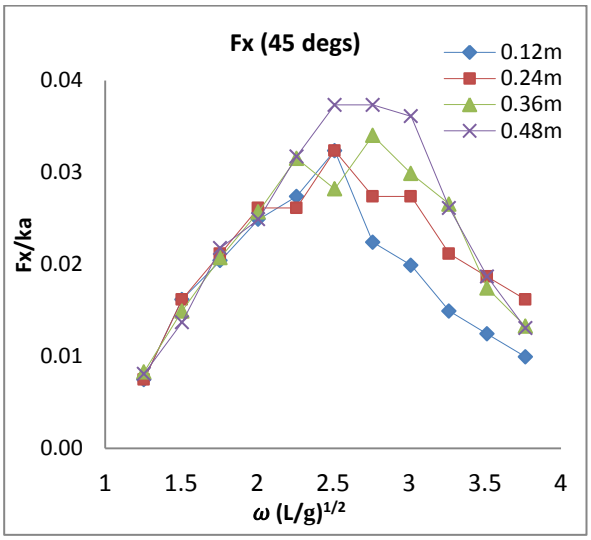

Figure 4.45: Longitudinal Shear Force (Fx) in Stern Quartering Seas (45°) at zero speed

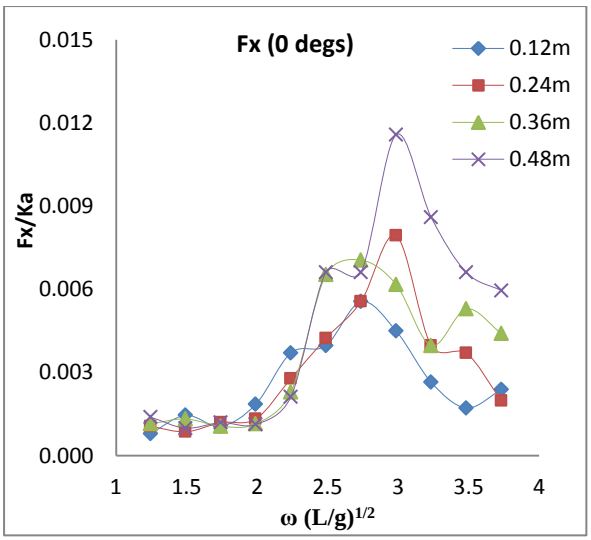

Figure 4.46: Longitudinal Shear Force (Fx) in Following Seas (0°) at zero speed

4.5.5.2 The Transverse (Side) Shear Force (Fy)

The plots of experimental responses for the wave-induced transverse shear (side) forces acting on the segmented model of the RV Princess Royal are presented in Figures 4-47 to 4-51. A summary of the peak magnitudes of these loads for each of the five vessel heading conditions is presented in Table 4.12.

The trend of the transverse shear (side) force response in ***Head Seas (180^o)*** **-** Figure 4.47**,** is similar to those that were observed in the longitudinal shear force response in the same ***Head Seas (180^o)***. The plots contain two distinct "Kinks" at non-dimensional frequencies of 2.26 and 3.10. One of these "kinks "occur at about the same frequency as the peak pitch motion response. The pitch motion response appears to be the most influencing factor in the transverse shear behaviour of the vessel in a stationary condition. There seems to be a considerable increase in the magnitude of response amplitudes for the side forces in comparison to the corresponding longitudinal shear forces for the Head Seas condition.

The physical trend of the plots for responses in the **Bow Quartering Seas condition (135^o)** - Figure 4.48, started as being a relatively linear response between non-dimensional frequency of 1.25 and 2.51. It then became somewhat nonlinear as the frequency increases at the mid-range until the end of the tests frequency of 3.77. The degree of nonlinearity is coupled together with separation of the plots of responses for higher wave amplitude from the lower amplitudes. One of the causes of this nonlinearity could be the low stiffness of the cross-deck structure of the model which contributes to the rapid relative movement between the demi-hulls of the segmented model. The effects of unsteady wave amplitudes on the model could also be a contributing factor to this condition.

In the ***Beam Seas (90^o)*** **-** Figure 4.49**,** the behaviour of the response plots is fairly linear but with some isolated cases of nonlinearity developing between the non-dimensional frequencies of 2.51 and 3.10. At some frequencies where the nonlinearities were observed, there appear to be a trend of the responses for higher wave amplitudes separating from the lower ones. This case of separation has been observed in the response for longitudinal shear in quite a number of headings. The cause of these separations, as in the previous conditions, needs to be further investigated

The plots of the transverse shear force response for the **Stern Quartering Seas (45^o)** - are presented in Figure 4.50. The trend begins as a linear response and then changes to being strongly nonlinear from non-dimensional frequency of 2.51 to 3.77. In the region of this nonlinearity, the plots also exhibit certain degree of separations of the individual plots as reported in the preceding sections. The nonlinear effect is stronger when the wavelength (λ) of the incident wave is in the region of $0.5L \leq \lambda \leq 1.0L$ of ship length (L). Other possible cause of these scenarios is the model station-keeping during testing and the possible effect of reflected waves due to tank-walls interference.

In the **Following Seas condition (0^o)** - Figure 4.51, the physical trend of the plots is predominantly linear but with a modest "kink" and then another big "Kink". These "Kink" only manifested in lower amplitudes responses. The behaviour of the responses is somewhat similar to that which has been observed in the **Head Sea (180^o)** except for the double "Kinks" that exits there as opposed to a single "Kink" in this condition. The magnitudes of the side force responses outside the range of the "Kink" are generally very small. This result is almost a direct opposite of that observed in the **Bow Quartering Seas (135^o)**.

A summary of the peak values of the non-dimensional responses for the side force (transverse shear force) is given in Table 4.12. This table reveals that the most dominant side force (transverse shear force) acting on the model was found to occur in the **Beam Seas (90^o)**.

Table 4.12: A Summary of the Transverse (Side) Force (Fy)

S/N	***Heading (Deg)***	***Side Force (Fy)***	
		Fy	$\omega(L/g)^{1/2}$
1	Head Seas (180^o)	0.025	3.10
2	Bow Quartering	0.080	3.10
3	Beam Seas	0.423	3.10
4	Stern Quartering	0.043	2.76
5	Following Seas	0.022	3.10

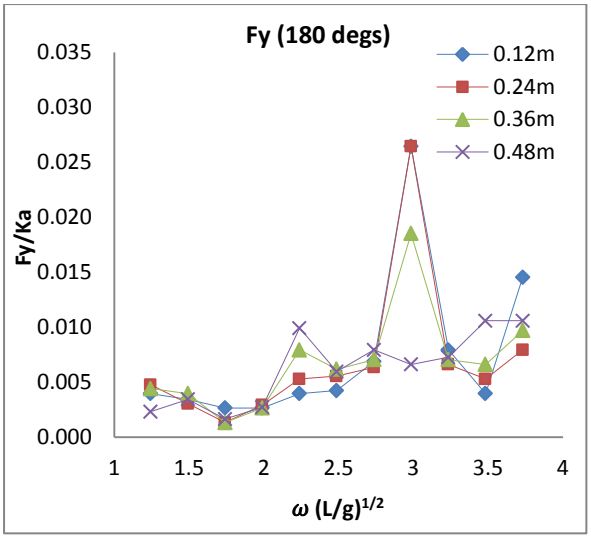

Figure 4.47: Transverse Shear Force (Fy) in Head Seas (180°) at zero speed

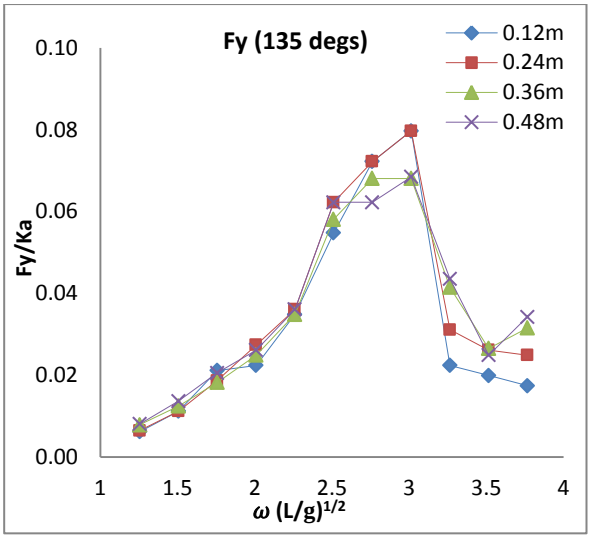

Figure 4.48: Transverse Shear Force (Fy) in Bow Quartering Seas (135°) at zero speed

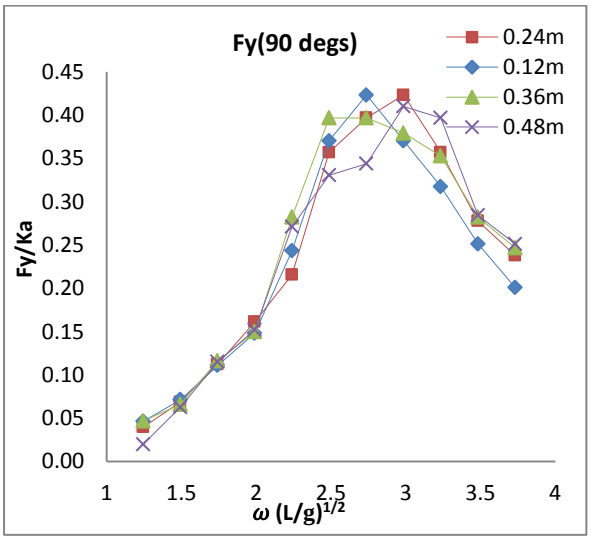

Figure 4.49: Transverse Shear Force (Fy) in Beam Seas (90°) at zero speed

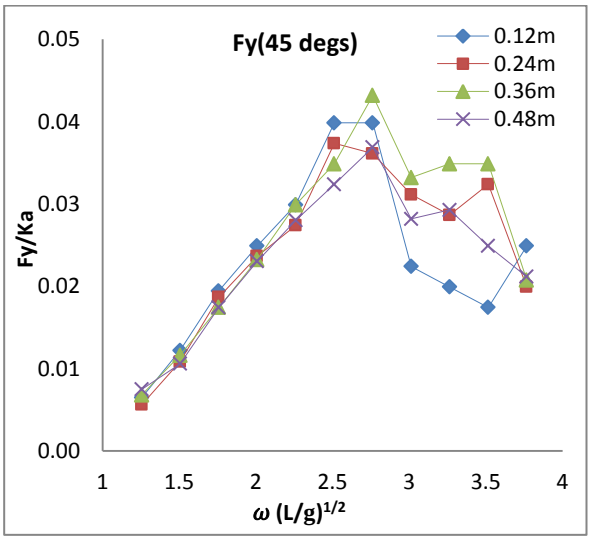

Figure 4.50: Transverse Shear Force (Fy) in Stern Quartering Seas (45°) at zero speed

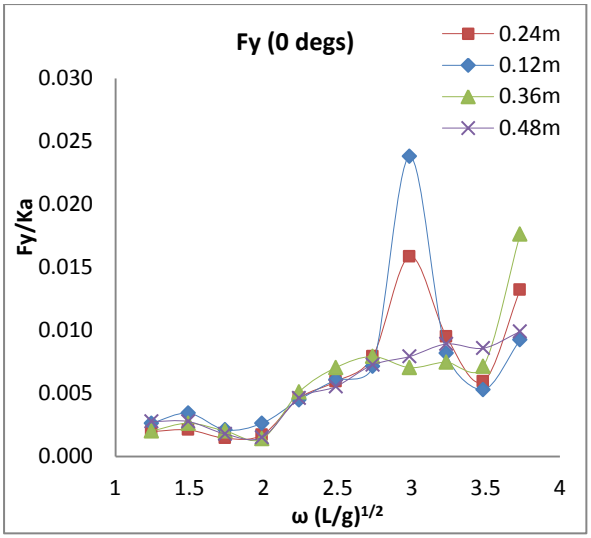

Figure 4.51: Transverse Shear Force (Fy) in Following Seas (0°) at zero speed

4.5.5.3 The Vertical Shear Force (Fz)

The vertical shear force responses that have been measured on the cross-deck structure of the segmented model are presented in Figures 4-52 to 4-56. A summary of the peak magnitudes of the wave-induced loads responses for each of the five wave heading conditions that have been measured is given in Table 4.13.

The plots of the vertical shear force responses in the **Head Seas (180^o)** are presented in Figure 4.52. The trend of these plots reveals some mixed results with the presence of nonlinearity due to the effects of wave amplitudes coupled with a separation of the responses. As it has been observed in the previous plots, this plot also contains some "Kinks" which are the manifestation of coupling of this response together with the responses (motion or resonant) of other modes of the vessel. There is a significant increase in the magnitudes of the vertical shear force response compared to those that were obtained in both the longitudinal and transverse shear forces.

In the **Bow Quartering Seas (135^o)** - Figure 4.53 the physical behaviour of the plots is largely linear with some modest signs of nonlinearity at the high non-dimensional frequencies range of 3.26 to 3.77. This has been the general trend for most of the responses in this heading. The nonlinearity occurs together with the separation of the responses for higher wave amplitudes from the lower wave amplitudes, a phenomenon that is similar to that which has been reported in other conditions. The frequency at which the peak response is measured is similar to those that been seen in other conditions.

The trend of the vertical shear force response plots in the **Beam Seas (90^o)** - Figure 4.54, have similar pattern of behaviour to those already reported. They started as fairly linear and then changed to being nonlinear at mid-range frequency. The nonlinearity then becomes stronger as the frequency increases. The trend is also the same in the **Stern Quartering Seas (45^o),** - Figure 4.55, except for their magnitudes. The peak magnitude of shear force in the **Stern Quartering Seas (45^o)** is about a half of that which had been measured in the **Bow Quartering (135^o)**.

The responses in this **Beam Seas (90^o)** are the most dominant of the vertical forces along the vertical axis. This is so when the impact of the hydroelasticity of the model is taken into accounts as it relates to the rigidity of the cross-deck structure.

The plot of the responses for the **Following Seas (0^o)** - Figure 4.56, is predominantly nonlinear especially at the higher frequencies. These plots contained some "Kinks" in about the same region where the nonlinearity is observed in the **Head Seas (180^o)**. Generally, the trends of the responses are somewhat similar to those that have been observed in the **Head Seas (180^o)** and also in the **Beam Seas (90^o)**. The similarity of these responses is common in both their magnitudes and the physical behaviours.

A summary of the peak non-dimensional responses for the vertical shear force is given in Table 4.13. This table reveals that the most dominant vertical shear force acting on the model was found in the Beam Seas condition.

Table 4.13: A Summary of the Vertical Shear Force (Fz)

S/N	***Heading (Deg)***	***Vertical Shear Force***	
		Fz	$\omega(L/g)^{1/2}$
1	Head Seas (180^o)	0.102	2.76
2	Bow Quartering	0.212	3.10
3	Beam Seas	0.290	3.10
4	Stern Quartering	0.125	3. 10
5	Following Seas	0.063	3.25

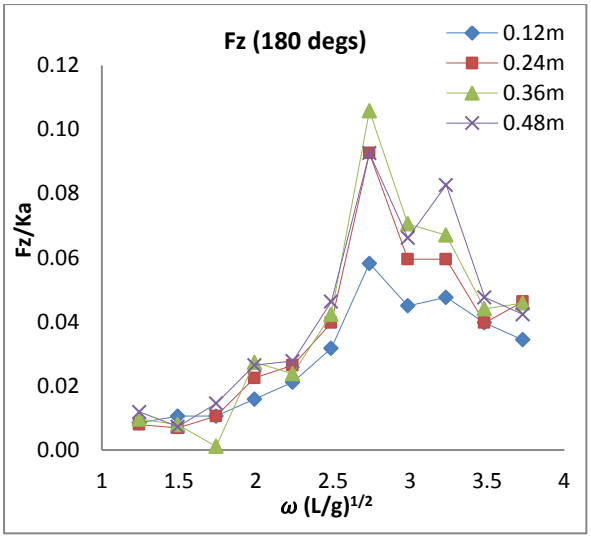

Figure 4.52: Vertical Shear Force (Fz) in Head Seas (180°) at zero speed

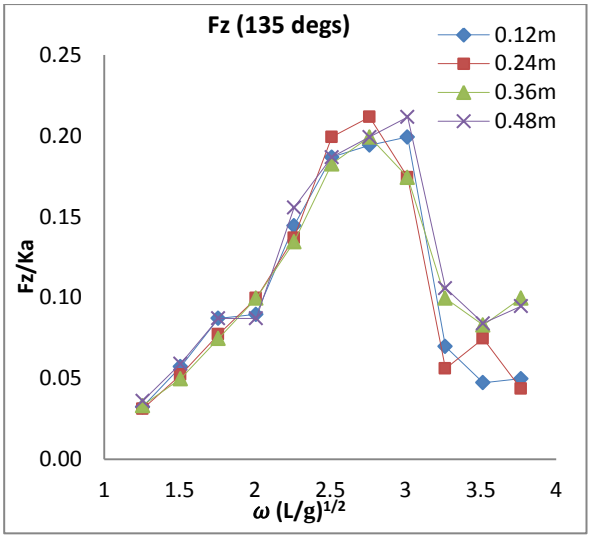

Figure 4.53: Vertical Shear Force (Fz) in Bow Quartering Seas (135°) at zero speed

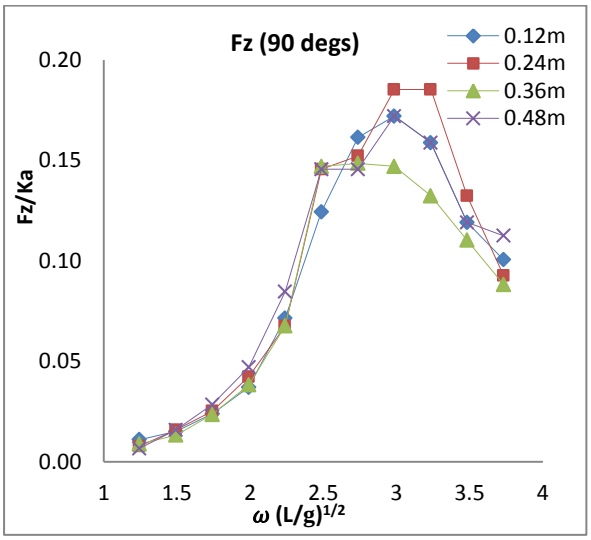

Figure 4.54: Vertical Shear Force (Fz) in Beam Seas (90°) at zero speed

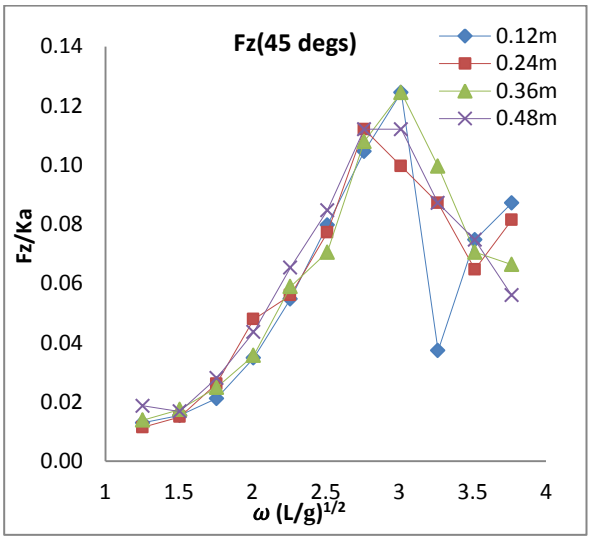

Figure 4.55: Vertical Shear Force (Fz) in Stern Quartering Seas (45°) at zero speed

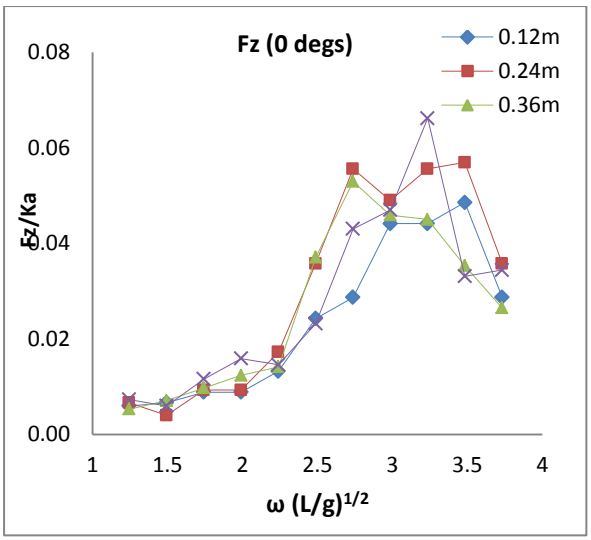

Figure 4.56 Vertical Shear Force (Fz) in Following Seas (0°) at zero speed

4.5.5.4 Prying (Longitudinal Bending) Moment (Mx)

The experimental results of the wave-induced prying moment acting on the segmented model of the RV Princess Royal are presented in Figures 4.57 to 4-61. A summary of the peak magnitudes of the prying moment responses for each of the five wave heading conditions that have been measured is presented in Table 4.14.

The plots of the non-dimensional prying moment response in the **Head Seas (180^o)** are presented in Figure 4.57. The trend of these plots is similar to that which has been observed in the **vertical shear force in the Head Seas (180^o),** Figure 4.52**,** but with little exception. These plots contain two "Kinks" that are more visible than in the vertical shear force plots. The physical behaviour of these plots is partially linear in spite of the presences of the double "Kinks" which is thought to be due to the influence of motions response and other external interferences on the wave-induced loads. These coupled effects that have manifested as "Kinks" at non-dimensional frequencies of 2.76 and 3.26 are peculiar to the forces in the Head Seas condition only. The pitch motion is found to be one of the influencing factors on the prying moment in this condition.

In the **Bow Quartering Seas (135^o)** - Figure 4.58, the physical behaviour of the prying moment plots is nonlinear with respect to the wave amplitudes. The nonlinearity occurs in three stages. The first of these stages occurs between the frequencies range of 1.25 – 2.10 with a strongly nonlinear trend despite being in the lowest range of frequency. The second stage ranges between the non-dimensional frequencies of 2.10 – 3.27. The behaviour of the plots within the group is also nonlinear, and it is in this same group that the separation of the lowest wave response amplitudes from the maximum responses begins. In the third group, the frequencies range is between 3.27 – 3.77. The trend is strongly nonlinear and its most dominant feature is the separation between the plots of the responses.

The plots of the prying moment responses in the **Beam Seas** (**90^o**) - Figure 4.59, are fairly linear at the beginning but then changed to nonlinear within the non-dimensional frequencies range of 2.26 to 3.1. The trend then changed back to a partial linearity for the reminder of the non-dimensional frequencies (3.10 – 3.77). The nonlinearity is manifested in the form of decrease in magnitude with the highest wave amplitudes producing the lowest responses while, at the same time, the lowest wave amplitudes producing the highest responses. The responses in this condition are the most dominant of the measured prying moments.

The **Stern Quartering Seas (45^o)** response plots for the prying moment are presented in Figure 4.60. The plots are generally linear until its attainment of the non-dimensional frequency of 2.76 at which point the responses became nonlinear. Within the nonlinear range, there is a partial separation of the individual response plots from one another. The plots change from being linear to strongly nonlinear as the frequency increases from a non-dimensional frequency of 2.51 to 3.77. This scenario is similar to that what has been observed as the effect of heading in the plots for the horizontal and transverse shear forces in the **Stern Quartering Seas (45^o)**.

This magnitude of the responses of this axis is about 40% less than that which had been measured in the **Bow Quartering Seas (135^o).**This trend, again, is very similar to the behaviour of the transverse shear force for both the **Bow Quartering Seas (135^o)** and **Stern Quartering Seas (45^o)** except for their magnitudes.

In the **Following Seas (0^o)** - Figure 4.61, the non-dimensional plot of the prying moment responses is predominantly nonlinear, especially at higher frequencies as it has been observed in the vertical shear force for the **Following Seas (0^o)**. The plots contained some random "Kinks" whose frequencies were found to be within the range of nonlinear plots. In spite of the presence of these "Kinks", the trends of the responses can be equated to those observed in the **Head Seas (180^o)**. This similarity is only limited to the trend itself but not the magnitude. Due to the random nature of these plots, especially in the high frequency region, the peak magnitude is only taken from the response due to the highest wave amplitude.

A summary of the peak responses for the prying moment is given Table 4.14. The table shows that the most dominant prying moment occurs in the Beam Seas condition.

Table 4.14: A summary of the Prying Moment (Mx)

S/N	***Heading (Deg)***	***Prying Moment***	
		Mx	$\omega(L/g)^{1/2}$
1	Head seas (180^o)	0.011	2.76
2	Bow Quartering	0.016	3.10
3	Beam Seas	0.043	2.76
4	Stern Quartering	0.016	3.27
5	Following Seas	0.006	3.27

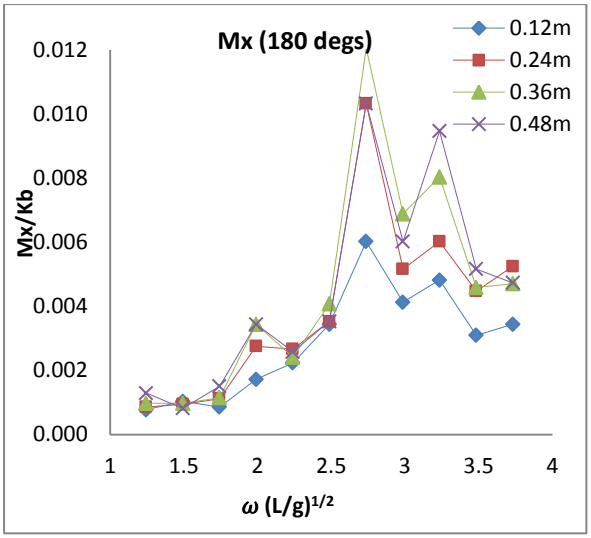

Figure 4.57: Prying moment (Mx) in Head Seas (180°) at zero speed

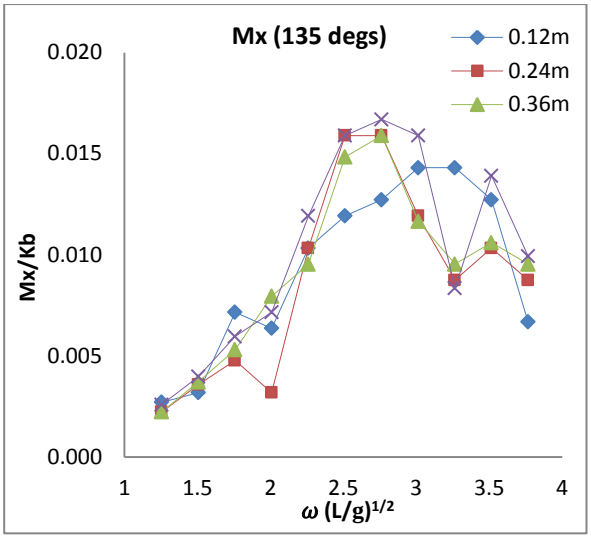

Figure 4.58: Prying moment (Mx) in Bow Quartering Seas (135°) at zero speed

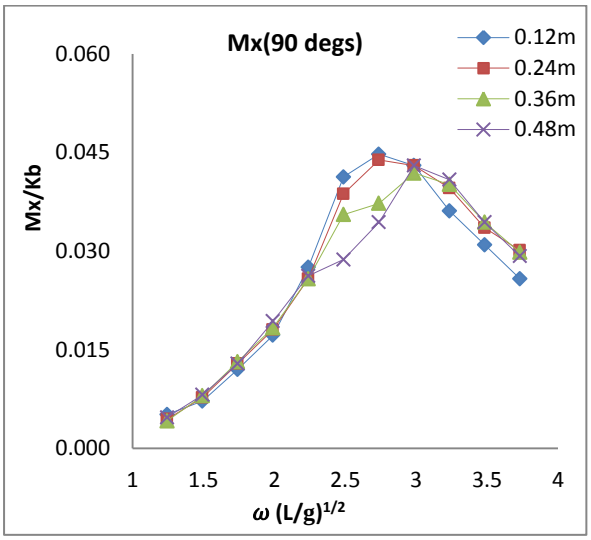

Figure 4.59: Prying moment (Mx) in Beam Seas (90°) at zero speed

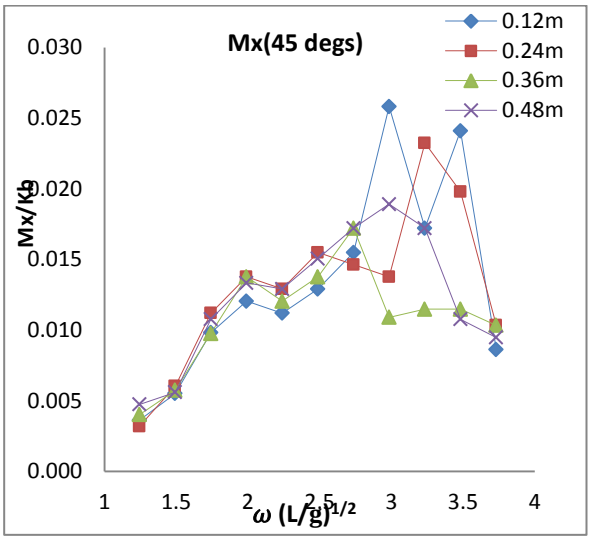

Figure 4.60: Prying moment (Mx) in Stern Quartering Seas (45°) at zero speed

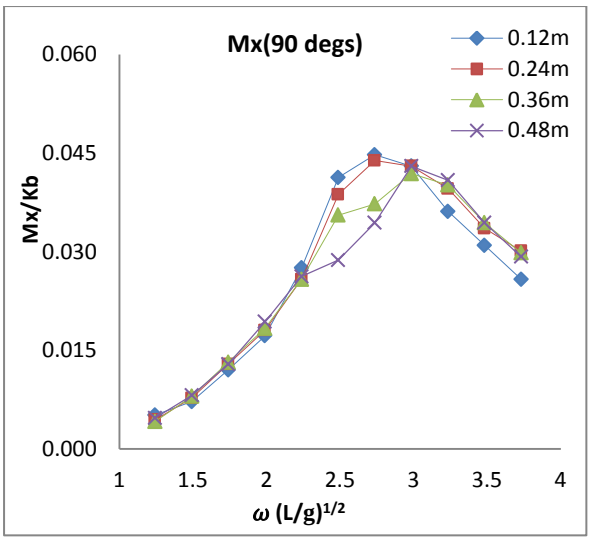

Figure 4.61: Prying moment (Mx) in Following Seas (0°) at zero speed

4.5.5.5 The Yaw Splitting Moment (Mz)

The experimental results of the non-dimensional wave-induced Yaw Splitting moment responses for the segmented model of the RV Princess Royal are presented in Figures 4.62 to 4.66. A summary of the peak magnitudes of the responses for each of the five wave heading conditions is given in Table 4.15.

Figure 4.62 presents the non-dimensional plots of the wave-induced yaw splitting moment responses in the **Head Seas (180^o).** The trend of these plots is similar to that which had been observed in the vertical shear force and the prying moment in the **Head Seas (180^o).** The plots contain two distinct "Kinks" at non-dimensional frequencies of 2.26 and 3.10. The general behaviour of these plots is linear albeit with modest degree of nonlinearity occurring within the peak magnitude of the responses. The plots also show that the coupling of the motion responses and the wave-induced load responses can easily be seen within the identified areas of nonlinearity.

The peak magnitudes are relatively small compared to that which had been obtained for the prying moment in the **Head Seas (180^o).** Since the coupled pitch motion response is one of the most visible factors affecting the magnitude of the yaw splitting moment, it is reasonable to assume that these factors, along with the flexibility of the cross-deck structure of the model, are some of the major cause of the nonlinearity.

The plot of the yaw splitting moment response in the **Bow Quartering Seas condition (135^o)** - Figure 4.63, is linear at low frequency but then becomes nonlinear as the wave frequency increases. The frequency at which this nonlinearity occurs is similar to that at which the coupled effects and the separation of the response amplitudes have been observed. The cause of these effects needs to be further investigated.

In the ***Beam Seas (90^o)*** - Figure 4.64, the non-dimensional plots of the yaw splitting moment responses is nonlinear, and the nonlinearity within the non-dimensional frequencies range of 2.10 to 3.77. The effect of this nonlinearity is strongest in the region where separation between the plots of the responses has been observed. Also, the frequencies range for the nonlinearity coincides with the frequency of the peak magnitude of the response amplitudes.

The plots of the responses for the **Stern Quartering Seas** (**45^o**) - Figure 4.65, are also nonlinear and they contain modest but random "kinks" that are similar to that which has been

observed in the **Bow Quartering Seas (135^o).** The nonlinearity was first observed at a non-dimensional frequency of 2.10 and it then continues until the end of the frequencies range of 3.77. This nonlinearity appears to be a major contributing factor to the separation between the plots for the individual wave response amplitudes as it has been observed throughout these experiments. Again, the magnitude of this response is about 40% less than what has been measured in the **Bow Quartering Seas (135^o)**, which is quite compatible with what has been observed in the responses for the prying moment in the **Stern Quartering Seas (135^o).**

In the ***Following Seas (0^o)*** **-** Figure 4.66**,** the plots of the yaw splitting moment responses is generally nonlinear within the mid-range frequencies of 1.76 to 3.25, but linear outsides this frequency range. These plots are somewhat similar to those of the **Head Seas (180^o).** The similarity is both in terms of their physical behaviour and their magnitudes despite the fact that the plots for the yaw splitting moment in **Head Seas (180^o)** have more "Kinks" than in the ***Following Seas (0^o).***

A summary of the peak responses for the yaw splitting moment is given in Table 4.15. This table shows that the most dominant response is found in the **Bow Quartering Seas (135^o)**.

Table 4.15:A summary of the Yaw Splitting Moment (Mz)

S/N	***Heading (Deg)***	***Yaw Splitting Moment***	
		Mz	$\omega(L/g)^{1/2}$
1	Head Seas (180^o)	0.010	3.10
2	Bow Quartering Seas	0.033	3.26
3	Beam Seas	0.020	3.10
4	Stern Quartering Seas	0.020	2.76
5	Following Seas	0.019	3.10

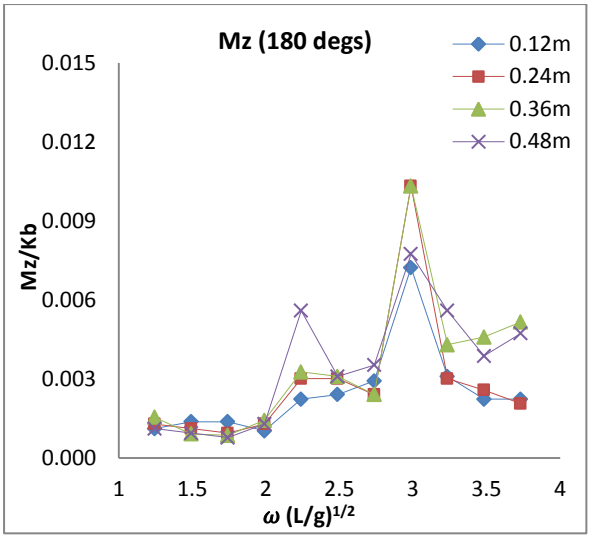

Figure 4.62: Yaw Splitting moment (Mz) in Head Seas (180°) at zero speed

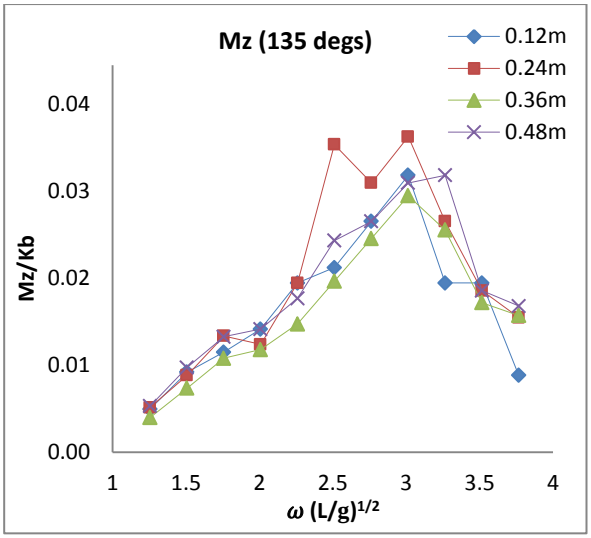

Figure 4.63: Yaw Splitting moment (Mz) in Bow Quartering Seas (135°) at zero speed

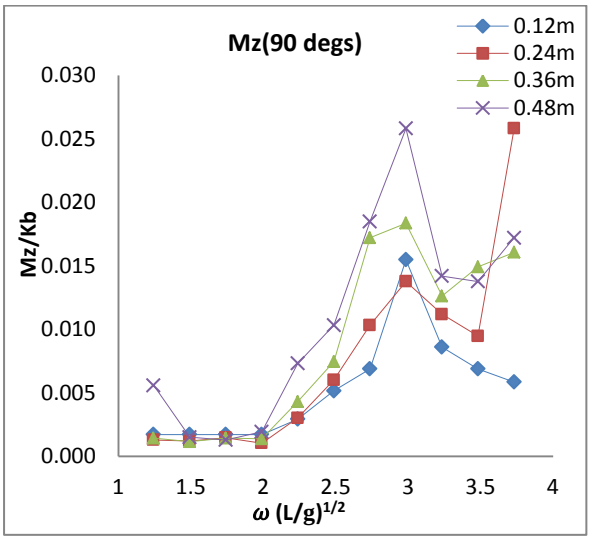

Figure 4.64: Yaw Splitting moment (Mz) in Beam Seas (90°) at zero speed

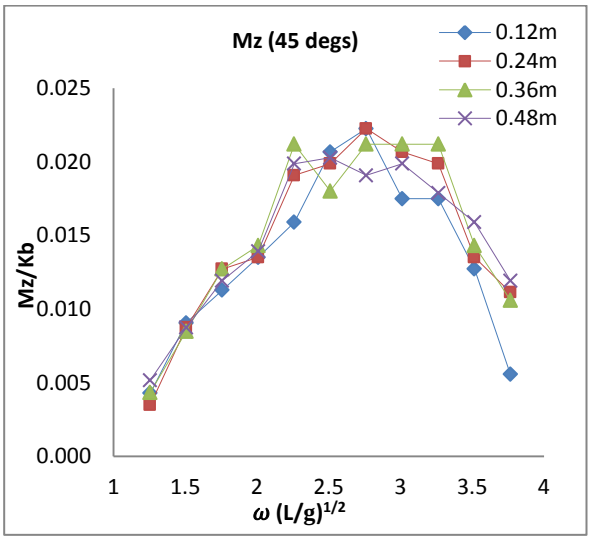

Figure 4.65: Yaw Splitting moment (Mz) in Stern Quartering Seas (45°) at zero speed

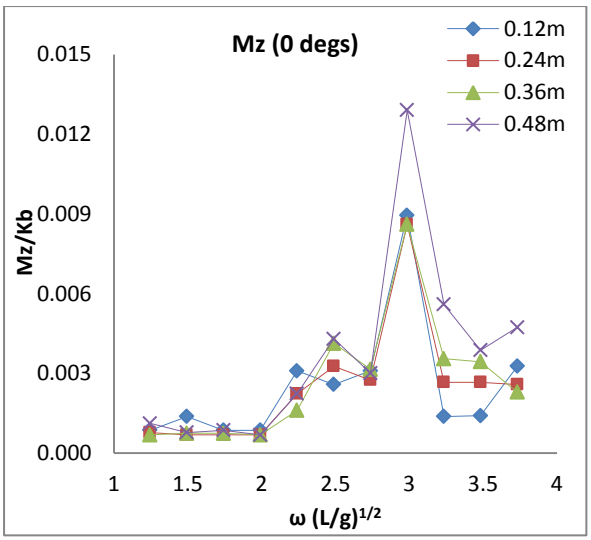

Figure 4.66: Yaw Splitting moment (Mz) in Following Seas (0°) at zero speed

4.5.6 The Forward Speed Wave-induced Loads Tests Results

The plots of the wave-induced loads acting on the cross-deck structure of the segmented model of the RV Princess Royal with forward speeds is being presented in this section. The plot are for the Longitudinal, Transverse and Vertical shear forces along with the Prying and Yaw Splitting moments that have been obtained with the model having different forward speeds corresponding to Froude numbers Fn = 0.2 and 0.6. A summary of the peak magnitudes of these responses for each of the degree of freedom and the two vessel speeds considered is given in Table 4.16.

4.5.6.1 The Horizontal (longitudinal) Shear Force (Fx*)*

The plots of the wave-induced longitudinal shear force responses in the **Head Seas (180^{o})** - Figure 4.67, for the model with vessel speeds of 15kn (Fn=0.6) and 5kn (Fn=0.2) are shown the presence of nonlinearity at lower frequencies. The nonlinearity disappears as the frequency increases thus exhibiting linear characteristics. The nonlinearity is largely due to the response behaviour of the Deep-V geometry in wave amplitudes rather than the vessel speeds.

In the slower speed condition (Fn=0.2), the nonlinearity is considered not to be strong enough as compared to those for a higher vessel speed (Fn=0.6).These results indicate a dynamic change in the magnitude of the response with respect to the vessel speed. These results should be cautiously used since the effects of speeds on the measured wave-induced loads has not been explored, hence the need for further investigation of these phenomena.

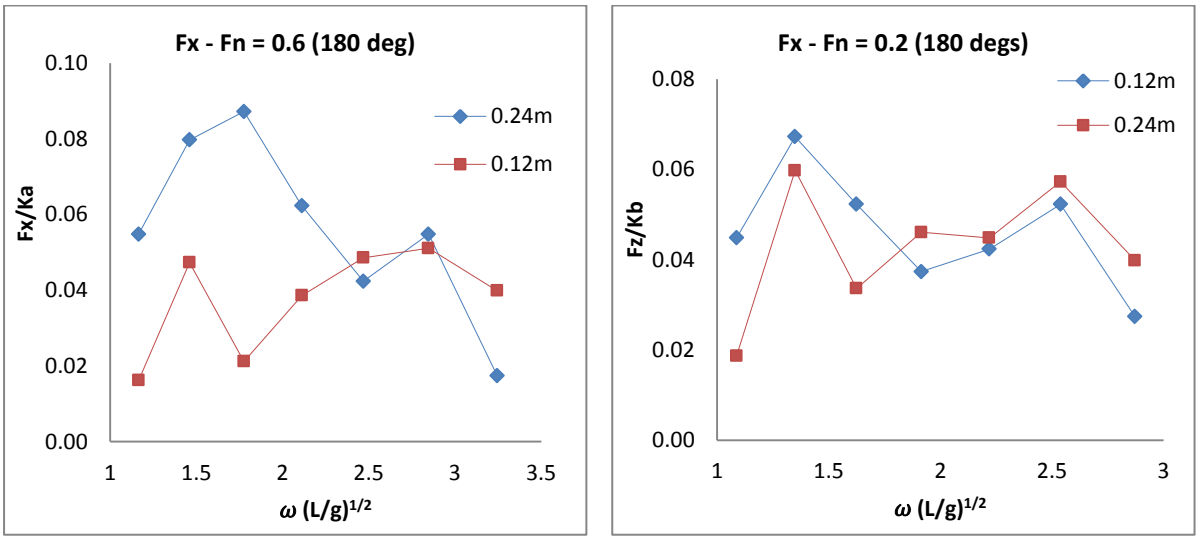

Figure 4.67: Horizontal Shear Force (Fx) for a forward speed condition.

4.5.6.2 The Transverse (Side) Shear Force

The plots of the non-dimensional transverse shear (side) force responses for the model with vessel speeds of 15kn (Fn=0.6) and 5kn (Fn=0.2) in the **Head Seas (180^{o})** are presented in Figure 4.68. The behaviour of these plots is slightly more predictable than in the plots of the longitudinal shear force. The plots are fairly linear with a small presence of nonlinearity at the lower and extreme ends frequencies. The plots appear to be stable and more linear within the mid-range frequencies of 2.55 to 3.25.

There is a significant similarity between the peak magnitude of the responses for this shear force (**Fy**), and the longitudinal shear force (**Fx**), that had been measured along the same direction for forward speeds of Fn = 0.6 and Fn = 0.2. There is virtually no difference between the magnitudes of these two results except for the shift in the frequencies at which they occur. The dynamism in the frequencies of the peak magnitudes of the response amplitudes with respect to the speed is, again, similar to that which had been observed in the longitudinal shear force.

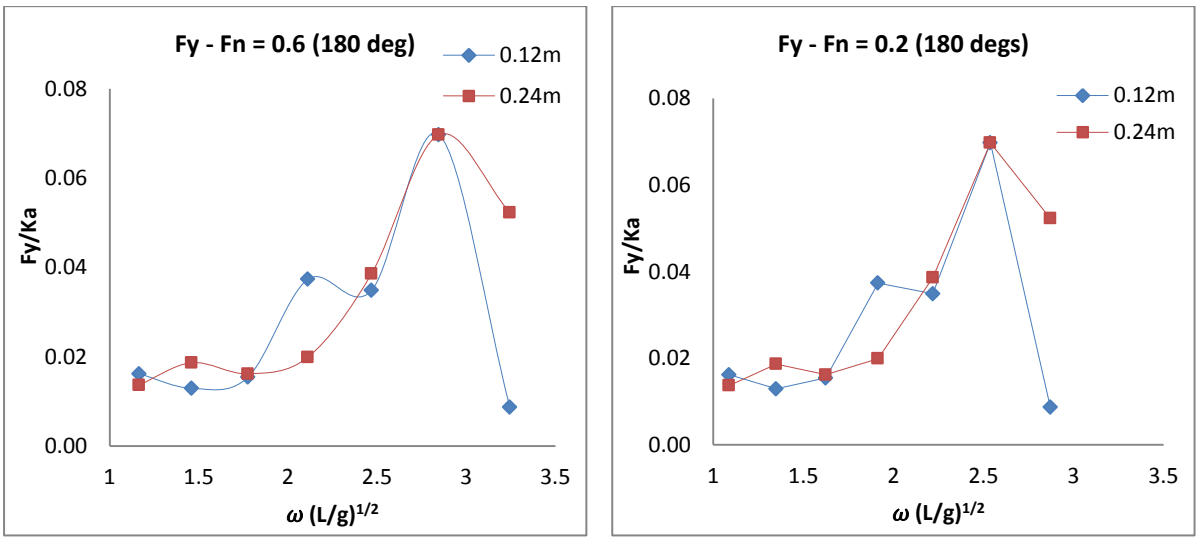

Figure 4.68: Transverse Shear Force (Fy - Side Force) at forward speed condition

4.5.6.3 The Vertical Shear Force

Figure 4.69 presents the plots of the responses for the vertical shear force in the Head Seas condition (**180^{o}**) for the segmented model with forward speeds of 15kn (Fn=0.6) and 5kn (Fn=0.2). The trend of these plots is linear but with certain degree of nonlinearity at the lower and the extreme ends frequencies. The linearity of these plots is coupled with small kinks at encountered frequencies 1.75 and 1.92. Again, the trends are quite similar, both in terms of

their peak magnitude and their physical appearance in forward speeds and waves, to the vertical shear force plots. The only noticeable difference between these two separate plots in waves is the shift in the peak frequencies where their peak magnitudes are measured. The vertical shear force is clearly the most dominant of the shear forces acting on the cross-deck structure of the model with forward speed in **Head Seas (180^{o})**.

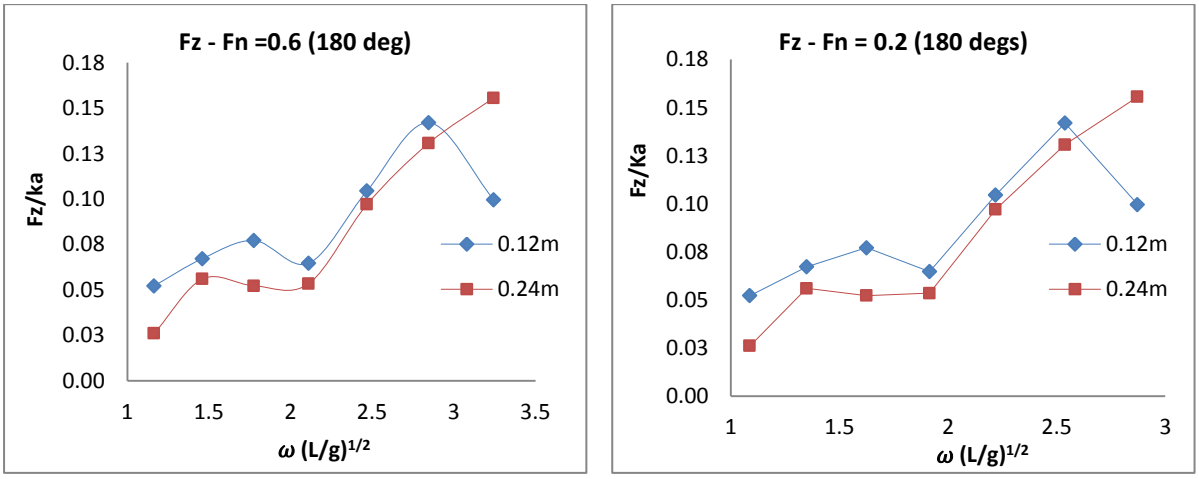

Figure 4.69: Vertical Shear Force (Fz) at forward speed condition

4.5.6.4 Prying (Longitudinal Bending) Moment

The plots of the prying moment responses acting on the model with forward speeds in the **Head Seas (180^{o}) -** Figure 4.70, presents some varying responses experienced by the cross-deck structure of the model in this heading. The plots contain a small kink at a non-dimensional frequency of 2.11 and it is really difficult to draw any meaningful inference on the results because of the difference and the negligible responses obtained for the model in the two wave amplitudes that have been measured.

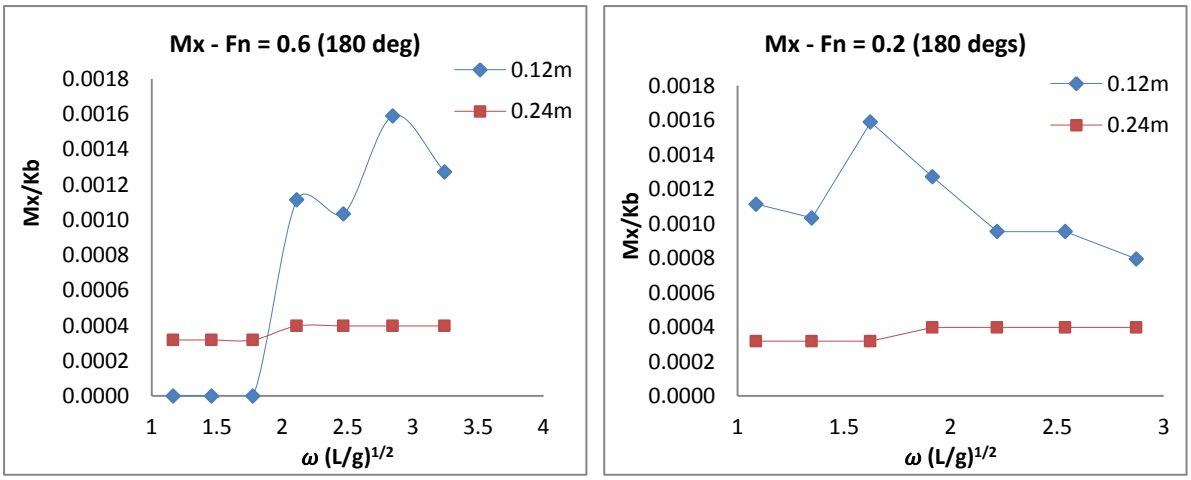

Figure 4.70: The prying moment plots for the model with forward speed condition

4.5.6.5 Yaw Splitting Moment

The trend of the yaw splitting moment response plots in the **Head Seas (180^{o})** - Figure 4.71, is generally nonlinear. The plots are somewhat similar to that which has been observed in the longitudinal shear force in the **Head Seas (180^{o}).**The responses in this heading are the most dominant of the wave-induced moments that have measured in the forward speed condition.

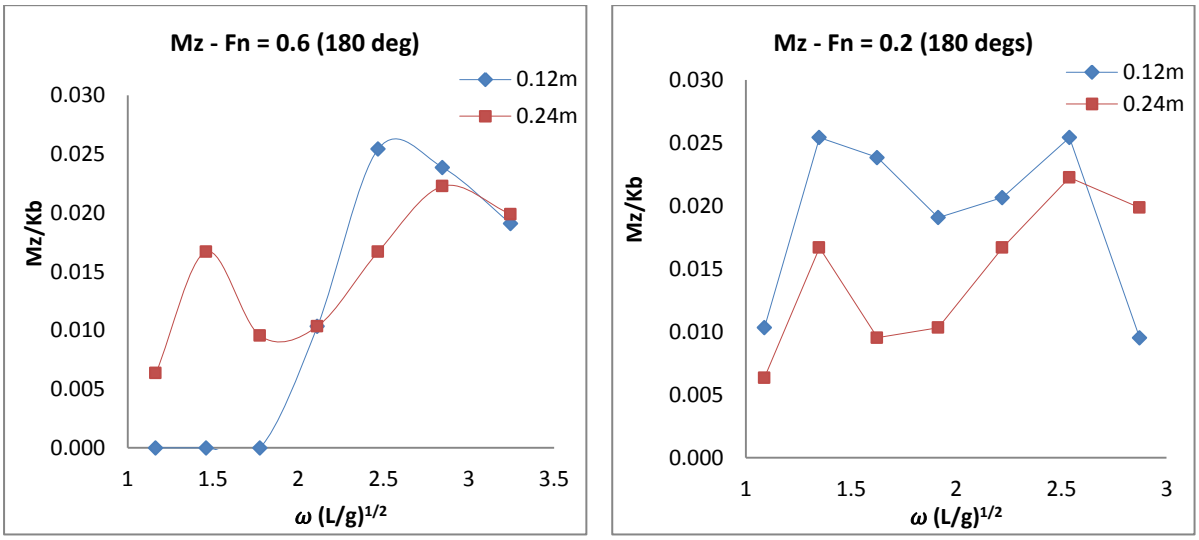

Figure 4.71: Vertical Bending Moment at forward speed condition

A summary of the peak responses for the shear forces and bending moments in the Head Seas condition for the two forward speeds of the vessel is given in Table 4.16. The vertical shear force is the most dominant of the shear forces measured.

Table 4.16: A summary of the peak magnitudes of wave-induced Shear Forces

S/N	***Heading (Deg)***	***10Kn***		***5Kn***	
		Fi	***$\omega(L/g)^{1/2}$***	***Fi***	***$\omega(L/g)^{1/2}$***
1	Fx	0.067	1.37	0.06	2.11
2	Fy	0.070	2.85	0.07	2.54
3	Fz	0.156	3.24	0.142	2.58
4	Mx	0.00159	2.85	0.00159	1.63
5	Mz	0.025	2.50	0.025	1.35

4.6 Conclusions

The experimental procedures for the measurements of motion responses and wave-induced loads on a twin hull vessel have been presented in this chapter. The main focus of the chapter was on the use of both the rigid body and the segmented models of the RV Princess Royal. The objective of the experiment has been the measurement of the motion response and wave-induced forces and moments acting on the cross-deck structure of a DVC concept. This was performed with the sole purpose of establishing a basis for validating the results of the numerical study on the same objective. The following is the summary of the tasks performed and the conclusions that have been drawn. .

i. The experimental prediction of the motion responses for a Deep-V Catamaran concept in zero and forward speed conditions using both a rigid and the segmented models of the RV Princess Royal have been performed. The measured motions responses comprised of the heave, the pitch and the roll responses in the Head Seas, the Bow Quartering Seas, the Beam Seas, the Stern Quartering Seas and the Following Seas.
ii. The experimental measurements of the wave-induced loads acting on the Deep-V hull concept have also been carried out. These loads comprised of the Longitudinal, the Transverse and the Vertical shear forces along with the Prying and the Yaw Splitting moments.
iii. The most dominant load parameters measured in the experiments for each of the vessel axis and for all the heading directions considered, have been identified and presented in this chapter.
iv. A comparison of the responses obtained using the rigid body model and the segmented models were made for the purpose of ascertaining the validity of their respective outputs.

The main conclusions that have been drawn from the experimental studies on the motions and wave-induced loads response measurements are as follows:

1. A significant reduction in the magnitudes of the motions response of the vessel was witnessed as the vessel heading changes. However, in the responses for the roll motion, such changes which are due to the vessel headings follow a Gaussian distribution in which the responses increase from lower magnitudes in the Head

Seas to the peak magnitudes in the Beam Seas then, finally lowest in the Following Seas.

2. A coupling between the respective motion responses (Heave, Roll and Pitch) at either (sometimes on both occasion) at resonant frequencies or the peak response frequency of that particular motion response have been observed in a number of wave heading conditions. The most prominent of this coupling was recorded in the responses that have been measured in the Beam Seas and then followed by the Bow and Stern Quartering Seas.
3. It has been established that the predictions of motion responses using the rigid body yield higher magnitudes of motion responses in the Head Seas and the Following Seas than it does in the measurement with a segmented model. On the other hand, the segmented model yields higher responses in the Beam Seas and the Bow and Stern Quartering Seas. The reason for such behaviour could be attributed to the unavoidable hydroelasticity of the segmented model due to the attachment of the load cell unit.
4. The behaviour of the motion responses that have been measured using both the rigid and the segmented models has been found to be mostly nonlinear. The nonlinearity featured very prominently at higher incident wave frequencies and on the responses where coupling with other motion responses were observed.
5. A shift in the motion response plots for individual wave amplitudes at higher frequencies have been observed in the plots for the wave-induced loads responses. The shifts in the responses occur mostly within the frequency range where nonlinearity was observed.
6. The most dominant load parameters due the wave-induced loads have been mostly found in the Head Seas, the Bow Quartering Seas and the Beam Seas. It has also been found that the magnitudes of these load parameters are strongly influenced by the coupling effects of the motion responses.
7. The most dominant wave-induced load response due to the longitudinal shear force in zero speed was found in the Bow Quartering Seas. The responses due to the shear force are predominantly nonlinear at higher frequencies and it also contains some separation of the plots for individual wave amplitude responses. The longitudinal shear force magnitude in the forward speed condition is slightly

higher than in the zero speed. The characteristic of the load responses in both the zero and forward speeds condition essentially remains the same.

Although Bow Quartering Seas offers the most dominant load parameters in the shear force; the vessel could still experience high response magnitude in other heading especially within the Oblique Seas angles.

8. The most dominant load parameter for the transverse shear (side) force in the zero speed condition was found in the Beam Seas. The magnitude of the responses in the forward speed condition is lower than those measured in the zero speed condition
9. The most dominant load parameter for the vertical shear force in zero speed condition was found in the Head Seas and it is quite higher than those that have been measured in the forward speed condition.
10. The most dominant wave-induced load parameter for the prying moment was found in the Beam Seas at zero speed condition. The magnitude of the prying moment decreases as the frequencies increase in the region where nonlinearity was observed.
11. The results of the Yaw Splitting moment revealed that the most dominant parameter occurred in the Bow Quartering Seas at zero speed condition. The responses contain some isolated nonlinearity that is coupled with a shift in the plots of individual responses for the various wave amplitudes. The magnitude of the Yaw Splitting moment in the forward speed condition is slightly higher than in the zero speed.

Chapter 5

Benchmark Studies

5.1 Introduction

This chapter presents the results of the benchmark studies in which the towing tank results were validated using the results obtained from the numerical study of the motions and wave loads on the models of the RV Princess Royal. The need for the validation of these experimental data is in compliance with the recommendations of ITTC (2006). It is also intended to demonstrate confidence in both the numerical studies and the towing tank tests data with regards to the capability and reliability of data obtained.

Section 5.1 of this chapter presents an overview of the chapter while Section 5.2 presents a brief overview of the numerical codes that have been used in performing the validations. The first bench mark studies in which comparison between the experimental and numerical results of the motions response for the Deep-V concept was made is presented in Section 5.3.while in Section 5.4, the benchmark studies on the experimental and numerical wave-induced loads predictions using the same Deep-V hull form model is presented. Section 5.5 presents the comparison of the Deep-V model with and without appendage whilst Section 5.6 concludes the chapter.

5.2 The Numerical codes

In line with the broader objectives of this study, two numerical codes were used for the prediction of the responses required for these benchmark studies. These codes are the MAESTRO-Wave and the PRECAL, both of which are specialised numerical codes for solving hydrodynamic problems of marine vehicles. The reason for the benchmark studies is to validate the numerical data using both the experimental data and the results from the multiple numerical codes in order to exploit the strength of these two codes together and also to add more credibility to the entire validations process. A brief overview of these codes and the theoretical background has already been stated in Chapter 3.

5.3 Benchmark Studies 1: Experimental versus Numerical Motions Response Validations

This section covers the validation of experimental motion using the two numerical programs mentioned earlier. The response measurement was performed using a Deep-V hull form model which is known to have only limited data on its motions response available at present. Some of these data were published by this author (Bashir *et al.*, 2011) and they are part of the overall results reported here in. For the purpose of this study, the MAESTRO-Wave and the PRECAL programs have been used in predicting these responses. Particulars of the model used for this study have been presented and discussed in Chapter 4.

This validation is primarily focused on some selected heave, roll and pitch motions response results in both zero and forward speed conditions for heading directions, namely, the Head Seas (180^o), the Bow Quartering Seas (135^o), the Beam Seas (90^o), Stern Quartering Seas (45^o) and the Following Seas (0^o).

5.3.1 Heave Motions Comparison

In this section, the results of the heave motion responses that have been obtained from the experimental studies using the rigid body model (**RB)** of the RV Princess Royal have been compared with those obtained from the numerical prediction for vessel speeds of Fn = 0.2 and Fn = 0.6. The plots of these comparisons are presented in Figure 5.1, Figure 5.2, Figure 5.4 and Figure 5.5, for vessel speed Fn = 0 in Head Seas, Beam Seas and Bow Quartering Seas and Following Seas respectively, while the plots for the vessel speed of Fn = 0.2 and Fn = 0.6 are given in Figure 5.3 and Figure 5.6 for Head Seas only.

From these plots, it can be seen that there exist a strong agreement between the numerical results – MAESTRO-Wave and PRECAL – when the vessel speed is at Fn = 0. The agreement is good both in terms of their respective trends and the magnitudes of their responses. The agreement applies to all the three heading conditions that have been considered. As for the comparison between the experimental and numerical results for vessel speeds of Fn = 0, a reasonably good agreement was also observed in the Head Seas and the Bow Quartering Seas. However the plot for the experimental responses in the Beam Seas appears to be an outlier and does not show the characteristic good agreement that has been seen between the experimental and the numerical results in other headings. This validation further confirms the existence of strongly coupling between the experimental responses for roll and pitch motions at frequencies of 3.2 and 2.4 respectively. One possible explanation to this scenario is the likely presence of interference due to the influence of standing waves between the demi-hulls in the towing tank (Table 4.7). This condition can easily be visualised when one considers the fact that the model is encountering the incident wave tangentially and that the mooring lines are expected to limit the translational movement of the model hence leading to the amplification of roll behaviour while the model is experiencing heave This condition has the potentials of causing adverse effects on the responses especially in the Beams Seas and the Bow and Stern Quartering and needs to be further investigated for this hull concept.

In the forward speed condition, the validation was made for two speed cases, namely, Fn = 0.2 (Figure 5.3) and Fn = 0.6 (Figure 5.6). The results show a good agreement between the responses for the experiment and the numerical codes. Their trends appear to be close enough to each other except that PRECAL did not record any Kink at vessel speed of Fn = 0.2. The

Kinks that appear in the results of experimental and the MAESTRO are consistent with the coupling of pitch motions response..

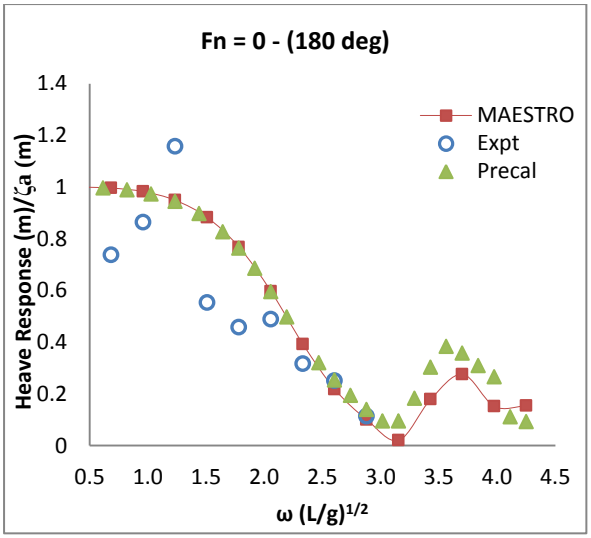

Figure 5.1: Heave motions response in Head Seas at Fn = 0

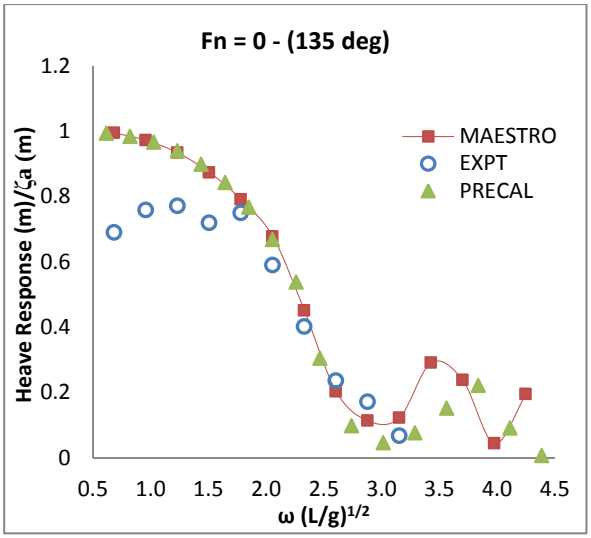

Figure 5.4: Heave motions response in Bow Quartering Seas at Fn = 0

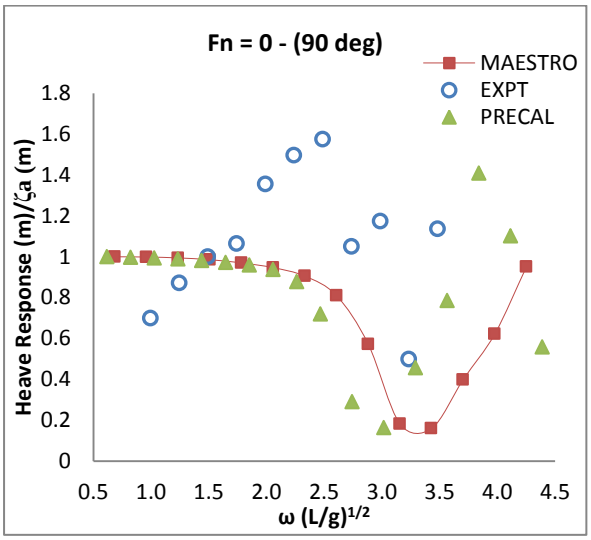

Figure 5.2: Heave motions response in Beam Seas at Fn = 0

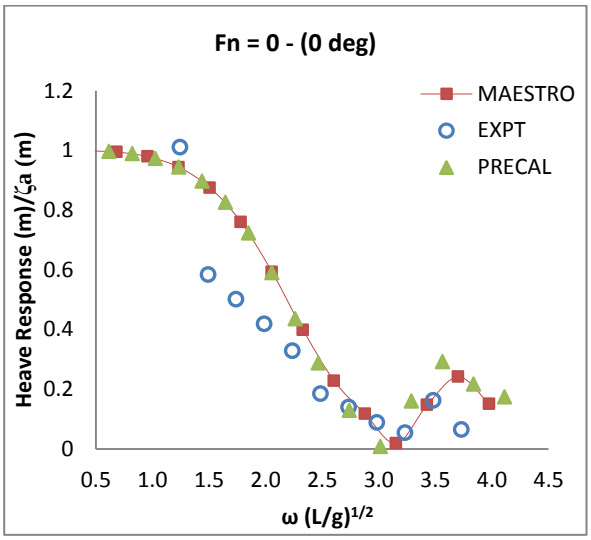

Figure 5.5: Heave motions response in Following Seas at Fn = 0

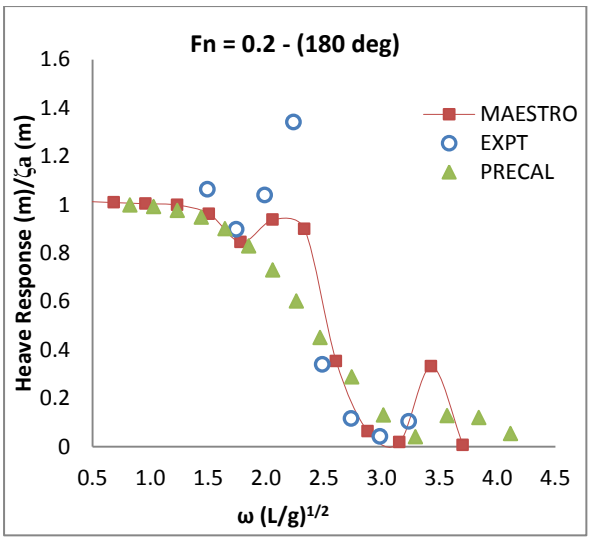

Figure 5.3: Heave motions response in Head Seas at Fn = 0.2

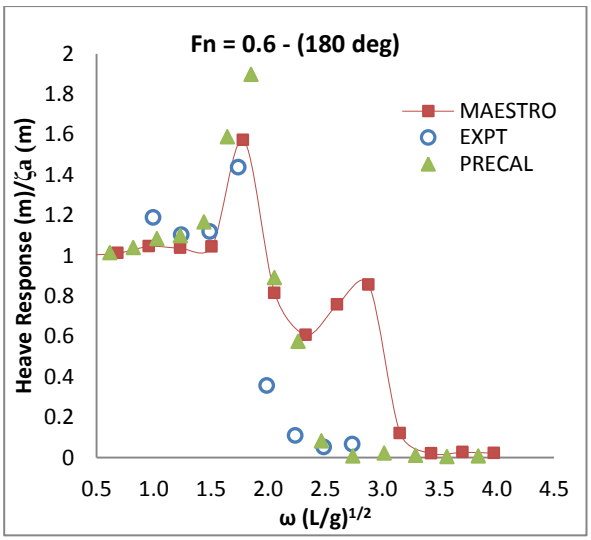

Figure 5.6: Heave motions response in Head Seas at Fn = 0.6

5.3.2 Roll Motions Comparison.

The comparison for the roll motion responses is limited to the zero speed condition because the model tests for roll motions in forward could not be measured due tank limitations. The roll responses for the experimental measurements have shown good correlation in the Beam Seas (Figure 5.8) and the Stern Quartering Seas (Figure 5.9) with those obtained from the numerical predictions. The magnitudes of the experimental results in the Bow Quartering Seas (Figure 5.7) and the Stern Quartering Seas reduce as the increase in frequency within the higher frequency range. Both of the numerical programs used correctly recorded the kinks which corresponds to the roll natural period in both the Bow Quartering Seas and the Stern Quartering Seas conditions.

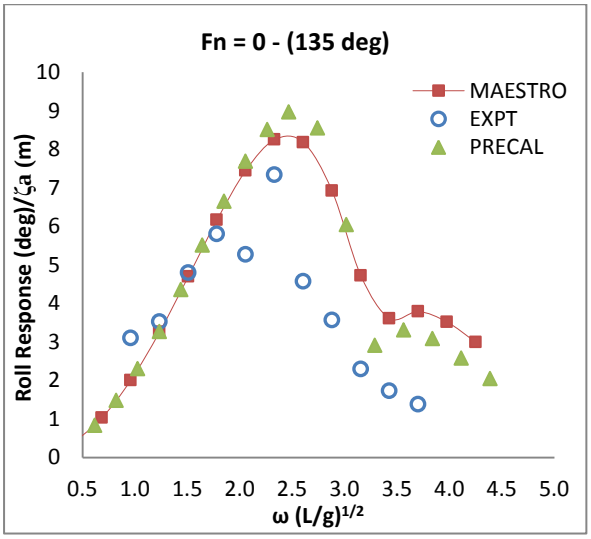

Figure 5.7: Roll motions response in Bow Quartering Seas

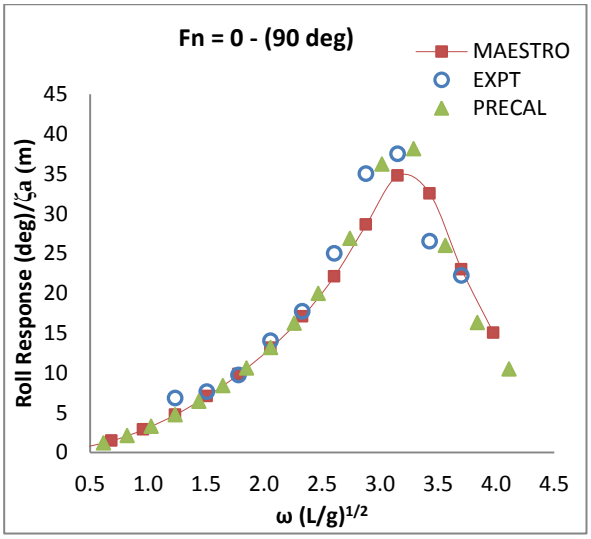

Figure 5.8: Roll motions response in Beam Seas

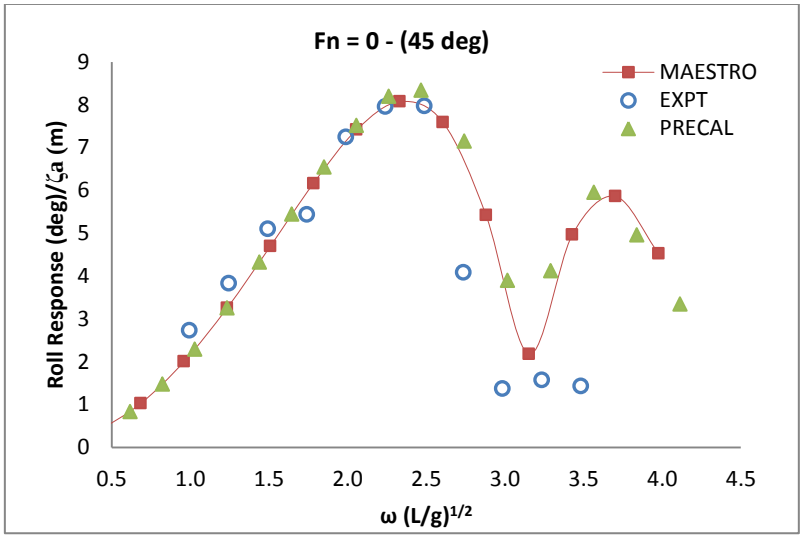

Figure 5.9 Roll motions response in Stern Quartering Seas

5.3.3 Pitch Motions Comparison

In the zero speed condition, Fn = 0, the trend of the pitch responses that have been measured using the numerical programs are in good agreement with each other and with the experimental responses. Their trend in zero speed condition (Fn = 0) in Head Seas (Figure 5.10) and the Following Seas (Figure 5.14) are similar in both the magnitude of the responses and the kinks corresponds to the pitch and heave natural frequencies. In the Bow Quartering Seas (Figure 5.13) and the Stern Quartering Seas (Figure 5.11) good agreement in the validation was achieved, but more specifically, at the lower frequency range (frequency of 0.5 to 2.5). As the frequency increases, the numerical programs appear to be slightly over-estimating the responses in the region of the natural frequencies of the vessel heave and pitch responses (or it could also be that the experimental underestimate the response within that range).

The comparison of the experimental and numerical pitch RAOs for the model speeds corresponding to Froude numbers Fn = 0.2 and Fn = 0.6 in the Following Seas and Head Seas is presented in Figure 5.12 and Figure 5.15 respectively. The trends of these results are equally in good agreement with the numerical codes' despite the fact that the experimental data in the Following Seas is limited to frequency range of 1.0 - 2.5. The two numerical programs correctly identify the two kinks whose frequencies are consistent with the peak heave motion response and the pitch resonance frequencies. This further affirms the presence of coupling of the pitch motions together with the motions of heave response.

In the comparison of pitch response for Fn =0.6 in the Head Seas, there appear to be a shift in the MAESTRO-Wave results away from both the experimental and the PRECAL results. This shift can be related to the formulation of the speed effects in these computer codes.

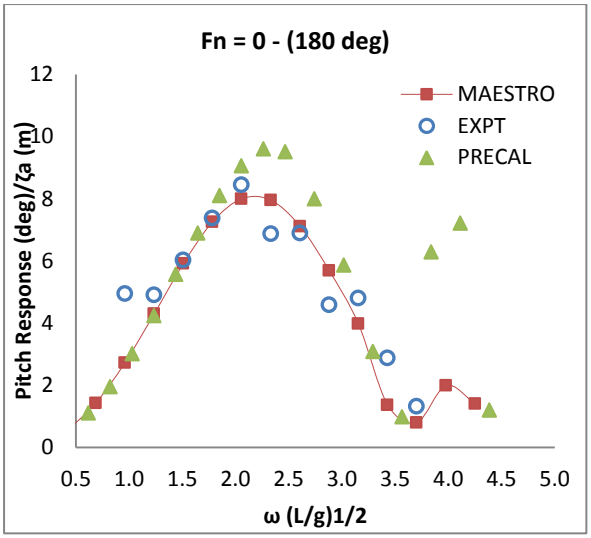

Figure 5.10: Pitch motions response in Head Seas at Fn = 0

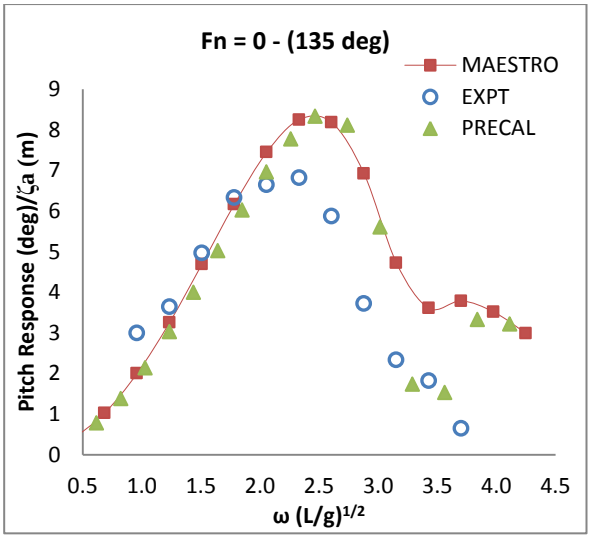

Figure 5.13: Pitch motions response in Bow Quartering Seas at Fn = 0

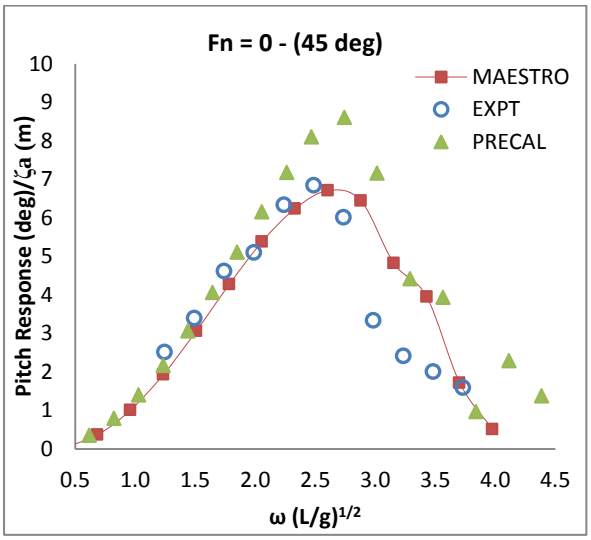

Figure 5.11: Pitch motions response in Stern Quartering Seas at Fn = 0

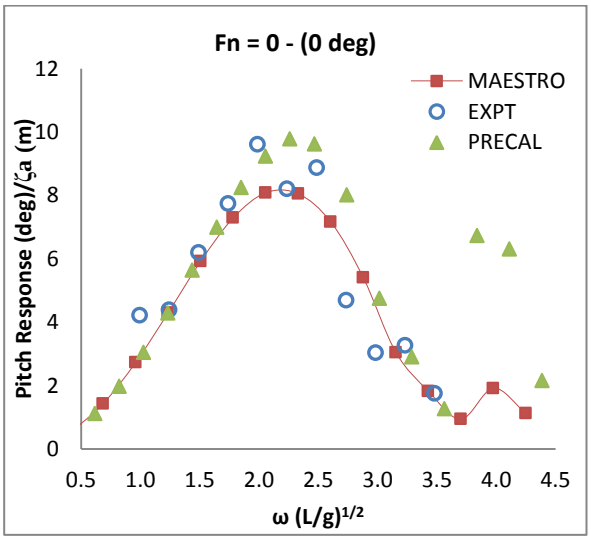

Figure 5.14: Pitch motions response in Following Seas at Fn = 0

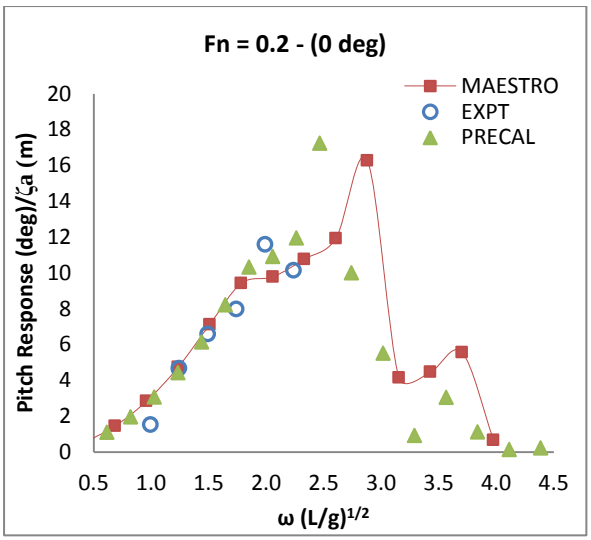

Figure 5.12: Pitch motions response in Following Seas at Fn = 0.2

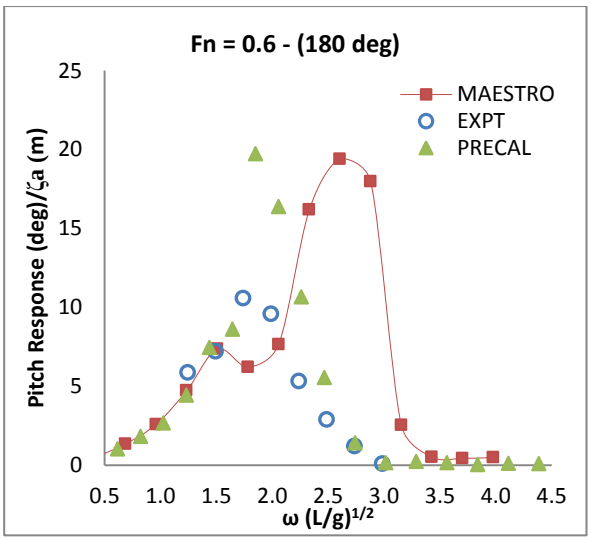

Figure 5.15: Pitch motions response in Head Seas at Fn = 0.6

5.4 Benchmark Studies 2: Experimental versus Numerical Wave-induced Loads Response Validations

The second benchmark studies compares the wave-induced shear forces obtained from both the towing tank experiment for vessel speeds of Fn = 0, Fn = 0.2 and Fn = 0.6 with the corresponding numerical predictions results using the MAESTRO-Wave program. The measured forces consist of the Longitudinal Shear force (Fx) and the Vertical forces (Fz) while the moments comprise of the Prying moment (Mx) and the Yaw Splitting moment (Mz) with some of the results already been published (Bashir *et al.*, 2013).

5.4.1 The Longitudinal Shear Force (Fx)

The trends of the Longitudinal Shear force (Fx) plots reveal a reasonably close agreement between the experimental measurement and the numerical predictions of this wave load. The results of the validation in the Head Seas (Figure 5.16) and the Bow Quartering Seas (Figure 5.17) show that the experimental measurement tends to predict higher responses than the numerical in these headings. In the Beam Seas (Figure 5.18) and the Stern Quartering Seas (Figure 5.19), the trends are generally in agreement at low to mid range frequency but the magnitudes of the experimental results reduce as the frequency increases to the higher range. Comparison of these responses, especially in the Bow and Stern Quartering Seas, highlights the dilemma that exist in the measurement and interpretation of the experimental wave loads at higher frequencies in the Oblique Seas as it has been reported by (Wellicome *et al.*, 1999; Thomas *et al.*, 2011).

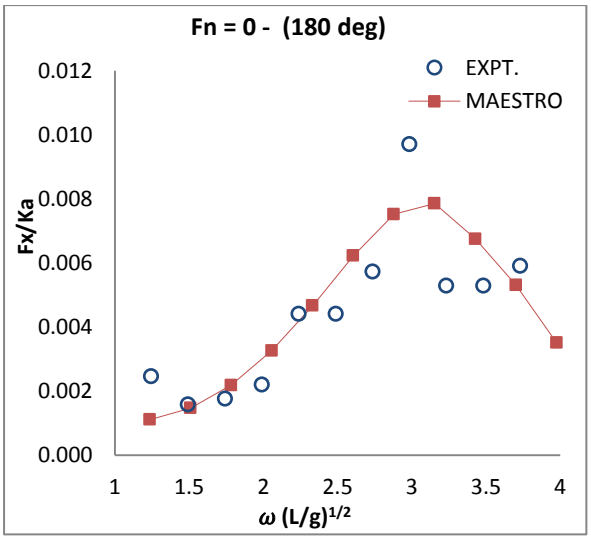

Figure 5.16: Comparison for Longitudinal Shear Force (Fx) in Head Seas (180°)

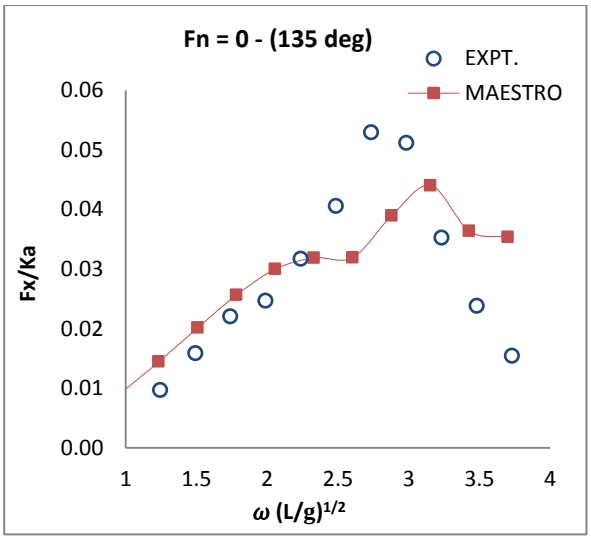

Figure 5.17: Comparison for Longitudinal Shear Force (Fx) in Bow Quartering Seas (135°)

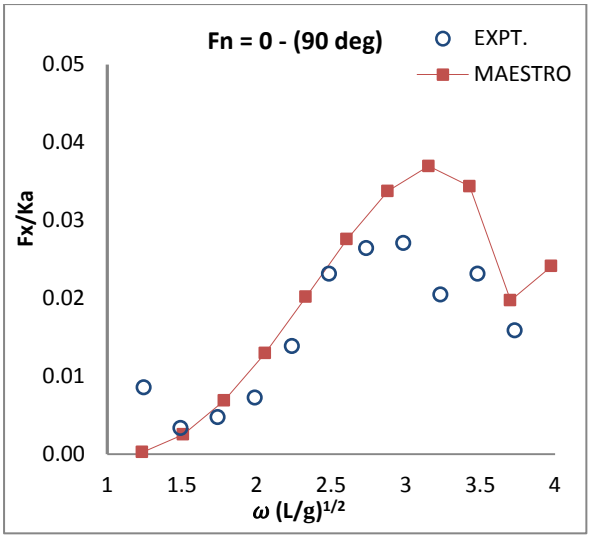

Figure 5.18: Comparison for Longitudinal Shear Force (Fx) in Beam Seas (90°)

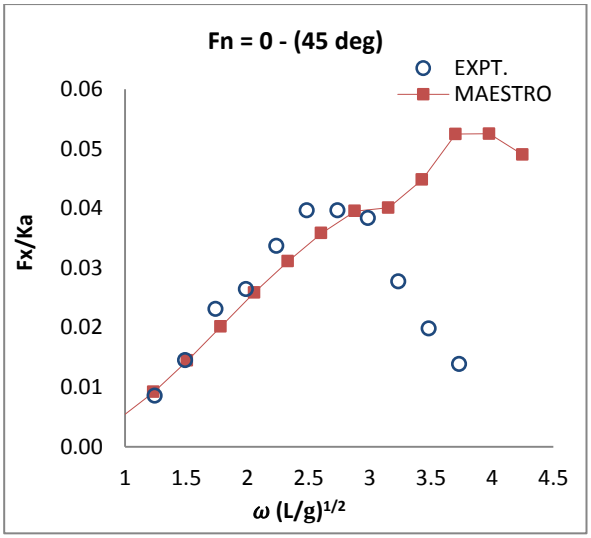

Figure 5.19: Comparison for Longitudinal Shear Force (Fx) in Stern Quartering Seas (45°)

5.4.2 The Vertical Shear Force (Fz)

The comparisons of the vertical shear force that have been measured in the four heading directions in zero speed condition and for a single heading in the forward speed condition are presented in the Figures below. The headings that have been considered in the measurements for zero speed, Fn =0, are the Head Seas (Figure 5.20), the Bow Quartering Seas (Figure 5.21), the Beam Seas, (Figure 5.22) and the Stern Quartering Seas (Figure 5.23) while the forward speed (Fn.= 0.2 and Fn = 0.6) was measured in the Head Seas only in Figure 5.24 and Figure 5.25.

The trends of the responses for zero speed (Fn = 0) show a very good agreement between the experimental measurement and also with the numerical predictions of the wave loads in all the headings presented with the exception of Beam Seas (Figure 5.22). The experimental results in the Beam Seas have been found to contain significant influence on the roll motions. This is so because the trend and the frequency of the peak responses for both the wave-induced loads and the motions response are consistently similar. The variation between these responses (Beam Seas) is very substantial and it renders the comparison as an outlier.

The results of the forward speeds comparison (Fn = 0.2 and Fn = 0.6), in the Head Seas are presented in Figure 5.24 and Figure 5.25 respectively. The trends of their responses for both of the heading directions are very similar except that the numerical program has shown some coupling with the pitch motion response. This is not entirely unexpected since if it accurately depicts the responses of the vessel in seaway.

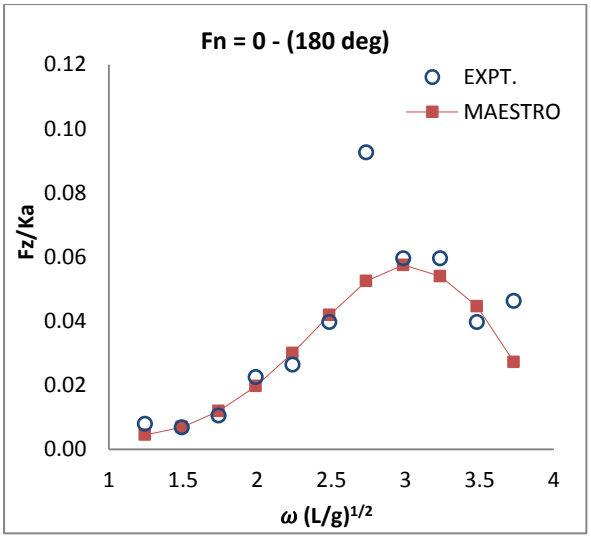

Figure 5.20: Comparison for Vertical Shear Force (Fz) in Head Seas (180°) at zero speed

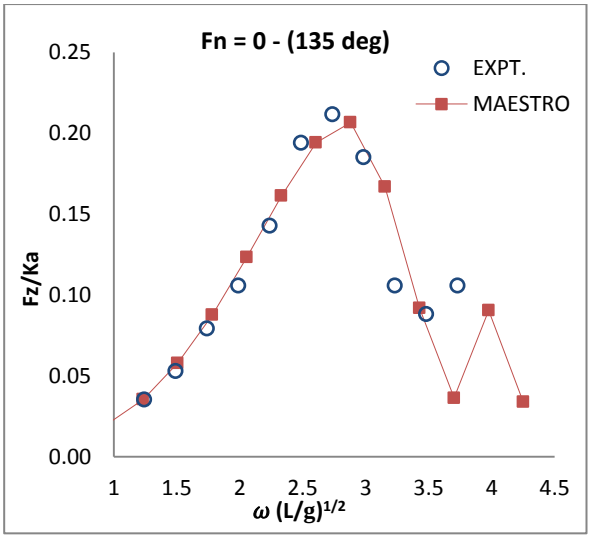

Figure 5.21: Comparison for Vertical Shear Force (Fz) in Bow Quartering Seas (135°) at zero speed

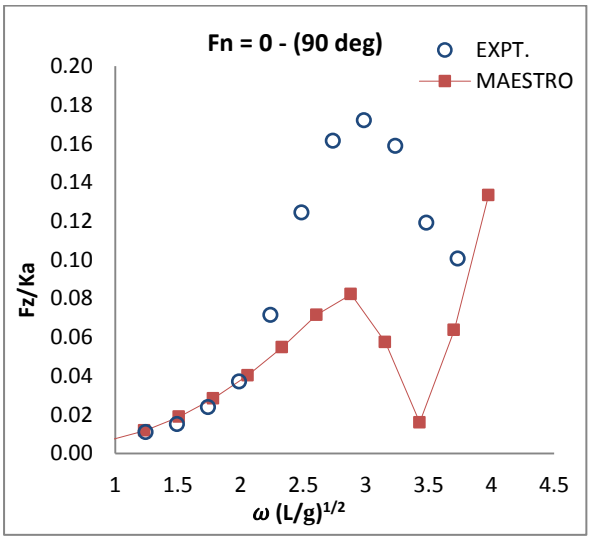

Figure 5.22: Comparison for Vertical Shear Force (Fz) in Beam Seas (90°) at zero speed

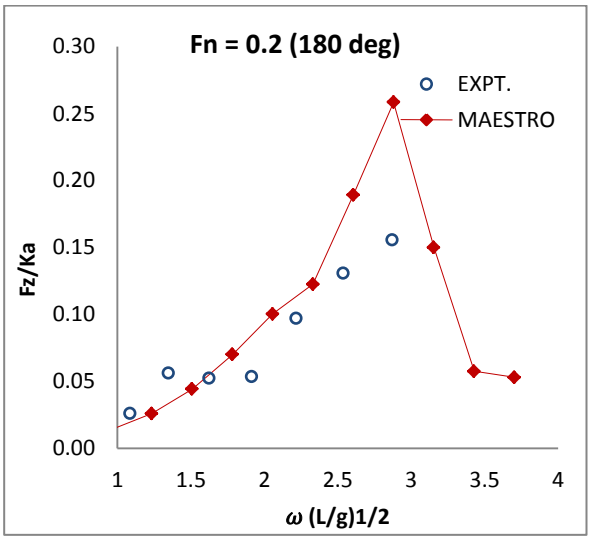

Figure 5.24: Comparison for Vertical Shear Force (Fz) in Head Seas (180°) at Fn = 0.2

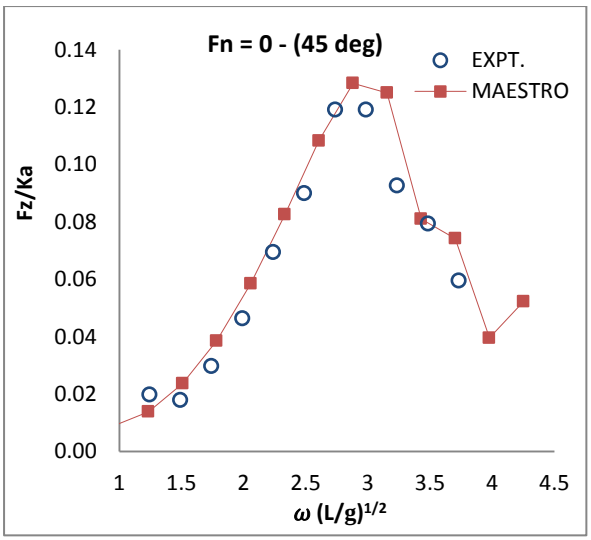

Figure 5.23: Comparison for Vertical Shear Force (Fz) in Stern Quartering Seas (45°) at zero speed

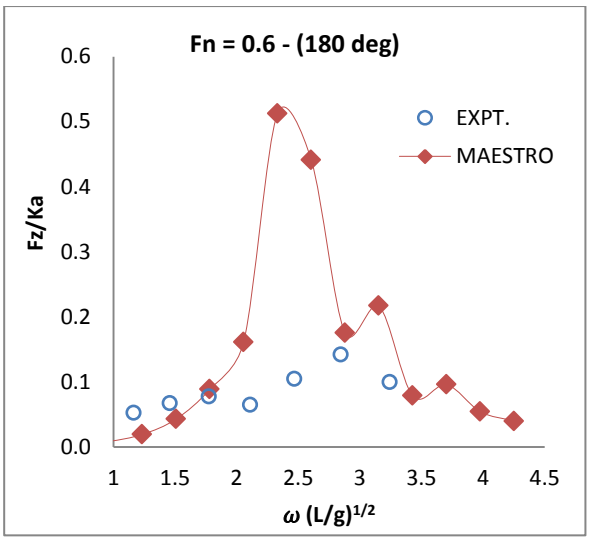

Figure 5.25: Comparison for Vertical Shear Force (Fz) in Head Seas (180°) at Fn = 0.6

5.4.3 The Prying (Mx) and Yaw Splitting Moments (Mz)

The results of the benchmark studies for the prying moments in three heading directions that have been identified as the source of the dominant load parameters are presented in the Bow Quartering Seas (Figure 5.26), Beam Seas (Figure 5.27) and the Stern Quartering Seas (Figure 5.28). The trends of these plots present some mixed results. There seem to be good agreement between the experimental and numerical responses in the Beam Seas but this correlation is not quite the same in other headings.

In the Bow and Stern Quartering Seas, in the plots of the numerical results a shift away from the experimental responses has been observed. Both the experimental and the numerical responses have a very similar peak magnitude but this peak in the Bow Quartering Seas is measured at different frequencies from that of thee experiment. This condition requires further study in order to accurately determine its cause.

The comparisons for the yaw splitting moment were also made for the three headings with the dominant load parameters. In addition to this, validation for the two forward speed cases (Fn = 0.2 and Fn = 0.6) in the Head Seas condition have been performed. The results of these comparisons are presented in Figure 5.29 – for Bow Quartering Seas for Fn = 0, Figure 5.30 – Beam Seas for Fn = 0 and Figure 5.31 – Stern Quartering Seas while Figure 5.32 represents Fn = 0.2 in the Head Seas and Figure 5.33 represents Fn = 0.6 in the Head Seas.

There seem to be good agreement between the trends of the responses for both the experimental and the numerical measurements in zero speed (Fn = 0). The magnitudes of both of these results are very close to each other, at least within the limit of the available experimental data. As for the forward speeds comparison (vessel speeds of Fn = 0.2 and Fn = 0.6), the trends are similar to those that been observed in the vertical shear force. Again, the plots of the numerical results contain some kinks at frequencies that are consistent with the peak pitch motions response. This condition shows the extent to which the coupling of the pitch motion responses influences the loads on catamaran in the Head Seas.

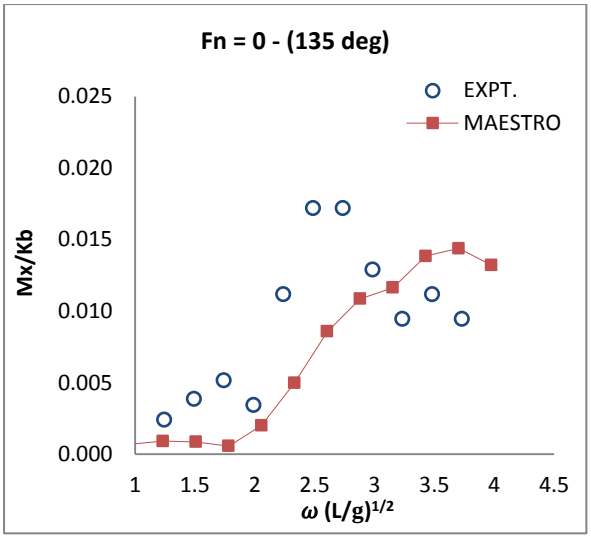

Figure 5.26: Comparison for prying moment (Mx) in Bow Quartering Seas (135°) at zero speed

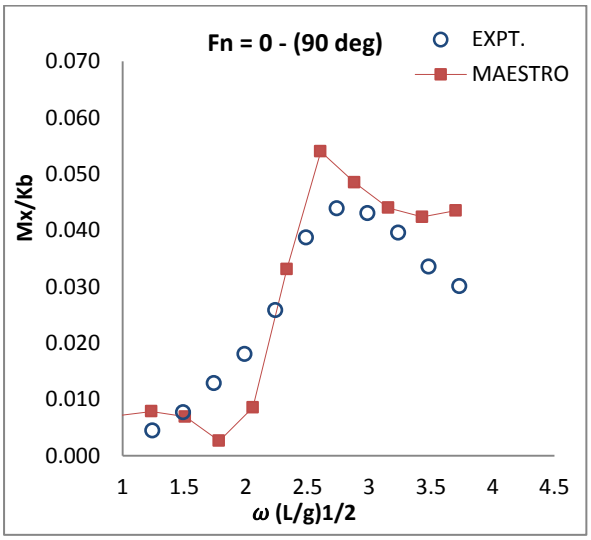

Figure 5.27: Comparison for prying moment (Mx) in Beam Seas (90°) at zero speed

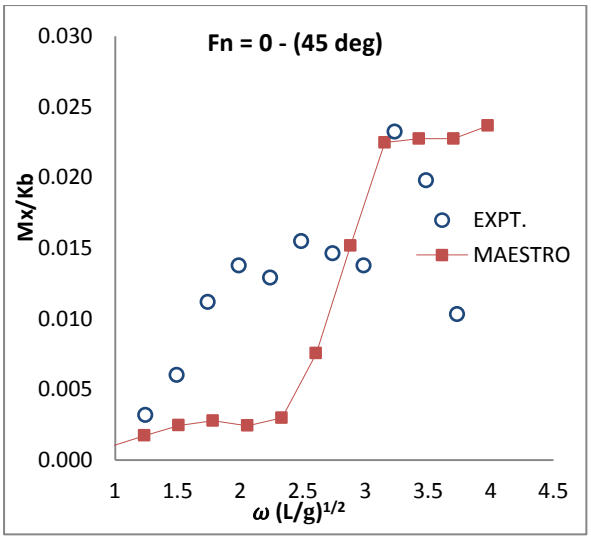

Figure 5.28: Comparison for prying moment (Mx) in Stern Quartering Seas (45o) at zero speed

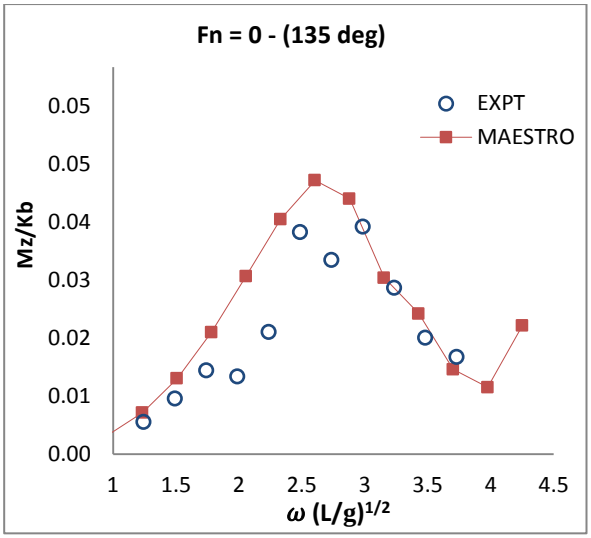

Figure 5.29: Comparison for Yaw Splitting moment (Mz) in Bow Quartering Seas (135°) at zero speed

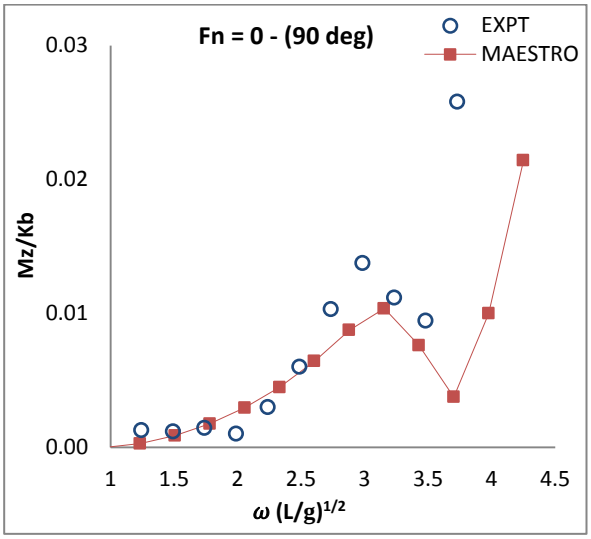

Figure 5.30: Comparison for Yaw Splitting moment (Mz) in Beam Seas (90°) at zero speed

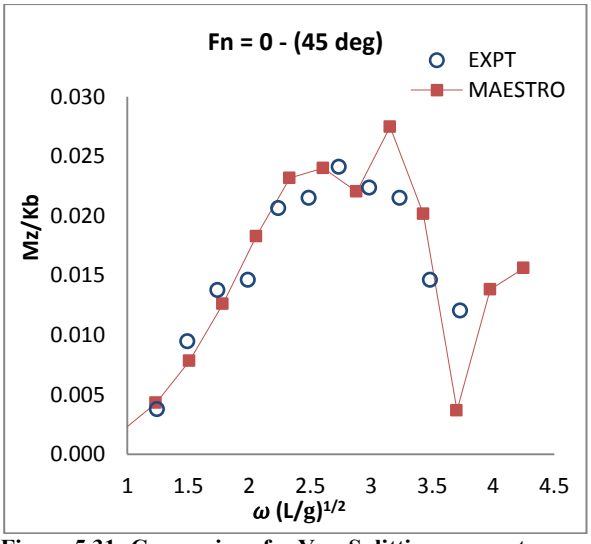

Figure 5.31: Comparison for Yaw Splitting moment (Mz) in Bow Quartering Seas (45°) at zero speed

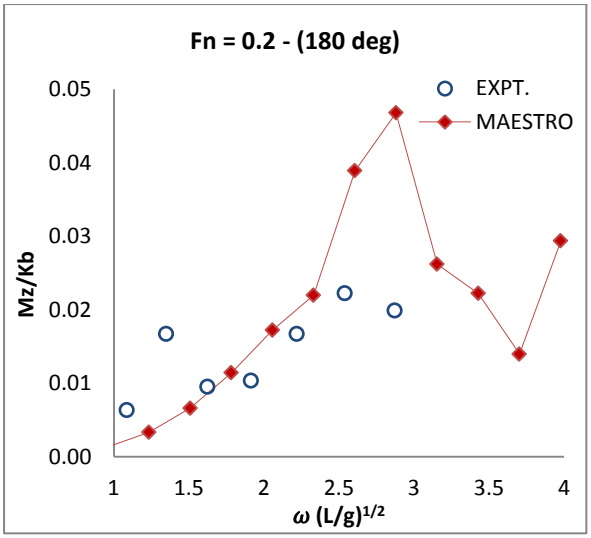

Figure 5.32: Comparison for Yaw Splitting moment (Mz) at Fn = 0.2 in Head Seas (180°)

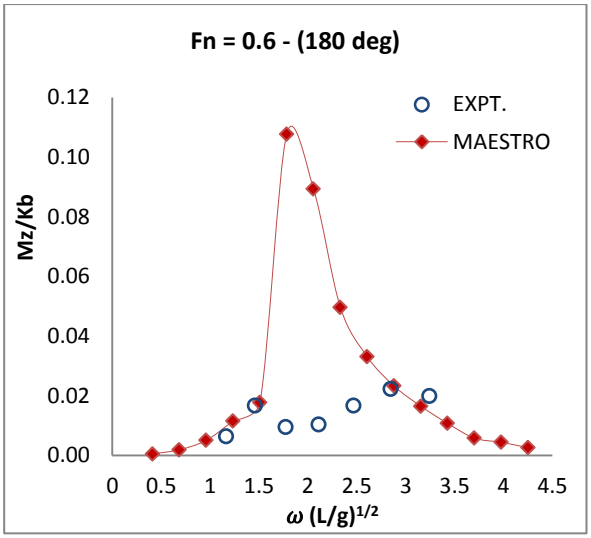

Figure 5.33: Comparison for Yaw Splitting moment (Mz) at Fn = 0.6in Head Seas (180°)

5.5 Benchmark Studies 3: DVC Model With and Without Appendage

The integrated skeg arrangement of the Princess Royal is quite a substantial appendages which was introduced to the vessel at later stages of the design in order to protect the vessel's propeller from potential grounding damage risk as well as to beach (dry out) the vessel securely. It is therefore appropriate to investigate the effect of this appendage arrangement on the motion responses of the vessel.

Furthermore, the proceeding Chapter of this thesis is intended to compare the motion and loads responses of the DVC with a round bilge hull form catamaran and hence it will be appropriate to make a decision on the inclusion of the appendages in the comparison or not For this reason, this section investigates the contributions of the appendage to the overall seakeeping performance of the DVC concept. MAESTRO-Wave and PRECAL numerical programs have been used in the prediction of the responses hence the need for the comparison of their results.

The results of the motion responses of the DVC model that is fitted with and without appendage are presented in Figure 5.34 – for Heave in the Head Seas at Fn = 0 and in Figure 5.35 – for the Heave in the Beam seas at Fn = 0. In addition, the results of the roll motions in Bow Quartering Seas at Fn = 0.4 (Figure 5.36) and in the Beam Seas at Fn = 0.6 (Figure 5.37), as well as for the pitch in the Bow Quartering Seas at Fn = 0 (Figure 5.38) and in the Head Seas at Fn = 0.6 (Figure 5.39) are presented. These results were obtained using the MAESTRO-Wave program and they have been compared with those that have been obtained from PRECAL using a DVC model without an appendage.

The trends of the responses for the model with and without the appendage are generally similar, irrespective of the heading and speed. The heave responses for the model without the appendage appear shift away from the rest of the plots as the frequency increases to higher frequency (≥2.0) in both of the Head Seas (Figure 5.34) and the Beam Seas (Figure 5.35).

The peak magnitudes of the roll and pitch responses for the model without the appendage are significantly higher than those for the model with appendage with forward speed in the Bow Quartering Seas (Fn = 0.4) and in the Beam Seas (Fn = 0.6). The differences in these responses represent some modest improvement in the seakeeping performance of the DVC model with appendage.

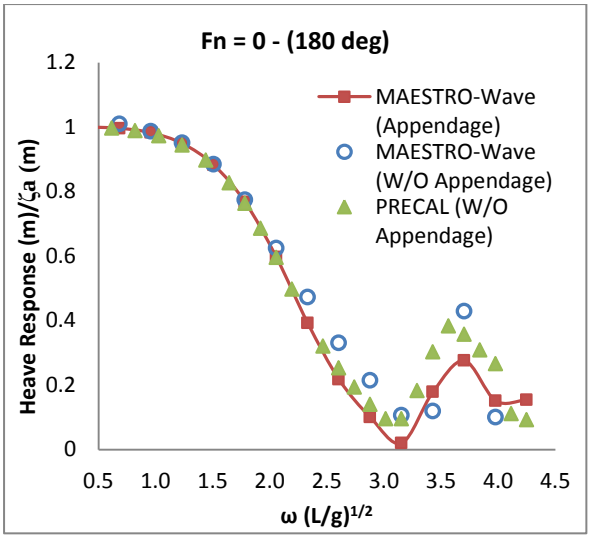

Figure 5.34: Heave motion comparison for models with and without appendage in Head Seas

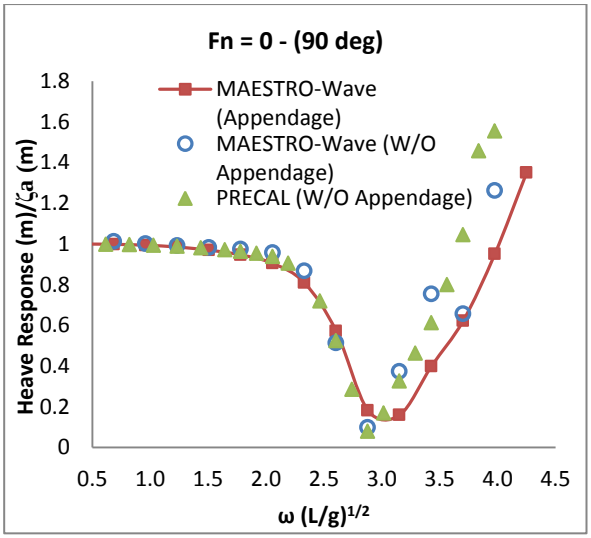

Figure 5.35: Heave motion comparison for models with and without appendage in Beam Seas

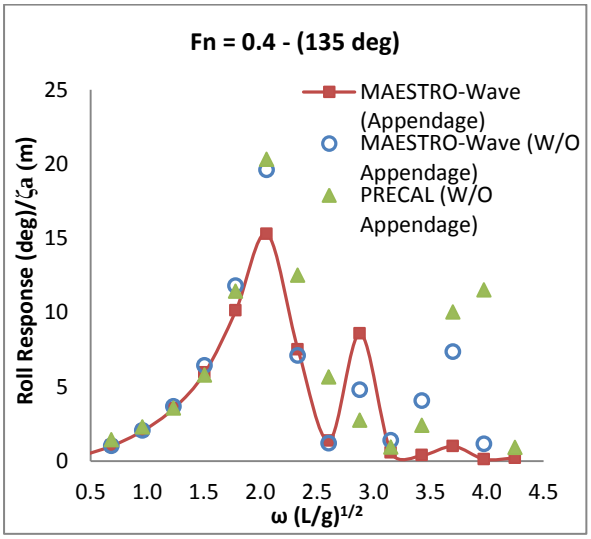

Figure 5.36: Roll motions comparison for models with and without appendage in Bow Quartering Seas

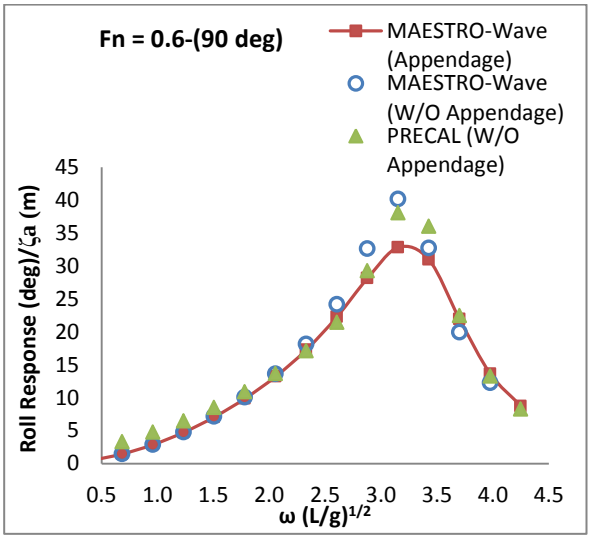

Figure 5.37: Roll motions comparison for models with and without appendage in Beam Seas

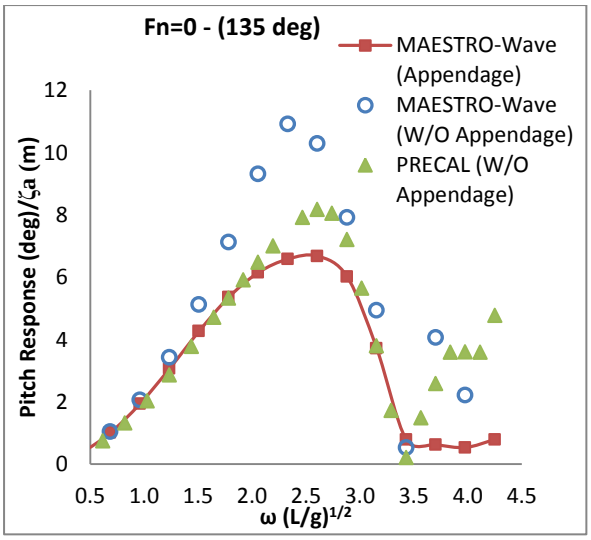

Figure 5.38: Pitch motion comparison for models with and without appendage in Bow Quartering Seas

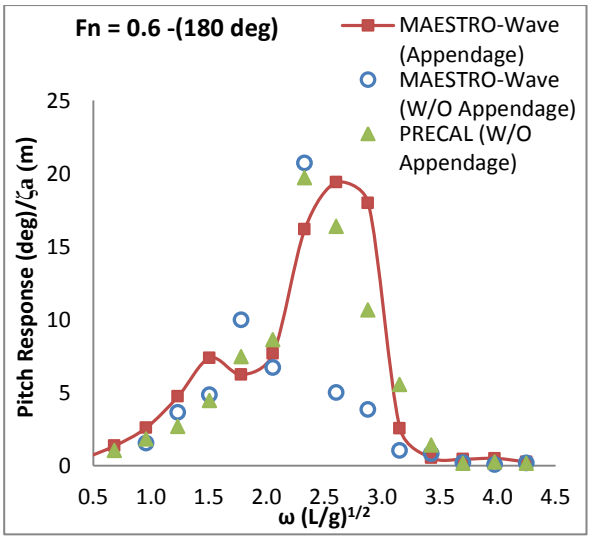

Figure 5.39: Pitch motion comparison for models with and without appendage in Head Seas

5.6 Conclusions

A validation of the responses for the motions and the wave-induced loads that have been measured in the towing tank experiments has been performed using the numerically predicted data for selected headings. This validation includes the comparison of the DVC model with and without the appendage. The following conclusions have been drawn up from the validation study:

1. In the entire comparisons, a good agreement was found between the results of the experimentally predicted motions and the wave-induced loads responses and those that have been predicted using the numerical codes. The agreement between the respective responses was particularly good within the non-dimensional frequencies range of 0.5 to 2.25.
2. The validation of the experimental motions confirmed that the selected numerical codes (the MAESTRO-Wave and the PRECAL) were able to predict the kinks that appeared in the experimental results, in both the zero speed and the forward speeds, correctly. However, there appear to be some irregular behaviour in the responses at higher frequencies ($\geq$3.0) from the numerical prediction results which needs to be further investigated.
3. The effect of changes in the vessel speed on the responses manifested in the form of a shift in the plots, especially the pitch motions response plots, in Head Seas and in the Prying moment response in the Bow Quartering Seas and the Stern Quartering Seas. This condition was observed in the response plots for the various vessel speeds in which the trends of the plots remain essentially the same but with changes in their peak magnitudes and the frequency at which they are recorded.
4. It has been found that the responses of the DVC model with appendage clearly yield lower responses than for the model without appendage. However, this difference in the responses only translates into some modest improvement in the seakeeping performance of the DVC model with appendage over the one without the appendage.
5. Overall, it has been established that the numerical tools can be relied upon to accurately predict the motion and wave-induced load response characteristics of the DVC model in the various wave conditions.

Chapter 6

Loads and Motions Response Analysis

6.1 Introduction

This chapter presents the analysis of numerical predictions of the motions and wave-induced loads acting on the Deep-V Catamaran (DVC) and its counterpart Round Bilge Catamaran (RBC) models. The objective of the chapter is to present the results of the motions response and wave-induced loads acting on these models and also to establish a direct basis for the comparisons of the hydrodynamic responses of the two models.

Section 5.1 presents an overview of the chapter while Section 5.2 provides a brief description of the numerical models, highlighting the basis for their comparison as well as their hydrostatic parameters. Section 5.3 presents the results of the numerically predicted motions response for the two models, and which also comprised of the detailed comparisons of these responses. In Section 5.4, the results and the comparisons of the numerical wave-induced loads for the two models are presented whilst Section 5.5 concludes the chapter.

6.2 Description of the Numerical Models

The Deep-V hullform vessel that has been used in this numerical study is the prototype of the RV Princess Royal vessel – a displacement-type hull form catamaran that was developed locally at Newcastle University by Mantouvalos (2009) based on the works of Atlar (1997b), Atlar et al(1998) and Haslam (1996). The model is fitted with an innovative anti-slamming bulbous bow, a stern tunnel and an extended skeg, which serves as appendage for improved stability.

The round bilge hull form is based on the benchmark semi-displacement NPL form (Bailey, 1976),developed at Southampton University by Insel and Molland in (1992) for applications in the design of catamaran but without a bulbous bow. The hullform is equally a displacement-type that is commonly used in the design of high speed (displacement) vessels.

A full scale of these two models were created using the MAESTRO Finite Element (FE) program (MAESTRO, 2012), for use in prediction of wave-induced responses using MAESTRO-Wave program. The code uses the FE mesh as the hydrodynamic panel element in the response predictions which has the advantage of ensuring equilibrium between the hydrodynamic panels and the FE mesh of the vessel in the structural analysis. It should be noted that the above waterline hull form of both Princess Royal and its counterpart the round bilge hull is assumed to be similar. However, their underwater hull forms are quite different with the Deep-V hull form concept having anti-slamming bulbous bow and an appendage.

The models consist of 1983 and 2232 hydrodynamic panel elements for the DVC and the RBC respectively. This panel elements represent the total wetted surface over which the hydrodynamic pressure induced on the vessel is predicted.

Both of these models were ballasted to a full scale displacement of 36.74tonnes, representing the light load departure condition of the actual vessel. Details of the masses used in the ballasting are presented in Table 6.1 while other hydrostatic parameters along with the radii of gyration of the two models are given in Table 6.2.

Table 6.1: Light load departure condition

Item	Total mass (kg)	LCG (m)	TCG (m)	VCG (m)
Lightship	36,935	7.74	-0.02	3.33
Crew	160	13.3	0	4.7
Passengers	0	9.8	0	4.2
Storage	250	8.9	0	3.5
Fuel (port side tank)	2,265	7.747	-2.470	1.231
Fuel (starboard side tank)	2,265	7.747	2.470	1.231
Waste water	40	7.9	1.95	1.722
Fresh water	400	7.0	2.55	2.097
Total	42,317	7.764	0.009	3.1

Table 6.2: The vessels hydrostatic parameters

	DVC Model	RBC Model
LOA	18.45m	18.80m
Bw	7.04m	7.12m
LCG	7.66m	7.66m
VCG	2.19m	2.19m
TCG	0.002m	0.009m
r_{xx}	0.35Bw	0.33Bw
r_{yy}	0.12LOA	0.12LOA
r_{zz}	0.12LOA	0.12LOA

6.3 Results of the Motions Response Prediction

The results of the numerical predictions of the motion responses for the **DVC** and its competing **RBC** models in various vessel headings with zero and forward speeds are presented in this section. These plots contain the responses due to four vessel speeds (Fn = 0, 0.4, 0.6 and 0.8 corresponding to 0kn, 10kn, 15kn, and 20kn) and in five heading conditions, namely, the Head Seas (180^o), the Bow Quartering Seas(135^o), Beam Seas, (90^o), the Stern Quartering Seas (45^o), and the Following Seas(0^o).The orientations of the axes of the plots for

the responses are similar to those that have been defined in section 4.5.3. The plots are for the results of the heave; roll and pitch motion responses of the two models, as explained in section 4.5.3.

6.3.1 DVC Motions Response Results

6.3.1.1 Heave Motions Response Amplitude Operator (RAO)

The results of the responses in the **Head Seas (180^o)** are presented in Figure 6.1. The behaviour of the plots is linear with respect to vessel speeds and their trend has shown some coupling with the pitch motions responses in the form of kinks". These kinks occurred are associated with the natural pitch motion responses at higher frequencies and shifts towards lower frequencies with different vessel speeds of Fn = 0.4, 0.6 and 0.8. The magnitudes of these kinks differ for the various vessel speeds of the model. These responses are nonlinear towards the end of the plots and in the region of higher frequencies. They are also similar to those that have been obtained in the **Following Seas (0^o)**

In the **Bow Quartering Seas (135^o)** and **Stern Quartering Seas (45^o), -** presented in Figure 6.2 and Figure 6.4 respectively, the responses are similar to each other but the **Bow Quartering Seas (135^o)** has higher response magnitudes than in the **Stern Quartering Seas (45^o)**. The plots of the responses for each of the vessel speeds contain kinks whose frequency is different from the kinks of other vessel speeds.

The plots of the responses in the **Beam Seas** (**90^o**) are presented in Figure 6.3. Their behaviour in this heading is almost constant with respect to the vessel speeds as expected since the speed does not affect the responses in the Beams Seas conditions.

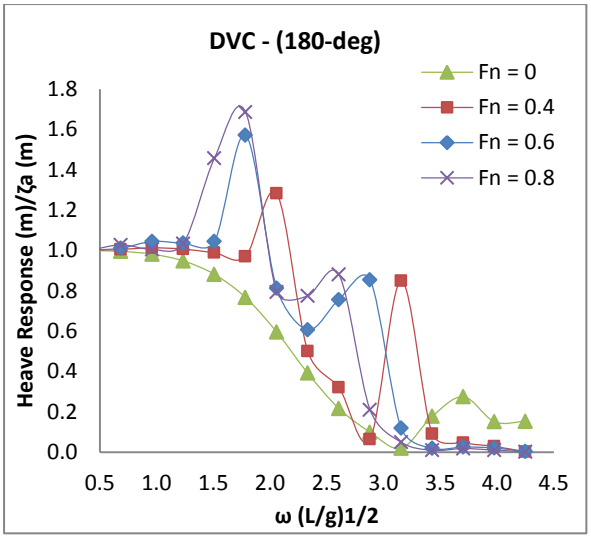

Figure 6.1: DVC numerical heave motion response in Head Seas

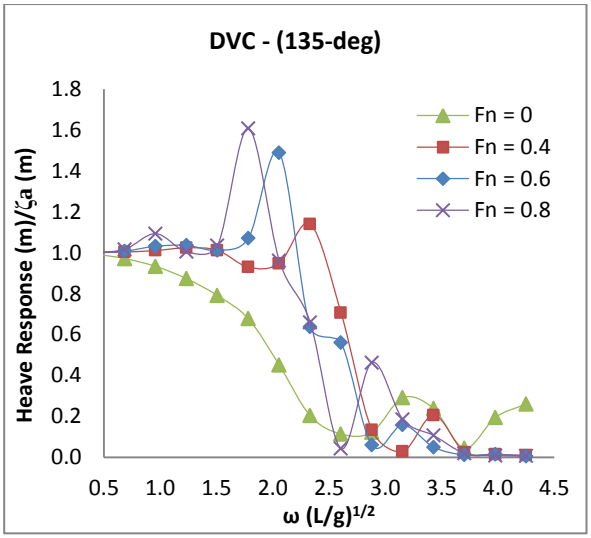

Figure 6.2: DVC numerical heave motion response in Bow Quartering Seas

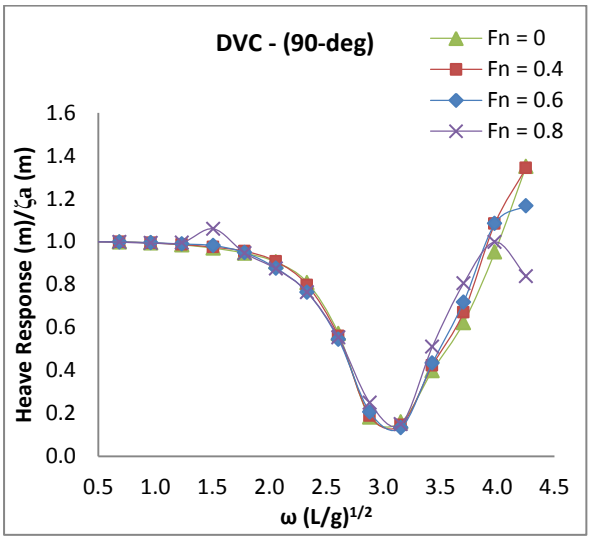

Figure 6.3: DVC numerical heave motion response in Beam Seas

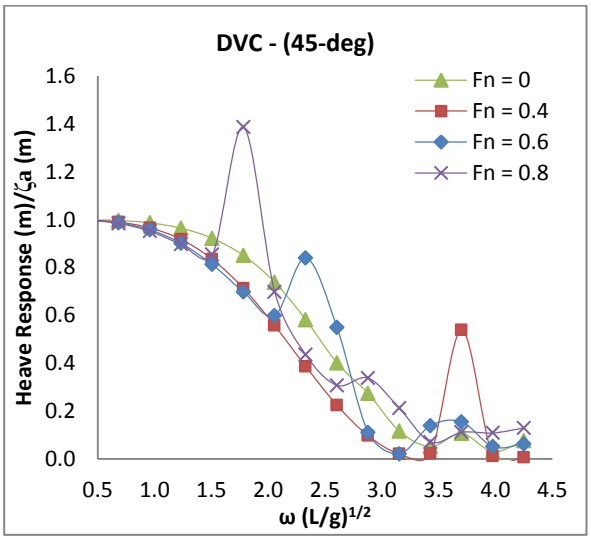

Figure 6.4: DVC numerical heave motion response in Stern Quartering Seas

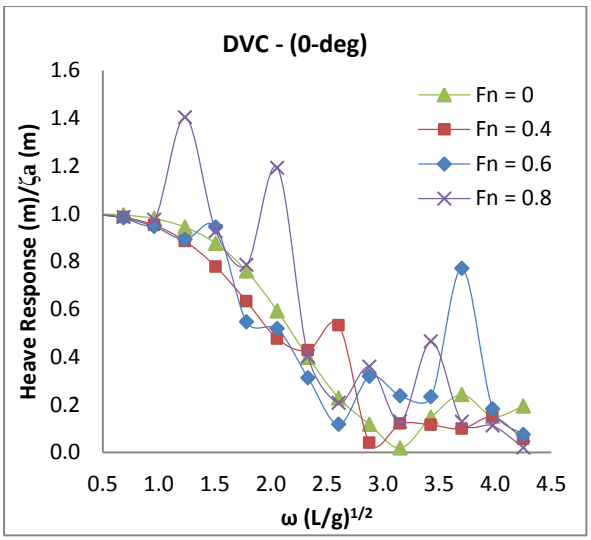

Figure 6.5: DVC numerical heave motion response in Following Seas

6.3.1.2 Roll Motions Response Amplitude Operator (RAO)

The plots of the roll motion responses in the **Bow Quartering Seas (135^o)** are presented in Figure 6.6. The trend of the plots is generally nonlinear, especially when the vessel speeds increase from Fn = 0 to Fn = 0.8 due to the effect of the natural frequencies. The responses for the forward speed cases contain some kinks in their plots for individual vessel speeds. In contrast, the responses in the **Stern Quartering Seas (45^o) -** Figure 6.7 are mildly nonlinear and they contain fewer kinks than in the **Bow Quartering Seas (135^o).** The **Bow Quartering Seas (135^o)** has higher magnitudes of response than does the **Stern Quartering Seas (45^o)**.

The plots in the **Beam Seas (90^o) -** Figure 6.8**,** are predominantly linear and they have not shown any particular feature of interest. The responses are found to be insensitive to the vessel speeds, and the condition is similar to what has been observed in the heave motions response plots in the **Beam Seas (90^o).**

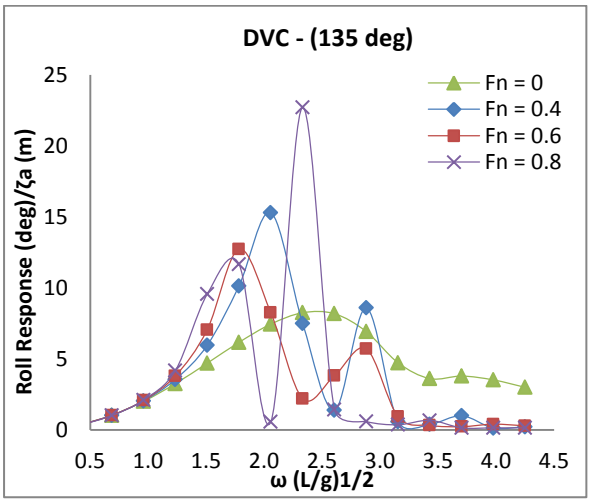

Figure 6.6: DVC numerical roll motions response in Bow Quartering Seas

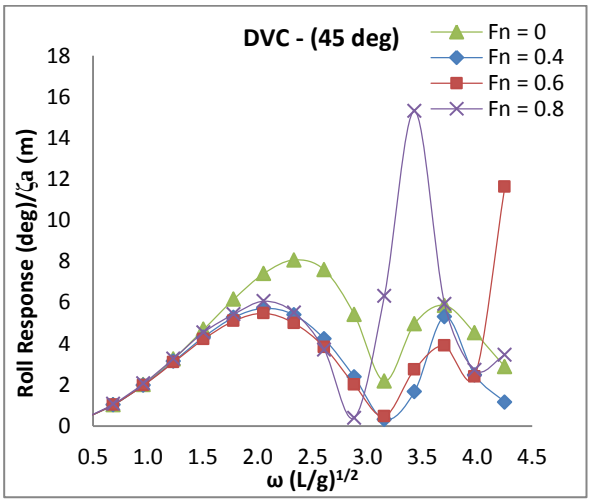

Figure 6.7: DVC numerical roll motions response in Stern Quartering Seas

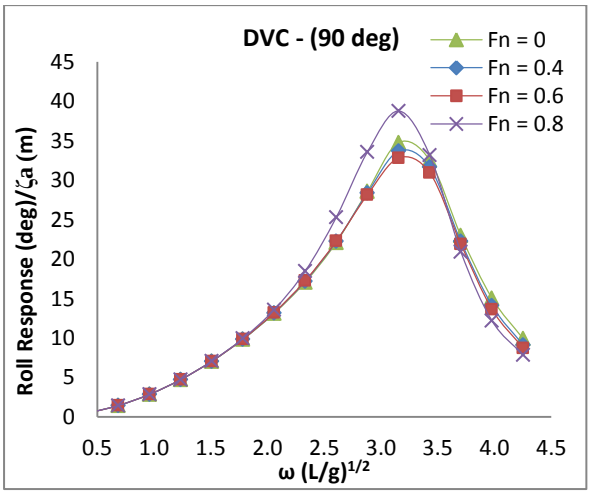

Figure 6.8: DVC numerical roll motions response in Beam Seas

6.3.1.3 Pitch Motions Response Amplitude Operator (RAO)

The plots of the pitch motion responses in the **Head Seas (180^o)** are presented in Figure 6.9. Their trend is nonlinear and the interactions between these motion responses and the resonant pitch are quite visible in the form of kinks. Some of these kinks are a direct manifestation of the resonance effects on the model. This is because the kinks' frequencies are similar to the resonant frequencies of the model. In addition, the effect of increase of the vessel speed is another reason for some of the kinks. A relatively gradual increase in the magnitudes of the responses at higher frequencies was observed.

In the **Bow Quartering Seas (135^o),** the responses are nonlinear as shown in Figure 6.10**.** The plots contain some kinks whose numbers and magnitudes increase as the vessel speeds increase. The responses due to Fn = 0.6 and Fn = 0.8 (which corresponds to the vessel cruise and top speeds), in particular, have the higher peak responses.

The pitch motions response plots in the **Beam Seas** (**90^o**) are presented in Figure 6.11. Unlike in the previous headings, the responses are somewhat nonlinear, especially at higher frequency ($\geq$ 3.0). However, the magnitudes of the responses of the vessel in this heading are smaller than those that have been obtained for pitch in other vessel modes. This change in trend is a clear demonstration of the effect of heading on the pitch motions response when vessel is in this mode.

The responses in the **Stern Quartering Seas (45^o)** are presented in Figure 6.12. While these plots have shown similar trend as in the plots for **Bow Quartering Seas (135^o),** –in terms of increase in their magnitudes when the vessel speed increases – but they have lower magnitudes when compared to the Bow Quartering Seas. The behaviour of the pitch response plots in this vessel mode is nonlinear at higher frequency.

The heave responses plots in the **Following Seas (0^o)** – Figure 6.13, are slightly different from those that have been obtained in other heading conditions. There is a rapid change in the linearity of the responses when the vessel speed increases. These responses become somewhat erratic at higher speed, especially when the vessel speed is equals to Fn = 0.8. The plots contain some mild kinks in responses for vessel speeds of up to Fn = 0.6, however, the response due to vessel speed of Fn = 0.8 contained three high magnitudes kinks. This suggests that the vessel's behaviour at higher speed is subject to interference from resonance or other external influences.

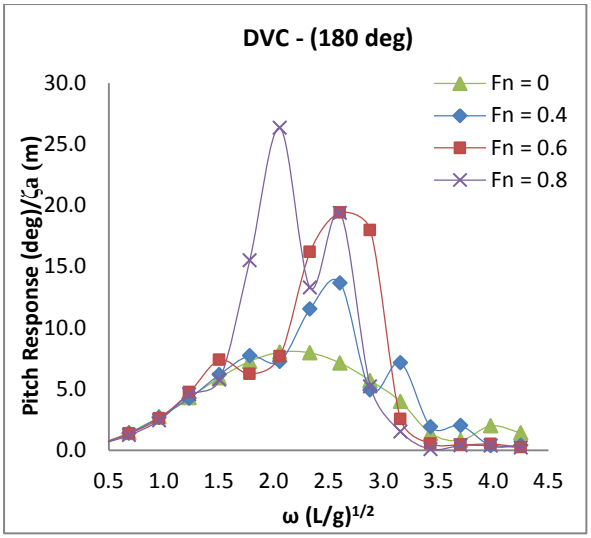

Figure 6.9: DVC numerical pitch motions response in Head Seas.

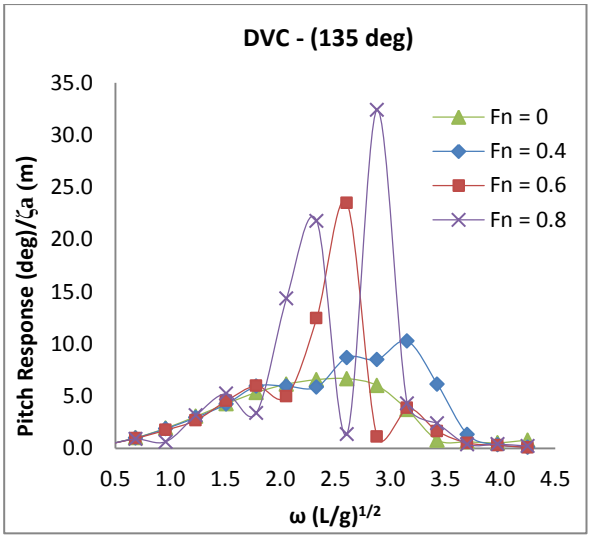

Figure 6.10: DVC numerical pitch motions response in Bow Quartering Seas.

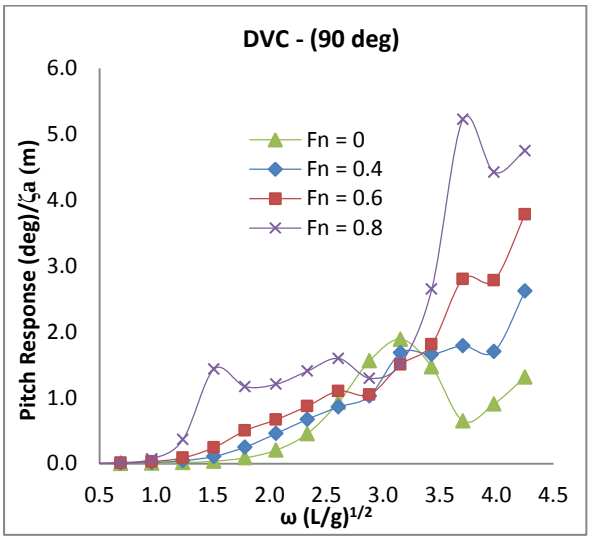

Figure 6.11: DVC numerical pitch motions response in Beam Seas

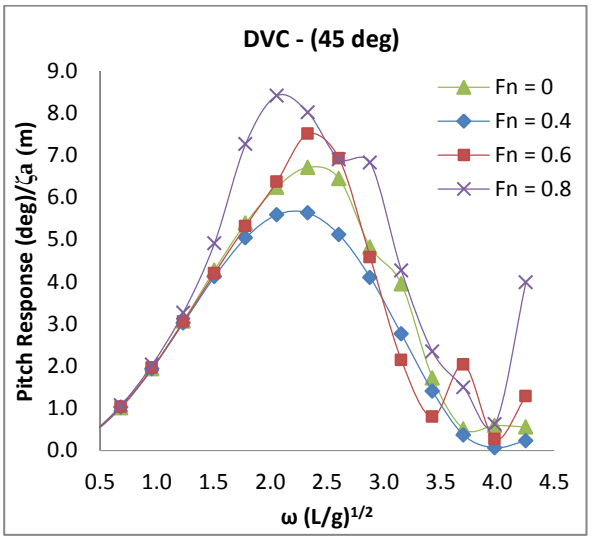

Figure 6.12: DVC numerical pitch motions response in Stern Quartering Seas.

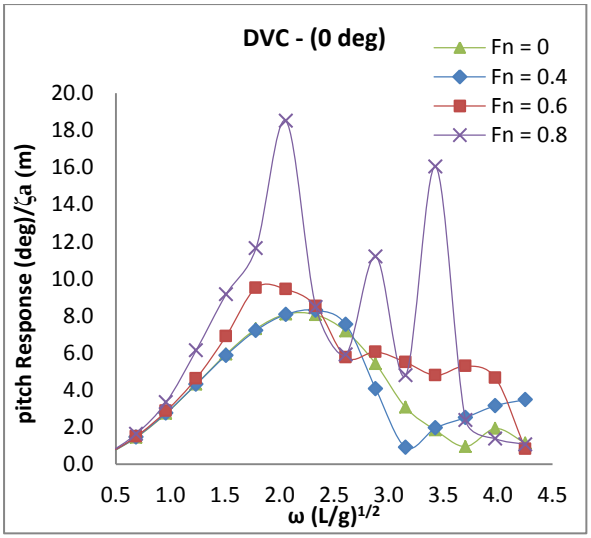

Figure 6.13: DVC numerical pitch motions response in Following Seas

6.3.2 RBC Motions Response Results

6.3.2.1 Heave Motions Response Amplitude Operator (RAO)

The heave motions response plots in the **Head Seas (180^o)** are presented in Figure 6.14. These plots contain some visible "kinks" on the individual responses within a frequency range of 1.2 – 3.0. The kinks are due to the coupling of the heave and pitch motion responses at their respective frequencies for the responses due to the various vessel speeds. The magnitudes of these kinks occurred at the same frequencies as the peak magnitudes of responses.

Figure 6.15 presents the plots of the responses in the **Bow Quartering Seas (135^o).** The trend of the plots is somewhat similar to those that have been observed in the **Head Seas (180^o)** except for the number and magnitude of kinks that were recorded in this heading. The responses are nonlinear within the frequency range of 2.3 -4.5 with respect to the vessel speeds.

The responses in the **Beam Seas** (**90^o**) are presented in Figure 6.16. Their plots show that they are largely linear in behaviour with respect to the vessel speeds and they are also not sensitive to changes in the vessel speeds. A similar phenomenon has been observed in the motion responses in the **Beam Seas** (**90^o**) for other vessel modes.

In the **Stern Quartering Seas (45^o),** the plots (Figure 6.17) contain some kinks which occurred at higher frequencies. The only exception this is in the responses due to speed of Fn = 0.8 where more than a kinks was identified. The magnitudes of these responses are much smaller than in the **Bow Quartering Seas (135^o)** which indicates the effects of change in the headings on the results.

The plots in the **Following Seas (0^o)** (Figure 6.18) bear some semblance to those observed in the **Stern Quartering Seas (45^o).** This result is in direct contrast to those that have been recorded in the responses for the **DVC** model, where the responses were observed to be similar to those in the **Head Sea (180^o)** of that particular vessel mode**.** However, just like in the DVC model, these responses are also highly nonlinear and the cause of this nonlinearity needs to be investigated.

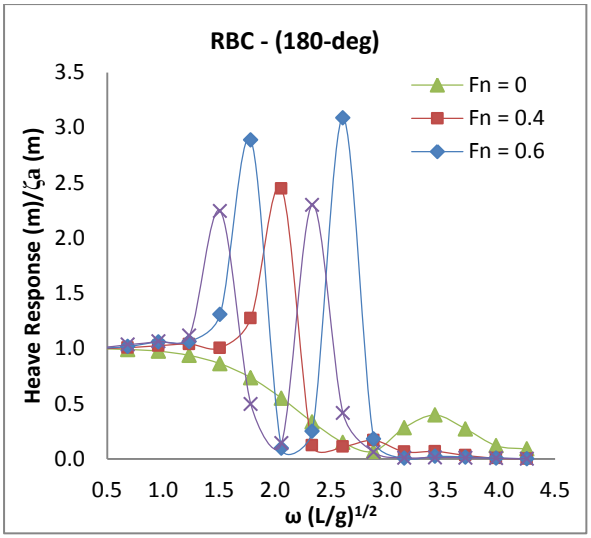

Figure 6.14: RBC numerical heave motion response in Head Seas

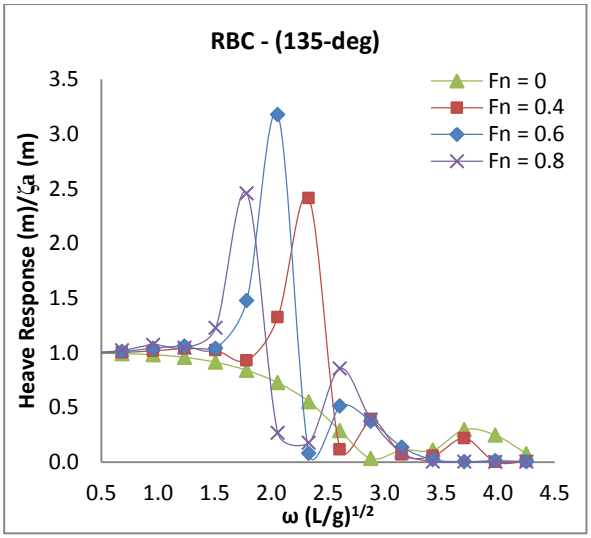

Figure 6.15: RBC numerical heave motion response in Bow Quartering Seas

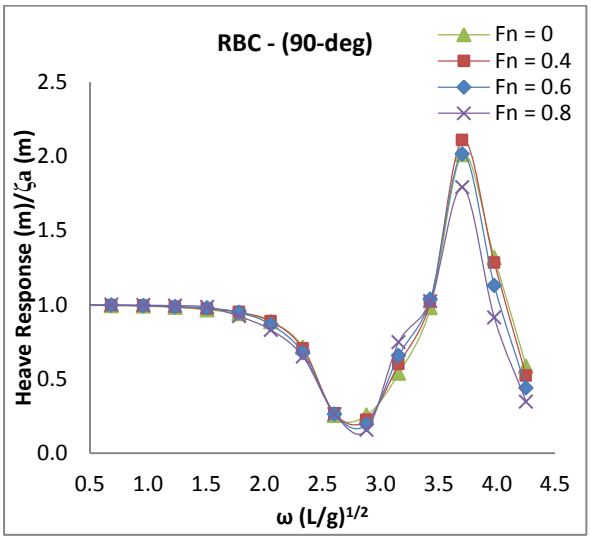

Figure 6.16: RBC numerical heave motion response in Beam Seas

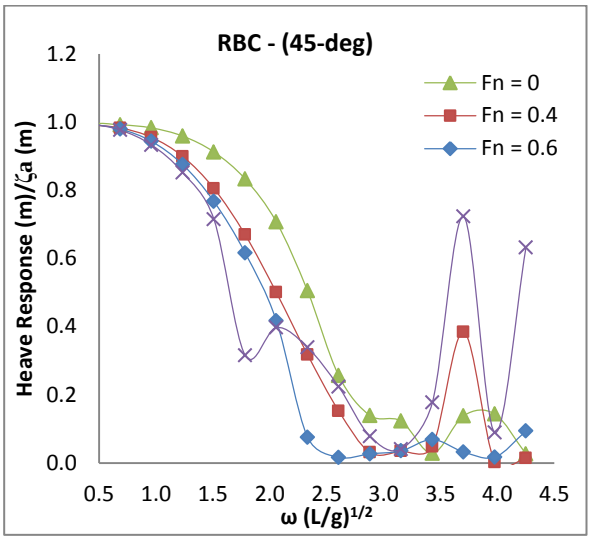

Figure 6.17: RBC numerical heave motion response in Stern Quartering Seas

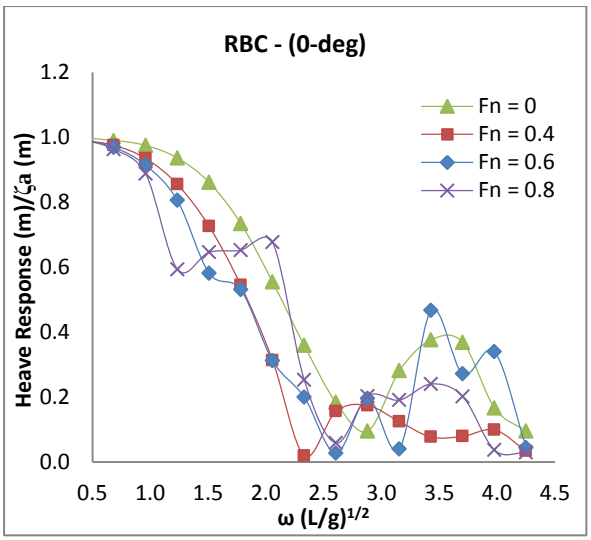

Figure 6.18: RBC numerical heave motion response in Following Seas

6.3.2.2 Roll Motions Response Amplitude Operator (RAO)

The roll motion response plots in the **Bow Quartering Seas (135^{o})** are presented in Figure 6.19. The behaviour of these plots is similar those observed in the same condition for the DVC model. The responses are nonlinear when the vessel speeds increases. The plots contain some kinks in the responses for the individual vessel speeds, seemingly due to the coupling of the roll motions with the pitch responses. This scenario suggests the likely occurrence of parametric rolling. The responses in the **Stern Quartering Seas (45^{o}) -** Figure 6.20 were initially linear but then become nonlinear when frequency reaches 2.0. They plots contain fewer kinks with lower response magnitudes than in the **Bow Quartering Seas (135^{o}).** The plots of the responses in the **Beam Seas (90^{o}) -** Figure 6.21, have a linear trend with no any distinct features. Again, they appear to be insensitive to changes in the vessel speeds.

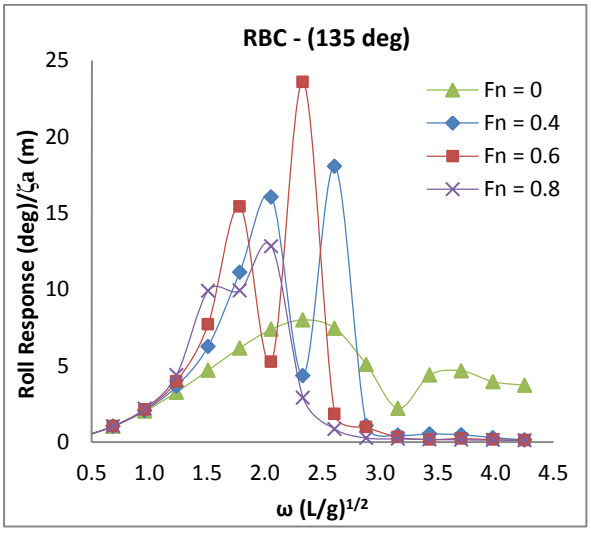

Figure 6.19: RBC numerical roll motion response in Bow Quartering Seas

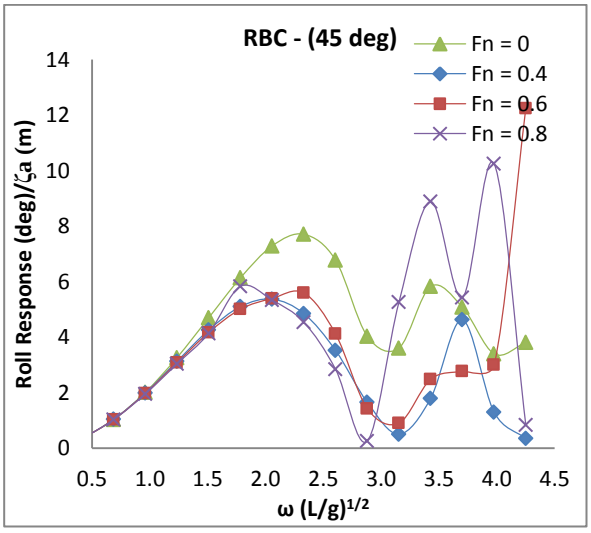

Figure 6.20: RBC numerical roll motion response in Stern Quartering Seas

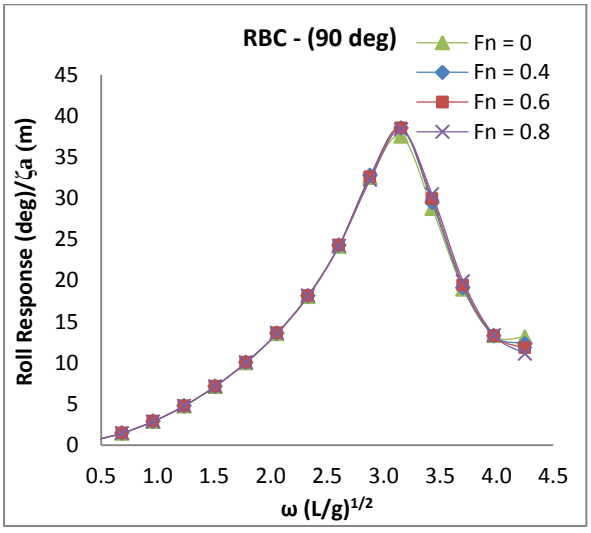

Figure 6.21: RBC numerical roll motion response in Beam Seas

6.3.2.3 Pitch Motions Response Amplitude Operator (RAO)

The pitch motion responses in the **Head Seas (180^o)** are presented in Figure 6.22. Their trend is nonlinear with respect to vessel speeds. The plots contain kinks that indicate the presence of coupling between the pitch and heave motions responses. These kinks are mainly distributed within a narrow frequency band than in the other responses that have been predicted in the **DVC** model. The top two vessel speeds (Fn = 0.6 and Fn = 0.8) have peak magnitudes of the responses that are significantly higher than in the other vessel speeds.

The plots in the **Bow Quartering Seas (135^o)** are also nonlinear as can be seen in Figure 6.23**.** The response due to vessel speed of Fn = 0.4, in particular, has higher magnitude of response than those due to the vessel's cruise speed of Fn = 0.6. These plots contain kinks whose peak magnitudes are not in any way proportional to the increase in the vessel speeds in which they occur.

In the **Beam Seas** (**90^o**), the pitch motions response plots which are presented in Figure 6.24 are relatively linear. The plots for the responses due to the individual vessel speeds are clearly detached from each other. The magnitudes of the responses also increase with increase in the vessel speeds.

The plots of the response in the **Stern Quartering Seas (45^o)** are presented in Figure 6.25. The behaviour of these plots is relatively linear with respect to the vessel speeds. The trend of the responses is quite opposite to those observed in the **Bow Quartering Seas (135^o)** since the responses in the **Stern Quartering Seas (45^o)** contain fewer (or none) kinks. The effects of vessel speeds on these responses are equally very mild because of the low magnitudes of responses that have been recorded as well as the lesser coupling effect in relation to the natural frequencies.

Figure 6.26 presents the plots of the response in the **Following Seas (0^o).** There is a clear distinction between these responses and those that have been recorded in the **DVC** model. These responses are slightly linear at lower frequency range but then gradually changed to nonlinear at higher frequencies when compared to those in the aforementioned model. The effect of vessel speeds on the responses are visible in the form of variation in their magnitudes due to the speeds of Fn = 0.6 and Fn = 0.8. The plots contain some kinks but at much higher frequencies than have been observed in the entire response plots in this study.

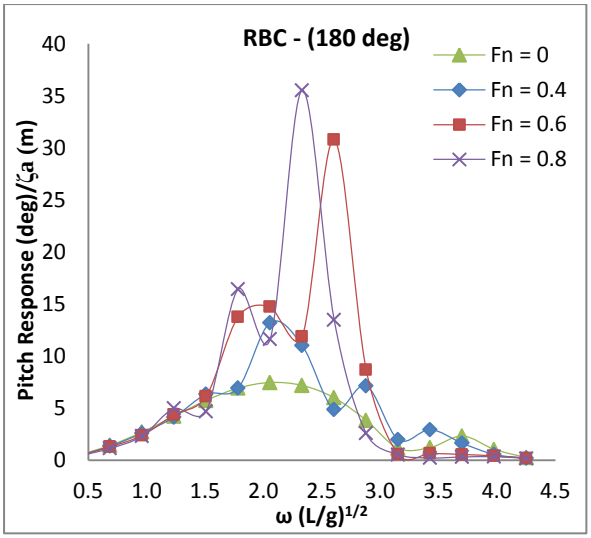

Figure 6.22: RBC numerical pitch motion response in Head Seas

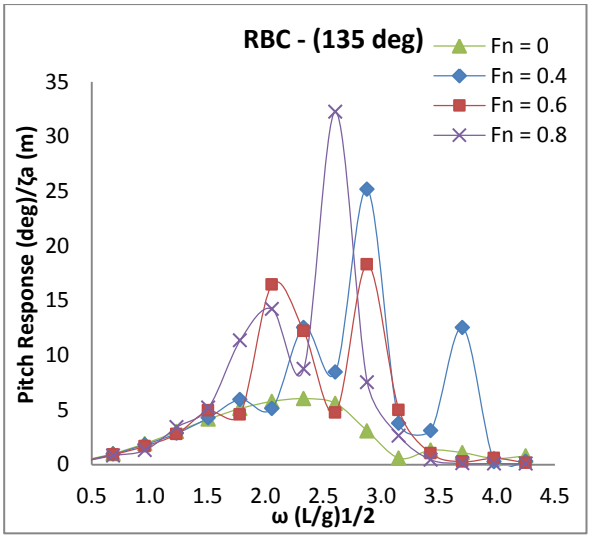

Figure 6.23: RBC numerical pitch motion response in Bow Quartering Seas

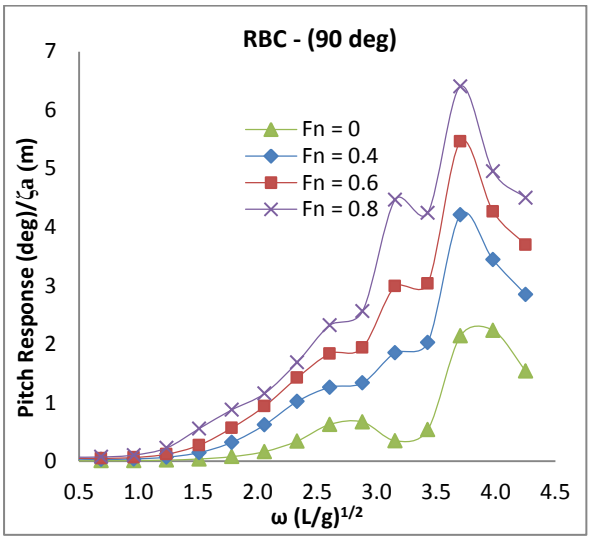

Figure 6.24: RBC numerical pitch motion response in Beam Seas

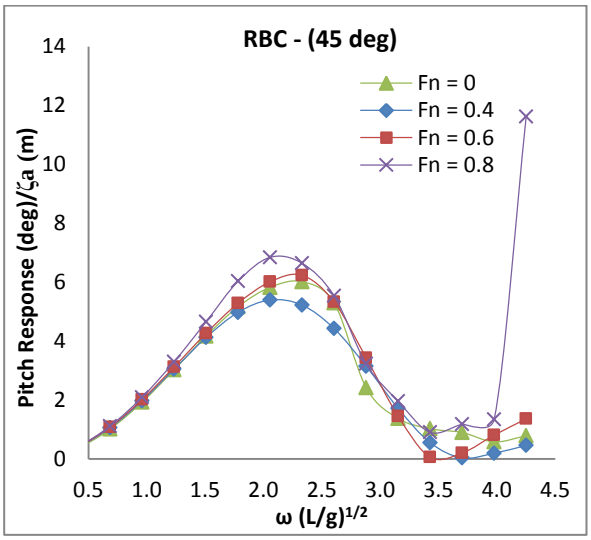

Figure 6.25: RBC numerical pitch motion response in Stern Quartering Seas

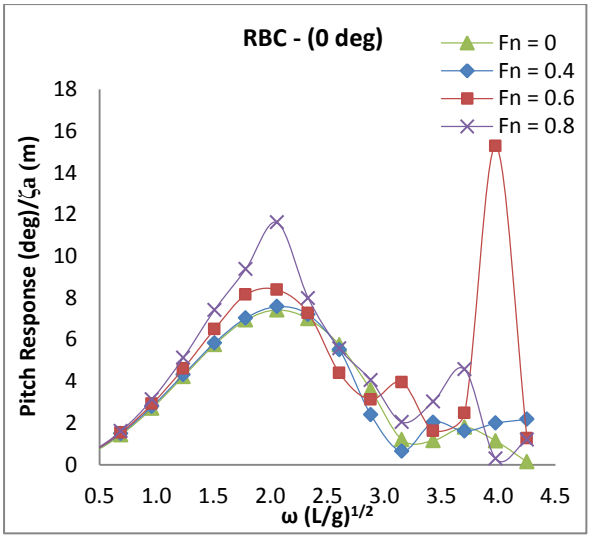

Figure 6.26: RBC numerical pitch motion response in Following Seas

6.3.3 Comparison of DVC and RBC motion responses

This section presents a detailed comparison of some selected results of the numerically predicted motion and spectral responses for the **DVC** and its competing **RBC** models. The comparison has been limited to the motion responses for the zero speed (Fn = 0.) and the vessel's cruising speed (Fn = 0.6) while the spectral response analyses were performed for vessel speeds for two vessel speeds, namely, Fn=0.4 and Fn=0.6. In addition spectral response analysis has been carried out for the two models (Deep-V [DV] and Round Bilge [RB]) at for sea states which correspond to significant wave heights of 1m, 2m, 3m, and 4m.This was done in order to evaluate the competiveness and performance of the concepts in these frequently used speed conditions.

6.3.3.1 Comparison of Heave Motions Response Amplitude Operator (RAO)

The plots of the heave motion responses for the **DVC** and **RBC** models at two different speeds in the **Head Seas (180^o)** condition are presented in Figure 6.27. The general trend of these plots in zero speed is identical to each other. The plots of the motion response (Figure 6.27) contain mild kinks at non-dimensional frequencies of 3.4 and 3.7 for the **RBC** and the **DVC** respectively. The frequencies of these kinks coincide with the natural pitch frequency of the **DVC** model. As the vessel speed increases to its cruising speed (Fn = 0.6), the responses for the models become very distinct in behaviour. While both of them contain double kinks, the frequencies and the peak magnitudes of these kinks differ from each other. The kinks in the response for DVC model occur at frequencies of 1.76 and 2.85 and with the magnitudes of 1.6m/m and 1.1m/m respectively, while in the **RBC** model, the kinks occur at frequencies of 1.76 and 2.7 and having magnitudes of 2.9m/m and 3.1m/m respectively. Both of these plots share a common frequency for one of the kinks and which happens to the same as for the pitch motions response in **Head Seas (180^o)**. The second kink is due to the shift in the resonance of the models as a result of the forward speed effects.

The comparative responses in the **Bow Quartering Seas (135^o)** condition are presented in Figure 6.28. The general trend of these plots is nonlinear within the frequencies range of 2.2 – 4.3. The plots for the zero speed responses, Fn = 0, for both of these models appear to be, understandably, isolated from each other but having higher magnitudes in the **RBC** model than in the **DVC** model. The forward speed response plots, Fn = 0.6, contain a visible kink and some other mild ones at a various frequencies. Again, the non-dimensional frequency of the kinks for both of the models is the same (2.10).

The trends of the responses in the **Beams Seas (90°)**, Figure 6.29, are linear but they have been found to be insensitive to the vessel speeds for both of the models. DVC model performs better in this condition and at higher frequency than the **RBC** model. In the **Stern Quartering Seas (45°)**, Figure 6.30, the magnitudes of the responses decreases as the vessel speed increases. The plots for the zero speed responses of the two models, Fn = 0, have similar trends whereas the trends for the vessel speed of Fn = 0.6 are different because of the presence of a kink in the responses for **DVC** model. The kink is due to the coupling of the Heave motions with the pitch motions in the same **Stern Quartering Seas.**

Generally, there is a reduction in both the magnitudes and the number of kinks that appeared in the plots of each of the responses when the heading condition changes from **Head Seas (180°)** to the **Following Seas (0°)**. In spite of these changes, responses for the **DVC** are less sensitive to these changes than those for **RBC** model.

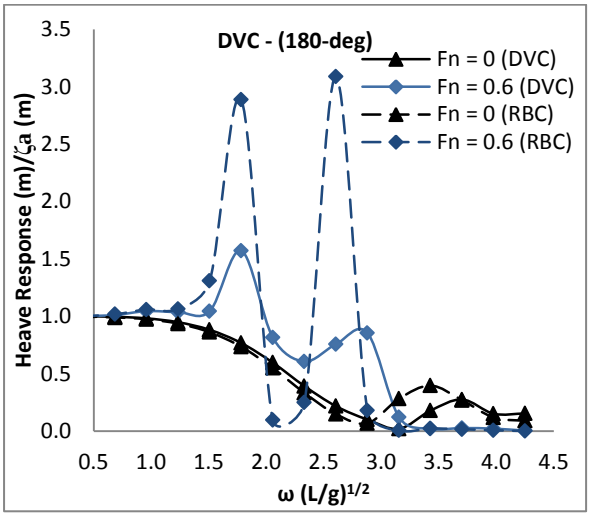

Figure 6.27: Comparison of heave motions RAO in Head Seas (90°)

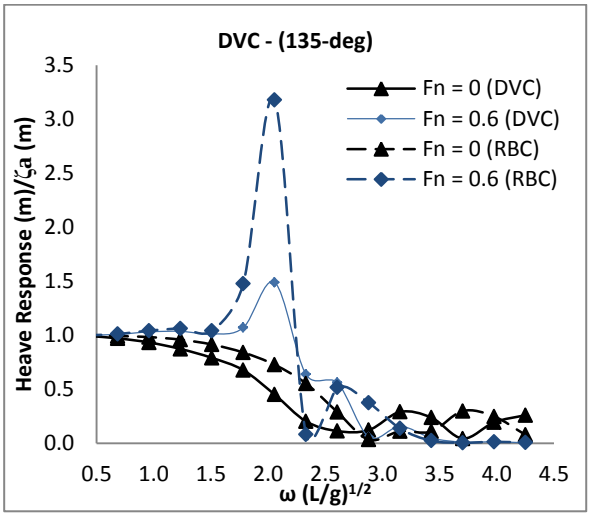

Figure 6.28: Comparison of heave motions RAO in Bow Quartering Seas (135°)

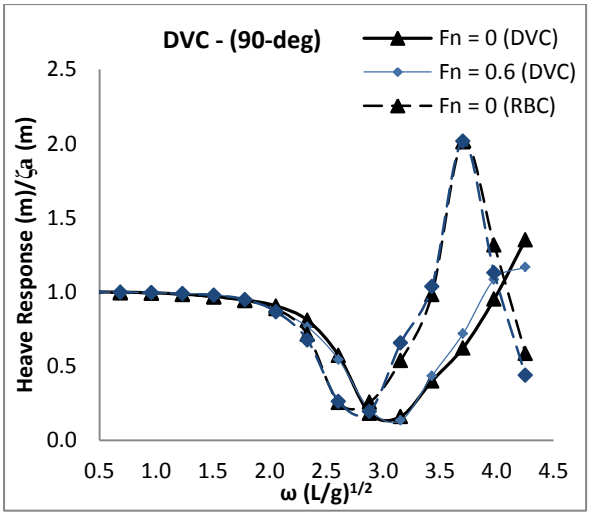

Figure 6.29: Comparison of heave motions Response Amplitude Operator (RAO) in Beam Seas (90°)

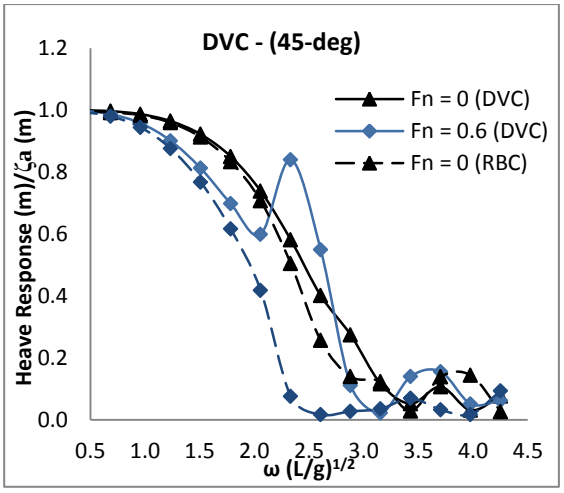

Figure 6.30: Comparison of heave motions Response Amplitude Operator (RAO) in Stern Quartering Seas (45°)

6.3.3.2 Performance Comparison of Heave Spectral Response

The plots of the heave motion spectral response analysis for the vessel speeds of Fn=0.4 and Fn=0.6 are presented in Figure 6.31 (Fn=0.4) and Figure 6.34 (Fn=0.6) - for **Head Seas (180^o),** Figure 6.32 (Fn=0.4) and Figure 6.35 (Fn=0.6) - for **Bow Quartering Seas (135^o),** and Figure 6.33 (Fn=0.4) and Figure 6.36 (Fn=0.6) - for **Beam Seas (180^o)**. The trends of the responses for the plots of both of these models (DVC and RBC) are similar.

A comparison of the performance of these models in the various wave heights that have been tested (ranging from 1m to 4m significant wave heights) revealed that the DVC concept has a slight (but probably insignificant) improvement in its performance over its RBC counterpart in **Head Seas (180^o)** and the **Bow Quartering Seas (180^o)**. However, in the **Beam Seas (180^o),** the performance of the two concepts is identical both in terms of their trends and magnitudes. A further study to quantify the impact of this slight difference is therefore required. A summary of the comparison for the behaviour of the two model concepts is presented in Table 6.3.

Table 6.3: Summary of performance comparison for DVC and RBC concepts in heaving condition

S/N	**Heading (Deg)**	***Motion Response***	***Spectral Response***
1	Head seas (180^o)	DVC (at higher speed)	DVC (at higher speed)
2	Bow Quartering	DVC (at all speed)	DVC (at all speed)
3	Beam Seas	Both models are similar	Both models are similar
4	Stern Quartering	RBC (at all speed)	-

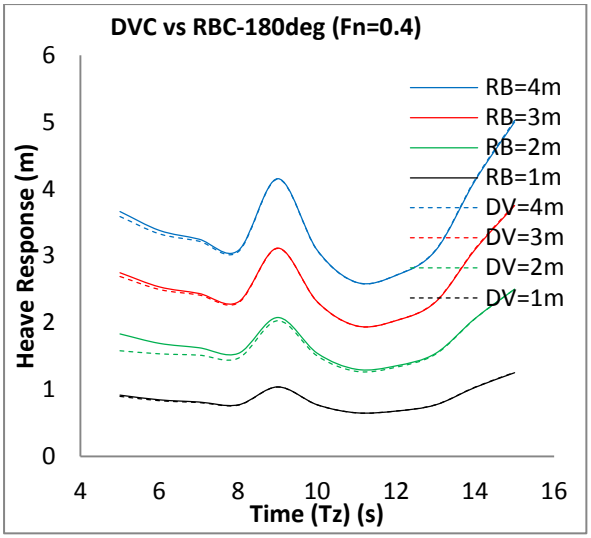

Figure 6.31: Spectral Response Comparison of Heave in Head Seas (180°) at Fn=0.4

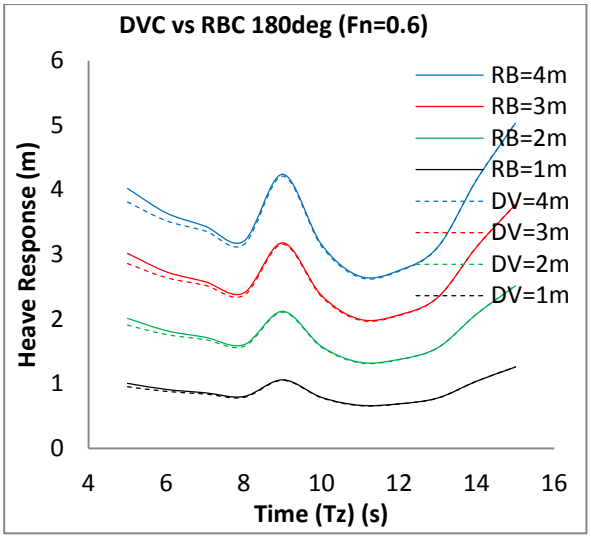

Figure 6.34: Spectral Response Comparison of Heave in Head Seas (180°) at Fn=0.6

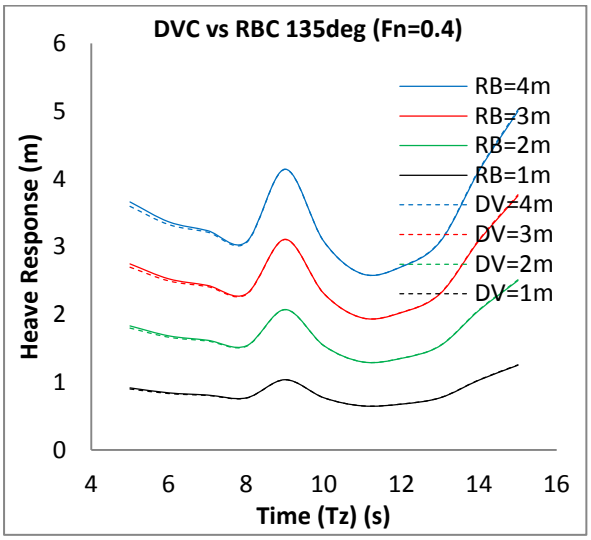

Figure 6.32: Spectral Response Comparison of Heave in Bow Quartering Seas (135°) at Fn=0.4

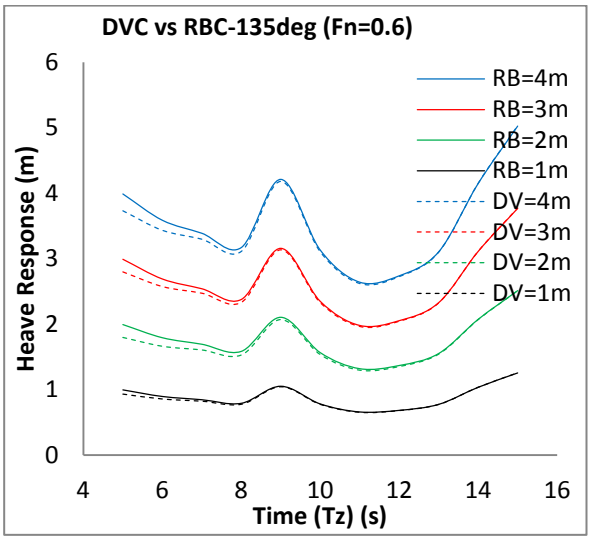

Figure 6.35: Spectral Response Comparison of Heave in Bow Quartering Seas (135°) at Fn=0.6

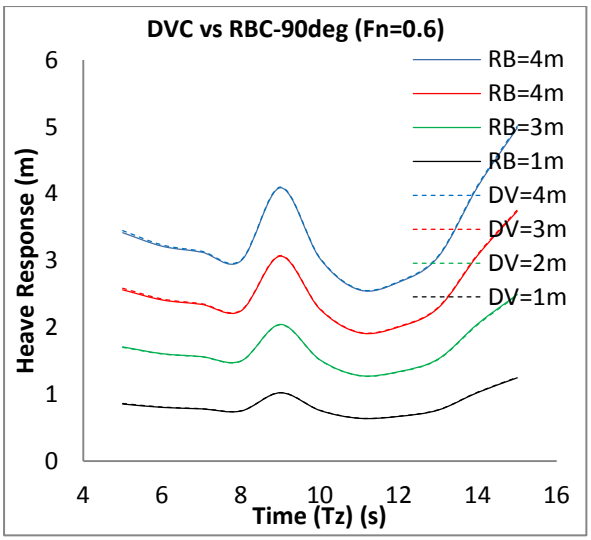

Figure 6.33: Spectral Response Comparison of Heave in Beam Seas (90°) at Fn=0.4

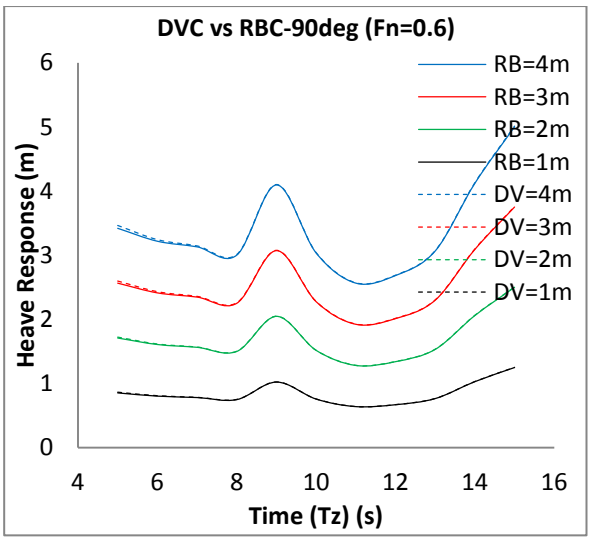

Figure 6.36: Spectral Response Comparison of Heave in Beam Seas (90°) at Fn=0.6

6.3.3.3 Comparison of Roll Motions Response Amplitude Operator (RAO)

The plots of the comparative roll motion responses for the two models in the ***Bow Quartering Seas (135^o)*** are presented in Figure 6.37. The trends of these responses contain some intermittent decrease in the magnitudes of the responses for the **DVC** model relative to those for the **RBC** at some specific frequencies. The **DVC** model has lower peak magnitude of the roll motion responses than the **RBC** model in this heading condition and the reason for this difference is the geometry of the **DVC** concept and some of its added features such as appendage and the anti-slamming bulbous bow that are lacking in the RBC model.

The plots contain some kinks in the responses for the vessel speed of Fn = 0.6 and at frequencies of 1.75 (in the two models) and 2.3 (in the **RBC** model only). Again, while the responses for both of these models contain two visible kinks, those for the **RBC** model have higher magnitudes and they are spread within a narrow frequency band than the **DVC**'s. The consequence of this phenomenon is that the **RBC** model is more susceptible to vibration of the hull structure than the **DVC** model. This is so if the kink is actually due to resonance (LR, 2006).

The plots of the responses in the **Beam Seas condition (90^o)** are presented in Figure 6.38. Their trends with respect to the vessel speeds are largely linear and they do not respond to changes in the vessel speeds. The magnitudes of the responses in the **DVC** model decrease marginally with an increase in the vessel speed which is a direct contrast to the **RBC** model.

In the ***Stern Quartering Seas (45^o),*** the trends of the plots are similar and the magnitudes of their responses decrease as the vessel speed increases. The responses contain a kink at frequency 3.7.

The effects of the change in the vessel headings on the responses of these models along the roll motions axis are manifested in the variation of their magnitudes. The responses in the **Bow Quartering Seas (135^o)** are significantly higher than those obtained in the ***Stern Quartering Seas (45^o)*** which confirms a reduction in the response as the headings change from **Bow Quartering Seas** to the **Stern Quartering Seas.**

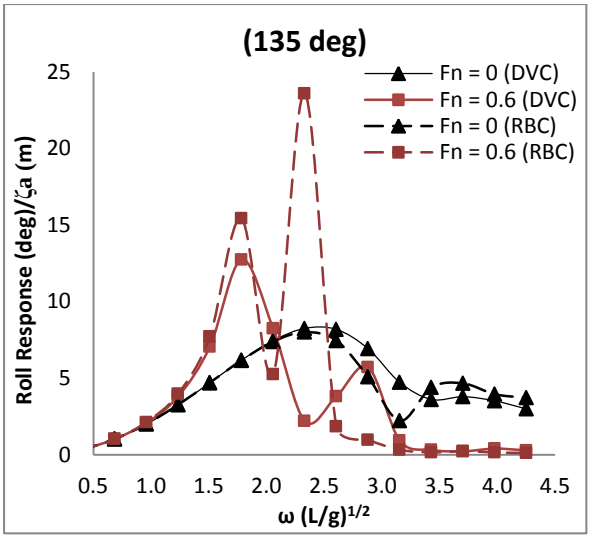

Figure 6.37: Comparison of roll motions Response Amplitude Operator (RAO) in Bow Quartering Seas (135°)

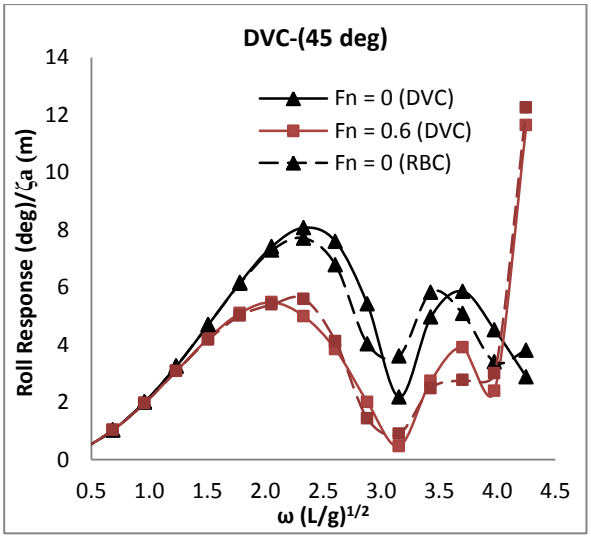

Figure 6.38: Comparison of roll motions Response Amplitude Operator (RAO) in Stern Quartering Seas (135°)

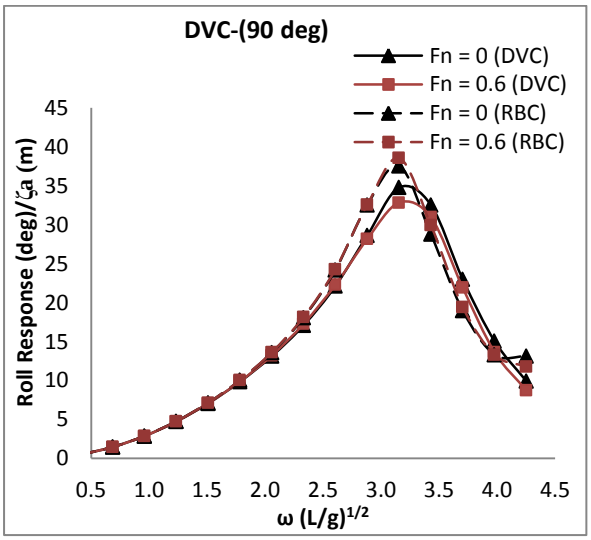

Figure 6.39: Comparison of roll motions Response Amplitude Operator (RAO) in Beam Seas (90°)

6.3.3.4 Performance Comparison of Roll Spectral Response

The plots of the spectral response in **Bow Quartering Seas (135^o)** for the two vessel speeds under consideration are presented in Figure 6.40 (Fn=0.4) and Figure 6.43 (Fn=0.6). The behaviour of the models of the two concepts are essentially similar at vessel speed of Fn=0.4, the RBC concept having a slightly lower responses in the 4 sea states that have been tested. A further comparison of the vessel performance at higher vessel speed of Fn=0.6 indicates that DVC concepts performs better, especially at medium wave heights of 2m – 3m.

The roll behaviour of the two concepts in **Beam Seas (90^o),** Figure 6.41(Fn=0.4) and Figure 6.44 (Fn=0.6), have been found to be insensitive to the increase in vessel speed. The RBC concept has a modest but negligible reduction in their responses in each of the seas states that have been considered when compared to the responses of the DVC concept. This difference could be explained in terms of the respective hull geometries of the two models.

In the **Stern Quartering Seas (45^o),** the behaviour of the two models are identical to each other at every sea state considered at a vessel speed of Fn=0.4 (Figure 6.42).The performance of the models at higher speed of Fn=0.6 Figure 6.45 is significantly different. The responses at low crossing period of 5s appear to be out of sync with rest of the results. The DVC concept performs better that the RBC's due to the lower magnitude of their responses.

A summary of the performance comparison for the two model concepts is presented in Table 6.4.

Table 6.4: Summary of performance comparison for DVC and RBC concepts in heaving condition

S/N	**Heading (Deg)**	***Motion Response Comparison***	***Spectral Response Comparison***
1	Bow Quartering Seas (135^o)	Similar (Slightly DVC)	Similar (Slightly DVC)
2	Beam Seas (90^o)	Similar	Similar (Slightly DVC)
3	Stern Quartering (45^o)	Similar (Slightly RBC)	DVC(at higher speed)

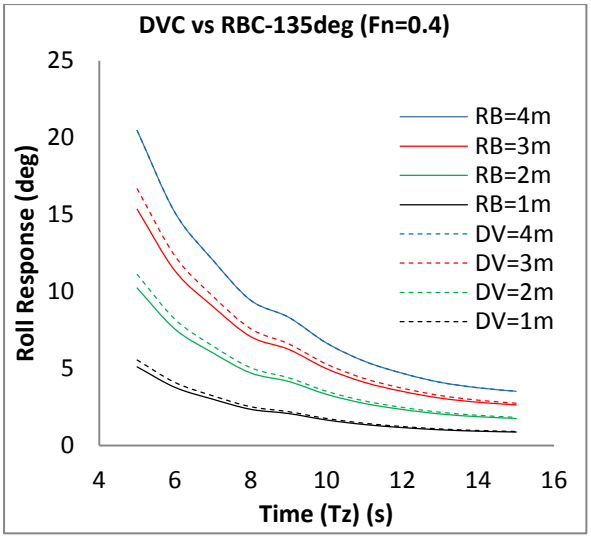

Figure 6.40: Spectral Response Comparison of Roll in Bow Quartering Seas (135°) at Fn=0.4

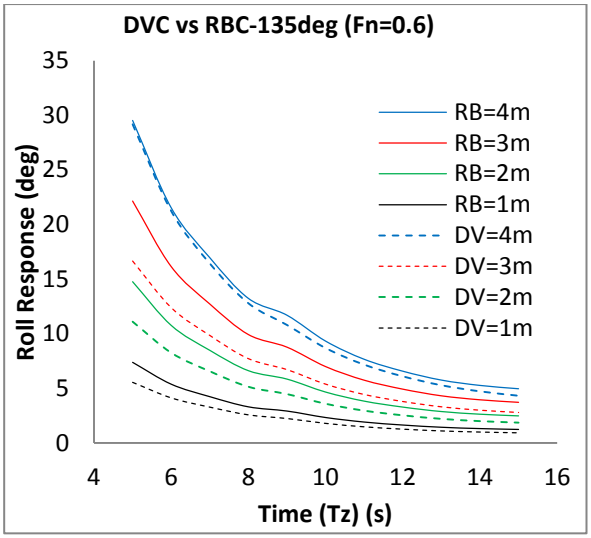

Figure 6.43: Spectral Response Comparison of Roll in Bow Quartering Seas (135°) at Fn=0.6

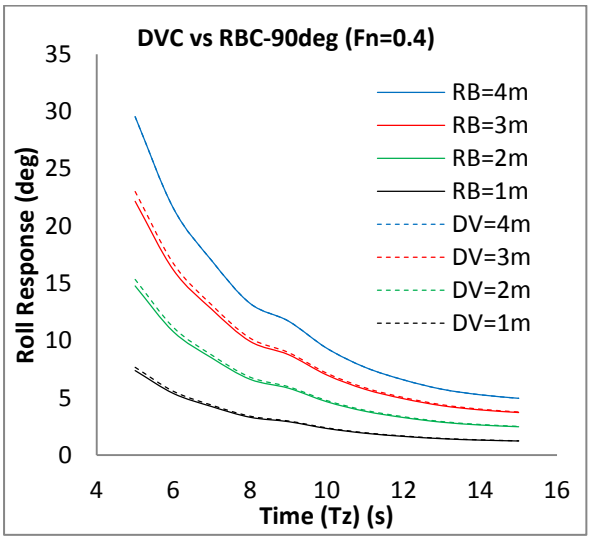

Figure 6.41: Spectral Response Comparison of Roll in Beam Seas (90°) at Fn=0.4

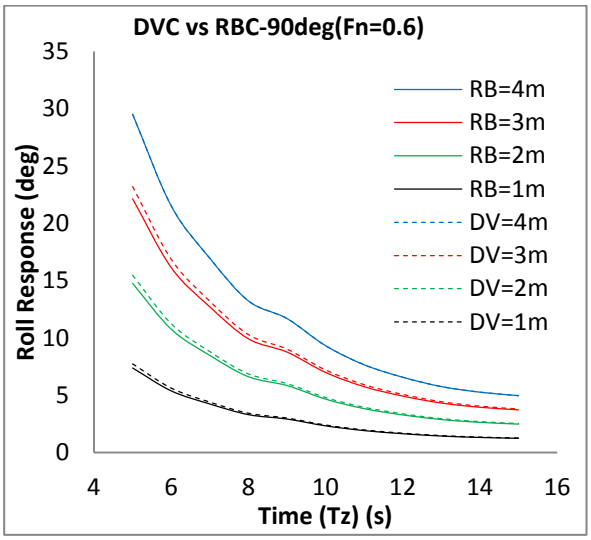

Figure 6.44: Spectral Response Comparison of Roll in Beam Seas (90°) at Fn=0.6

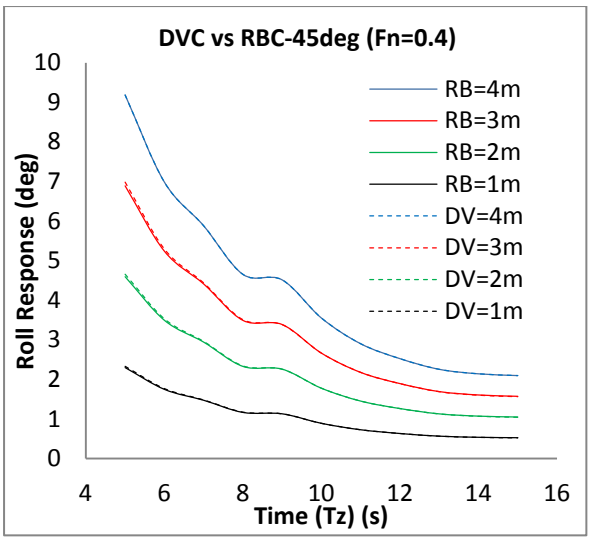

Figure 6.42: Spectral Response Comparison of Roll in Stern Quartering Seas (45°) at Fn=0.4

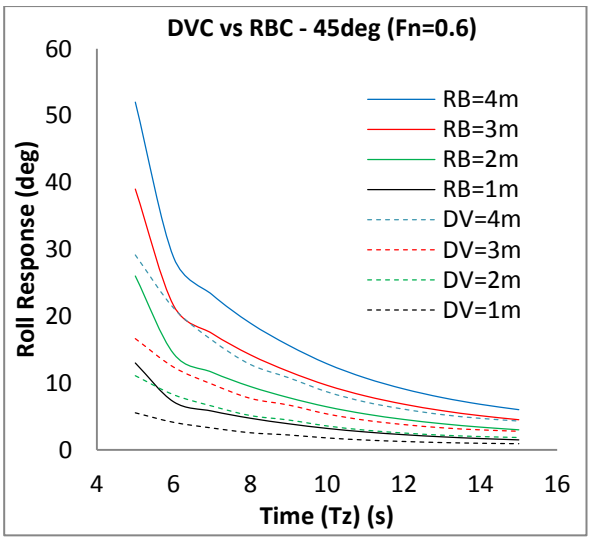

Figure 6.45: Spectral Response Comparison of Roll in Stern Quartering Seas (45°) at Fn=0.6

6.3.3.5 Comparison of Pitch Motions Response Amplitude Operator (RAO)

The comparisons of the pitch motion responses in the **Head Seas (180^o)** for the **DVC** and the **RBC** models are presented in Figure 6.46. The trends of these plots for the vessel speed of Fn = 0 are relatively similar to each other, while in the vessel speed of Fn = 0.6, responses contain kinks at frequency of 2.7 (in the **DVC** model) and at frequencies of 1.9 and 2.6 (in the **RBC** model). The kink that occurs at a frequency of 2.65 is clearly within the range of the DVC model's roll motions frequency. The **RBC** model has higher pitch motions response magnitude than the **DVC** model, confirming that the **DVC** performs better in roll and in this heading condition.

The comparison of the pitch motion responses in the ***Bow Quartering Seas (135^o)*** are presented in Figure 6.47. The trends of these plots in the zero speed, Fn = 0, are similar to each other. The **RBC** model has lower magnitudes responses at higher frequency than the **DVC** model. Apart from this, there is no any distinct difference between the responses of these two models in this heading and speed conditions.

In the forward speed condition, Fn = 0.6, the responses for the **DVC** model contain a visible kink with high magnitude at a frequency of 2.6. The kink coincides with the standing wave interference frequency in the transverse direction due to asymmetric mode of n =2.5 (Table 4.7), which suggest that the magnitude of the kink is due to the disturbance resulting from demi-hull interference. The responses for the **RBC** model contain two kinks at frequencies of 2.0 and 2.85. The second of these frequencies is likely due to the coupling of pitch motions and the heave motions response.

The difference between the magnitudes of the responses of the two models is very small if the responses at "kinks" are taken out as the effects of disturbance during numerical predictions especially in the **DVC** model. This would have meant that the **DVC** performs better in seaway than the **RBC** model.

The effects of changes in the vessel heading have resulted in the reduction in the magnitudes of responses from the **Head Seas (180^o)** down to the **Following Seas (0^o).** The responses of the models in the **Beam Seas (90^o)** (Figure 6.48) and the **Stern Quartering (45^o)** (Figure 6.49) have lower pitch response amplitudes than in the **Head Seas (180^o)** (Figure 6.39) and the **Bow Quartering Seas (135^o)** (Figure 6.46).

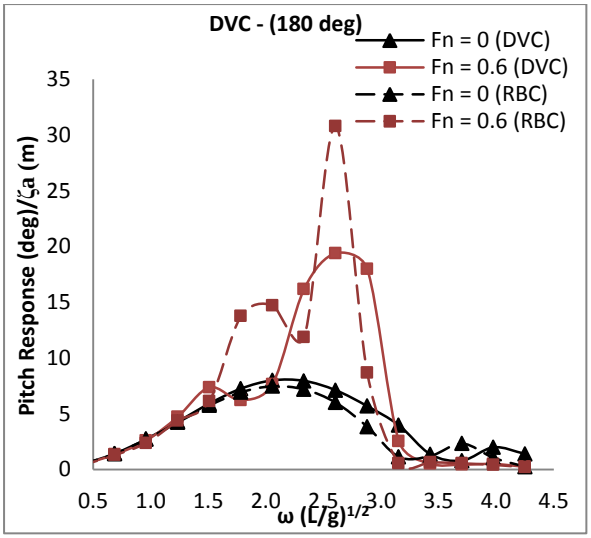

Figure 6.46: Comparison of pitch motions Response Amplitude Operator (RAO) in Head Seas (180°).

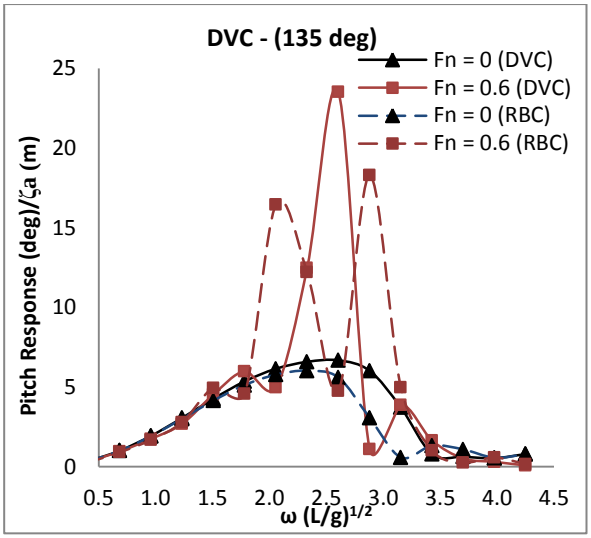

Figure 6.47: Comparison of pitch motions Response Amplitude Operator (RAO) in Bow Quartering Seas (135°).

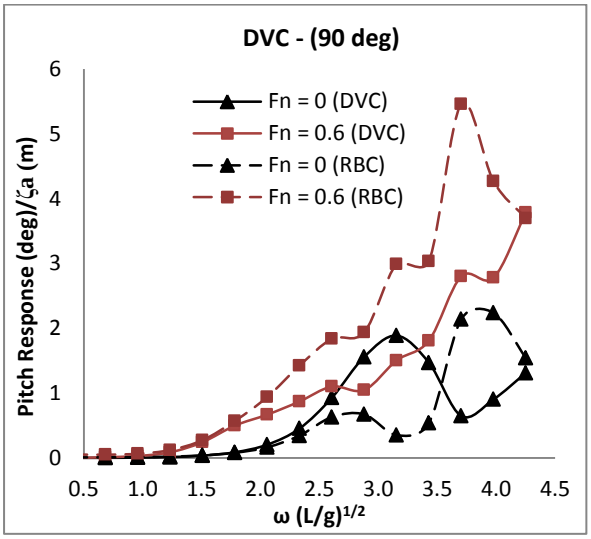

Figure 6.48: Comparison of pitch motions Response Amplitude Operator (RAO) in Beam Seas (90°)

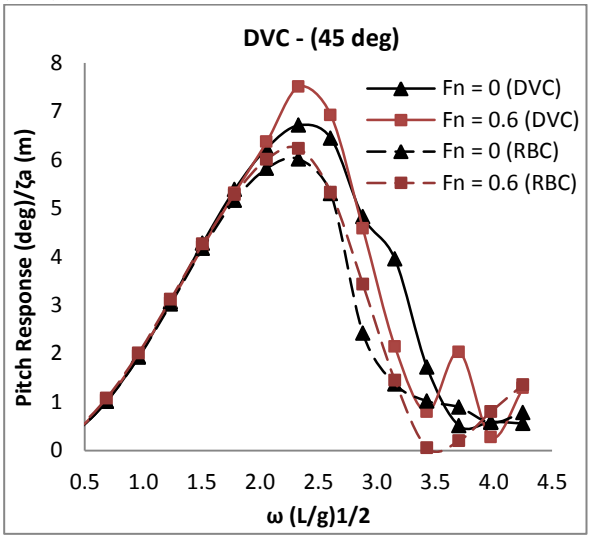

Figure 6.49: Comparison of pitch motions Response Amplitude Operator (RAO) in Stern Quartering Seas (45°)

6.3.3.6 Performance Comparison of Pitch Spectral Response

The plots of the pitch responses in **Head Seas (180^o),** for the two vessel speeds of Fn=04 (Figure 6.51) and Fn=0.6(Figure 6.54) in four sea states, namely, Hs=1m, Hs=2m, Hs=3m and Hs=4m, which have been obtained from the spectral analysis, are presented in this section. The trend of the responses in various wave heights and at a vessel speed of Fn=0.4 are similar for both of the two hull form concepts. In addition, there is virtually no difference in the magnitudes of the responses, which means that he performance of the concepts are essentially the same when vessel is at this condition. However, the performance of the DVC concept improves marginally as the vessel speed increases.

In the **Bow Quartering Seas (135^o),** Figure 6.50 (Fn=0.4) and Figure 6.53 (Fn=0.6), the two models offer a conflicting performance. The DVC concepts performs better than the RBC at moderate speed of Fn=0.4 whereas the RBC models offers a slightly better performance when the vessel speed increases to Fn=0.6. In spite of this, the DVC concept performs, marginally, better than the RBC in this condition.

The spectral response for the analysis of pitching performance of the models in the **Following Seas (0^o)** and at vessel speeds of Fn=0.4 and Fn=0.6 are presented in Figure 6.52 and Figure 6.55 respectively. Again, the trends of the responses for both these models (DVC and RBC) are similar for a vessel of Fn=0.4. As the speed increases to Fn=0.6, the RBC concept appears to have a marginally lower response magnitudes when compared to that of the DVC concept. This equally translates to mean that the RBC performs slightly better that the DVC concept.

A summary of the comparison for the behaviour of the two model concepts is presented in Table 6.7.

Table 6.5: Summary of performance comparison for DVC and RBC concepts in pitching mode

S/N	Heading (Deg)	*Motion Response Comparison*	*Spectral Response Comparison*
1	Head seas (180^o)	RBC (marginally)	DVC (as the speed increases)
2	Bow Quartering	DVC (marginally)	DVC (at low speed)
3	Beam Seas	Inconclusive	-
4	Stern Quartering	RBC (at all speed)	-
5	Following Seas (0^o)	DVC (at higher speed)	RBC (marginally)

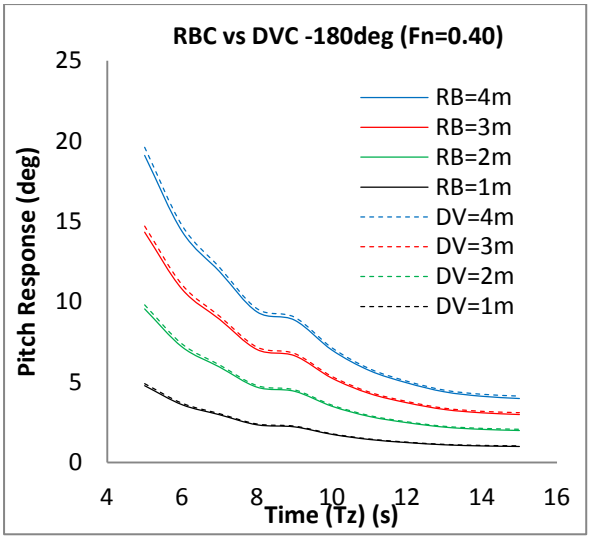

Figure 6.50: Spectral Response Comparison of Pitch in Head Seas (180°) at Fn=0.4

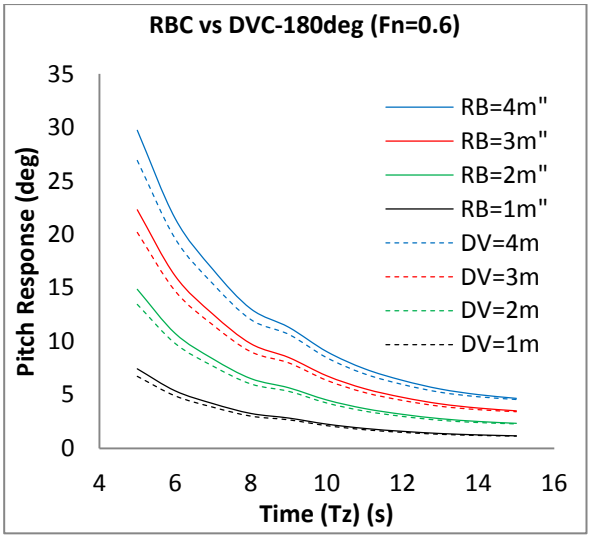

Figure 6.53: Spectral Response Comparison of Pitch in Head Seas (180°) at Fn=0.6

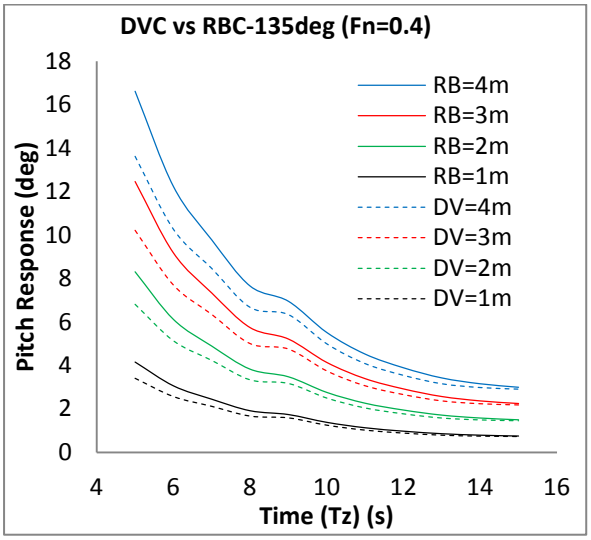

Figure 6.51: Spectral Response Comparison of Pitch in Bow Quartering Seas (135°) at Fn=0.4

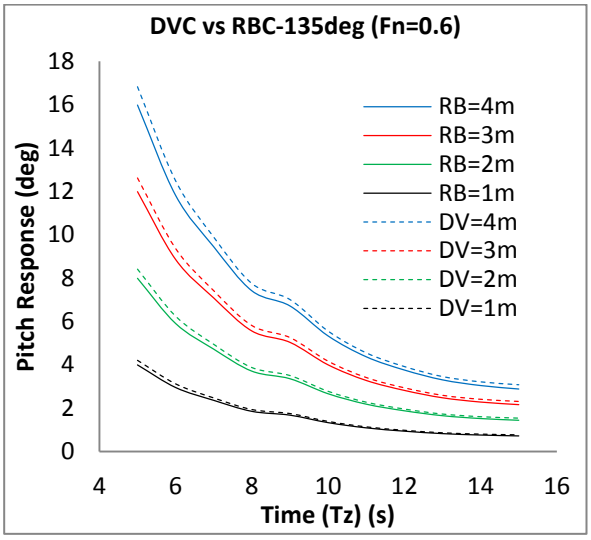

Figure 6.54: Spectral Response Comparison of Pitch in Bow Quartering Seas (135°) for Fn=0.6

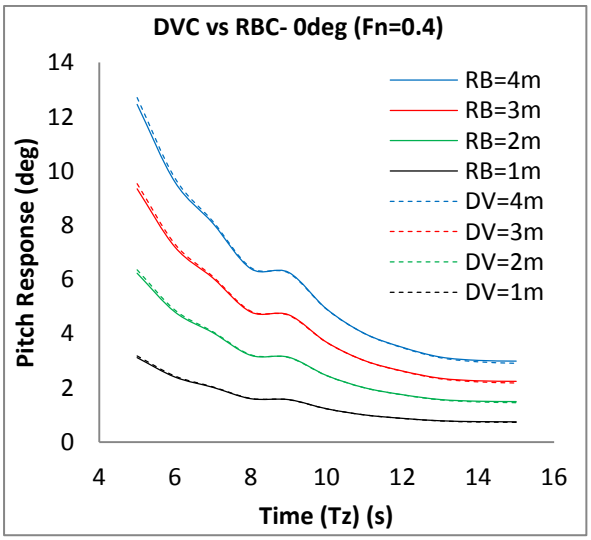

Figure 6.52: Spectral Response Comparison of Pitch in Following Seas (0°) at Fn=0.4

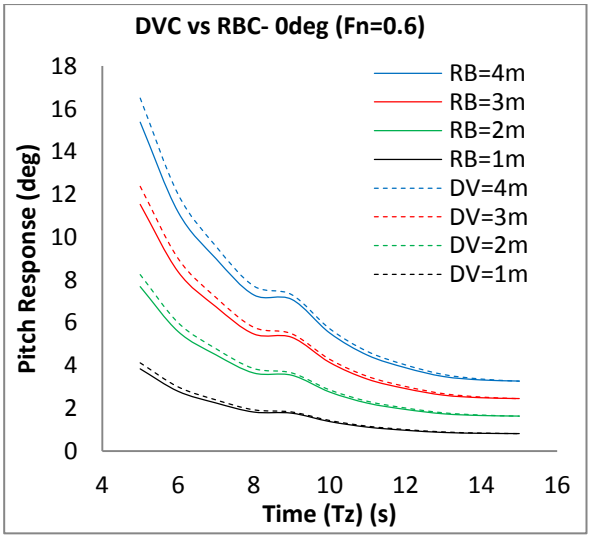

Figure 6.55: Spectral Response Comparison of Pitch in Following Seas (0°) at Fn=0.6

6.4 Results of the Wave-induced Loads Response Prediction

This section presents the results of the numerical predictions of the wave-induced loads acting on the two models that have used in this study. The section comprised of the results of the shear forces along the longitudinal and the vertical axes together with the Prying moment, the Yaw splitting moment and the Longitudinal Torsional moment. These results have been presented in non-dimensional forms as earlier defined in Chapter 4.5.3.

6.4.1 DVC Wave-induced Loads Response Results

6.4.1.1 The Longitudinal Shear Force (Fx)

The results of the longitudinal shear force for the **DVC** model in **Head Seas (180^o)** are presented in Figure 6.56. The magnitudes of these responses are significantly small despite the effect of vessel speeds (Fn = 0.6 and Fn = 0.8) on the peaks responses The trends of the responses are quite nonlinear with respect to vessel speeds, especially for the speeds of Fn = 0 and Fn = 0.4.

In the **Bow Quartering Seas (135^o),** Figure 6.57, the responses are also nonlinear and they contained a visibly high magnitude kink in the response due to the speed of Fn = 0.4. The kink appears within a very low non-dimensional frequency of 0.67. The irregularities become more prominent as the encountered frequencies increases. The trends bear some semblance to those for the responses in the **Head Seas (180^o).** The cause of these kinks is the coupling of the longitudinal shear force responses with the pitch motions, in addition to the speed effect.

The longitudinal shear force in the **Beam Seas** (**90^o**) is presented in Figure 6.58 and their responses are linear between a frequency range of 0 -2.5. This response then became nonlinear throughout the remainder of the frequencies. The effect of the vessel speeds on the results is very limited because the vessel did not to respond to changes in the vessel speeds.

Figure 6.17 presents the longitudinal shear force in the **Stern Quartering Seas (45^o).** The trend of their responses is mildly nonlinear especially at the higher frequencies. The responses due to the speed of Fn = 0 is slightly different from the rest of the vessel speeds

In the **Following Seas (0^o),** (Figure 6.60), the responses for the speeds of Fn = 0, 0.4, and 0.6 have similar trend at lower frequency, but then changed to nonlinear as the frequency increases. The numerical code could not measure the responses due to the speed of Fn = 0.8.

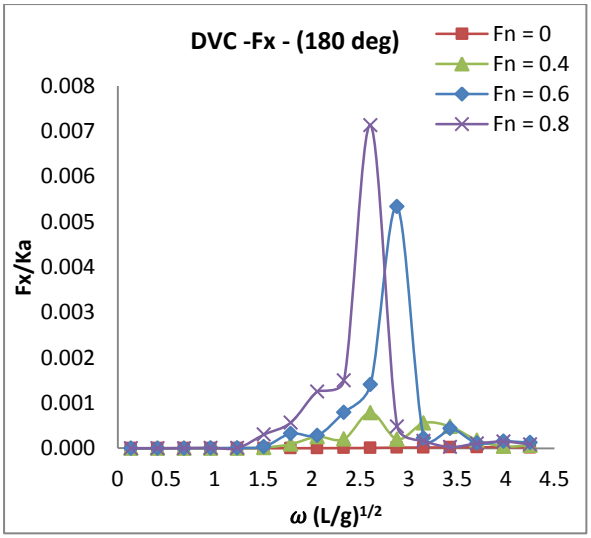

Figure 6.56: DVC numerical longitudinal shear force in Head Seas

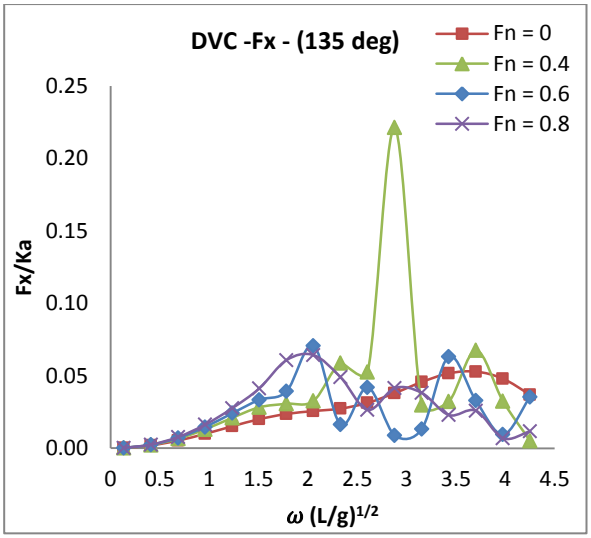

Figure 6.57: DVC numerical longitudinal shear force in Bow Quartering Seas

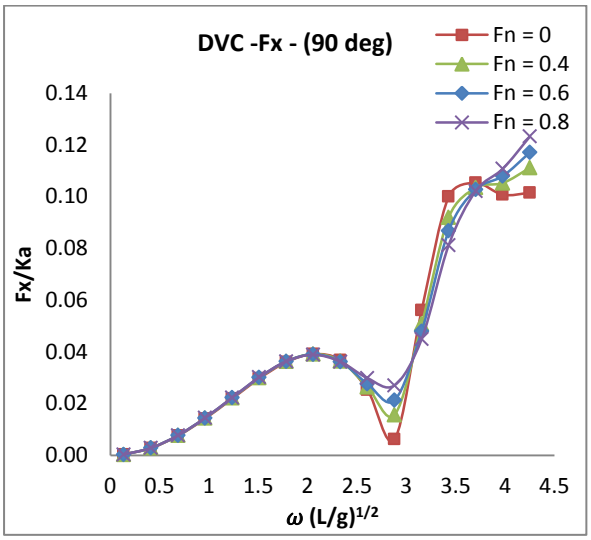

Figure 6.58: DVC numerical longitudinal shear force in Beam Seas

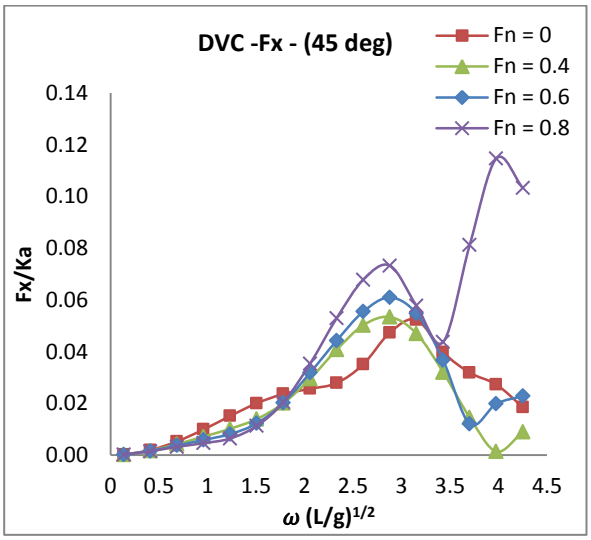

Figure 6.59: DVC numerical longitudinal shear force in Stern Quartering Seas

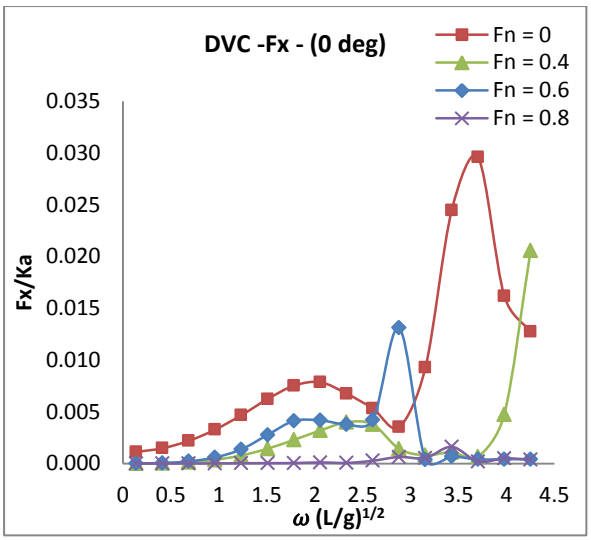

Figure 6.60: DVC numerical longitudinal shear force in Following Seas

6.4.1.2 The Vertical Shear Force (Fz)

The plots of the vertical shear force in the **Head Seas (180^o)** are presented in Figure 6.61. The trends of the responses are similar to those for the longitudinal shear force in the **Head Seas,** the only exception being their magnitudes. The responses are nonlinear between the frequency ranges of 1.25 to 3.5. The vertical shear force due to the speed of Fn = 0 has lower magnitudes in comparison to those for the vessel speeds of Fn = 0.4, Fn = 0.6 and Fn = 0.8. The plots contain kinks at the same frequency as the pitch motion response.

The responses for the vertical shear force plots in the **Bow Quartering Seas (135^o),** Figure 6.62, are nonlinear and they contained a visibly high magnitude kink in the response due to vessel speed of Fn = 0.48. There are other random kinks in these plots whose magnitudes are less than the peak magnitude of the individual responses due the various speeds. Again, the responses have a similar trend to those that have been observed in the longitudinal shear force in and the same heading albeit with some few exceptions.

The vertical shear force plots in the **Beam Seas** (**90^o**) are presented in Figure 6.63. The responses are linear in behaviour and their magnitudes remain the same in all the vessel speeds and at their respective frequencies. The magnitudes also increase as the frequency increases. Again, the responses in this heading condition are not sensitive to the vessel speeds.

The vertical shear force plots in the **Stern Quartering Seas (45^o)** are presented in Figure 6.65. These plots have not shown any specific pattern and their responses are nonlinear and with shifts for individual vessel speeds. The response due to vessel speed of Fn = 0 has a high magnitude that is only comparable to the speed of Fn = 0.8.

In the **Following Seas (0^o),** Figure 6.64, the trend is somewhat similar to those that have been observed in the **Head Seas**. The peak magnitudes of the responses due to the various vessel speeds occur within the high frequency region of the plots and their trends are equally nonlinear especially within the same high frequency region.

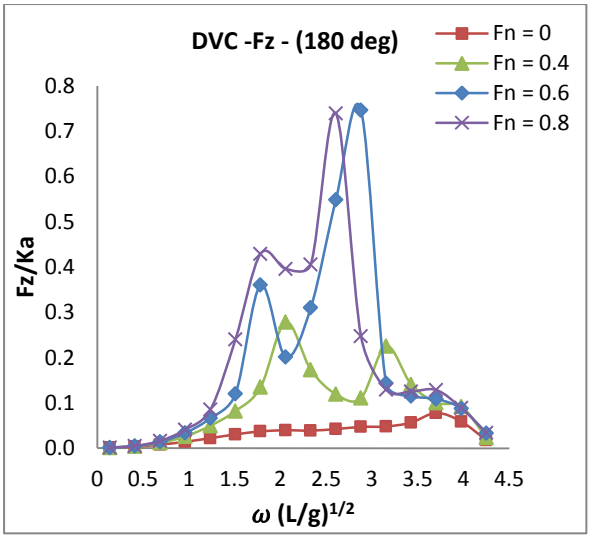

Figure 6.61: DVC numerical vertical shear force in Head Seas

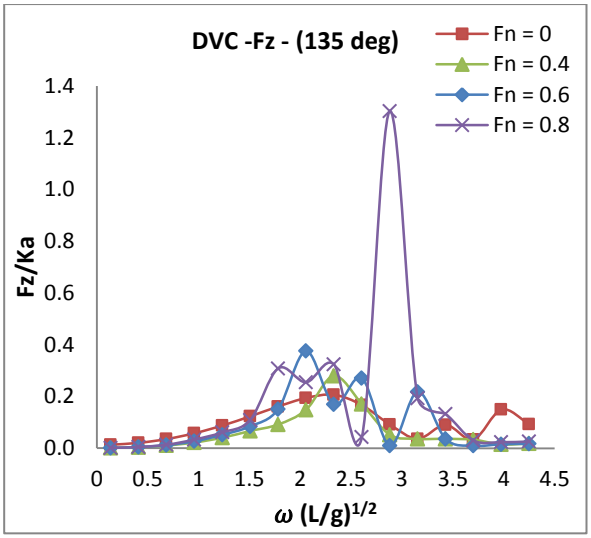

Figure 6.62: DVC numerical vertical shear force in Bow Quartering Seas

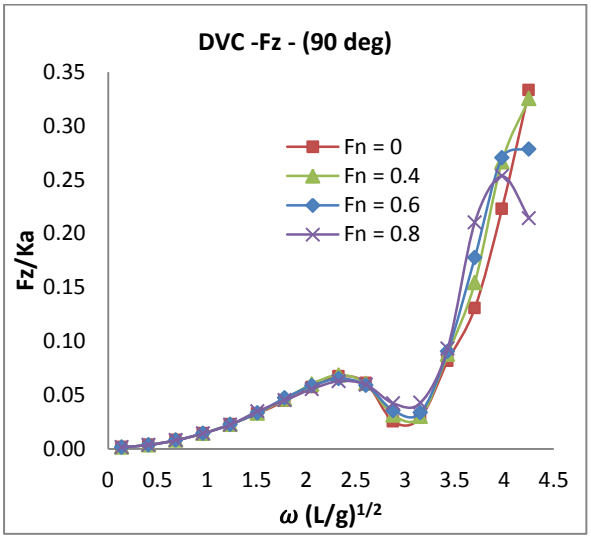

Figure 6.63 DVC numerical vertical shear force in Beam Seas

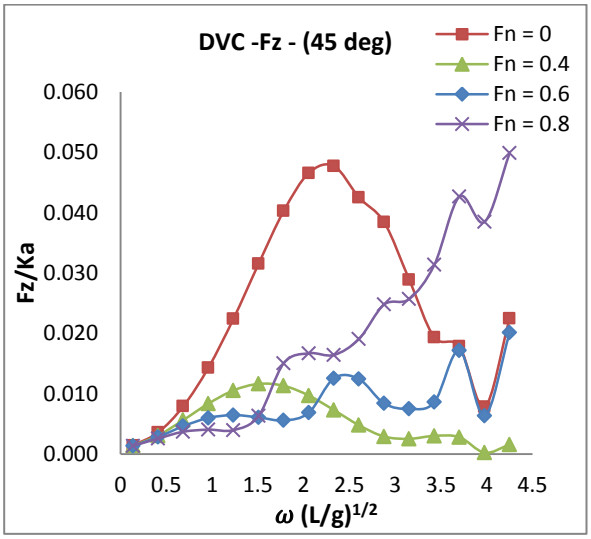

Figure 6.65: DVC numerical vertical shear force in Stern Quartering Seas

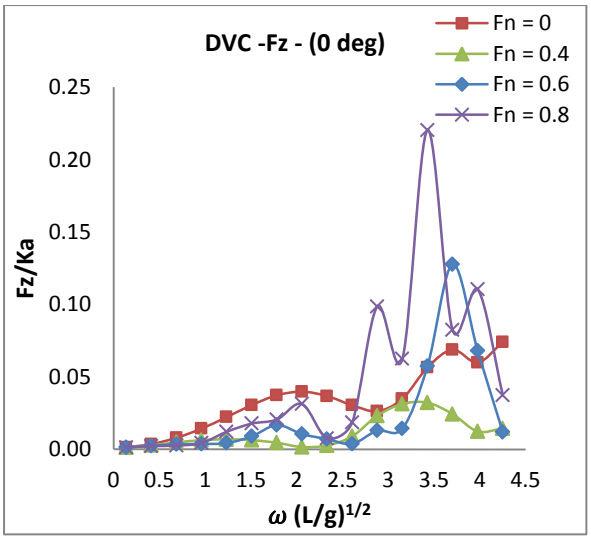

Figure 6.64 DVC numerical vertical shear force in Following Seas

6.4.1.3 Prying (Longitudinal Bending) Moment (Mx)

The plots of the prying moment in the **Bow Quartering Seas (135^{o})** for the various vessel speeds are presented in Figure 6.66. Their trends are generally nonlinear and they are similar to those for the other responses due to different loading condition in this heading.

The prying moment responses in the **Beam Seas (90^{o}) -** Figure 6.67**,** are linear and they are without any particular feature. Their plots appear to be insensitive to the vessel speeds, which is similar to what has been observed in the **Beam Seas (90^{o}),** so far**.**

In the **Stern Quartering Seas (45^{o}),** Figure 6.68**,** the responses are mildly nonlinear and they contain some kinks at higher frequency, especially in the responses due to vessel speed of Fn = 0.6 and Fn = 0.8. Their magnitudes are lower than those that have been obtained in the **Bow Quartering Seas (135^{o})**

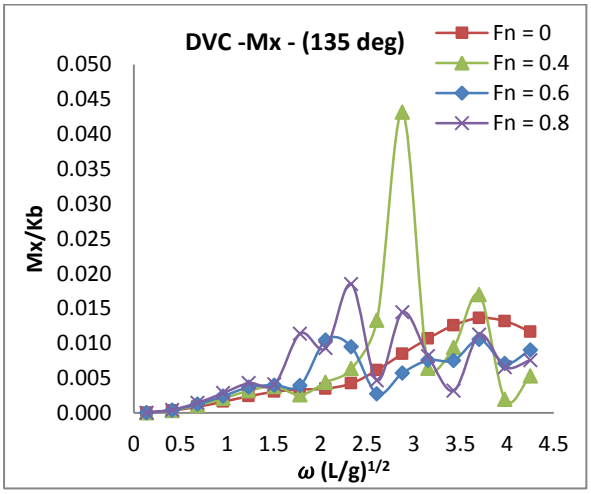

Figure 6.66 DVC numerical prying moment in Bow Quartering Seas

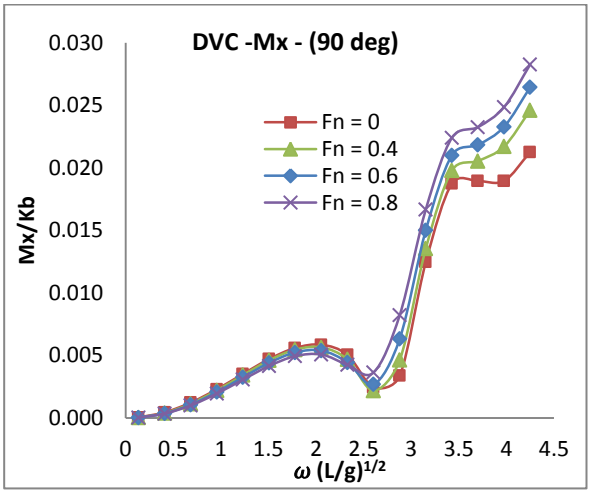

Figure 6.67 DVC numerical prying moment in Beam Seas

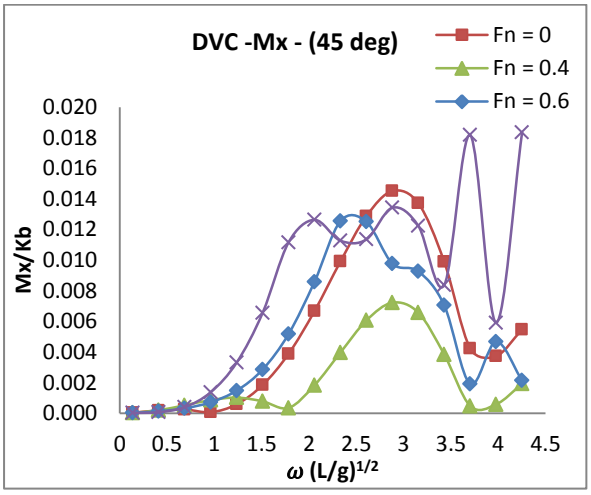

Figure 6.68 DVC numerical prying moment in Following Seas

6.4.1.4 The Yaw Splitting Moment (Mz)

The results of the yaw splitting moment in the **Head Seas (180^o)** are presented in Figure 6.69 The trend of the plot has some similarity with those in the vertical shear force in the Head Seas with the exception of their magnitudes. The similarity extends to coupling of these responses with the pitch motions response. This condition is adjudged to be an indication of the influence the pitch motions response has on the yaw splitting moment. The plots contained some kinks which are mainly found in the responses due to the forward speeds (Fn = 0.4, Fn = 0.6 and Fn = 0.8) and they are within a distributed frequency range of 1.5 – 3.5.

The plots for the yaw splitting moment in the **Bow Quartering Seas (135^o)** have shown some nonlinear characteristics as the frequency progresses forward, which can be seen in Figure 6.70**.** The plot contains some kinks that whose frequencies vary with the vessel speeds. The magnitudes of the kinks are also not in any way proportional to vessel speeds

In the **Beam Seas** (**90^o**), Figure 6.71, the yaw splitting moment plots is relatively linear. The trends of the magnitudes due to the individual responses are similar to each other, and hence they do not change with changes in the vessel speeds. At higher frequency range, 3.1 – 4.3, the moment increases as the encountered frequencies increase in a given vessel speed.

The plots of the responses in the **Stern Quartering Seas (45^o)** are presented in Figure 6.72. The plots exhibited two distinct features. These are: the magnitudes of the responses for zero speed are significantly higher and also detached from those for the forward speeds. And secondly, the trends of the plots for the forward speed conditions are relatively nonlinear with respect to the vessel speeds.

In the **Following Seas (0^o),** Figure 6.73, there is a gradual change in the linearity of the responses as the vessel speed increases. The responses are slightly linear at lower frequency range but then they gradually changed to nonlinear at higher frequencies. The effects of vessel speed on the responses were observed in the form of a shift in the frequencies of the kinks in the responses for vessel speed of Fn = 0.6 and Fn = 0.8

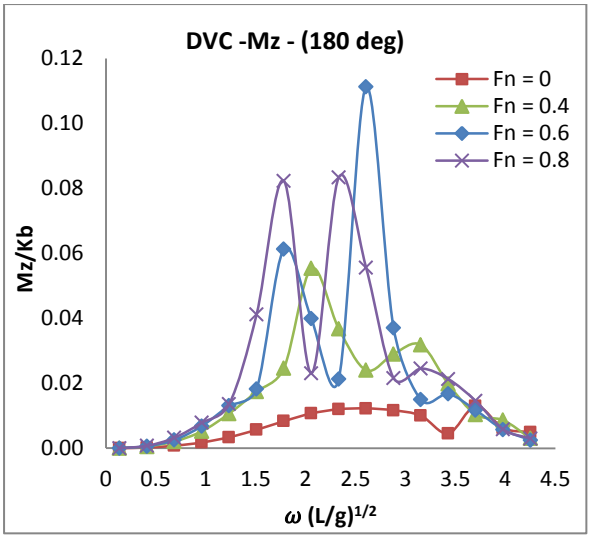

Figure 6.69: DVC numerical yaw splitting moment in Head Seas

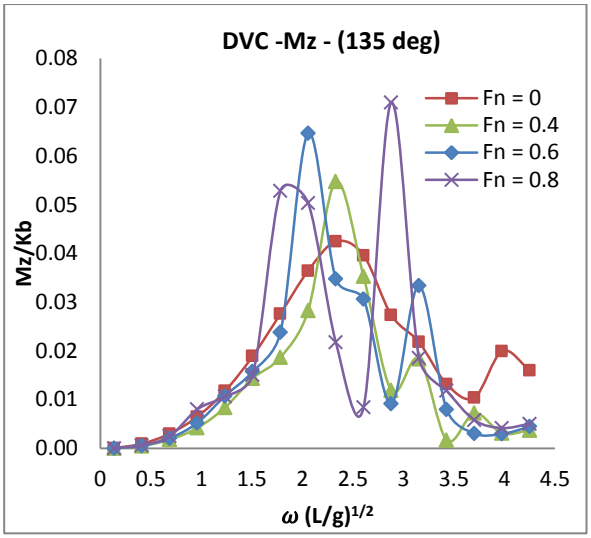

Figure 6.70: DVC numerical yaw splitting moment in Bow Quartering Seas

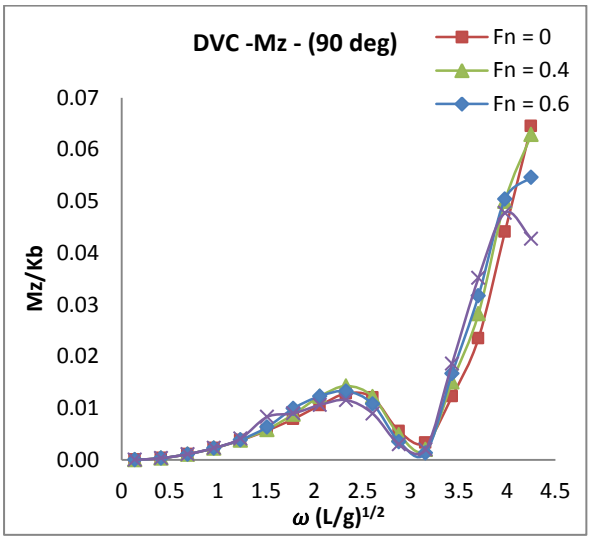

Figure 6.71: DVC numerical yaw splitting moment in Beam Seas

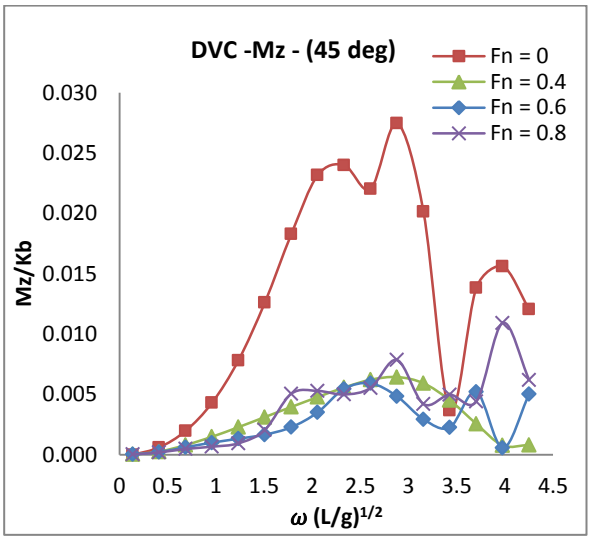

Figure 6.72: DVC numerical yaw splitting moment in Stern Quartering Seas

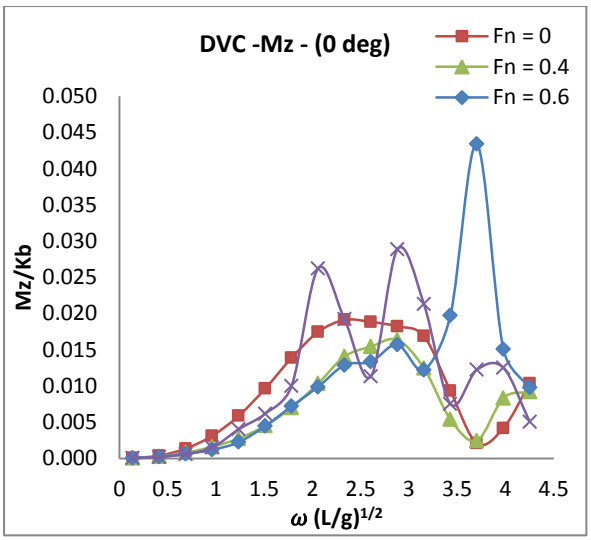

Figure 6.73: DVC numerical yaw splitting moment in Following Seas

6.4.1.5 Torsional (Longitudinal) Moment (Mx)

The plots of the longitudinal Torsional moment in the **Bow Quartering Seas (135^{o})** are presented in Figure 6.74. The general trends of these plots are nonlinear. The plots for the responses due to the forward speeds contain kinks and they are detached from those for the zero speed. The peak magnitudes of these kinks shift with changes in the vessel speeds.

The plots in the **Beam Seas (90^{o}) -** Figure 6.75**,** are linear but they have shown an inverse relationship between the increase in the vessel speeds and magnitudes of the response at higher frequency. The plots appear to be less sensitive to the vessel speeds.

The Torsional moment responses in the **Stern Quartering Seas (45^{o}),** Figure 6.76**,** are nonlinear at higher frequency and they also contain some kinks, especially in the plots due to vessel speed of Fn = 0.6 and Fn = 0.8. Their response magnitudes is about similar to those obtained in the **Bow Quartering Seas (135^{o})**

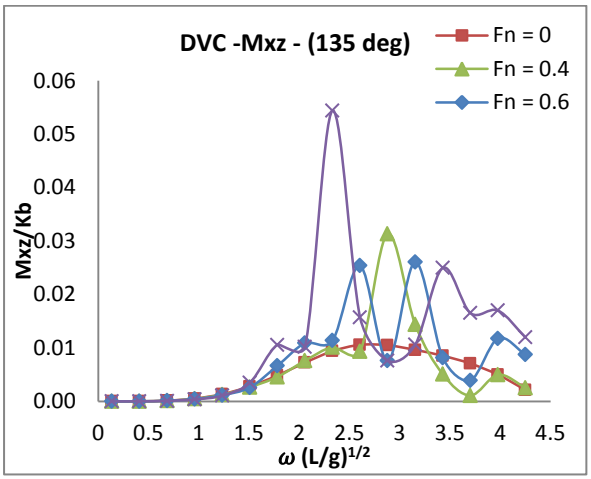

Figure 6.74: DVC numerical longitudinal Torsional moment in Bow Quartering Seas

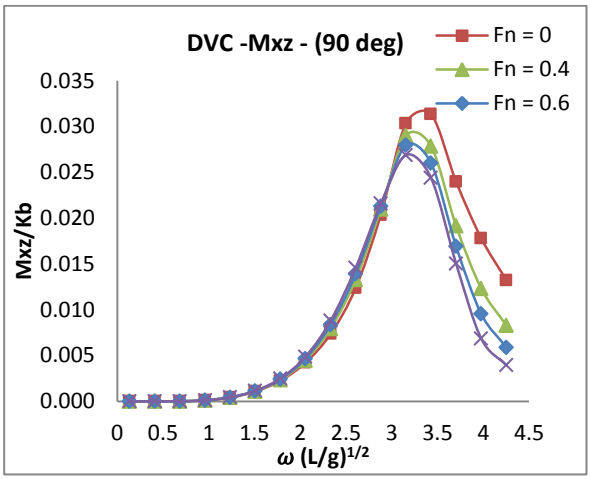

Figure 6.75: DVC numerical longitudinal Torsional moment in Beam Seas

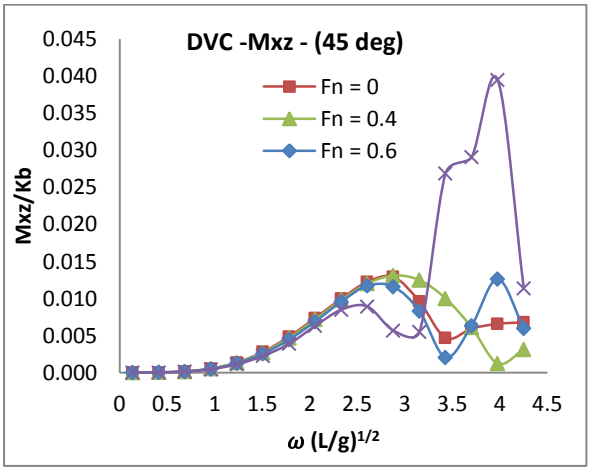

Figure 6.76: DVC numerical longitudinal Torsional moment in Stern Quartering Seas

6.4.2 RBC Wave-induced Loads Response Results

6.4.2.1 The Longitudinal Shear Force (Fx)

The trend of the responses in the **Bow Quartering Seas (135^o),** Figure 6.77, is nonlinear with high magnitude kinks in the plots for the vessel speeds of Fn = 0.4, Fn =0.6 & Fn = 0.8 and within the frequency range of 1.8 – 3.2. There is a shift in the frequencies of the peak responses due to changes in the vessel speeds. However, the plots in the **Beam Seas** (**90^o**), Figure 6.78, are linear between frequencies of 0 - 2.5, but then became nonlinear for the rest of the frequencies. The effect of the vessel speeds on the responses in this heading is very limited and the responses appear not to respond to changes in the vessel speeds. In the **Stern Quartering Seas (45^o),** Figure 6.79,the trend is mildly nonlinear, especially at the higher frequencies. The responses for Fn = 0.8 contain a kink at the same frequency within which other speeds (Fn = 0.4 and Fn = 0.6) have experienced a depression in their plots.

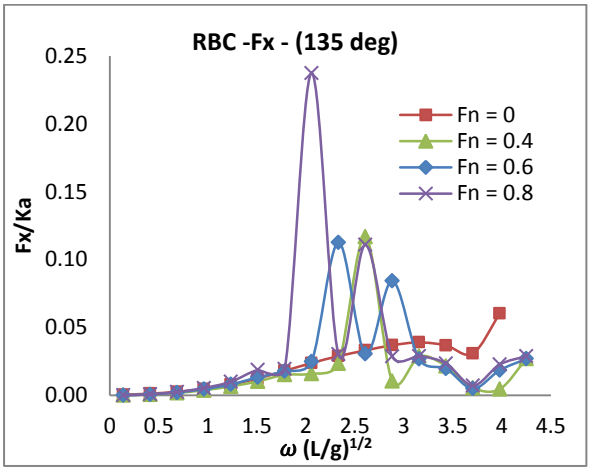

Figure 6.77: RBC numerical longitudinal shear force in Bow Quartering Seas

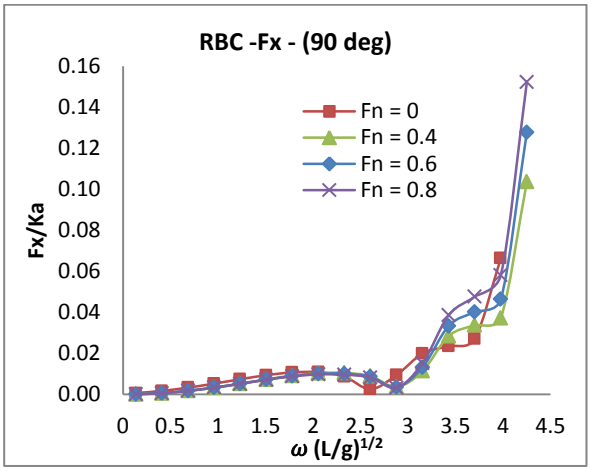

Figure 6.78: RBC numerical longitudinal shear force in Beam Sea

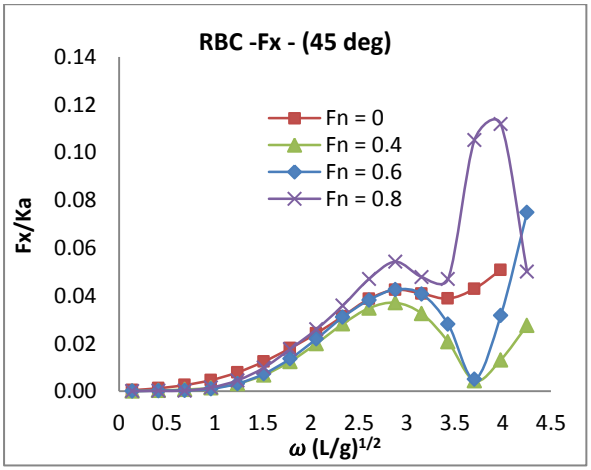

Figure 6.79: RBC numerical longitudinal shear force in Stern Quartering Seas

6.4.2.2 The Vertical Shear Force (Fz)

The vertical shear force for the **RBC** model in **Head Seas (180^o)** is presented in Figure 6.80. The responses for the force along this axis are nonlinear between the frequency ranges of 1.25 to 3.5. This is similar to those that have been observed in the **DVC** model in Head Seas but for their magnitudes. The vertical shear force due to the speed of Fn = 0 has the lowest magnitudes when compared to other speeds (Fn = 0.4, Fn = 0.6 and Fn = 0.8). The plots contain some kinks at frequencies that are consistent with the pitch motion responses. The shift in the frequencies of these kinks indicates the effects of vessel speeds on the responses.

The trends in the **Bow Quartering Seas (135^o),** Figure 6.81, are also nonlinear and with high magnitude kinks appearing in the plots for the vessel speeds of Fn = 0.4, Fn = 0.6 and Fn = 0.8.There other random kinks in the plots whose magnitudes are milder than those for the peak responses. The frequency band within which these kinks occur are wider than for those in the Head Seas but the peaks, in both cases, occurred in the vessel speed of Fn = 0.6.

The plots of the vertical shear force in the **Beam Seas** (**90^o**) are presented in Figure 6.82. The responses are mostly linear in behaviour and their magnitudes remain relatively the same for all the vessel speeds at their respective frequencies range. The magnitudes also increase as the frequency increases. Unlike in the longitudinal shear force, the plots in this case contain kink in all the responses and they have about the same magnitudes and within the same high frequency

The plots in the **Stern Quartering Seas (45^o)** are presented in Figure 6.83. The responses are nonlinear with separation between the responses due to individual vessel speeds. The peak magnitudes of the responses occurred within the high frequency range and, at the same time, the position of kinks. The responses due to the speed of Fn = 0 has the peak magnitude outside the high frequency region and it is then followed by a gradual reduction in response magnitudes as the speed increases.

In the **Following Seas (0^o),** Figure 6.84, the trend is somewhat similar to those that have been observed in the Stern Quartering Seas. While the peak of these responses occurs at about the same frequencies, the general trends of the responses themselves are nonlinear. The plots contains some modest kinks within the mid range frequencies of 1.5 – 3.0. The peak magnitudes of the responses for the various vessel speeds that have been considered occur within the high frequency range.

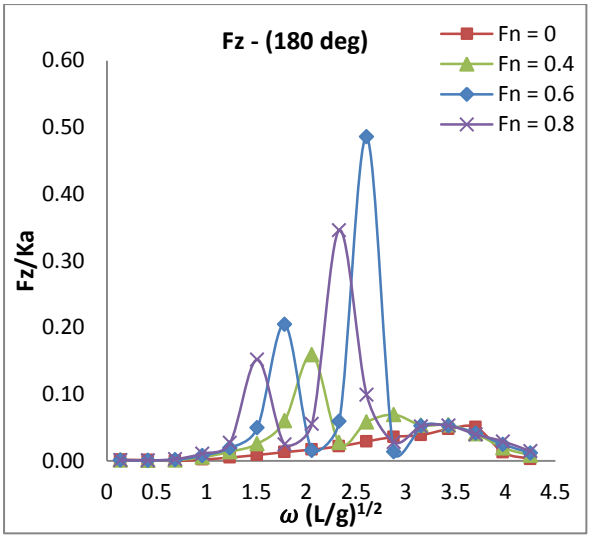

Figure 6.80 RBC numerical vertical shear force in Head Seas

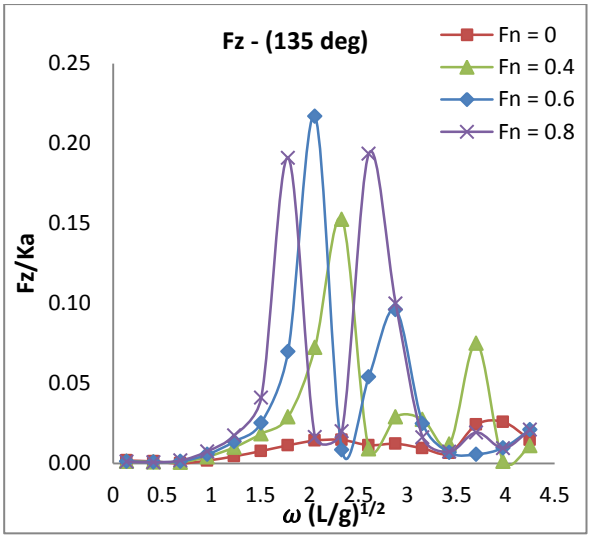

Figure 6.81: RBC numerical vertical shear force in Bow Quartering Sea

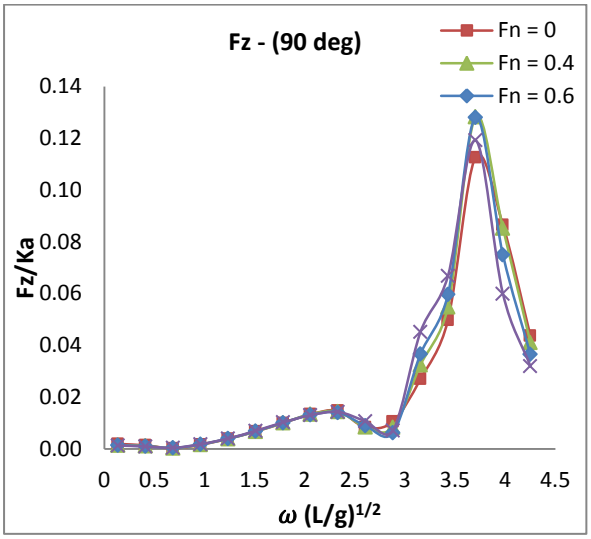

Figure 6.82 RBC numerical vertical shear force in Beam Seas

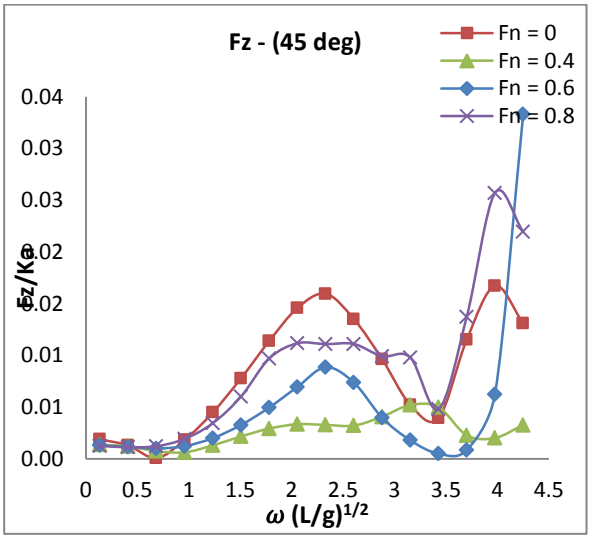

Figure 6.83: RBC numerical vertical shear force in Stern Quartering Sea

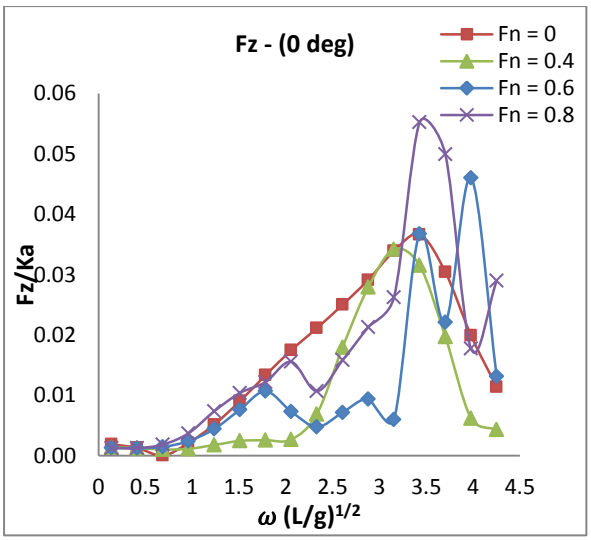

Figure 6.84: RBC numerical vertical shear force in Following Seas

6.4.2.3 Prying (Longitudinal Bending) Moment (Mx)

The trend of the results in the **Bow Quartering Seas (135^o),** Figure 6.85, is nonlinear and it contain high magnitude kinks in the responses due to vessel speed of Fn = 0.4, Fn =0.6 & Fn = 0.8 and within the non-dimensional frequency range of 1.8 – 3.2. The kinks and subsequent shift in their peak response frequencies are due to the changes in the vessel speeds. the plots in the **Beam Seas** (**90^o**), Figure 6.86, the effects of speeds on response remain linear within a frequency range of 0 -2.5, and then nonlinear for the reminder of the frequencies. The responses in this heading are not sensitive to changes in the vessel speeds. In the **Stern Quartering Seas (45^o),** Figure 6.87, the trend is mildly nonlinear especially at higher frequencies. The plot of the Fn = 0.8 responses contain a kink at a frequency in which the other speeds (Fn = 0.4 and Fn = 0.6) are experiencing depression. This change is due to the influence of speeds change and the roll motions coupling on these responses.

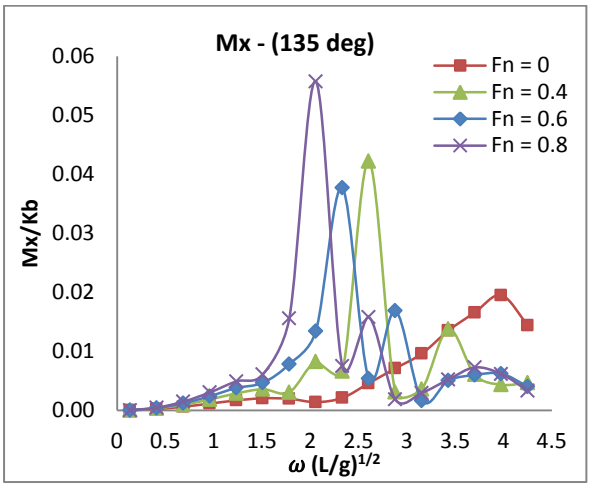

Figure 6.85: RBC numerical prying moment in Bow Quartering Seas

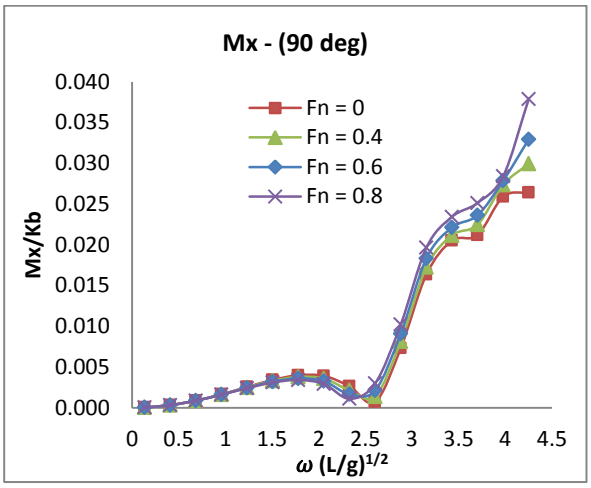

Figure 6.86: RBC numerical prying moment in Beam Seas

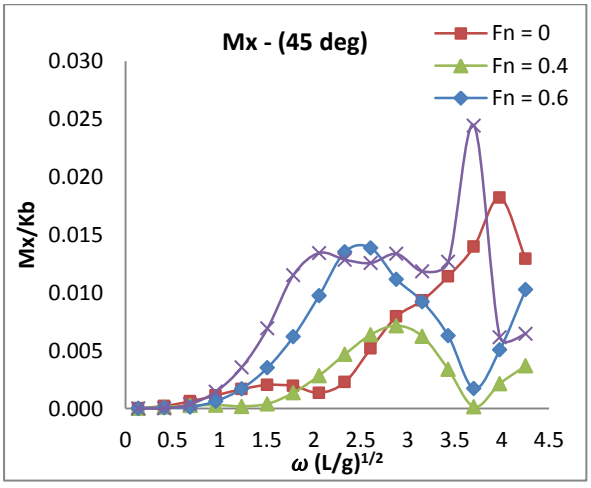

Figure 6.87 RBC numerical prying moment in Stern Quartering Seas

6.4.2.4 The Yaw Splitting Moment (Mz)

The plots of the yaw splitting moment in the **Head Seas (180^o),** Figure 6.88, have shown some similarities in their responses with those for the vertical shear force in the **Head Seas**, except in their magnitudes. The principal similarity is the coupling of the responses with the pitch motions, a trend that appeared as kinks at specified frequencies. These kinks are mainly found in the responses for the forward speeds condition (Fn = 0.4, Fn = 0.6 and Fn = 0.8) and they are distributed within a frequency range of 1.5 – 3.5.This condition confirms the influence the pitch motions have on the behaviour of the yaw splitting.

The plots in the **Bow Quartering Seas (135^o),** Figure 6.89**,** contain some shifts in the frequencies of their respective peak responses. These peaks occurred at the positions of the kinks and their magnitudes are also not in any way proportional to the vessel speeds. The trends of these responses are nonlinear and the kinks occurred in the plots for forward speeds condition responses (Fn = 0, Fn= .6 and Fn = 0.8), as the frequency progresses. This change is, as expected, due to the effects of vessel speeds on the responses.

In the **Beam Seas** (**90^o**), Figure 6.86, the plots have shown relatively linear characteristics and with consistently similar magnitudes due to their individual vessel speed responses. Again, the plots contain a kink at high frequency which is due to influence of the coupling with roll motions. The responses do not change with the changes in the vessel speeds.

The plots of the responses in the **Stern Quartering Seas (45^o)** are presented in Figure 6.92 The distinct features of these plots are the high responses due to vessel speed of Fn = 0 and the peak responses due to Fn = 0.8. The magnitude of response for the zero speed, Fn = 0, is significantly higher within the mid-range frequencies and they are also detached from those for the forward speeds. Also, the trend of the forward speed plots is nonlinear with respect to the vessel speeds which suggest that the forward speeds effect only kicks in at higher frequencies.

The plots in the **Following Seas (0^o),** Figure 6.91, have shown a gradual change in the linearity of the responses as the vessel speed increases. They also contained some kinks at higher frequencies. The responses due to zero speed, Fn = 0, are the most dominant within a frequency range of 0 - 3.0. The effects of vessel speed on the responses are shown in terms of slight shift in the frequencies of the kinks in the plots for vessel speed of Fn = 0.4 and Fn = 0.8

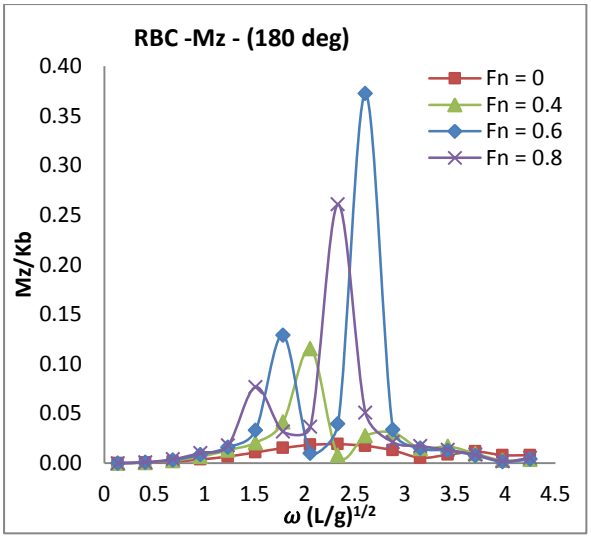

Figure 6.88: RBC numerical yaw splitting moment in Head Seas

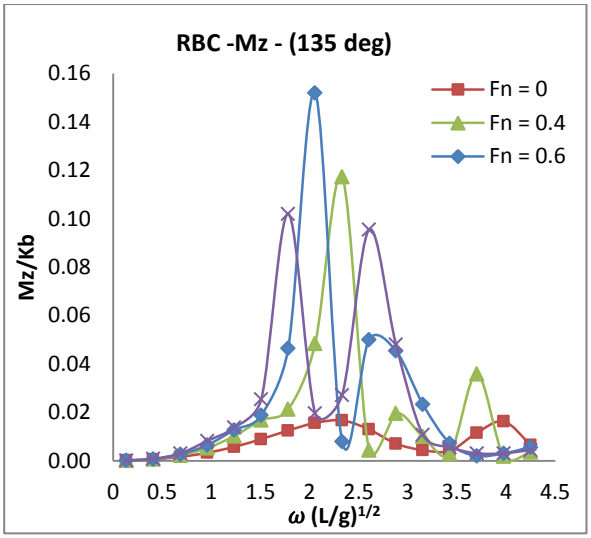

Figure 6.89: RBC numerical yaw splitting moment in Bow Quartering Seas

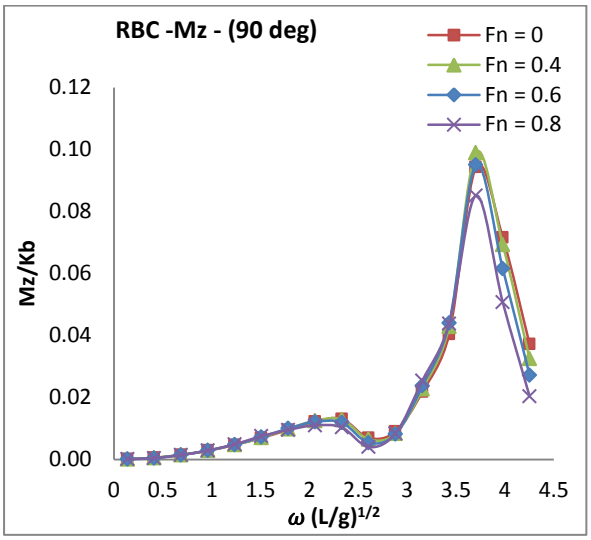

Figure 6.90 RBC numerical yaw splitting moment in Beam Seas

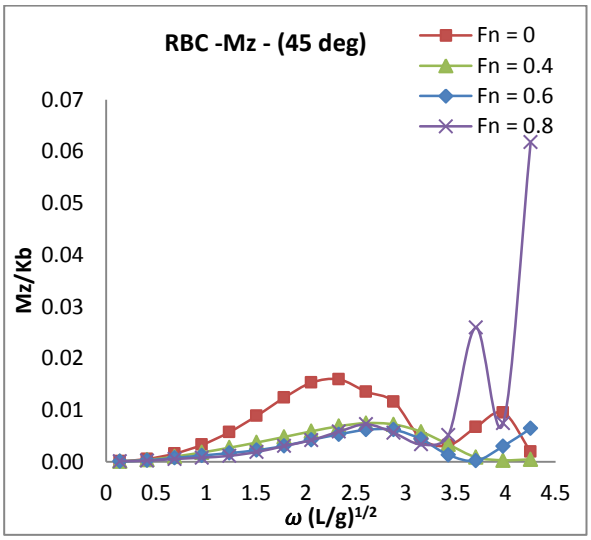

Figure 6.92: RBC numerical yaw splitting moment in Stern Quartering Seas

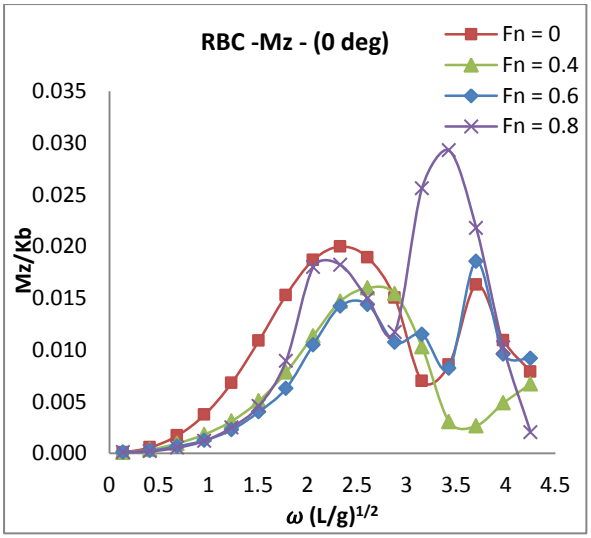

Figure 6.91 RBC numerical yaw splitting moment in Following Seas

6.4.2.5 Torsional (Longitudinal) Moment (Mxz)

The longitudinal Torsional moment in the **Bow Quartering Seas (135^o)** are presented in Figure 6.93. The trends of these plots are generally nonlinear, especially in the forward speed condition (Fn = 0.4, Fn = 0.6 and Fn = 0.8) .The forward speeds responses contain kinks at varying frequencies and they are detached from those for the zero speed. The changes in the frequencies of these kinks are due to effects of the vessel speeds. On the other hand, plots for the **Beam Seas (90^o) -** Figure 6.94**,** are linear but they have shown an inverse relationship between the vessel speeds and the magnitudes of the response at higher frequencies. The plots are less sensitive to the changes in vessel speeds. The responses in the **Stern Quartering Seas (45^o),** Figure 6.95**,** are somewhat nonlinear but at higher frequencies. They also contain some kinks that have shifted as the vessel speeds increase.

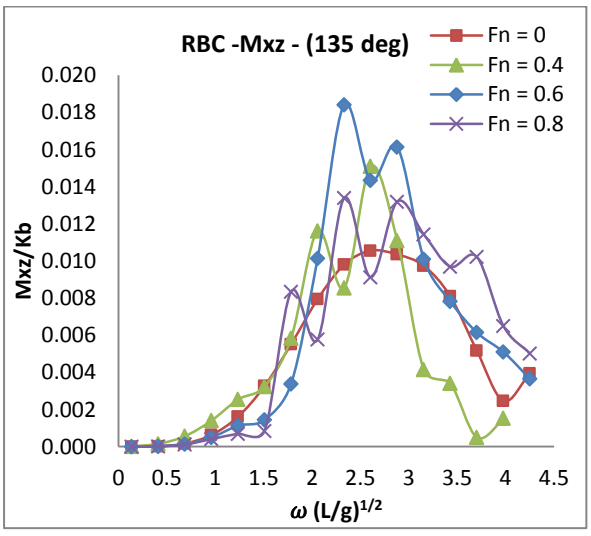

Figure 6.93: RBC numerical longitudinal Torsional moment in Bow Quartering Seas

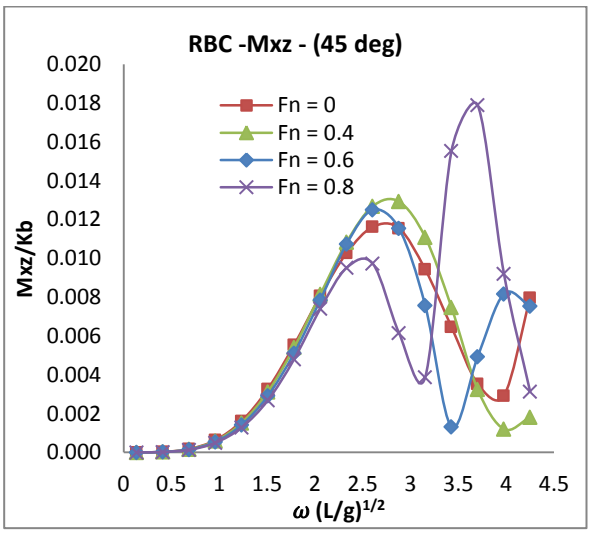

Figure 6.95: RBC numerical longitudinal Torsional moment in Stern Quartering Seas

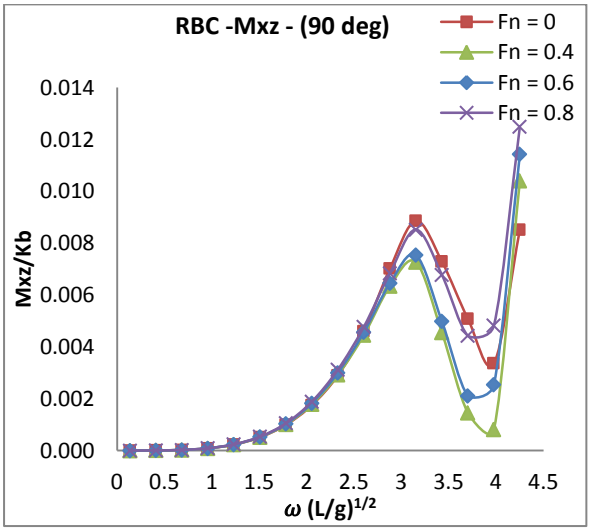

Figure 6.94: RBC numerical longitudinal Torsional moment in Beam Seas

6.4.3 Comparison Between DVC and RBC Wave-induced Loads Response Results

This section presents a detailed comparisons of the numerically predicted wave-induced load responses for the **DVC** model and its competing **RBC** model due to the vessel speeds of Fn =0 and Fn = 0.6 (corresponding to vessel speeds of 0kn and 15kn) in some selected headings. The orientations of the axes of these plots are similar to those that have been defined in section 4.5.3.

6.4.3.1 Comparisons of the Longitudinal Shear Force (Fx)

The comparisons of the longitudinal shear force in the **Bow Quartering Seas (135^o)** for the two models are presented in Figure 6.96. The trends of these plots present mixed results. At zero speed, Fn = 0, the responses appear to be similar but having different magnitudes while in the forward speed, Fn = 0.6, the responses for the **DVC** contain three kinks and over a wider frequency band as opposed to the two kinks within a narrow frequency band in the **RBC** model. The effects of the frequency range over which the load acts on the model has a significant relationship with the fatigue life of the vessels, hence this effect needs to be further investigated (Lavroff *et al.*, 2007).

The **DVC** model has a peak magnitudes of 0.07 at a frequency of 2.10 and which is recorded at a vessel speed of Fn = 0.6. On the other hand, the **RBC** model has a peak magnitude of 0.113 at a frequency of 2.33 due to a vessel speed of Fn = 0.6. The kinks in the forward speed are due to the coupling of the wave-induced responses with the pitch motions and the natural pitch frequency of the model, in addition to the vessel speed effect.

The responses in the **Beam Seas (90^o),** Figure 6.97, for these models are similar in many respects in terms of their respective magnitudes and the trends. The trends of the responses change linearly with the vessel speeds, but the similarity of their magnitudes is limited to higher frequencies. The responses are also not sensitive to the changes in the vessel speeds. The effects of vessel headings changes (from Head Seas to the Following Seas) on the responses manifested in the form of reduced responses magnitudes and the number of kinks that occurred in the plots.

A summary of the peak magnitudes of the responses for the longitudinal shear force in all the vessel headings is given in Table 6.6. The table also shows that the most dominant longitudinal shear force acting on the vessel was found in the **Bow Quartering Seas**

condition. Of these two models, the **RBC** has the highest peak magnitude of the responses than the **DVC** which leads to the conclusion that the **DVC** is less sensitive to the most dominant loads than the **RBC** model.

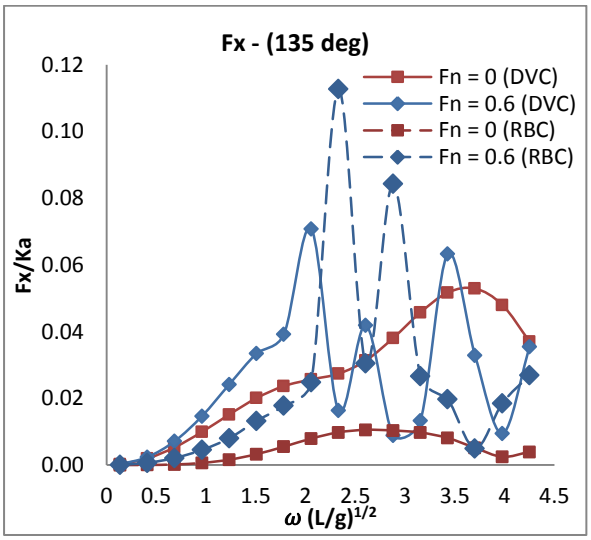

Figure 6.96: Comparison of the Longitudinal Shear Force in Bow Quartering Seas

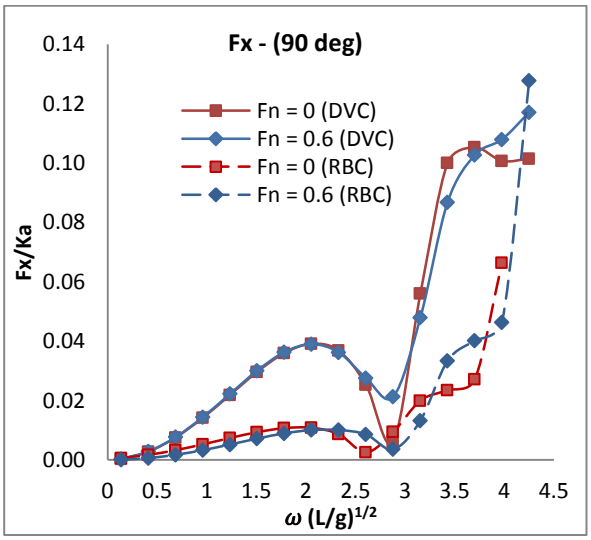

Figure 6.97: Comparison of the Longitudinal Shear Force in Beam Seas

Table 6.6: A Summary of the peak magnitudes of the Longitudinal Shear Force (Fx)

S/N	Heading (Deg)	*DVC Model*		*RBC Model*	
		Fx	***ω(L/g)$^{1/2}$***	***Fx***	***ω(L/g)$^{1/2}$***
1	Head seas (180^{o})	0.0071	2.60	-	-
2	Bow Quartering	0.221	2.88	0.237	2.06
3	Beam Seas	0.117	4.25	0.152	4.25
4	Stern Quartering	0.115	3.98	0.112	3.98
5	Following Seas	0.0025	2.90	-	-

6.4.3.2 Comparison for the Vertical Shear Force (Fz)

The results of the comparisons of the vertical shear force for the **DVC** and the **RBC** models in the **Head Seas (180^o)** are presented in Figure 6.98. The trends of these responses at zero speed, Fn = 0, and the forward speeds are similar. The forward speed responses, Fn = 0.6, for both of these models contain two kinks but they are within a different frequency range. These kinks are due to the coupling of the pitch motions with the responses of the vertical shear force. The condition is similar to those that have been observed in the longitudinal shear force that has been reported earlier.

In the **Bow Quartering Seas (135^o),** Figure 6.99, the responses are nonlinear and they have shown a wide variation in their magnitudes for the vessel speeds that have been presented. The responses for the **DVC** model at zero speed, Fn = 0, contained kinks that are within the higher frequency region and which then shifted to the mid-range frequency region. The reason for this change is due to the effects of the vessel speed changes. The three kinks that appeared in the plots the response for the **DVC** model at zero speed are due to the coupling of the vertical shear force responses with the pitch motions and the resonant heave response; while in the **RBC**, the coupling is between the vertical shear force and the roll resonance.

In the **Head Seas (180^o)**, the **DVC** model has a peak magnitudes of 0.75 at a frequency of 2.90 due the vessel speed of Fn = 0.6 compared to the **RBC** model's of 0.49 at a frequency of 2.6 due to the same vessel speed of Fn = 0.6. Similarly, the peak magnitudes of responses for the **DVC** model in the **Bow Quartering Seas (135^o)** is 0.38 and which occurs at a frequency of 2.9 due to the speed of Fn = 0.6 while the **RBC** model has a peak magnitude of 0.22 at the frequency of 2.1 due to same vessel speed. There is also a remarkable reduction in the magnitudes of these responses as the heading conditions changes from the **Head Seas (180^o)** to the **Following Seas (0^o)**.

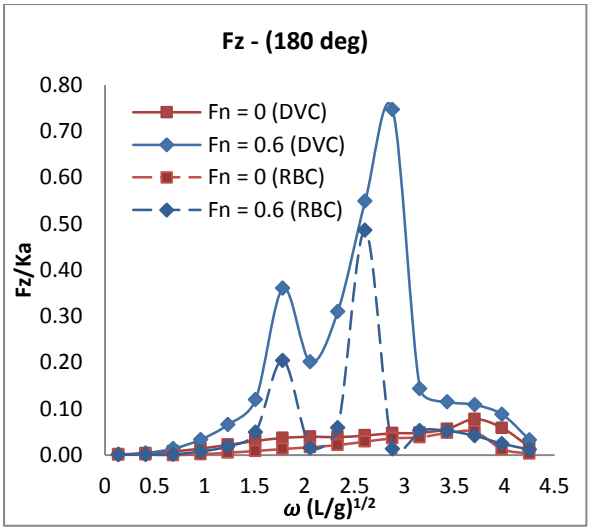

Figure 6.98: Comparison of the Vertical Shear Force in Head Seas

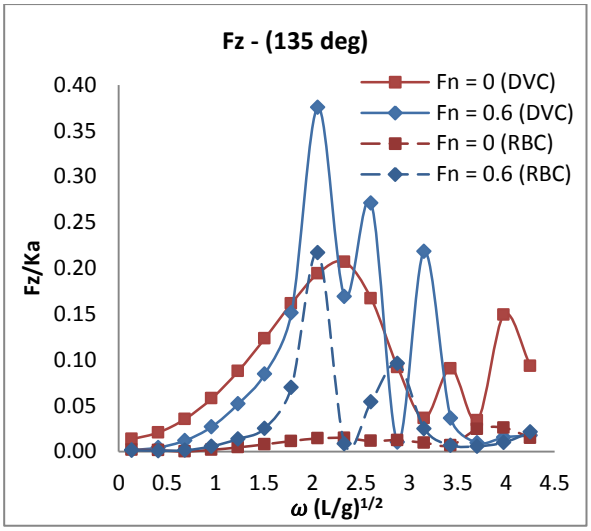

Figure 6.99: Comparison of the Vertical Shear Force in Bow Quartering Seas

A summary of the peak magnitudes of the responses for the vertical shear force in all the vessel headings is given in Table 6.7. The table also shows that the most dominant longitudinal shear force acting on the vessel was found in the **Bow Quartering Seas** condition. Of these two models, the **DVC** has the highest peak magnitude of the responses than the **RBC.**

Table 6.7: A Summary of the peak magnitudes of the Vertical Shear Force (Fz)

S/N	*Heading (Deg)*	*DVC Model*		*RBC Model*	
		Fz	$\omega(L/g)^{1/2}$	*Fz*	$\omega(L/g)^{1/2}$
1	Head seas (180^o)	0.750	2.88	0.486	2.60
2	Bow Quartering	1.330	2.88	0.217	2.06
3	Beam Seas	0.325	4.25	0.119	3.70
4	Stern Quartering	0.048	2.33	0.038	4.25
5	Following Seas	0.063	3.15	0.055	3.43

6.4.3.3 Comparison for the Prying Moment (Mx)

The comparisons for the prying moment in the **Bow Quartering Seas (135^o)** for the two models are presented in Figure 6.100. The trends of their responses at zero speed, Fn = 0, are essentially the same and they have not shown any significant feature. The magnitude of the responses increases almost linearly with the frequencies. In the forward speed condition, Fn = 0.6, the responses for the **RBC** contain two kinks, one of which is due to the coupling with

the roll motions. The **RBC** model has higher magnitudes at the same vessel speed and frequency than the **DVC** model.

The trends of the responses in the **Stern Quartering Seas (45^o),** Figure 6.101, are somewhat similar in the sense that the plots for the Fn = 0.6 have shifted away from those for the Fn = 0. This shift has resulted in a reduction in their magnitudes. While the **DVC** model has higher magnitude of response in the zero speed condition, the magnitudes for the **RBC** models are higher in the forward speed conditions. The magnitude of the responses reduces as the vessel headings changes from the **Head Seas** to the **Following Seas** (Table 6.8). This effect has also resulted in their respective plots having reduced number of kinks.

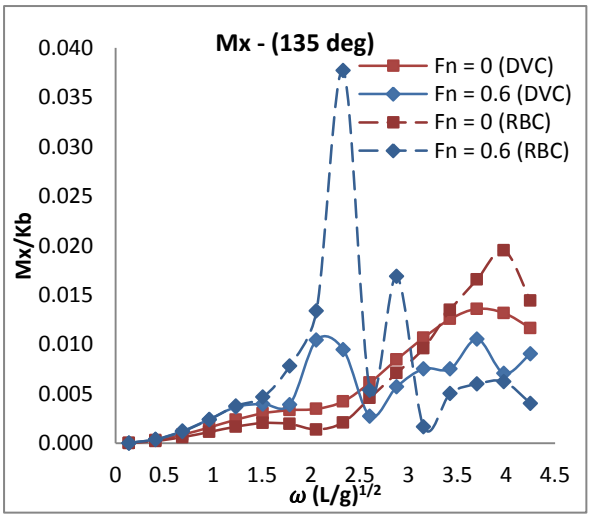

Figure 6.100: Comparison of the prying moment in Bow Quartering Seas

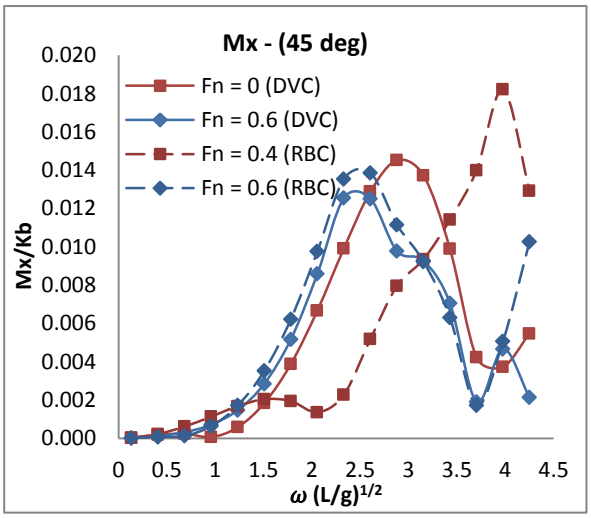

Figure 6.101 Comparison of the prying moment in Stern Quartering Seas

Table 6.8: A Summary of the peak magnitudes of prying moment (Mx)

S/N	***Heading (Deg)***	***DVC Model***		***RBC Model***	
		Mx	***$\omega(L/g)^{1/2}$***	***Mx***	***$\omega(L/g)^{1/2}$***
1	Bow Quartering Seas	0.043	2.88	0.016	1.78
2	Beam Seas	0.028	4.25	0.037	4.25
3	Stern Quartering Seas	0.018	3.70	0.024	3.70

6.4.3.4 Comparison for the Yaw Splitting Moment (Mz)

The plots for the yaw splitting moment comparisons in the **Bow Quartering Seas (135^o)** are presented in Figure 6.102. The characteristics of these plots are nonlinear with respect to the vessel speed. A significant difference between the magnitudes of responses for the two models was observed in the forward speed condition, Fn = 0. The **RBC** model suffers from having higher as result of the kinks that appeared in its response. The responses for both of

the models at zero speed, Fn = 0, are largely similar, even though **DVC** model has slightly higher responses. The kinks in the **RBC** model's responses are due to the coupling of the yaw splitting moment with the roll motions.

The magnitudes of the responses for the two vessel speeds considered in the **Stern Quartering Seas (45^{o}),** are presented in Figure 6.103. The plots have nearly the same trends. The responses due to the forward speed are lower than those for the Zero Speed. The zero speed condition for both of the models clearly offers the most dominant yaw splitting moment. It is difficult to determine the actual effects of change in headings on the results of the responses because of the presence of such a high magnitude of the kinks in the **RBC** model response at Fn = 0.6. However, in spite of this, there is still a reduction in the responses as the vessel headings changes from **Head Seas** to the **Following Seas** (Table 6.9).

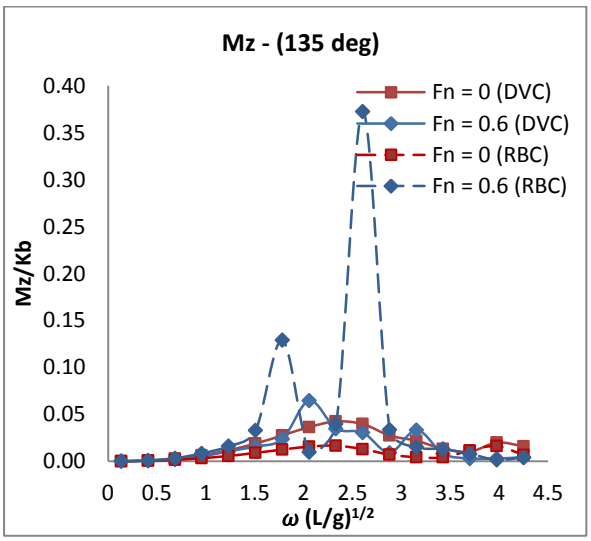

Figure 6.102: Comparison of the yaw splitting moment in Bow Quartering Seas

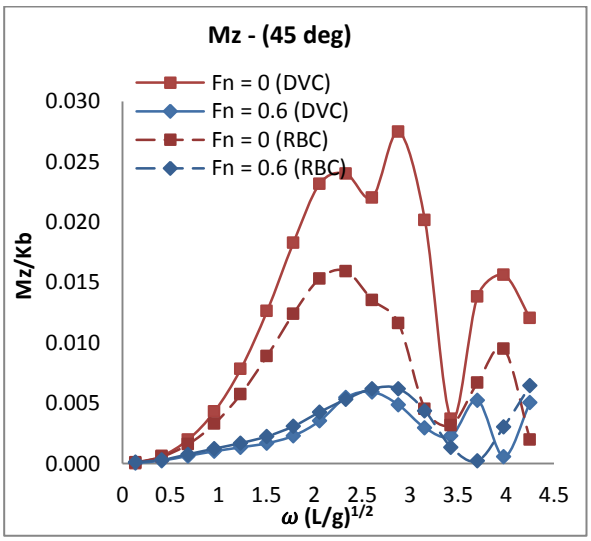

Figure 6.103: Comparison of the yaw splitting moment in Stern Quartering Seas

Table 6.9: A Summary of the peak magnitudes of the Yaw Splitting Moment (Mz)

S/N	*Heading (Deg)*	*DVC Model*		*RBC Model*	
		Mz	*$\omega(L/g)^{1/2}$*	*Mz*	*$\omega(L/g)^{1/2}$*
1	Head seas (180^{o})	0.110	2.60	0.370	2.60
2	Bow Quartering	0.071	2.60	0.150	2.06
3	Beam Seas	0.060	4.25	0.095	3.70
4	Stern Quartering	0.028	2.87	0.064	4.25
5	Following Seas	0.043	3.70	0.029	3.43

6.4.3.5 Comparison for the Torsional (Longitudinal) Moment (Mxz)

The comparisons of the longitudinal Torsional moment for the two models in the **Bow Quartering Seas (135^{o})** are presented in Figure 6.104. The trends of these plots are generally nonlinear in the forward speed condition (Fn = 0.6) .The responses for both of the models in the forward speeds condition contain kinks at varying frequencies. The changes in the frequencies of these kinks are due to effects of the vessel speeds on the responses. On the other hand, while the plots for the **Beam Seas (90^{o}) -** Figure 6.105**,** are linear, there is a clear distinction between their peak magnitudes with the **DVC** model having the highest responses. There is also an inverse relationship between the vessel speeds and their response magnitudes at higher frequencies. These changes in the vessel speeds do not affect the response of the models in this heading. This phenomenon is similar to what has been observed in the **Stern Quartering Seas (45^{o}),** Figure 6.68**.** The **RBC** models appears to be less sensitive to the Torsional moment, hence it performs better than the **DVC** concept (Table 6.10).

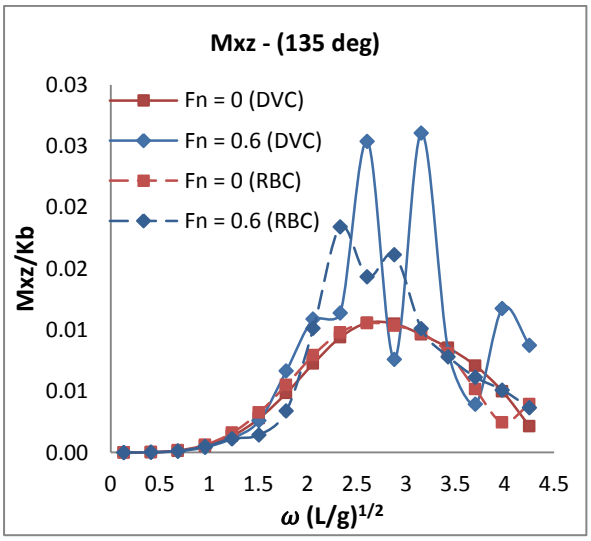

Figure 6.104: Comparison for the longitudinal Torsional moment in Bow Quartering Seas

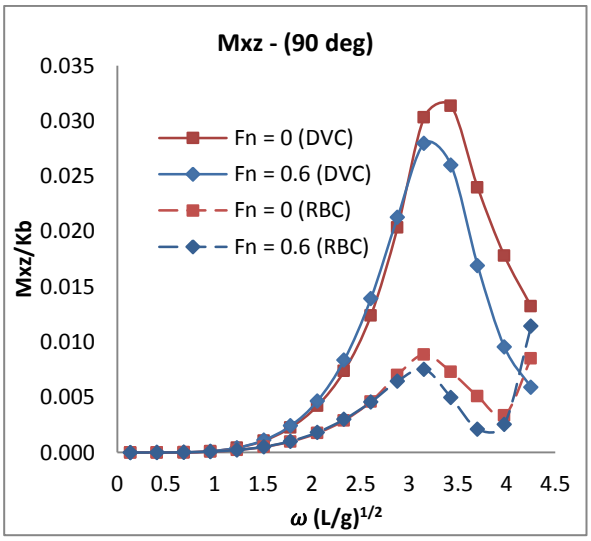

Figure 6.105: Comparison for the longitudinal Torsional moment in Beam Seas

Table 6.10: A Summary of the peak magnitudes of Torsional Moment (Mxz)

S/N	*Heading (Deg)*	*DVC Model*		*RBC Model*	
		Mxz	*$\omega(L/g)^{1/2}$*	*Mxz*	*$\omega(L/g)^{1/2}$*
1	Bow Quartering Seas	0.054	2.33	0.010	2.06
2	Beam Seas	0.030	3.15	0.018	3.70
3	Stern Quartering Seas	0.040	3.98	0.013	4.25

6.5 Conclusions

In this chapter, the motions and the wave-induced loads response characteristics of the Deep-V Catamaran (**DVC**) concepts and its equivalent Round Bilge Catamaran (**RBC**) have been predicted and compared. The significance of these results is that they would serve as useful tools in the understanding into the seakeeping and structural response behaviour of the **DVC** vessels. The results will also be beneficial to the naval architects and the ship designers engaged in the concepts selection and the design, especially in the preliminary stage, of multihull vessels.

A comparison of the results of the **DVC** concepts with those for the **RBC** vessel has also been performed in line with the broader objectives of this thesis. Based on these results, the following is the summary of the findings that have been made:

1. In the motions response comparisons, it has been established that the **DVC** concept performs better than its competing equivalent **RBC** vessel in the Head Seas and the Bow Quartering Seas conditions in terms of having lower magnitudes of motions responses. The behaviour of the models in the Beams Seas is relatively similar in terms of their respective trends.
2. To further corroborate the findings reported in item 1 above, spectral response analysis using the various response amplitudes operator (RAO) that have been predicted in the study were performed for vessel operations in 4 sea states. The result of this analysis indicates that the better performance that the DVC concepts offer in comparison to the performance of the RBC concept in waves appears not to be very significant, hence further study is required in order to have a clearer understanding of this aspect of the performance.
3. The motions and wave-induced loads responses for both of these models in the forward speed conditions have been found to be strongly nonlinear with respect to the increase in the vessel speed. This condition was quite visible in the Head Seas and in the Bow Quartering Seas, and especially at higher frequencies. The effect of this nonlinearity reduces in the responses for the Stern Quartering and the Following Seas.
4. The motions and the wave-induced loads responses in the Beams Seas have been found to be insensitive to the effects of the changes in vessel speeds. In addition, the Beam Seas responses have also exhibited a relatively linear behaviour and with very similar trend throughout the study.

5. The interactions between the individual motion responses with one another, on one hand, and with the wave-induced loads, on the other hand, have resulted in the frequent appearance of kinks in a coupled form with the responses of other motions or wave-induced loads. Such kinks are also attributed to the effects of changes in the vessel speed since their magnitudes usually increase when the vessel speeds increases. The effects of these coupling could be adverse to the performance of the vessel, hence it requires further investigation.
6. The effects of changes in the vessel/wave headings have resulted in the reduction of both the motions and wave-induced load response magnitudes for these models. However, an exception to this observation applies only in the Beam Seas and in a condition in which the magnitudes of the responses are considered to be of negligible consequence to the overall performance of the vessel, especially in the Head Seas – for roll motions, and the Prying Moment - wave-induced loads.
7. In the plots for the RBC model responses, it has been observed that the frequency range of the responses, in most of the headings, occurred within a narrow frequency band and at the same time, behaving nonlinearly at higher frequencies. Such phenomenon is directly related to the cause of hull structure's vibrations and it could cause fatigue problem to the vessel structure. This condition needs to be further investigated
8. From the perspective of wave-induced load response on the DVC and the RBC concepts, DVC concepts is less sensitive to wave-induced load in the critical headings hence it offers further opportunity of having increased operational life cycle than the RBC concept.
9. Finally, the dominant loads parameters of the Deep-V Catamaran concept have been identified.

Chapter 7

Case Study: Structural Response Analysis of the RV Princess Royal

7.1 Introduction

The design of a vessel structure generally involves a skilful selection of the materials that are required in order to resist the forces due to dynamic wave loads, hydrostatic pressures, self-weights of the vessel and its components. For this reason, the forces and the resulting combinations of stresses and moments (Bending and Torsional) acting on the hull structure must be properly evaluated in order to ensure that their integrity is adequate and it is safe for its intended through-life time purpose. In addition, the structure must be fit for purpose both in terms of strength, stiffness, fatigue life and cost.

In view of this, the objective of this chapter is to investigate the structural response behaviour of the DVC hull structure to the various wave induced loads that have been predicted. This would consist of assessing the overall strength of the cross-deck structure, in addition to other global and local strength demands on the vessel.

This section (Section 7.1) provides a brief introduction and concise objective of the chapter. Section 7.2 describes the structural configuration of the model of the RV Princess Royal vessel. The section also discusses the mechanical properties of the structural materials that have been utilised in the design, in addition to the modelling techniques that were applied.

The Section also highlights the key assumptions that were made with respect to the analytical boundary conditions. The philosophy adopted in evaluating the loading conditions and strength assessment of the vessel is described in Section 7.3. The Section provides the description of the methodologies adopted for the structural elastic strength analyses of the model. Also, the section comprised of a definition of the operational profile of the vessel which was then used as a practical basis for determining the extreme design wave-induced loads in relation to the vessel's overall operations. A comparison of the predicted wave-induced loads with those that are determined based on the classifications societies' generalised recommendations as spelt out in the Lloyds Register's Rules and Regulations for Classification of Special Service Craft (LR, 2012); is also presented in this Section. Section 7.4 presents the results and discussions of the structural responses due to the effects of the predicted loads on the vessel whilst Section 7.5 concludes the chapter with a summary of the key observations made with regards to the results of the structural analyses.

7.2 The Structural Configuration of the Deep-V model

7.2.1 The Model Description

A global Finite Element (**FE**) model of the Princess Royal research vessel was developed using the MAESTRO program (MAESTRO, 2012). The model consists of the two demi-hulls and it is rigidly connected by a cross-deck structure. The vessel is also fitted with a bulbous bow and an appendage in the form of an extended skeg and it is symmetrical along the longitudinal centreline. The main particulars of the vessel have been defined earlier in Table 4.1**.** Since the vessel is symmetrical along the centreline, only a half of its full scale global FE model was created. This half was then mirrored using the command tools available in the program to produce the full scale vessel. The significance of modelling a half of the vessel is that it allows for the application end-moments to the model as a cut-model – an essential requirement in the structural analysis using fixed-ends moment. On the other hand, the full scale model allows for an adequate definition of the boundary conditions and the application of the design loads at their actual position on the vessel.

The FE model was created using five sub structural units which collectively formed the half side of the vessel along the line of symmetry. The structural configuration of the model, which consists of 3 traverse frames per meter, 31,000 structural nodes, and 186,000 degrees of freedom, was created in such a way that the stiffeners and frames were modelled as strake elements. The FE model created using the MAESTRO is shown in Figure 7.3.

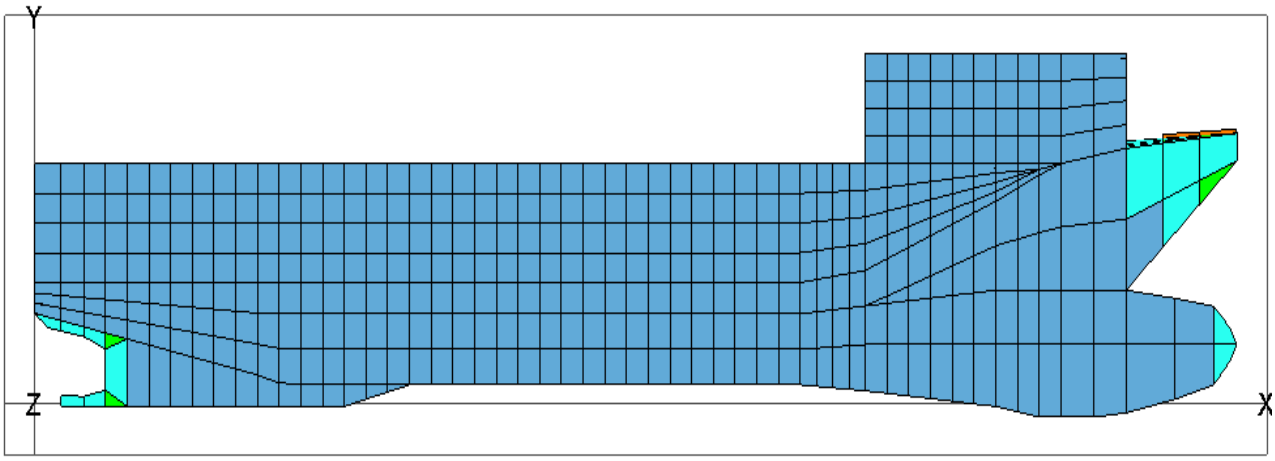

Figure 7.1: The profile view of the model

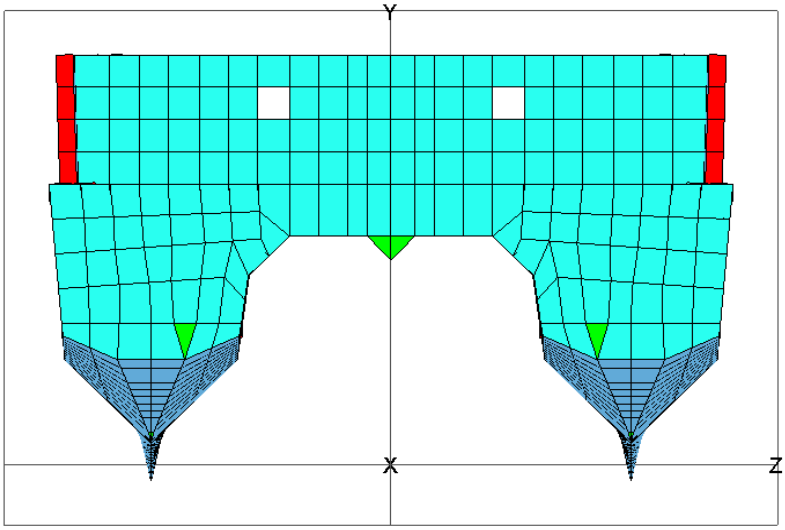

Figure 7.2: The body plan of the model

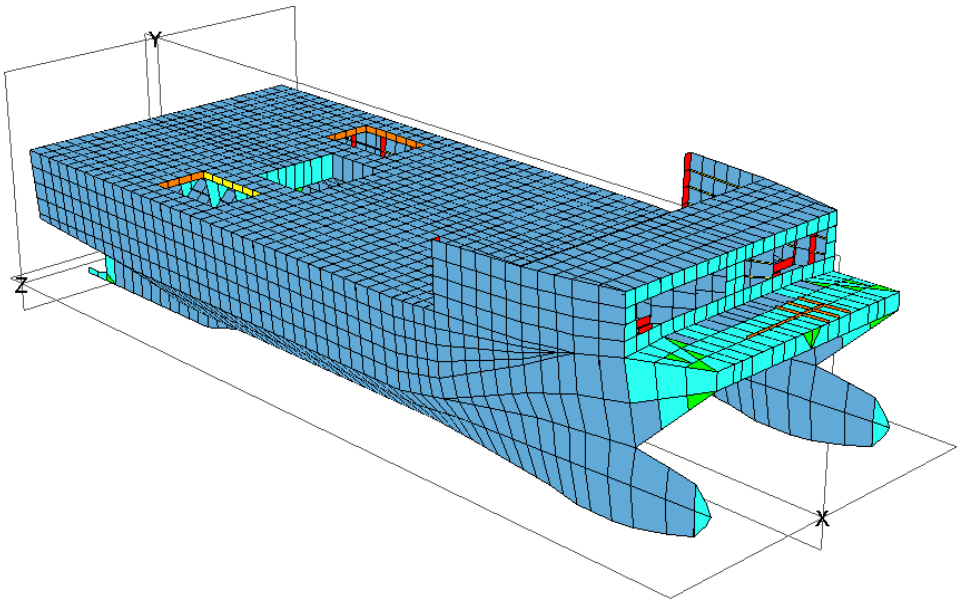

Figure 7.3: A global FE model of the RV the Princess Royal

7.2.2 The MAESTRO FEA and the Modelling Process

Given the geometric and structural complexity of a twin hull vessel, such as the RV Princess Royal, the Finite Element Method of analysis, FEM is the most appropriate approach that one can use to determine both the internal and external responses of the vessel structure to the various applied loads. This method allows for the stresses in the structure to be determined according to the stiffness of the elements and it does not necessarily require some simplified assumptions to produce results. The MAESTRO (**M**ethod for **A**nalysis, **E**valuation and **Str**uctural **O**ptimisation), which is an FE analysis program that has the capability of performing failure analysis based on limit state philosophy and structural optimization, was thus selected. The program has the added advantage of having an in-built capability to determine the both static and dynamic wave-induced responses and other loading systems of the vessel. This characteristic ensures that there is equilibrium between the hydrodynamic panels used in the wave-induced loads predictions and the geometrical FE mesh that is required for the structural analysis. It is important to note that the MAESTRO software was specifically developed for ship structures and that it has been continuously developed and enhanced to be able it to carter for the progressively with larger range of marine structural configurations(MAESTRO, 2012).

The construction of this model involved the use of the combination of quadrilaterals; triangular plates; beams and bars elements which formed structural panels. The design process requires that the model is subdivided into smaller units, called modules which offer unique advantage of having a good control over the entire design process. This subdivision facilitates the modelling of the structure as a sub-structural units that consists of the "substructure", "modules", "strake" and "members (element)" (MAESTRO, 2012).

7.2.2.1 The Elements

In MAESTRO, the elements have a relatively large size which can take the size the entire panel between the frames. The program has some sets of elements that are particularly unique in shapes and sizes. Of these elements, the types that have been used in modelling of this vessel are summarised in Table 7.1:

Table 7.1: Panel elements in MAESTRO

Element	Type	Nodes
CQuadR	Flat/Stiffened Panel	4
Hybrid CBAR	Beam Element	2
CTRIR	Triangle Element	3

7.2.2.2 The Modules and Strakes

The module is a uni-directional group of three-dimensional elements that are located at a specified distance from each other. These members can be found along the transverse or the longitudinal directions of the model and they usually have similar geometry. The modules are normally created using the combinations of the strakes. The strake is a form of a stiffener which occurs at specific intervals and they are used to define the locations of beams and the panels that make up the module. The definition of the location of endpoints in a transverse plane and at both ends of the module helps in generating the mesh within an element. The module is an important part of the building block of a structural model.

7.2.2.3 The Substructure

This consists of a group of modules that are used in modelling either a section or part of the model itself that have similar geometrical properties. The substructures allows for the creation of the components of the model by categorizing them into modules – or a smaller units, based on their intended usage. The coordinates of each substructure is required when building the entire model in order to have ease of assembling into a complete model.

7.2.3 Materials Properties

Catamarans are inherently sensitive to lightship weights due to their geometrical configuration. For this reason, this type of vessel is generally designed using relatively lightweight materials such as aluminium alloys, Fibre Reinforced Polymers, etc. The lightweight materials help it to achieve a higher allowable deadweight fraction and which is a critical requirement for this class of vessel during the design stages.

The Marine-grade weldable aluminium alloys were used as the main structural materials in the design of the Princess Royal vessel. The selected properties of these materials are given in

Table 7.2. The **5083-H116** material comes in various forms typically as aluminium sheets with plate thickness range of up to 50mm thick (DNV, 2009). The **6082-T6** material, on the other hand, comes in extruded forms as aluminium sections with section thickness range of up to 12.5mm thick (DNV, 2009). This grade of material is mainly used as bars, beams and stiffeners in the design of the vessel and their strength is derived from the combination of the above listed characteristics. These two alloys can be welded together and have no compatibility problems with each other. The mechanical characteristics of these materials have been explained in **Chapter 2** of this thesis.

Table 7.2: Marine-grade Aluminium Alloys Material Properties

Material Properties	***5083-H116***	***6082-T6***
Young's Modulus of Elasticity **(GPa)**	70	70
Poisson Ratio	0.33	0.33
Material Density **(kg/mm^3)**	2.66e-006	2.66e-006
Yield Stress**(N/mm^2)**	215	260
Ultimate Strength **(N/mm^2)**	165	205
Reduced Yield Stress in AL HAZ **(N/mm^2)**	185	260
Weld Residual Stress/Yield Stress Ratio	1.0	1.0

The **5083-H116** material is widely used in the high speed craft construction industry mainly because it offers some beneficial characteristics compared to other similar weld-able marine-grade aluminium alloys. These characteristics included the following:

1. Relatively high strength
2. Corrosion resistance,
3. Toughness
4. Ductile
5. Weld-ability

7.2.4 The Boundary Conditions

The determination of the stresses on the hull structure and their resultant effects on the cross-deck structure rely on the accurate application of the boundary conditions on each of the demi-hull in order for the model to attain the state of equilibrium. The interaction between the

various structural components such as frames, longitudinal girders, shell plates and stiffeners allows for normal flow of loads and stresses across the elements. Although only half of the model (along the longitudinal plane) was modelled due to the symmetry, the boundary conditions were applied to the full model having mirrored it to create a full extent model. The application of these boundary conditions was done on the basis of the coordinate system that has been presented in Table 7.3. For the purpose of this study, the boundary conditions given in Table 7.4 were then applied to the model of the DVC hull form in the MAESTRO program.

Table 7.3: Definition of the structural coordinate system

X	**Longitudinal direction**
Y	**Vertical direction**
Z	**Transverse direction**

Table 7.4: Boundary conditions that were applied to the FE model

	Type of Constraints	Position of the Constraints
1	FIXED-X, FIXED-Y, FIXED-Z	X = 0m; Y = 1.15m & Z = -2.750m
2	FREE-X, FIXED-Y, FREE-Z	X = 0m; Y = 1.15m & Z = 2.750m
3	FREE-X, FIXED-Y, FREE-Z	X = 16.75m; Y = 1.15m & Z = -2.750m
4	FREE-X, FIXED-Y, FREE-Z	X = 16.75m; Y = 1.15m & Z = 2.750m

7.3 Analysis of Structural Design Loads

7.3.1 Methodology for the Structural Response Analysis of a DVC Vessel

The premise for the initial strength design of the hull structure of a catamaran is similar to that which is used for monohull in the sense that both of them largely employ the principles and assumptions of the small deflection elastic bending theory of beams and plates (Heggelund *et al.*, 2002; Hughes and Paik, 2010). The bending theory allows for the quick determination of the stresses and strength of the hull structure using the appropriate limiting criteria and by assuming that the hull girder structure itself behaves as a simple elastic beam. The basis for the calculations of the stresses and moments acting on this type of structure is the 'elastic bending' formula which is expressed as follows:

$$\sigma = \frac{My}{I} \qquad \textbf{Eqn 7 - 1}$$

Where: σ = Bending stress

M = Moment about the neutral axis

y = Coordinate of the plate measured from the cross section neutral axis

I = Moment of inertia of the cross section

The structural analysis used in the design of this catamaran employs the bending principles for the purpose of determining the global and local stresses on the vessel structures. These stresses include those due to the combined effects of the wave-induced responses results from dynamic loads, still water and the static loads due to the localised weights of cargo and machinery, or direct loads due to local impacts such as the green seas, transient slamming, etc (Brown *et al.*, 1991). In any of these scenarios, the elastic bending theory can give an idea of the global strength of the hull structure (when associated with simple stress criteria and component buckling checks) under these loads. Initial uncertainties and approximations in the stress analysis are typically provided for by the careful use of the safety factor.

7.3.2 Evaluation of Failure Modes and Acceptance Criterion

The principles for the evaluation of structural adequacy for structural elements and members in the MAESTRO FE Program are based on failure modes of their constituent structural elements. The evaluation of these failure modes for a hull structure has been carried out based on failure of structure in yielding and buckling. These failure modes are directly depended on

the structural geometry of the ship, their appropriate boundary conditions, and most importantly, the structural loads applications. For a given ship structural system and other relevant loading conditions, the calculated stresses must not be greater than the limits prescribed and/or computed for these failure modes (MAESTRO, 2012)

The acceptance criterion for this structure is based on the failure modes due to the resulting stresses that were observed on the cross-deck structures and within connections between the cross-deck and the two demi-hulls. The acceptance criteria for failure due to these stresses in MAESTRO is such that adequacy ratio, $\boldsymbol{g(R)}$, as defined in Eqn 7.3 is not more than 1.0.

$$\boldsymbol{g(R) = \frac{1 - \gamma . R}{1 + \gamma . R}} \qquad \textbf{Eq 7 - 2}$$

Where: $\boldsymbol{\gamma}$ is safety factor and R is the strength ratio due to the loads **Q** and the load limits $\mathbf{Q_L}$ which further defined as $\boldsymbol{R = \frac{Q}{Q_l}}$.

The determination of whether the ship structure design is satisfactory or not is based on the adequacy parameters due to the ultimate and serviceability limit states design criterion. The ultimate limit state design mainly deals with failure of the structure due to the applied loads while the serviceability limit states involve the prediction of failures of structure in the form of deterioration of the structure during its operational life cycle.

The MAESTRO FEA Program (MAESTRO, 2012), considers two distinct failures modes. These modes comprised of the Panel Failure Modes and the Beam Failure Modes.

7.3.2.1 Panel Failure Modes

There are eight different types of panel failure modes that have been implemented in the MAESTRO FEA Program and they are presented below. These modes comprised of the panel failures due to collapse, yielding and the serviceability limit state and they have covered the various failure scenarios that typically occur in stiffened panel as used in the design of ship structure. A concise explanation of these failure modes is presented in this section based on the work presented in the following references (Hughes and Paik, 2010; MAESTRO, 2012)

i. Panel collapse due to stiffener bending (Flexure – (PCSF)
ii. Panel collapse due to combined buckling of plate (Flexure – (PCCB)

iii. Panel collapse due to the effects of stiffener buckling (Flexure – (PCB)
iv. Panel collapse due to membrane yielding (Flexure – (PCMY)
v. Panel failure due to flange yielding (PYF)
vi. Panel failure due to plate yielding (PYP)
vii. Serviceability panel failure for plate in bending (PSPB)
viii. Panel failure due to local buckling (PFLB)

There are three different types of failure modes that govern the underlying theory of the failure mechanisms in the PCSF. These modes are very essential to elastic analysis of the structure and they depend on the orientation (positive or negative) of the bending moment and the deflection of the plates and the flanges. The three critical failure modes are given as follows:

i. Stiffener-induced collapse of panels: This failure mode is due to compression failure of the stiffener and it is caused by the combination of in-plane compression and negative bending. The failure occurs when the stress in the middle laminar (thickness) of the flange material equals to the minimum of yield stress or the elastic tripping stress of the flange. Stresses due to this failure can be calculated by using equation **(Eq 7-3)**

$$\sigma_f = \sigma_a + \frac{M_o y_f}{I} + \frac{\sigma_a A(\delta_o + \Delta) y_f}{I} \Phi \qquad \textbf{Eq 7 - 3}$$

ii. Plate induced collapse of panels due to compression failure of the plating: The failure mode can be calculated using equation **(Eq 7-4).** This failure mode is somewhat opposite to the stiffener induced failure

$$\sigma_F = \sigma_{a,tr} + \frac{M_o y_{p,tr}}{I_{tr}} + \frac{\sigma_{a,tr} A_{tr}(\delta_o + \Delta) y_{p,tr}}{I_{tr}} \Phi \qquad \textbf{Eq 7 – 4}$$

iii. Combined failure of stiffener and plating: This failure occurs due to the formation of large positive bending moment that results in excessive tensile stress in the stiffener as a result of concurrent tensile yielding of stiffener and compressive yielding of the plate. The failure stress can be calculated using equation **(Eq 7-5).**

$$\sigma_{Ys} = \sigma_{a,ult} + \frac{M_o y_{f,tr}}{I_{tr}} + \frac{(\sigma_{a,tr})_{ult} A_{tr}(\delta_o + \Delta) y_{f,tr}}{I_{tr}} \Phi + \frac{(\sigma_{a,tr})_{ult} A_{tr} \Delta_p y_{p,tr}}{I_{tr}} \qquad \textbf{Eq 7 – 5}$$

When calculating the PCSF modes, the MAESTRO code requires that the effects of transverse compression and in-plane shear should be considered. In doing so, the respective reduction factors that are needed to achieve this are given in equation **(Eq 7-6)** and **(Eq 7-7).**as follows**:**

$$r_{ay} = 1 - \frac{\sigma_{ay}}{\sigma_{ay,u}}. \qquad \textbf{Eq 7 – 6}$$

$$r_{\tau} = \sqrt{1 - 3\left(\frac{\tau}{\sigma_{Yp}}\right)^2} \qquad \textbf{Eq 7 – 7}$$

Where: σ_f is the collapse stress in the flange

σ_a is the elastic stress in the flange

$\sigma_{a,i}$ is the elastic tripping stress where $i = f$, for flange; and $i = p$ for plate

$\mathbf{M_o}$ is the bending moment

δ_o is the deflection due to lateral loads

A is the cross sectional area

I is the moment of Inertia

$\mathbf{y_f}$ is the distance from the centroidal axis of the flange of stiffeners

Δ is the eccentricity

$\mathbf{r_T}$ is the in plane shear reduction factor while $\mathbf{r_{ay}}$ is the transverse compression reduction factor

$\boldsymbol{\tau}$ is in plane shear stress

Other important failure modes in this category are presented as follows:

Panel Collapse, Combined Buckling (PCCB)

The calculation of the effects of combined buckling on a stiffened panel that is subjected to the combination of longitudinal, transverse, and shear loads induced buckling is calculated by using an interaction formula based on combined strength ratios for longitudinal buckling,

transverse buckling and shear buckling for the panel. The equation for this collapse calculation is given as

$$\boldsymbol{R_x + \frac{0.625\left(1+\frac{0.6}{\alpha}\right)R_y}{1+R_x} + R_s^2 = 1 \ where\ (\alpha \geq 1).} \qquad \textbf{Eq 7 – 8}$$

Where: $\boldsymbol{\sigma_x; \sigma_y;\ and\ \tau_y}$ are the critical uniaxial stresses while $\boldsymbol{R_x; R_y;\ and\ R_s}$ are the uniaxial strength ratios which are further defined in equations (**Eq 3 -9, Eq 3-10** and **Eq 3-11**) respectively

$$\boldsymbol{R_y = \frac{\sigma_y}{\sigma_{y,cr}}} \qquad \textbf{Eq 7 – 9}$$

$$\boldsymbol{R_y = \frac{\sigma_y}{\sigma_{y,cr}}} \qquad \textbf{Eq 7 – 10}$$

$$\boldsymbol{R_s = \frac{\tau_y}{\tau_{y,cr}}} \qquad \textbf{Eq 7 – 11}$$

Panel Collapse, Membrane Yield (PCMY)

The failure due to yielding of the panel occurs through the thickness of the plating and can be calculated using the von Misses equation as presented in equation **(Eq 7 -12)**

In the local design of the other components of the hull structures, the resulting stresses acting on plate element's discrete stiffeners could be in the form of biaxial stresses. The biaxial stresses will be the combinations of the direct local beam and plate bending, shear and/or torsion acting on more than one orientation (coordinate) of a plane section of a framing or beam. The Von-Mises criterion has been used in determining the resultant effects of the internal stresses and it is given in Equation **(7-2):**

$$\boldsymbol{\sigma_t = \sqrt{\sigma_x^2 + \sigma_y^2 - \sigma_x\sigma_y + 3\tau_{xy}^2}} \qquad \textbf{Eqn 7 - 12}$$

Where: σ_x = normal stress in the *x* coordinate direction of the element

σ_y = normal stress in the *y* coordinate direction of the element

τ_{xy} = in-plane shearing stress

The calculated stress from Equation 7-2 is then compared with the material yield strength (or in the case of aluminium, the proof stress criteria), and the appropriate factor of safety. There

are various acceptance criterion of the total equivalent stress (von-Mises stress) acting on a plane section of a beam or plate. These criterions differ from classification societies, hence other criteria, such as the local buckling (elastic and inelastic effects in plates and stiffeners); need to be complied with at the beam or plate element levels.

7.3.2.2 Beam Failure Modes

The application of the limit states design principles to design of beam in MAESTRO program deals with six different failures. The failure modes are presented as follows:

i. Beam collapse due to tripping (BCT)
ii. Beam collapse due to comprehension in flange (BCCF)
iii. Beam collapse due to comprehension in plate (BCCP)
iv. Yielding in the beam flange (BYF)
v. Yielding in the beam web plate (BYP)
vi. Beam collapse due to the formation of plastic hinges (BCPH)

These failure modes have been presented based on whether the failure is due to ultimate limit state or the serviceability limit state. The ultimate limit state failure in this case covers the collapse failure due to the load carrying capacity of the structural members while the serviceability deals with deterioration of the members. Detailed discussion on these failure modes are given in these references: (Hughes and Ma, 1996; Hughes and Ma, 1997; MAESTRO, 2012)

7.3.3 The Operational Profile

The operational deduce profile, in combination with the wave parameters of the operating environment, has been used in the calculation of the extreme design loads experienced by the vessel during its operational life. Their calculation is based on the probability that the vessel would stay in a given wave conditions at certain speed and heading for a given period. Its importance is expressed in the relationship between the significant wave height and the vessel speeds under which the vessel operates(Heggelund *et al.*, 2002).

A typical operational profile that a vessel such as the Princess Royal vessel would encounter during its service years and the probability of occurrence of such speeds are presented in Table 7.5 and Table 7.6 respectively. The maximum operating seeped of the vessel is 20kn while its cruising speed is 15kn. An intermediate speed of 10kn along with the 0kn for

sheltered condition has been considered in this study. The vessel operational profile is only intended to demonstrate the importance of the operational profile in the design process of a vessel.

Table 7.5: Typical vessel operation profile

	Significant Wave Height (m)	**Vessel Speed (knots)**
1	> 3	Sheltered condition at low speed
2	≤ 2.5	10
3	≤ 2.0	15
4	≤ 1.5	20

Table 7.6 Probability of occurrence (%) of the vessel operationsfor different Hs (m) and headings (o)

	Significant Wave Height Hs (m)	0	45	90	135	180
1	> 3	2.5	1	1	1	5
2	≤ 2.5	47	1.0	1.0	1.0	50
3	≤ 2.0	34.5	2.0	1.5	2.0	60
4	≤ 1.5	13	2.0	2	3	80

7.3.4 The Loading Conditions

The structural loads acting on a vessel are classified according to the influence of their magnitudes on the design process of the structures of the vessel (Hughes and Paik, 2010). These loads are broadly classified as either the static or the dynamic loads.

The static loads basically consist of those loads that included the lightship weights of the vessel, wheel house, machinery and other fixed or movable loads like the cargo, passengers etc. The loads are mostly obtained from the known weights of the components of the vessel that are permanently fixed on the structure. The responses of the vessel to these loads are easily determined by multiplying the accelerations due to the vessel's motions with the weights.

The dynamic loads, on the other hand, are those loads that the vessel experiences in its operating environment throughout its design life. These loads include the combination of the responses due to still water and the wave-induced loads due to the inter-actions of the long

and/or short crested waves together with the vessel speeds on the whole or part of the vessel. The methods used in measuring the magnitude of these loads on any sea-going vessel prior to its design remain an important consideration in the design of the vessel.

In view of this, the following are the three sources of the structural loads acting the vessel that have been considered in this study.

1. Numerically predicted loads: These are the loads predicted using integral equations that have been developed as a computer code. The predicted loads are the hydrodynamic wave loads (Still water and the wave-induced loads) the vessel experiences in a seaway. In addition, the extreme loads were also predicted using this method based on the operation profile of the vessel.
2. Experimental loads: These are the wave-induced loads acting on the model that have measured using a scaled model of the vessel in the towing tank. The loads obtained from this exercise are then converted into full scale based on established scaling process in order to obtain the anticipated loads on the vessel.
3. Rule-based loads: These are the loads obtained by the empirical formulations developed by the classifications societies based on the combination of their field experience with a particular class of vessels, previous data obtained from the model tests and sea trials, and the numerical simulations.

7.3.4.1 Lightship Weights on the RV the Princess Royal

The static weights (Stillwater loads) acting on this vessel are the same as the weights that were used in ballasting the vessel in order to achieve a static equilibrium. These loads comprised of the lightship load that have been defined in Table 6.1. The source of these loads is the stability booklet of the vessel. The details of these loads have been presented in Table 6.1, giving the lightship weights of the major components of the vessel.

However, the MAESTRO program has an in-built capability to perform the static equilibrium analysis by rebalancing the total static weights acting on the vessel in order to achieve the desired (design) static equilibrium of the vessel. The program calculates the still water loads and the other properties such as the vessel's draught, longitudinal and transverse centres of gravity, and the vessel's trim angle. The results of the static equilibrium are needed for the predictions of the total wave-induced loads on the vessel based on the determined stability conditions of the vessel.

7.3.4.2 Rule-based Wave-induced Loads predictions

The Lloyd's Register's Rule for the Classification of Special Service Craft was used in the predictions of the loads and structural analysis of the model of the RV the Princess Royal (LR, 2012). The calculations of the wave-induced loads were performed for both the global loads acting on the vessel as well as the local primary loads acting on the cross-deck structure (Transverse loads).

The global loads are the longitudinal loads acting along the vessel length and they are presented in Table 7.7. The response of the model due to these loads were calculated as the magnitude of the vertical bending moments and the shear forces which induce the maximum hogging and sagging of the vessel in the worst operating sea state and for different vessel operating conditions. In addition, the shear forces due to similar wave action on the model were calculated. As a general rule, the transverse moments and forces were compared with the local loads for the purpose of determining the actual loads on the cross-deck structures of the vessel. A summary of the main loads that have been used in the design are given below:

i. The maximum vertical bending moment due to the global loads, M_R (based on the rule length of the vessel)
ii. The maximum transverse bending moment due to global loads acting on the vessel, M_B
iii. The maximum Torsional (pitch-connecting) moment due to global loads acting on the vessel, M_T

The maximum responses experienced by the cross-deck structures were calculated using the guidelines recommended in the LR rules (LR, 2012). The combination of these loads were performed in order to ensure that the structural integrity of the cross-deck structure is adequate enough to withstand any kind of failure due to the loads experienced by the vessel in various operating conditions as recommended by (LR, 2012). These combinations are presented in Table 7.8 based on the following:

i. $0.1\ M_B + M_R + 0.1\ M_T$ (in the Head seas conditions (180^o):
ii. MB + 0.1 MR + 0.2 MT (in the Beam seas conditions (90^o)
iii. 0.1 MB + 0.4 MR + MT (in the Bow & Stern Quartering seas conditions (45^o & 135^o)

Table 7.7: A summary of the calculated Rule-Based global wave-induced loads.

	Global Wave-induced Loads		**Sagging**	**Hogging**
1	Vertical Bending Moment (kNm)	M_{MW}	-974	1558
2	Wave Shear Force (kN)	Q_{MW}	*-162*	260

Table 7.8: A summary of the Rule-Based transverse (local) wave-induced loads

	Local Wave-induced Loads		**Loads**
1	Rule Bending Moment (Sagging) (kNm)	M_R	-974
2	Rule Bending Moment (Hogging) (kNm)	M_R	974
3	Transverse Bending Moment (kNm)	M_B	838
4	Torsional Connecting Moment (kNm)	M_T	1257
5	Rule Shear Force (kN)	Q_T	140

A summary of the design loads that have been obtained, based on the combinations of loads for individual vessel heading condition, from the rule-based calculations of the wave-induced loads are presented in Table 7.9.

Table 7.9: A summary of the calculated Rule-Based local loads combination.

		Sagging (kNm)	***Hogging (kNm)***
1	Head Seas	-1184	1768
2	Beam Seas	-1187	1245
3	Quartering Seas	-1964	1964

A direct comparison of the magnitudes of the loads that have been obtained using the rule-based calculations of the wave-induced loads have been to those obtained from the experimental numerical studies have been performed and presented in Table 7.10.

Table 7.10: Comparison between the maximum numerical and rule-based loads

	Headings	***Numerical (kNm) (MAESTRO Wave)***	***Rule Based (kNm)***
1	Head Seas	1314	1768
2	Beam Seas	778	1245
3	Quartering Seas	1052	1964

7.3.4.3 Extreme design loads

The basis for the computation of the extreme design loads acting on the vessel is by using the results of the numerically measured linear wave-induced loads (Schellin *et al.*, 2013). The process involves the determination of the hull girder load response amplitude operators (RAO) in order to predict the resulting extreme short-term and long-term statistical values of the maximum loads. The results of the RAOs obtained from these calculations are based on the use of the wave scatter diagrams, operational profiles, and wave spectra for a defined operational area of the vessel so that the most dominant load responses for the load components and be defined. These analyses of the loads are done using the in-built capability of MAESTRO program and the details description of the calculations procedure can be found in the MAESTRO-Wave user manual (MAESTRO, 2012).

The extreme dominant load parameters have been calculated using the North Atlantic 2 wave spectra and the results of the RAOs for the wave headings that have been predicted. The wave parameters that have been used for this calculation are based on the General Atlantic, which has been defined in the program. For a given response, the calculation is based on the relationship between the combinations of the wave heading (**μ**), the significant wave height (**Hs**), mean wave crossing period (**Tz**) and the vessel speed (**V**). The profile of the wave response follows a normal distribution, hence a statistical method is employed to calculate the probability that the maximum encountered loads by the vessel in a given wave conditions does not exceed certain values.

An example of the calculations of the probability of exceeding a given response sung the case of vertical bending moment (Mv) due to the long term wave effect on a vessel was defined by (Brown *et al.*, 1991) as shown in the this equation:

$$\boldsymbol{P(M_v) = \iiint P(V,H)P(\mu,H)P\,(H_s,T_z)\left(\frac{-M_v^2}{2M_{V0}(V,\mu,H_s,T_1,}\right)dVd\mu dH_s dT_z} \quad \textbf{Eq 7 – 13}$$

Mvo is the mean square amplitude of the vertical bending moment response, **Mv,** which has been obtained by using the results of the regular wave predictions. The extreme loads that have been obtained from the extreme loads analysis are presented in (Brown *et al.*, 1991). These loads are the extreme loads that have been used as individual load cases (**LC**) for the purpose of determining the maximum impact of wave-induced loads on the vessel. Typically, dynamic pressure (See Appendix B for plots) was used in this calculations and the probability of exceedance for this analysis is within a range of $1 - 10^{-10}$.

Table 7.11: The results of the extreme load analysis

LC	DLP	Heading (deg)	Speeds (knot)	Period (s)	Wave-length	Exposure (yr)	Extreme Load
1	Vertical BM (kNm)	180	20	3.70	21.23m	11.7	2362
2	Vertical SF (kN)	180	20	3.31	17.07m	10.4	793
3	Horizontal BM (kNm)	45	15	3.70	21.23m	8.0	760
4	Horizontal SF (kN)	45	15	3.70	21.23m	8.3	175
5	LTM (kNm)	135	20	3.70	21.23m	7.8	654

7.4 Results and Discussions

The results of the structural assessment of the DVC vessel that has been performed using MAESTRO FEA are presented in this Section. The discussion on these results is based on the responses that have been obtained from the loads on the longitudinal and the transverse axes of the vessel. The load cases considered are those that produced the Stillwater loads (light load departure conditions) and the extreme loads condition (for both sagging and hogging). The longitudinal loads consist of the peak magnitudes of the transverse response on each frame along the longitudinal axis. These loads are considered as the global loads and they are found to be acting along the length of the vessel. The transverse loads are the peak magnitudes of the loads acting on the frames and their maximum is considered as the peak loads on the cross-deck structure of the vessel. The stress distributions due to the effect of these loading conditions and there resulting deformation and displacement have been considered along their respective loading axes (longitudinal and the transverse). The combined stresses resulting from these loads have been discussed under the local loads effects on the strength of the vessel.

7.4.1 Longitudinal Strength

The results of the Stillwater bending moment and its resulting shear force that have been obtained from the load analyses are presented Figure 7.4 and Figure 7.6 respectively. These responses have been determined based on the vessel's light load departure condition as spelt out in Table 6.1. On the other hand, the longitudinal bending moment and the longitudinal shear force results due the extreme wave loads acting on the vessel are presented in Figure 7.5 and Figure 7.7 respectively. These plots are the results of the effects of the extreme loads such as the vertical bending moment on the vessel.

The maximum bending moment based on the light departure loading condition is 570 kNm, and the maximum shear force is +174kN. These results were obtained from the effects of the Stillwater on the model and they are essential in the predictions of the dynamic responses on the vessel, especially the transverse bending moment and shear force as required by the LR rules (LR, 2012).

The maximum longitudinal bending moment due to the extreme wave-induced loads is 2930 kNm, and its corresponding longitudinal shear force is -711 kN. These loads have been predicted by using the dynamic pressure which induces the maximum vertical bending and the shear force that one out of hundred of such a vessel would experience over its entire design life. The responses due to the extreme loads are higher by a factor of 1.8 than the design loads predicted on the basis of the rule-based, which is within the acceptable limit of ≥ 1.2 (LR, 2012).The maximum loads were measured in the Hogging conditions and they are significantly higher than in the sagging condition. The variation in these loads is could be attributed to the changes in the ballast conditions which is occasioned by the wave conditions and the effect of speed change.

The failure modes due to these stresses were observed on the cross-deck structures and within connections between the cross-deck and the two demi-hulls. In addition, stress concentration on the plates around the hatch and moon pool opening were also observed. The acceptance criteria for failure due to these stresses in MAESTRO is such that adequacy ratio, $\boldsymbol{g}(\boldsymbol{R})$, as defined in Eqn 7.3 is not more than 1.0.

The partial factor of safety of 1.25 for the serviceability requirement and 1.5 for the collapse failure has been used in the MAESTRO analysis. Plots of the limiting yield stress, which based on limit state design, are presented in Figure 7.12 and Figure 7.13 for plates and flange.

The plots revealed that failure occurred within the skeg structure, which is understandable giving that is treated as a cantilever

.

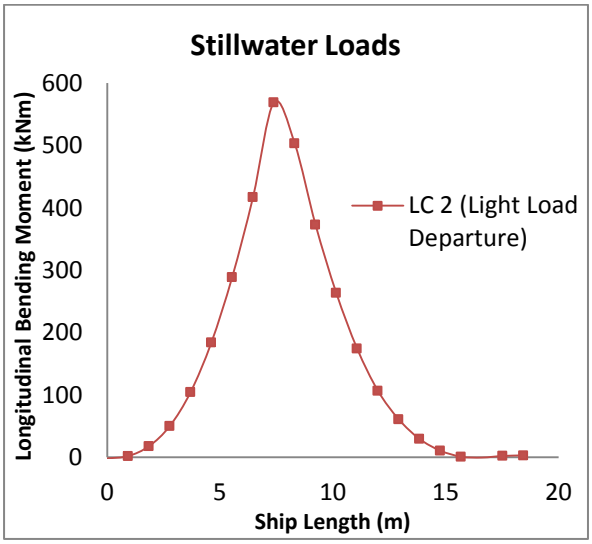

Figure 7.4: Stillwater Longitudinal Bending Moment

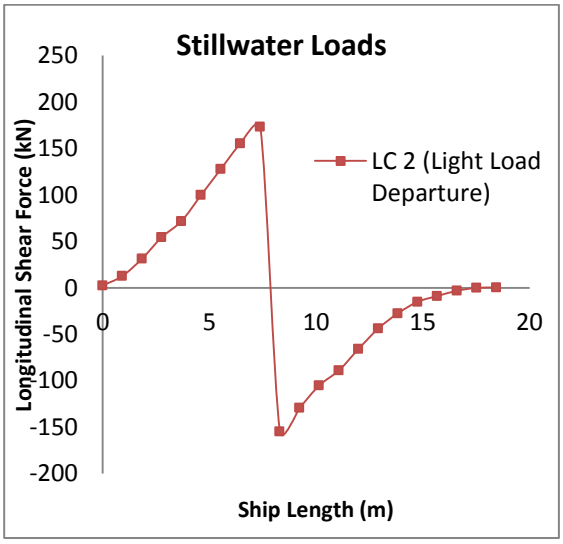

Figure 7.6: Stillwater Longitudinal Shear Force

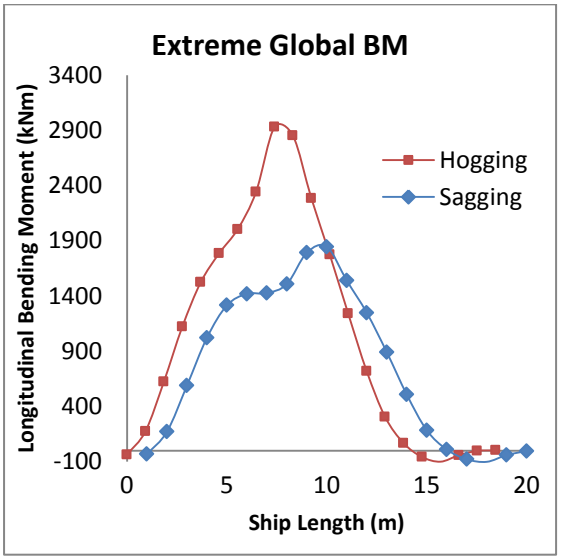

Figure 7.5: Extreme Longitudinal Bending Moment

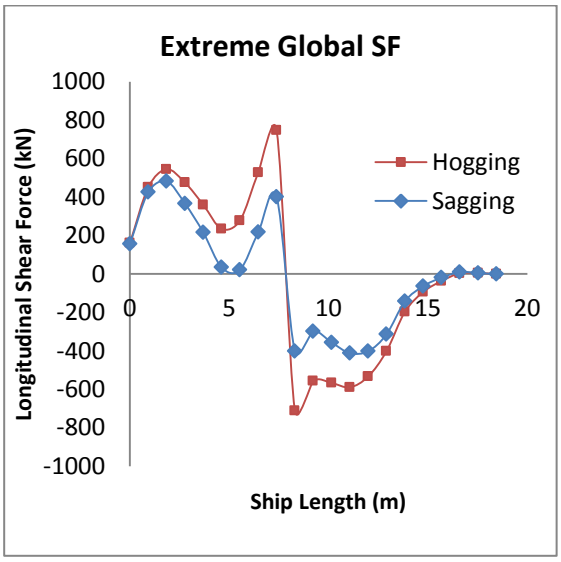

Figure 7.7: Extreme Longitudinal Shear Force

The deflection of the vessel has been measured in all the five load cases that have been considered. The maximum deflection, $\boldsymbol{\delta_z}$, in the vessel was measured as the displacement due to the extreme vertical bending in sagging condition as 135mm. The maximum deflections, $\boldsymbol{\delta_z}$ has been recorded at the tip of the bulbous bow and this positions is similar to other loading conditions. The reason for the occurrence of the deflections at this position is directly related to the stiffness of the vessel which, in turn, is also the result of the boundary

conditions that have been applied. Although the LR rule for special service craft (LR, 2012), has not explicitly set out the requirements for the deflections for this group vessels, the magnitudes of these deflections are generally low in comparison to those obtained by elastic bending theory.

The wave-induced stresses, $\boldsymbol{\sigma_x}$, due to the contributions of the Stillwater loads on the vessel have been found to be insignificant in terms of its magnitudes when compared, for instance, to the vertical bending moment. However, the combination of these loads with the dynamic effects on the vessel is responsible for the maximum dynamic bending and the shear loads on the vessel in the transverse condition and which gives the extreme stresses on the vessel.

In the calculations of the distributed stresses on the hull structure, vertical accelerations were applied by using the 'inertia relief' tool in the MAESTRO program, in order to ensure that internal stress equilibrium is achieved. This process is an essential requirement for ensuring that compatibility in stress distribution over the entire structure of the vessel is achieved. The acceleration is applied to the pressure distribution for each of the respective load case over the idealised FE model in the calculations of the sectional and hull girder loads. The stresses are then transferred across the entire structure through the interconnection of nodes of each element.

The bending stresses due to the Stillwater loads have low magnitudes as shown in Figure 7.9. The maximum deformation due to these stresses is found to be on the keel plating of the hull structure and also on the deck plate for area around the moon pool on the cross-deck structure. The deformations due to the extreme loads for both the sagging and the hogging conditions are presented in Figure 7.10 and Figure 7.11 respectively. (The plots of the longitudinal stress distribution due to the load cases for the full scale model are presented in Appendix B).

The distribution of these deformations across the hull structure is non linear as it should have been, by using the elastic bending theory. The effect of the loads are concentrated around the hatch and the moon pool openings and the distribution of the stresses relies on the interconnecting stiffness between the constituent elements of the model. A slight stress concentration was observed in the model for the sagging load case (LC3) just after the hatch openings at about 9.0m from the aft perpendicular. The reason for the occurrence of this stress concentration is that the weights due to the lightship of the vessel and equipment such

as the engines fuel, cargo etc have beam modelled as points loads, hence their efficient distribution across the model has not been realised as expected. A summary of the peak magnitudes of the longitudinal stress for the load case, LC2,LC3 and LC4 are presented in Table 7.12.

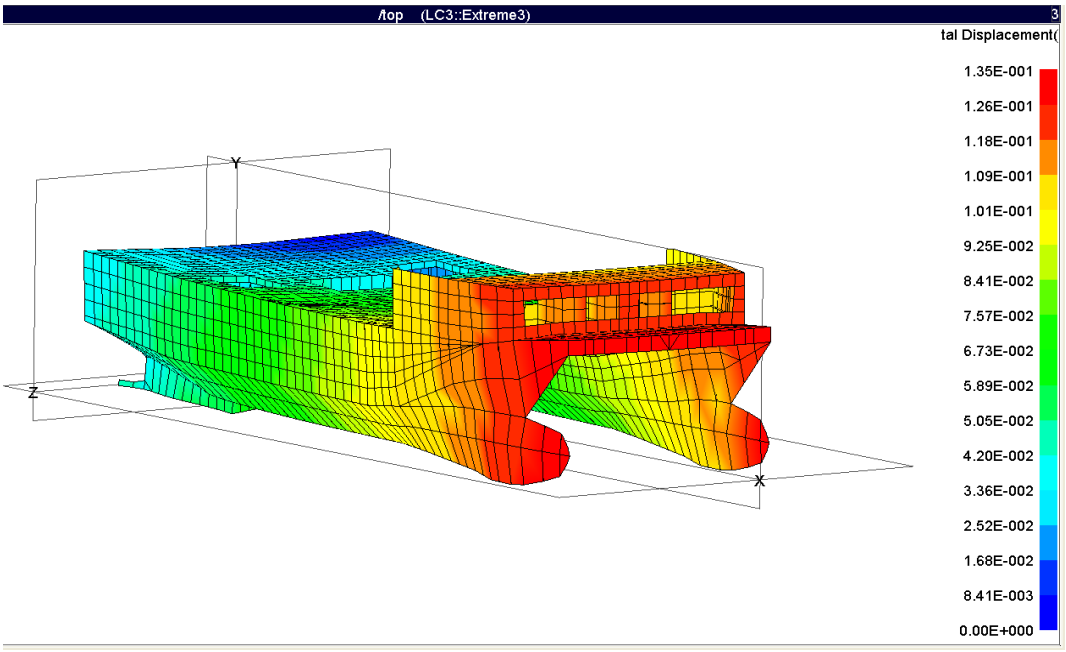

Figure 7.8: Displacement plots for Load Case 3 – Sagging

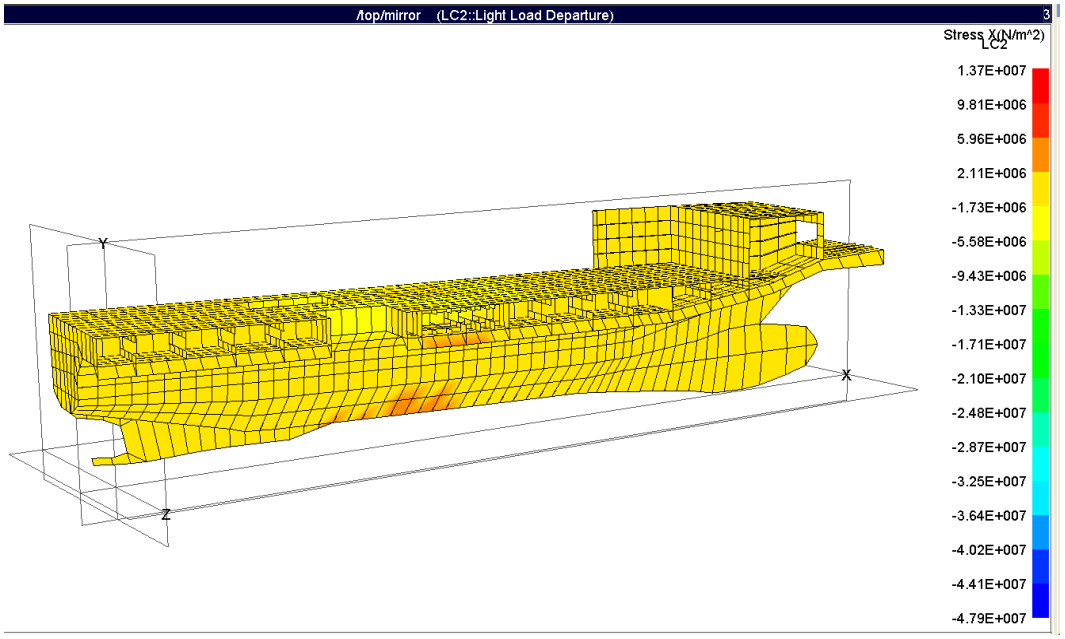

Figure 7.9 Longitudinal bending stress distribution for Load Case 2(LC 2)

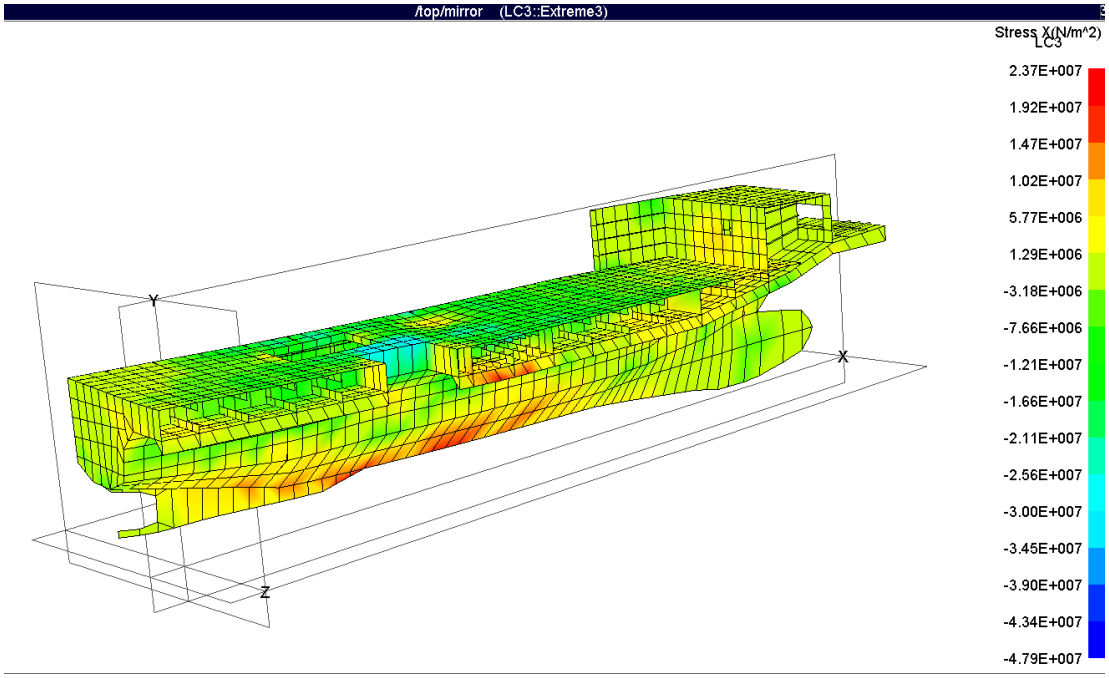

Figure 7.10: Longitudinal bending stress distribution for Load Case 3 (Sagging)

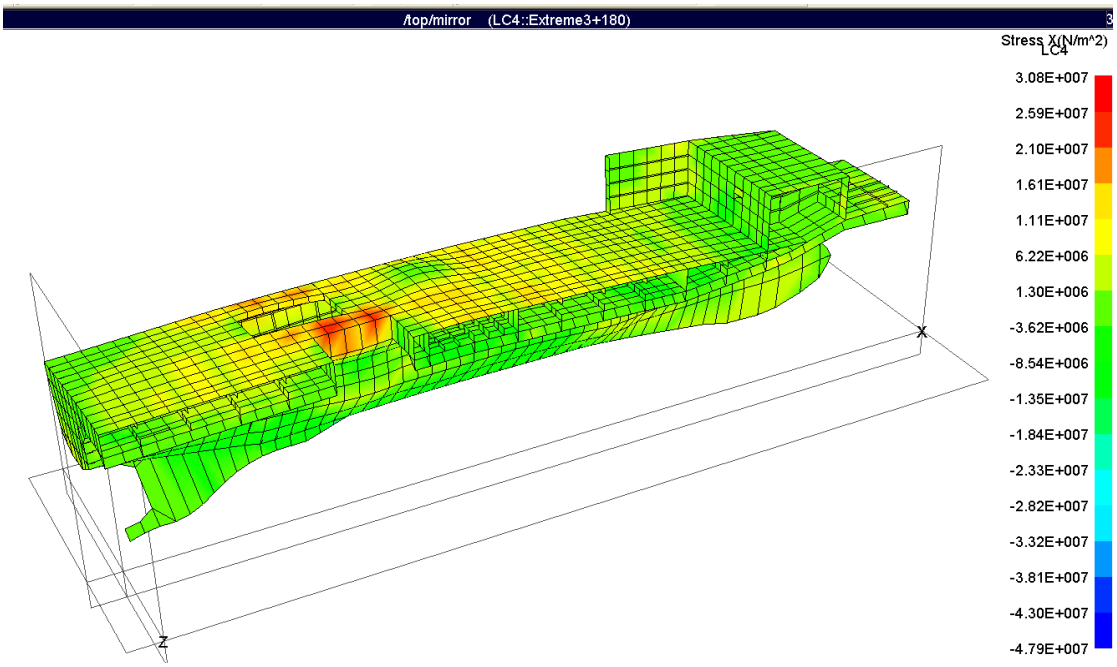

Figure 7.11: Longitudinal bending stress distribution for Load Case 4 (Hogging)

Table 7.12: Summary of longitudinal stress distribution on the vessel

Load Case (LC)	**Bending Stress (N/mm^2)**	**Shear Stress (N/mm^2)**
LC2 (Light load departure)	11.2	9.6
LC3 (Sagging – Extreme VBM)	25.2	17.7
LC4 (Hogging – Extreme VBM)	30.4	20.6

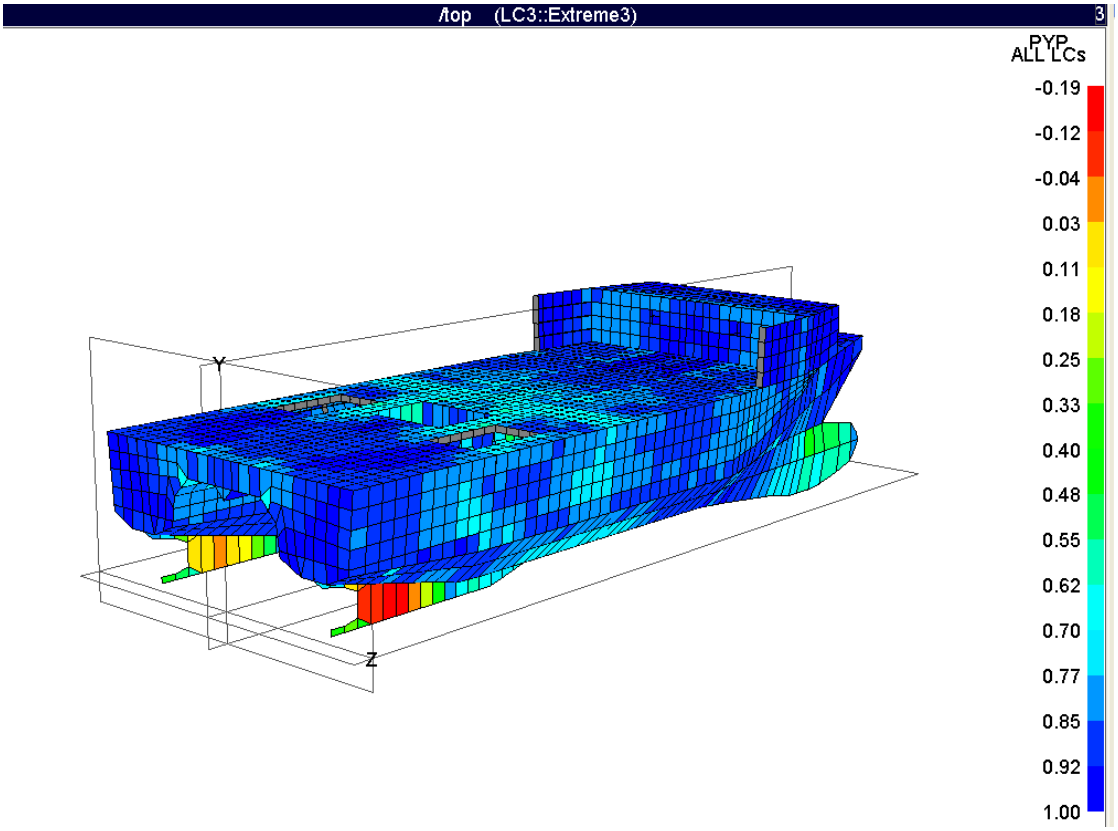

Figure 7.12: Plots of the limiting yield for plate for all load cases (PYP)

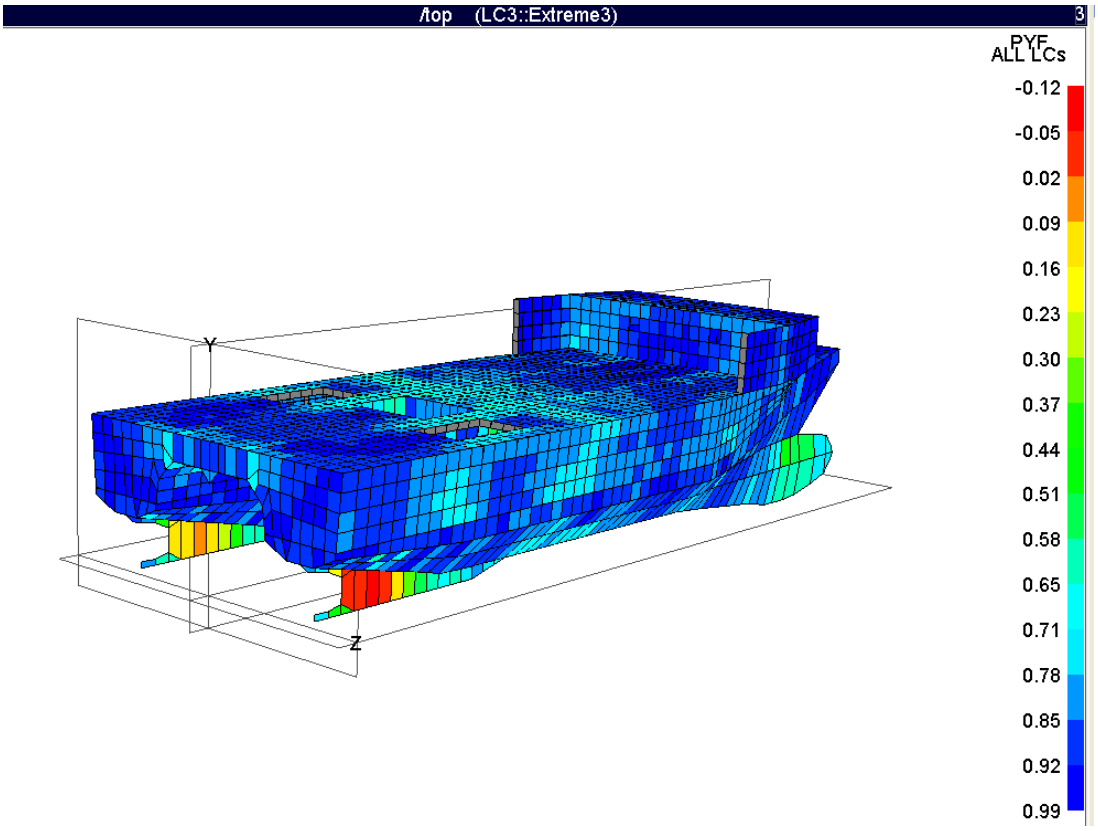

Figure 7.13:Plots of the limiting yield for flange for all load cases (PYF)

7.4.2 Transverse Strength (Cross-deck structure)

The assessment of the transverse strength of this vessel has been performed using the same FE model of the RV Princess Royal, based on the LR rules. The transverse loads of the models consist of the transverse bending moment acting on the hull structure have been calculated by using the combination of the Stillwater, the vertical forces and the extreme horizontal forces along the line of action of the forces . The extreme horizontal bending moment, which is also the prying moment, $\mathbf{M_x}$ is given as load case 3 (**LC 3**), while the horizontal shear force is considered as the side forces, **Fy**, and it is given as the load case 4 (**LC 4**), in the loading conditions presented in Table 7.11. The maximum bending moment occurs at the longitudinal centreline of vessel, hence increasing the stresses on the cross-deck structure within this region. The peak magnitude of the transverse shear force is distributed around the connection between the demi-hull and the cross-deck structure Figure 7.19.

The transverse distribution of the bending moment and the transverse shear force due to the combinations of the Stillwater loads and horizontal loads on the hull structure is presented in Figure 7.14 - Figure 7.17. The Torsional bending moment on the vessel in the transverse axis is presented in Figure 7.18.

The maximum deformations, $\boldsymbol{\sigma_y}$**,** due to the bending of the model in the transverse direction occur within the cross-deck structure. The peak of these stresses has been recorded on part of the transverse bulkheads and also the transverse frames that is located within the cross-deck structure. The impact of these stresses in combination with other bending and in-plane shearing stress on the structure has been analysed using the von Mises approach in the local FE analysis

The results of the loads and the resulting deformations indicate that the bulkheads and the transverse frames are significantly responsible for resisting the transverse loads induced on the vessel. These results indicate that the transverse capacity of the cross-deck structure of this vessel is adequate and one of the reasons for this adequacy is the number of transverse frames available in the vessel. The vessel has about 3 transverse frames per meter up to 12 m of the entire length of the vessel. These frames bear substantial magnitudes of the transverse bending stress as well as the transverse shear force. The geometry of these frames, which also reflects the geometry of the vessel, also contributes to the shear resistance on the vessel.

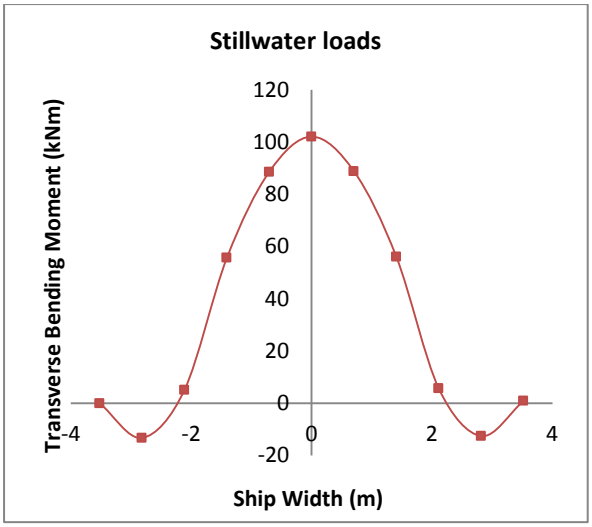

Figure 7.14: Stillwater Transverse Bending Moment

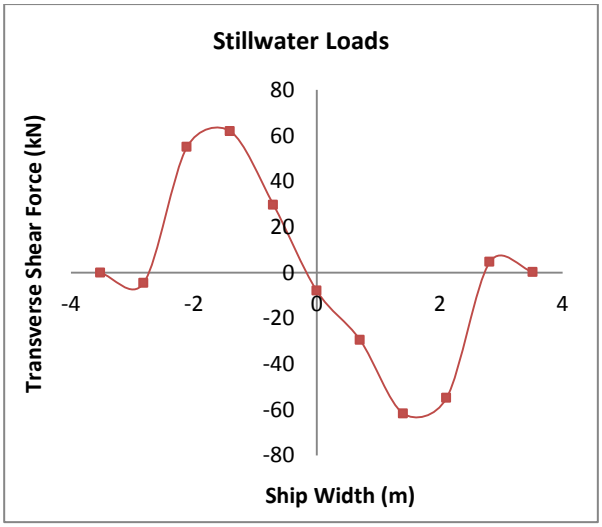

Figure 7.15: Stillwater Transverse Shear Force

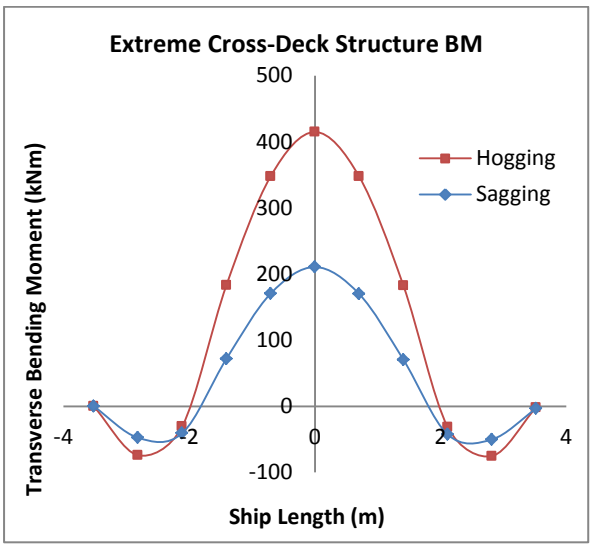

Figure 7.16: Extreme Transverse Bending Moment

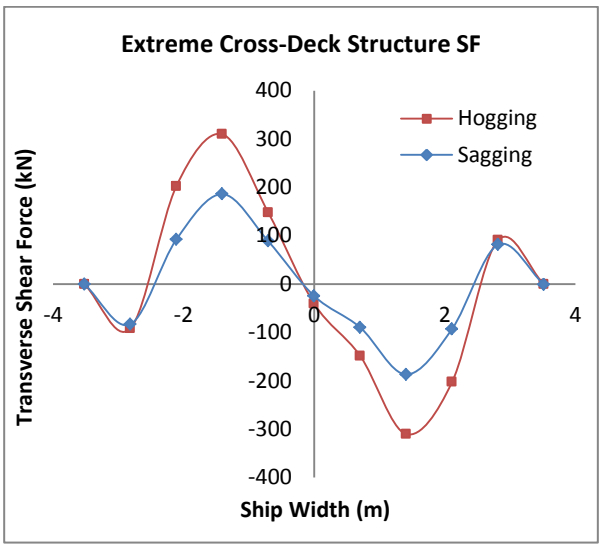

Figure 7.17: Extreme Transverse Shear Force

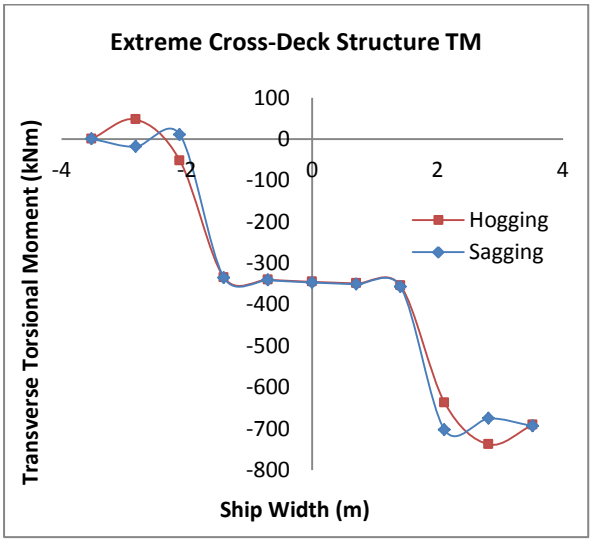

Figure 7.18 :Extreme Transverse Torsional Moment

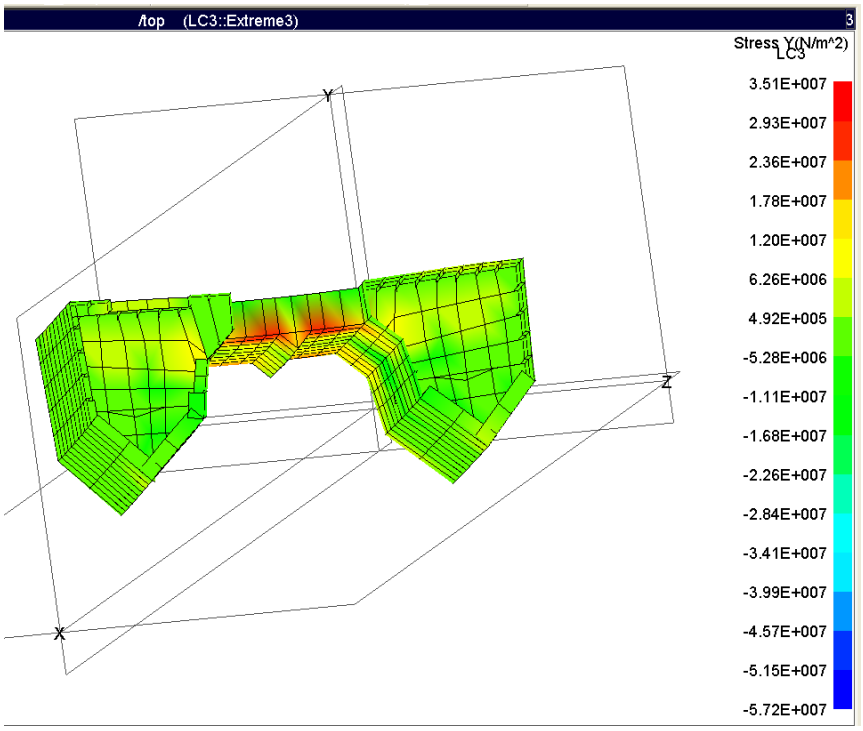

Figure 7.19: Transverse bending stress distribution for Load Case 3 (LC 3 – Sagging)

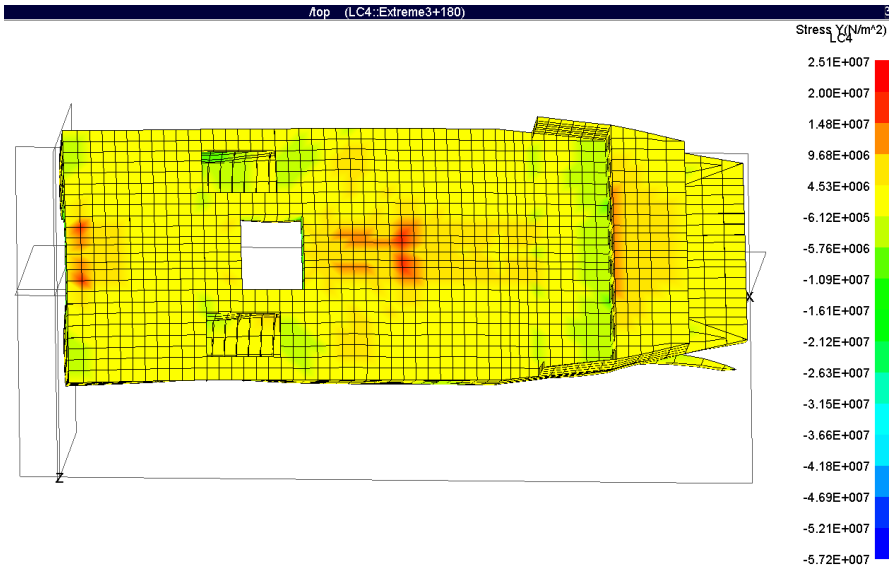

Figure 7.20: Transverse bending stress distribution for Load Case 4 (LC 4 – Hogging)

Table 7.13 Summary of the transverse stress distribution on the vessel

Load Case (LC)	**Von Mises Stress (N/mm^2)**	**Shear Stress (N/mm^2)**
LC2 (Light load departure)	11.2	9.6
LC3 (Sagging – Extreme VBM)	25.2	17.7
LC4 (Hogging – Extreme VBM)	30.4	20.6
LC 5 (Torsional)		

7.4.3 Local Strength

The local strength considerations in the design of catamaran focus on the net effect of the wave-induced loads on the demi-hulls that is borne by the cross-deck structure. These loads, combination with the Stillwater and the dead weight on the vessel are required for the design of the cross-deck structure. The consideration for the design of this structure entails the use of the stresses resulting from the FE analysis using the longitudinal and the transverse bending and the in-plane shear stresses, the von Mises stress, ($\boldsymbol{\sigma_t}$). In addition, the stresses induced by the Torsional loads effects on the structures are also included in the design. For this purpose, distribution on the vessel has been used for the local strength assessment of the failure modes of the various structural component of the vessel.

The LR (LR, 2012) requirements for the local strength is mostly depended on the scantlings ability to resist the design pressures. This criterion is also the rule's acceptable method of determining the strength of the hull structure for a displacement vessel of less that 50m in length. The limiting condition for the design of these scantlings is depended on their respective positions on the vessel, in addition to the design pressure that they would have to resist during their service years. However, the most important consideration in this assessment is the ability to ensure that the minimum thickness of these scantlings determine based on the results of the MAESTRO analysis do not fall below the specified minimum in the LR Rule's requirement.

A summary of the peak magnitude of the results of Von Misses stresses that have been obtained from the FE analysis is given in Table 7.14

Table 7.14: Summary of the combined stresses (von Mises) on the hull structure

Load Case (LC)	**Von Mises Stress (N/mm^2)**
LC2 (Light load departure)	42.5
LC3 (Sagging – Extreme VBM)	36.2
LC4 (Hogging – Extreme VBM)	57.2
LC7 (Sagging – Extreme HBM)	57.2
LC9 (Hogging – Extreme HBM)	39.4
LC11 (Torsional)	32.3

These results have been compared with the LR recommended limiting stress for an aluminium vessel. This limiting value is taken as the 0.85% of the yield stress or the proof stress of the material. A representative plot of the von Mises stress distributions for load case 3 -sagging is presented in Figure 7.21. The plots of other individual load cases are presented in Appendix A.

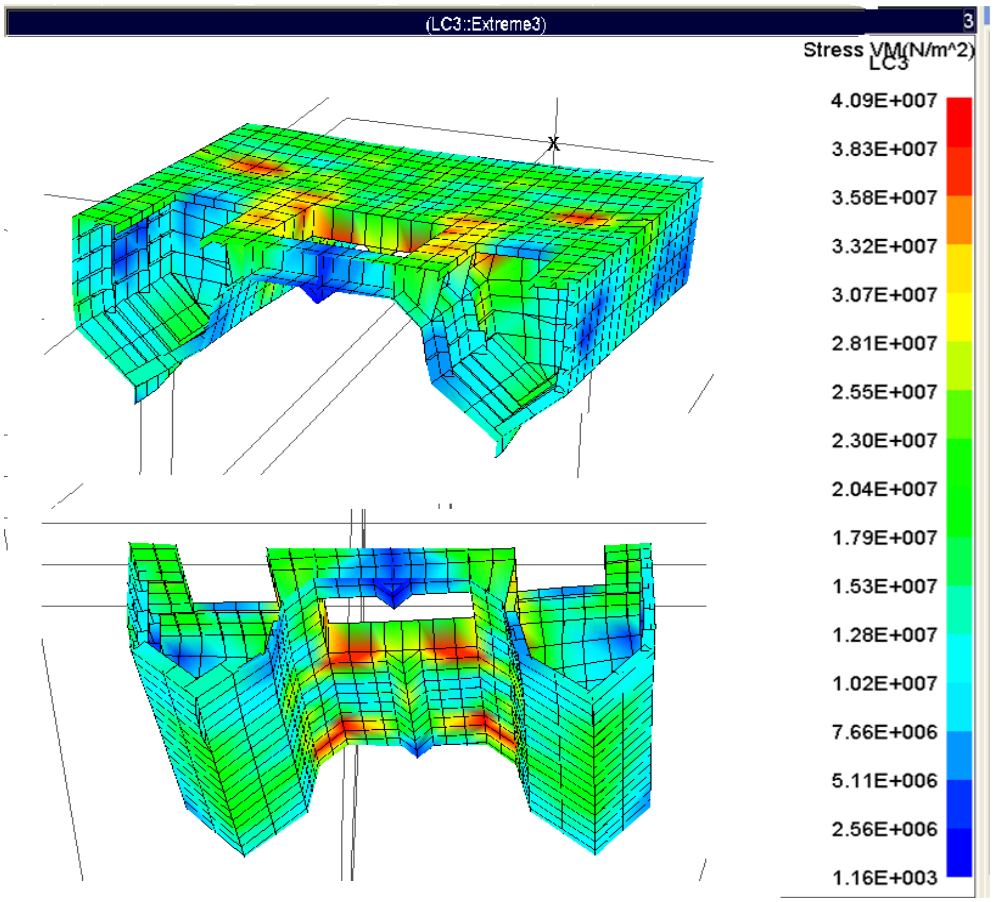

Figure 7.21: Von Mises stress distribution for Load Case 3 (Sagging)

7.5 Conclusions

In this chapter, the results of the extreme load analysis based on the prediction of the long term loads on the vessel have been performed. The loads have been compared with the design loads that have been obtained using the rule –based approach as contained in the LR Rules for the Classification and Regulation of Special Service Craft. A simple demonstration of the effects of these loads on the vessel structure has been carried out using an FE analysis. The summary of the finding from the structural loads predictions and the analysis are presented below:

1. The wave-induced loads that have been predicted using the experimentally validated numerical codes have been found to be, at least, 40% lower than those that have been predicted using the Rule-based approach as contained in the LR rules for the classification of special service craft, the although rule-based approach is based on stochastic method that uses higher safety margin to account for other scenarios that have not been considered in this study.
2. The extreme long term loads, which have a probability of exceedance of 1 in 100, that have been predicted using the numerical method have been used in the FE design of the vessel structure. The structural deformation resulting from the FE analysis based on these loads, which are almost 80% higher than the rule based design loads, were still found to have yielded lower stress distribution than the required limiting stress recommended by the codes based on the limit state design principles.
3. Some isolated cases of stress concentrations have been observed on the cross-deck structure around the openings of the moon pool and the hatches. These concentrations are predominantly due to the axial forces resulting from the equipment and machinery loads.
4. The stress distribution on the anti-slamming bulb and the skeg were found to be about twice the average stress on the vessel but it was still within the acceptable limit. However, these stresses were due to the effects of horizontal loads which have resulted in causing the structural elements to have higher deflections. This conclusion has been supported by the manifestation of structural cracks at the connection point between the skeg and the demi-hull of the vessel. Hence there is need for further study to determine the optimum structural configuration of these elements.

5. Considering the fact that these design have been performed using the extreme loads that were 80% higher than the rule-based design loads, the structural deformations on the vessel are still very low. This indicates that either the actual vessel might have been overdesigned.
6. From the results of this structural response analysis, it has been seen that the current structural arrangement of the cross-deck structure is robust enough to withstand high stresses. However, the impact of this configuration of the cross-deck structure on the whole cycle cost of the vessel needs to be considered

Chapter 8

Conclusions and Recommendations for Future Work

8.1 Introduction

This Chapter presents the overall summary and conclusions of the research on the hydrodynamic motions and load performance as well as the strength assessment of a Deep-V Catamaran. The chapter also covers a section on the recommendations for future research.

Section 8.2 of this Chapter presents the general summary of entire research. The main conclusions of the research are presented in Section 8.3 whilst Section 8.4 presents the recommendations for further study.

8.2 General Summary

The main focus of this thesis has been on the investigation of the hydrodynamic loading and strength of a Deep-V Catamaran (DVC). The research contributes towards the understanding of the motion and wave induced load response characteristics of a DVC concept in order to advance its structural design methodology and its subsequent application as better alternative to the more conventional Round Bilge Catamaran (RBC) concept.

In line with its stated objectives, as presented in Chapter 1, the first chapter of this thesis presents an introduction to the DVC concept, the motivation and the intended outcomes for this research. The first objective of the study was to perform a review of the current state of knowledge in relevant areas to support the research on the wave-induced motions and load

analysis and of the strength assessment of a catamaran using a Deep-V hullform concept. This objective is covered in Chapter 2.

The second objective was to carry out the predictions of the motion and wave-induced load response characteristics using a numerical method for the Deep-V and Round Bilge hull form concepts. The basis for doing so was presented in the form of theoretical background of motion and wave load response prediction methods and associated numerical tools in Chapter 3.

The Deep-V hull form, as used in the design of catamaran, is a new concept, hence it has been identified that there was lack of experimental data on the motion response and wave-induced load behaviour of this concept. As a result of this, the third objective of this study was focused on the experimental measurements and analyses of the motion and load responses of the hull form using both the rigid and the segmented scaled models. The model tests data that have been obtained from the experimental study are required in order to validate the numerical tools and prediction data that would be obtained from the tools. The facilities and procedures that were used for these experiments have been described as well as the discussion of the analysed motion and load responses are presented in Chapter 4.

The fourth objective of this study was to use the motion and load response data that have been obtained from the experimental study in order to validate the numerical tools and results obtained from the numerical predictions. The numerical study has been performed using two different sets of numerical codes, namely, the MAESTRO-Wave and the PRECAL. The latter code was used only for validation of the motion responses as an alternative to the former code which was the main tool for the motion and load analysis. The results of the validations for both the motion response and the wave-induced response characteristics have been presented in Chapter 5.

Following the reasonable success recorded in the validation, the numerical study was conducted to predict the motion and load responses of the DVC and its counterpart Round Bilge Catamaran (RBC) concepts in order to establish a direct basis for the comparison of their motion and load response amplitudes as well as their performance in seaway. This was in line with the fifth objective, which was to compare the motion and wave-induced loads responses of the DVC and the RBC concepts. The procedure for this comparison and the results that have been obtained thereof have been presented in Chapter 6 of this thesis.

The last two objectives were focused on predicting the loads on the DVC concept using the rule-based approach as obtainable in the Lloyds Registers Rules for Special Service Craft. The objectives also demand the evaluation of the strength performance in order to determine the influence of the hull form geometry on the strength of the cross deck structure. The results of the study on these objectives have been presented in Chapter 7.

The overall conclusions of the thesis have been presented in this Chapter (Chapter 8) and it also comprised of the findings that have been made in the course of the research. The chapter more specifically summarises the conclusions that have been presented in the last four Chapters of this thesis, which cover the experimental prediction of motion response and the wave-induced loads, the validation of the numerical tools, the comparisons of the responses for the DVC and RBC models and the Structural Response analysis.

Appendix A, presents the plots of stress distribution on the structure of the DVC.

8.3 Main Conclusions

The focus of this research has been on making contribution to the understanding of the motion and wave load response characteristics of a Deep-V Catamaran concept. The result of this study is intended to advance the structural design methods of the DVC concept. Hence, based on the results that have been obtained and the observations made from this research, the followings are the main conclusions that have been drawn in this thesis.

8.3.1 Experimental Motion Response and Wave-induced Load Measurements

The experimental study on the measurements of motion and wave-induced load responses on the DVC model have been performed using a scaled model of the RV Princess Royal. These results have provided useful insight into the seakeeping performance and the wave-induced loads behaviour of the DVC concept, presented as follows:

1. It has been established that the predictions of motion responses using the rigid model yield higher magnitudes of motion responses in the Head Seas and the Following Seas than in the measurement with a segmented model of the same vessel. On the other hand, the segmented model yields higher responses in the Beam Seas and the Bow and Stern Quartering Seas. The reason for such behaviour is attributed to the hydroelasticity of the segmented model that was the effect of the load cell arrangement.

2. A significant reduction in the magnitudes of the motions response of the vessel was also witnessed as the vessel heading changes. However, in the responses for the roll motion, such changes due to the vessel headings follow a Gaussian distribution in which the responses increase from lower magnitudes in the Head Seas to the peak magnitudes in the Beam Seas then, finally, the lowest in the Following Seas.
3. The effect of changes in the vessel speeds on the responses of both the DVC and the RBC models manifested itself in the form of a shift in the plots, especially on the pitch motions response plots in the Head Seas and in the Prying moment response in the Bow Quartering Seas and the Stern Quartering Seas. This same trend was observed in the response for the various vessel speeds in which the behaviour of the plots remain essentially the same but with some changes in their peak magnitudes and the frequency at which they were recorded.
4. The coupling of the pitch motions together with the roll motions responses has been observed. The consequence of this observation is that there is a credible potential for the occurrence of parametric rolling in both of these models in the Oblique Seas (Bow Quartering and Stern Quartering Seas).
5. A coupling between the respective motion responses (Heave, Roll and Pitch) at either (sometimes on both occasion) at resonant frequencies or at the peak response frequency of that particular motion response have been observed in a number of wave heading conditions. The most prominent of these couplings was recorded in the responses that have been measured in the Beam Seas and the Bow and Stern Quartering Seas.
6. The behaviour of the motion responses that have been obtained from the experimental study is predominantly nonlinear. The nonlinearity featured very prominently at higher incident wave frequencies and on the response plots where coupling with other motion responses were observed.
7. The most dominant load parameters due to the wave-induced loads have been mostly found in the Head Seas, the Bow Quartering Seas and the Beam Seas. It has been found that the magnitudes of these load parameters are strongly influenced by the coupling effects of the motion and the wave-induced responses. A summary of these dominant load parameters according to the vessel heading is given below.

i. The most dominant wave-induced load response due to the longitudinal shear force in zero speed was found in the Bow Quartering Seas and the trend of the load responses in both the zero and forward speeds condition are essentially the same.
ii. The most dominant load parameter for the transverse shear (side) force in the zero speed condition was found in the Beam Seas. The magnitude of the responses in the forward speed condition is lower than in the zero speed condition
iii. The most dominant load parameter for the vertical shear force in zero speed condition was found in the Head Seas and it is quite higher than those that have been measured in the forward speed condition.
iv. The most dominant wave-induced load parameter due to the prying moment was found in the Beam Seas at zero speed condition. The magnitude of the prying moment decreases as the frequencies increase in the region where nonlinearity was observed.
v. The most dominant parameter due to the Yaw Splitting moment revealed occurred in the Bow Quartering Seas at zero speed condition. The magnitude of the Yaw Splitting moment in the forward speed condition is slightly higher than in the zero speed

8.3.2 Numerical Load and Motion Response Comparisons

The main conclusions that have been drawn from the comparison of the numerical study on the load and motion responses are mainly between the Deep-V and its counterpart Round Bilge catamaran are presented in this section.

1. A specialised commercial numerical tool for solving hydrodynamic problems, called the MAESTRO-Wave has been used in the prediction of the motion and wave-induced load response characteristics of the models. This tool is a three-dimensional potential flow solver based on the zero-speed Green's function in frequency domain. The tool has been validated using another potential flow solver, called the PRECAL and also using the results of the experimental study. Benchmark studies that have been carried using the combination of these results have shown reasonable agreement between the responses that have been obtained using the numerical tools and the experimental studies. The result of validation study confirmed that the tool is indeed

capable of providing accurate data motion responses and wave-induced loads on the DVC concept.

2. The behaviour of the DVC model due to the motions and wave-induced loads responses were nonlinear in all the heading condition with the exception of the Beam Seas conditions. The nonlinearity is with respect to the vessel speed; hence increase in the vessel speed has resulted in the increase in the nonlinearity. The nonlinearity was predominantly found within the frequency range where coupling of the responses with others, or at the resonant frequencies, were observed and this phenomenon featured mostly at higher frequencies. However, the motions and the wave-induced loads responses in the Beams Seas were found to be insensitive to the effects of the changes in the vessel speeds. In addition, the responses in the Beam Seas were found to be predominantly linear but with some occasional coupling with the roll resonance.
3. In the motions response comparisons, it has been established that the DVC concept performs better than its competing equivalent, the RBC vessel, in the Head Seas and the Bow Quartering Seas conditions in terms of having lower magnitudes of motion responses. The behaviour of the models in the Beams Seas is relatively similar in terms of their respective trends. The Head Seas and the Bow Quartering Seas are two of the most critical headings; hence it has been concluded that the DVC concept has a superior seakeeping performance than the RBC concept on the basis of their motion responses.
4. Spectral response analyses in four different sea states that the vessel of the size of these model are expected to operate (using the various response amplitudes operator) that have been predicted in other to assess their performance. The result of these analyses indicate that the DVC concepts offer slightly better performance in waves in comparison to the RBC concept but the difference appears not to be very significant, hence further study to quantity significance of this changes to the performance of these concepts is required
5. The motions and wave-induced loads responses for both of these models in the forward speed conditions have been found to be strongly nonlinear with respect to the increase in the vessel speed. This condition was quite remarkable in the Head Seas and in the Bow Quartering Seas, and especially at higher encountered wave frequencies. The effect of this nonlinearity reduces in the responses for the Stern Quartering and the Following Seas. There also was a reduction in the number of kinks that appeared in a coupled form with the responses of other motions or wave-induced

loads as the headings changed. This situation that, irrespective of the vessel speeds, the changes in the vessel/wave headings determines the magnitudes of the motion responses.

6. In the plots for the RBC model responses, it has been observed that the frequency range of the responses, in most of the headings, occurred within a narrow frequency band and at the same time, the responses for the model were nonlinear at higher frequencies. Such phenomenon is directly related to the cause of hull structure's vibrations and it could cause fatigue problem to the vessel structure.

8.3.3 The Structural Response Analysis

A Finite Element analysis using the MAESTRO FEA program has been performed. The program had a good interface with the MAESTRO-Wave hydrodynamic tool that was used in the loads prediction. The following conclusions that have been drawn from study on the structural performance of the DVC concept:

1. The design loads of the DVC vessel have been calculated using the Rule-based approach as contained in the LR rules for the classification of special service craft. These predicted loads have been compared with those that have been obtained from the experimentally validated numerical codes. The result of these comparisons indicates that the numerically predicted loads are, at least, 40% lower than those that have been predicted using the Rule-based approach when the a direct comparison is made. However, the rule-based approach comprised of other factors such as fatigue, safety margin which could easily explain the reason for the variation in the two results.
2. The extreme design loads, which have been predicted using the long-term wave-induced loads with a probability of exceedance of 1 in 100, have been used in the FE design of the vessel structure. This was done in order to investigate the capability of the existing configuration to withstand the worst possible loading conditions. The structural deformation that was obtained from the FE analysis based on the extreme loads, which are almost 80% higher than the rule based design loads, were found to have yielded the combined stresses of less than 50% of the yield strength of the vessel structural materials and the required limiting stress recommended by the codes which are based on the limit state design principles.

3. Some isolated cases of stress concentrations have been observed on the cross-deck structure around the openings of the moon pool and the hatches. These concentrations are predominantly due to the axial forces resulting from the equipment and the machinery loads. Also, the stresses on the anti slamming bulb and the skeg were found to be about twice the average stress on the vessel structure, but it was still within the acceptable limit. These stresses were due to the effects of horizontal loads on the structural elements and which have resulted in causing these elements to have higher deflections than the remaining parts of the vessel.
4. Based on the stresses that have been obtained from the FE analysis, it has been seen that the current structural arrangement of the cross-deck structure is very robust and enough to withstand high load with an adequate strength threshold. However, the impact of this particular structural configuration of the cross-deck structure on the whole cycle cost of the vessel needs to be considered.
5. In addition to the conclusion number 4 (depending on the structural arrangement of the transverse frame), the geometry of the Deep-V Catamaran appears to offer more robust structural performance than the RBC concept. This also is one of the benefits that can be derived from the insensitivity of the DVC to the wave-induced loads.
6. The results of the wave-induced load responses and the resulting stresses from their applications to the structural assessment of the hull structure have demonstrated that a strength assessment of the DVC hull structure during the preliminary design stage can be carried out based on the simplified methodology of the load/ strength ratio of the material used in for this vessel design. This approach provides a rapid method of performing the preliminary scantling of the vessel structure.

.

8.4 Recommendations for Future Works

The concept and the applications of the Deep-V hullform in the design of twin hulls and high-speed craft is still evolving. The recent success achieved in the launching of Newcastle University's research vessel "The Princess Royal", 4 (four) Harbour Patrol Launches for the Port of London Authority and 1 (one) Environmental Survey vessel for Briggs Marine based on the Newcastle DVC concept have demonstrated the need for this hull form concept to be thoroughly investigated especially for larger sizes. This study and the others that have been previously performed indicate that the DVC hull form concept has good potentials for wider applications in the maritime industry. In view of this, the following aspects of the DVC concept need further understanding.

1. In the prediction of the motion response and wave-induced loads on the DVC concept, it has been observed that the hull form concept behaves nonlinearly at higher frequencies. The nonlinearity in the motion and the wave-induced loads responses are some of the known attributes of fatigue failure. Since the fatigue strength of this hull form concept is not within the remit of this thesis, it is therefore recommended that the fatigue load and strength, especially of the cross-deck structure of the vessel, be investigated.
2. The coupling of the roll motion and the pitch motion responses was observed in the model experiments. This condition, also known as "cork-screwing", can induce high Torsional stress on the hull girder structure of vessels. A simplified structural check that has been carried out using the Torsional loads indicated that the hull structure of this concept is structurally safe. However, a more detailed study on the effect of this phenomenon on the ultimate strength of the hull and the cross-deck structure – being the most weight-sensitive element, and also the effects on passenger comfort should be established.
3. During the numerical prediction of the motion and load responses by using the current codes, which are linear frequency domain codes using zero-speed Green functions, it has been noted that the accurate prediction of the forward speed effects and various non-linearities associated with the coupling effect of the out of plane motion modes (e.g. cork-screwing due to roll-pitch) cannot be achieved. The representation of these non-linearities as well as the others due to large amplitude motions and the

hydroelasticity would require better modelling of the speed effects and simulation of the motion and load responses in time-domain.

4. In the study using the RBC model, it has been observed that the frequency range of the responses, in most of the headings, occurred within a narrow frequency band and at the same time, behaving nonlinearly at higher frequencies. Such phenomenon is directly related to the cause of hull structure's vibrations and it could cause fatigue problem to the vessel structure. This condition needs to be further investigated.
5. The experimental study in this research was performed using the Deep-V model which enabled a comprehensive validation of the numerical prediction for the Deep-V hull form concept under investigation. In view of this, it is recommended that same experimental study using the round bilge model shall be performed in order to ensure consistency in both the validation of the results as well as in the comparison with the Deep-V concept's responses.
6. In the measurement of both the motion and wave-induced load characteristics, the effects of the changes in vessel speed on the responses have been observed. However, the direct contributions of these effects to the magnitudes of the responses and the resulting consequence on the strength and performance of the hull form structure needs to be investigated.
7. It has been established that the used of the rule-based approach in the calculation of the design loads tends to over predict the design loads. The use of direct method of load prediction that rely on the use of the numerical tool, that is properly validated by experimental data, should be encouraged in order to achieve a robust structural design of which offers a cost-effective structural system. This goal can further be realised through continuous study on the optimisation of the structural frames and the cross-deck structure.
8. The current International Association of Classification Societies (IACS) requirements for the design of hull structure of a vessel having less than 50m length depend strongly on the design for local pressures. This approach usually leads to the over design of the structural member. In order to further enhance the attractiveness of the hull form, there is need to establish the source of these local loads which principally comprised of wet deck slamming, green load etc.
9. The structural assessment of the hull structure was performed using aluminium material; hence it is recommended that the behaviour of this structure when design with other material such as composites is further investigated.

References

References

Abdul Gani, M. P. (2003) *Design Aspects of Catamarans Operating at High Speed in Shallow Water.* thesis. University of Southampton.

ABS. (2005) *Commentary of the Guideline for Buckling and Ultimate StrengthAssessment for Offshore Structures*.

ABS. (2011) *Guidance notes on Structural Direct Analysis for High-Speed Craft*. American Bureau of Shipping.

Allseas (2012) *Pieter Schelte*. Available at: http://www.allseas.com/uk/19/equipment (Accessed: 31/09/2012).

Amin, W., Davis, M. R., Thomas, G. A. and Holloway, D. S. (2013) 'Analysis of wave slam induced hull vibrations using continuous wavelet transforms', *Ocean Engineering,* 58, (0), pp. 154-166.

Atlar, M. (1997a) 'Recent Developments and Emerging State-of-the-Art in the High-Speed Vessel World with a Personal View on a Large Deep-V Hulls and their Further Potential*', The 6th International Marine Design Conference.* Newcastle upon Tyne, UK, June 1997. pp.

Atlar, M. (1997b) 'Recent Developments and Emerging State of the Art in High Speed Vessel World with a Personal View on Large Deep-V Hulls and their future Potentials*', 6th International Marine Design Conference, IMDC,*. Newcastle, UK, 1997. pp.

Atlar, M. (2011) 'Recent Upgrading of Marine Testing Facilities at Newcastle University*', AMT (Advanced Model Measurement)* Newcastle, UK, 4th -6th April 2011. pp.

Atlar, M., Haslam, B. and Mesbahi, E. (1998) 'Deep-Vee hullforms and their Applications to Multi-hulls "Deep-VV" Catamaran.*', 1st European Symposium on Yacht and Small Craft Design* University of Genova, La Spezia, Italy, October 1998. pp.

Atlar, M., Sampson, R., Wightman-Smith, J. R., Seo, K.-C., Glover, E. J., Danisman, D. B. and Mantouvalos, A. (2010) 'An Innovative Research Vessel Replacement for Newcastle University*', HIPER '10: The 7th International Conference on High-Performance Marine Vehicles,*. Melbourne, Florida, USA, 11th -15th October 2010. pp.

Atlar, M., Seo, K.-C., Sampson, R. and D.V, D. (2013) 'Anti-Slamming Bulbows Bow Tunnel Stern Applications on a Novel Deep-V Catamaran for Improved Performance', *International Journal of Naval Architecture and Ocean Engineering,* Vol. 5, (No. 2).

Atlar, M., Seren, D. B. and Validakis, J. (1985) 'The Effect of Tilt and Interference on the hydrodynamic Coefficients of SWATH-Type Sections *', SWATH Ships and Advanced Multi-Hulled Vessels.* London, UK, 17th -19th April 1985. pp.

Bailey, D. (1976) *The NPL High Speed Round Bilge Displacement Hull Series.* London: The Royal Institution of Naval Architect.

Bashir, M. B., Tao, L., Atlar, M. and Dow, R. S. (2011) 'Hydrodynamic Performance of a Deep-Vee Hull Form Catamaran in Regular Waves', *ASME Conference Proceedings,* 2011, (44380), pp. 45-54.

Bashir, M. B., Tao, L., Atlar, M. and Dow, R. S. (2013) 'Experimental and Numerical Prediction of Wave-induced Loads on a Deep-Vee Hull Form Catamaran in Regular Waves (Accepted)', *ASME Conference Proceedings,* 2013, (44380).

Brown, J. C., Clarke, J. D., Dow, R. S., Jones, G. L. and Smith, C. S. (1991) *The Dynamics of Ships: A Royal Society Discussion Meeting.* London, Uk:The Royal Society.

Chan, H. S. (1993) 'Prediction of motion and wave loads of twin-hull ships', *Marine Structures,* 6, (1), pp. 75-102.

Chen, N.-Z. and Guedes Soares, C. (2007a) 'Longitudinal strength analysis of ship hulls of composite materials under sagging moments', *Composite Structures,* 77, (1), pp. 36-44.

Chen, N.-Z. and Guedes Soares, C. (2007b) 'Reliability assessment for ultimate longitudinal strength of ship hulls in composite materials', *Probabilistic Engineering Mechanics,* 22, (4), pp. 330-342.

Clark, D. J., Ellsworth, W. M. and Meyer, J. R. (2004) 'The Quest for Speed at Sea', NSWC Technical Digest,

Cramer, E. H., LÃ¸seth, R. and Olaisen, K. (1995) 'Fatigue assessment of ship structures', *Marine Structures,* 8, (4), pp. 359-383.

Dallinga, R. P. and Tikka, T. T. (1986) 'A Design Procedure for Catamaran Cross Structure Loads', *Offshore Technology Conference.* Houston, USA, pp.

Davis, M. R. and Holloway, D. S. (2003) 'The influence of hull form on the motions of high speed vessels in head seas', *Ocean Engineering,* 30, (16), pp. 2091-2115.

Davis, M. R. and Whelan, J. R. (2007) 'Computation of wet deck bow slam loads for catamaran arched cross sections', *Ocean Engineering,* 34, (17â€“18), pp. 2265-2276.

DNV. (2011) *Rules for Classification of High Speed, Light Craft, and Naval Surface Craft*. Det Norske Veritas.

Dow, R., Benson, S. and Downes, J. (2009) 'Ultimate strength characteristics of aluminium plates for high speed vessels', in *Analysis and Design of Marine Structures.* CRC Press, pp. 121-131.

Dow, R. S., Hughes, O. F. and McNatt, T. R. (1997) 'Unified First-Principles Ship Structural Design Based on the Maestro Methodology', *INTERNATIONAL CONFERENCE ON*

COMPUTER APPLICATIONS IN SHIPBUILDING. Society of Naval Architects of Japan, pp.

Dubrovski, V. (2004) *Ships with Outriggers.* Backbone Publishers.

Fang, C. C., Chan, H. S. and Incecik, A. (1996) 'Investigation of motions of catamarans in regular waves--I', *Ocean Engineering*, 23, (1), pp. 89-105.

Fang, C. C., Chan, H. S. and Incecik, A. (1997) 'Investigation of motions of catamarans in regular waves--II', *Ocean Engineering*, 24, (10), pp. 949-966.

Fang, M.-C. and Chen, T.-Y. (2008) 'A parametric study of wave loads on trimaran ships traveling in waves', *Ocean Engineering*, 35, (8-9), pp. 749-762.

Haslam, B. (1996) *Deep-Vee hull Forms and their Suitability to High Speed Catamaran.* thesis. Newcastle University.

Heggelund, S. E., Moan, T. and Oma, S. (2002) 'Determination of global design loads for large high-speed catamarans', *Proceedings of the Institution of Mechanical Engineers, Part M: Journal of Engineering for the Maritime Environment*, 216, (1), pp. 79-94.

Heggelund, S. E., Tveiten, B. W. and Moan, T. (1998) 'Fatigue Analysis of High Speed Aluminium Catamarans*', The Third International Forum on Aluminium Ships.* Kent, UK, Quantic Media Ltd, pp.

Huang, Z. J. and Hsuing, C. C. (1993) 'An improved 3-D Method to Compute m-terms for Ship Motion*', 2nd Canadian Marine Dynamics Conference.* Vancouver, Canada, Butterworth-Heinemann, pp.

Hughes, O. F. and Ma, M. (1996) 'Elastic Tripping Analysi of Asymmetric Stiffners', *Computers and Structures,* 60, (3), pp. 369 - 389.

Hughes, O. F. and Ma, M. (1997) 'Inelastic Stiffner Buckling and Panel Collapse', *Computers and Structures*, 61, (1), pp. 101 - 117.

Hughes, O. F. and Paik, J. K. (2010) 'Ship Structural Analysis and Design', in Society of Naval Architects and Marine Engineers (SNAME).

Huijsmans, R. H. M., Van't Veer, A. P. and Willemstein, A. (1999) *PRECAL (Pressure Calculation Program) Manual,* in *MARIN Report (User Manual),* Delft, Netherlands.

Iijima, K., Yao, T. and Moan, T. (2008) 'Structural response of a ship in severe seas considering global hydroelastic vibrations', *Marine Structures,* 21, (4), pp. 420-445.

Insel, M. (1990) *An Investigation into Resistance Components of High-Speed Displacement Catamarans.* Technical Report thesis. Southampton University, UK.

Insel, M. and Molland, A. F. (1992) 'An Investigation into Resistance Components of High-Speed Displacement Catamarans', Transactions of The Royal Institute of Naval Architects, Vol. 134, p.1-20.

ITTC. (2006) *ITTC Recommended Procedures and Guidelines (7.5-02 07-02.1): Testing and Extrapolation Methods Loads and Response, Sea Keeping Experiments,* in *ITTC Recommended Procedures and Guidelines*,

Korkut, E., Atlar, M. and Incecik, A. (2004) 'An experimental study of motion behaviour with an intact and damaged Ro-Ro ship model', *Ocean Engineering,* 31, (3-4), pp. 483-512.

Krammer, R. K., Rampolla, B. and Magnusson, A. (2000) *Fatigue of Aluminium Structural Weldments.* Washington, D.C, USA: US Coast Guard

Lavroff, J., Davies, M. R., Holloway, D. S. and Thomas, G. (2007) 'The Whipping Vibratory Response of a Hydroelastic Segmented Catamaran Model*', Ninth International Conference on Fast Sea Transportation FAST2007* Shanghai, China, , September 2007. pp.

Lee, C. M., John¸H.D and Curphey, R. M. (1973) 'Prediction of Motions and Hydrodynamic Loads of Catamaran', *Marine Technology,* Vol. 10, pp. 334-360.

Liu, D., Chen, H. and Lee, F. (1981) *Extreme Loads Response Symposium, (The Ship Structure Committee/SNAME).* Arlington, VA, USA,

LR. (2006) *Guidance Notes on Ship Vibration and Noise*. Lloyd's Register.

LR. (2012) *Rules and Regulations for the Classification of Special Service Craft*. Lloyd's Register.

Ma, M., Zhao, C. and Danese, N. (2012) *Conference on Computer Applications and Information Technology, COMPIT.* Liege, Belgium,

Maddox, S. J. (2003) 'Review of fatigue assessment procedures for welded aluminium structures', *International Journal of Fatigue,* 25, (12), pp. 1359-1378.

MAESTRO. (2012) *MAESTRO Users Manual* (9.2)

Mansour, D. A. and Fenton, L. P. H. (1973) 'Structural Analysis and Design of a Catamaran Cross-Sstructure by the Finite Element Method', *Naval Engineers Journal,* 85, (1), pp. 33-42.

Mantouvalos, A. (2009) *The Development of the First Deep-V Catamaran (DVC) Systematic Series.* thesis. Newcastle University.

Martec. (2006) *FD-Wave Load Theory Manual.* Martec Limited.

Matsubara, S. (2011) *Ship Motions and Wave-induced Loads on High-Speed Catamarans.* thesis. The University of Tasmania, Australia.

Matsubara, S., Thomas, G., Davis, M. R., Holloway, D. S. and Roberts, T. (2011) *International Conference on Fast Sea Transportation.* Honolulu, Hawaii, USA, September 2011 American Society of Naval Engineers.

Molland, A. F. and Lee, A. R. (1995) *The theoretical investigation of a series of high speed displacement catamaran forms: variation of prismatic coefficient.* (87).

Nordenstrom, N., Faltinsen, O. M. and Pedersen, B. (1971) *Offshore Technology Conference.* Houston, Texas, 19-21 April 2012.

Ochi, M. K. (1981) *Extreme Loads Response Symposium, (The Ship Structure Committee/SNAME).* Arlington, VA, USA,

Ohkusu, M. (1999) *Twenty-Second Symposium on Naval Hydromechanical.*

Ojeda, R., Gangadhara Prusty, B. and Salas, M. (2004) 'Finite element investigation on the static response of a composite catamaran under slamming loads', *Ocean Engineering,* 31, (7), pp. 901-929.

Paik, J. K. (2007) 'Empirical formulations for predicting the ultimate compressive strength of welded aluminum stiffened panels', *Thin-Walled Structures,* 45, (2), pp. 171-184.

Paik, J. K. and Kim, B. J. (2002) 'Ultimate Limit State Design of Ship Hulls', *Society of Naval Architiects and Marine Engineers, SNAME, Transactions,* 110.

Paik, J. K. and Mansour, A. E. (1995) 'A simple formulation for predicting the ultimate strength of ships', *Marine Science and Technology*, Vol. 1, pp. 52-62.

Paik, J. K. and Thayamballi, A. K. (2007) *Ship-shaped Offshore Installations: Design, Building, and Operation.* Cambridge University Press.

Paik, J. K., Thayamballi, A. K., Pedersen, P. T. and Park, Y. I. (2001) 'Ultimate strength of ship hulls under torsion', *Ocean Engineering,* 28, (8), pp. 1097-1133.

Paik, J. K., van der Veen, S., Duran, A. and Collette, M. (2005) 'Ultimate compressive strength design methods of aluminum welded stiffened panel structures for aerospace, marine and land-based applications: A benchmark study', *Thin-Walled Structures,* 43, (10), pp. 1550-1566.

Qin, Z. and Batra, R. C. (2009) 'Local slamming impact of sandwich composite hulls', *International Journal of Solids and Structures,* 46, (10), pp. 2011-2035.

Qiu, W., Ando, S. and Hsuing, C. C. (1999) 'Validation of WAVELOAD, a 3-D Frequency Domain Computer Program for Ship Motions and Hull Pressures', *5th Canadian Marine Hydromechanics and Structures Conference.* St. john's, Newfoundland, Canada, Butterworth-Heinemann, pp.

Qualisys. (2010) 'Qualisys Motion Capture Systems', in Gothenburg, Sweden.

Sahoo, P. K. (2003) 'Hydrodynamics of High-Speed Vessels', *International Workshop on Hydrodynamics of High-Speed Vessels.* Australia, Australian Maritime Hydrodynamics Research Centre, pp.

Sahoo, P. K., Salas, M. and Schwetz, A. (2007) 'Practical evaluation of resistance of high-speed catamaran hull formsâ€"Part I', *Ships and Offshore Structures,* 2, (4), pp. 307-324.

Sarioz, K. and Narli, E. (1998) 'Seakeeping Performance Assessment of High-Speed Warship Hull Forms: Deep Vee versus Round Bilge', *Proceedings of International Conference*

on Ship Motions and Manoeuvrability. London, The Royal Institute of Naval Architects, RINA, pp. 1-9.

Schellin, T. E., Shigunov, V., Troesch, A. W., Kim, D.-H. and Maki, K. J. (2013) 'Prediction of Loads for Ship Structural Design', *Ship Structures Technical Track, ASNE Day* Arlington, VA, USA, pp.

Schmitke, R. T. (1978) '"Ship sway, roll, and yaw motion in oblique seas"', *Transactions of Society of Naval Architect and Marine Engineers, SNAME,* 86.

Serter, E. (1993a) *Hydrodynamics and Naval Architecture of Deep Vee Hull Forms.* Blackwell Publishing Ltd.

Serter, E. (1993b) *Naval Architecture and Hydrodynamics of Deep Vee Hull Forms.* Blackwell Publishing Ltd.

Soares, C. G. and Maron, M. (1999) 'Model Tests of the Motions of a Catamaran Hull in Waves', *Hydrodynamics of High Speed Craft.* London, UK, The Royal Institute of Naval Architects, pp.

Thomas, G., Davis, M., Holloway, D. and Roberts, T. (2008) 'The vibratory damping of large high-speed catamarans', *Marine Structures,* 21, (1), pp. 1-22.

Thomas, G., Kibby, L., Ford, A., Binns, J. R., Finnie, I. and Kavanagh, N. (2011) 'Experimental investigation into wave-induced design loads on a large moored catamaran', *Ships and Offshore Structures,* 6, (4), pp. 273-295.

Van't Veer, A. P. (2009) 'Theoretical Manual for 3D Hydrodynamic Pressure Calculation Program', PRECAL V6.5 (Theory Manual), V6.5,

Varyani, K. S., Gatiganti, R. M. and Gerigk, M. (2000) 'Motions and slamming impact on catamaran', *Ocean Engineering,* 27, (7), pp. 729-747.

Wahab, R., Pritchett¸C. and Ruth, L. C. (1971) 'On the behaviour of the ASR catamaran in waves', *Marine Technology,* Vol. 8, pp. 334-360.

Wellicome, J. F., Temarel, P., Molland, A. F. and Hudson, D. A. (1995) *Theoretical prediction of the seakeeping characteristics of fast displacement catamarans.* (93).

Wellicome, J. F., Temarel, P., Molland, A. F. and Hudson, D. A. (1999) *Theoretical prediction of the seakeeping characteristics of two fast displacement catamarans in oblique seas.* (113).

Yao, T. (2003) 'Hull girder strength', *Marine Structures,* 16, (1), pp. 1-13.

Zha, Y. and Moan, T. (2001) 'Ultimate strength of stiffened aluminium panels with predominantly torsional failure modes', *Thin-Walled Structures,* 39, (8), pp. 631-648.

Appendix A: Structural Response (Stress) Plots

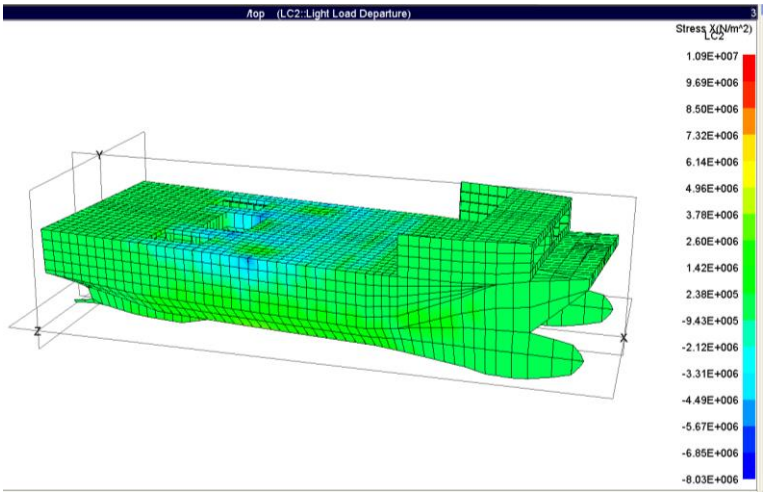

Figure A.0.1: Longitudinal stress distribution for load case 2(LC 2)

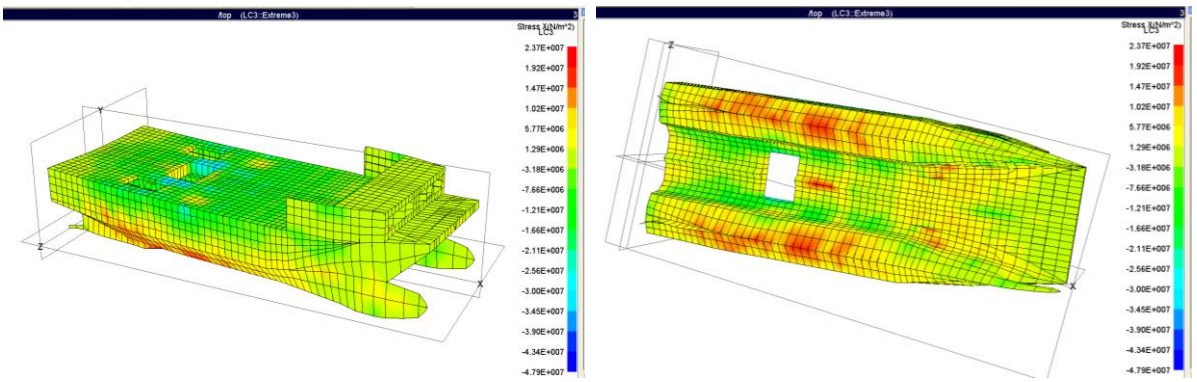

Figure A.0.2: Longitudinal stress distribution for load case 3(LC 3 – Sagging)

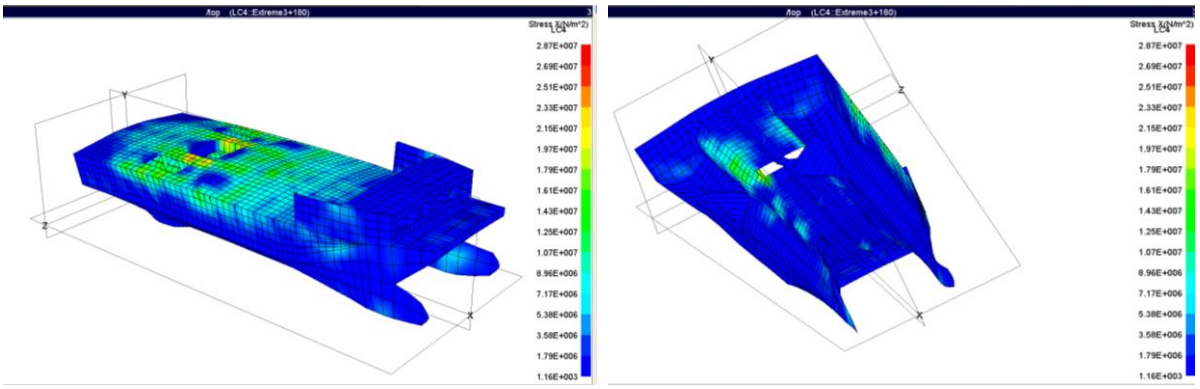

Figure A.0.3: Longitudinal stress distribution for load case 4 (LC 4 - Hogging)

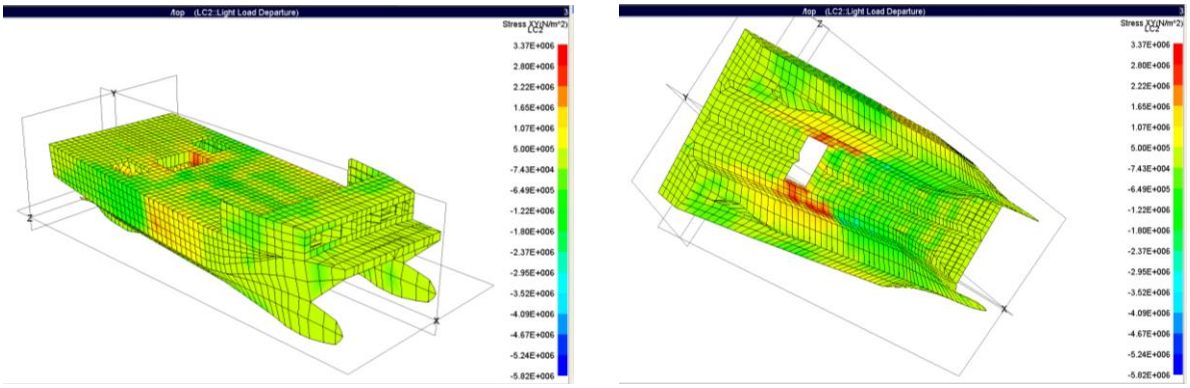

Figure A.0.4: XY in- plane shearing stress (LC 2 – X)

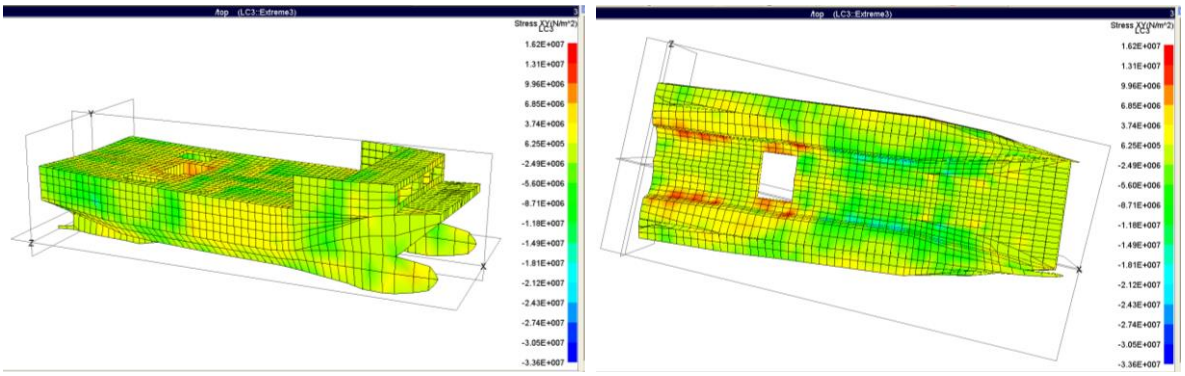

Figure A.0.5: XY in- plane shearing stress (LC 3 – X)

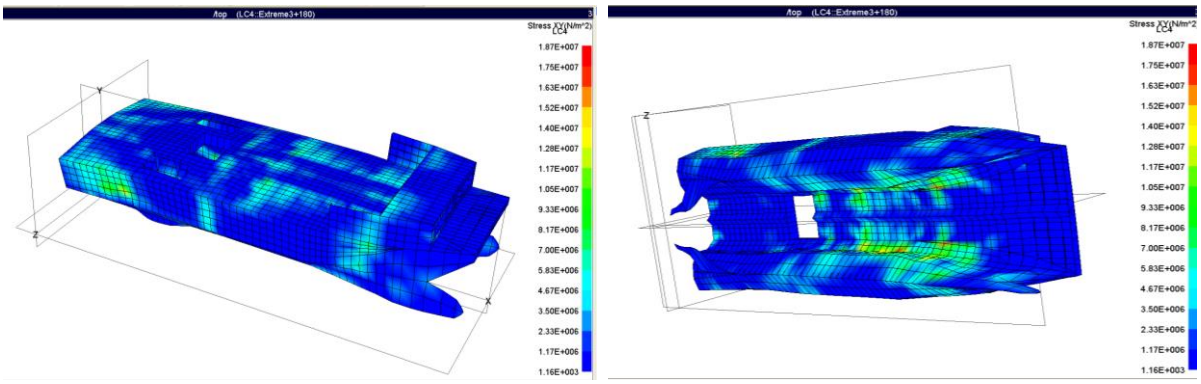

Figure A.0.6: XY in- plane shearing stress (LC 4 – X)

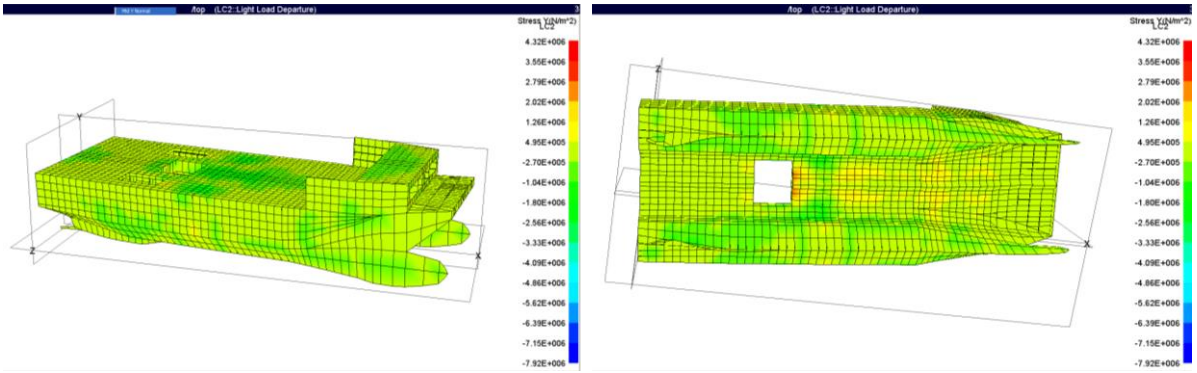

Figure A.0.7: XY in- plane shearing stress (LC 2 – Y)

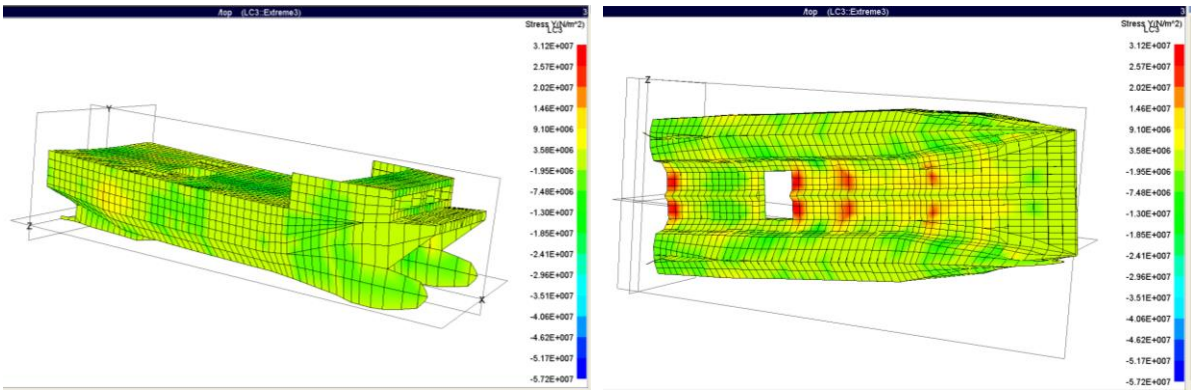

Figure A.0.8: XY in- plane shearing stress (LC 3 – Y)

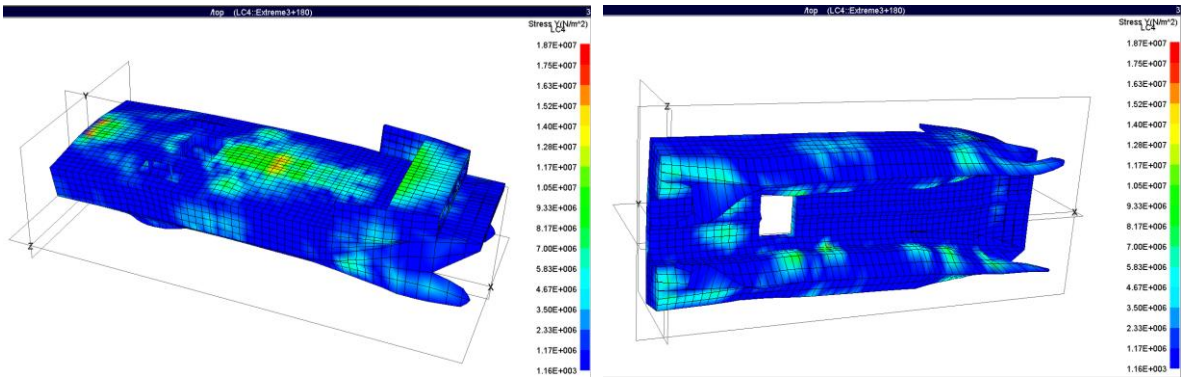

Figure A.0.9: XY in- plane shearing stress (LC 4 – Y)

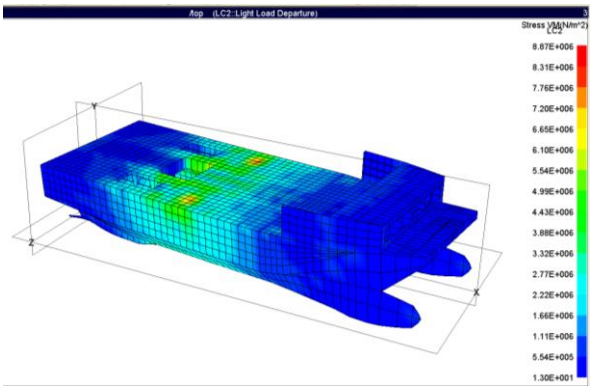

Figure A.0.10: XY in- plane shearing stress (LC 2 – VM)

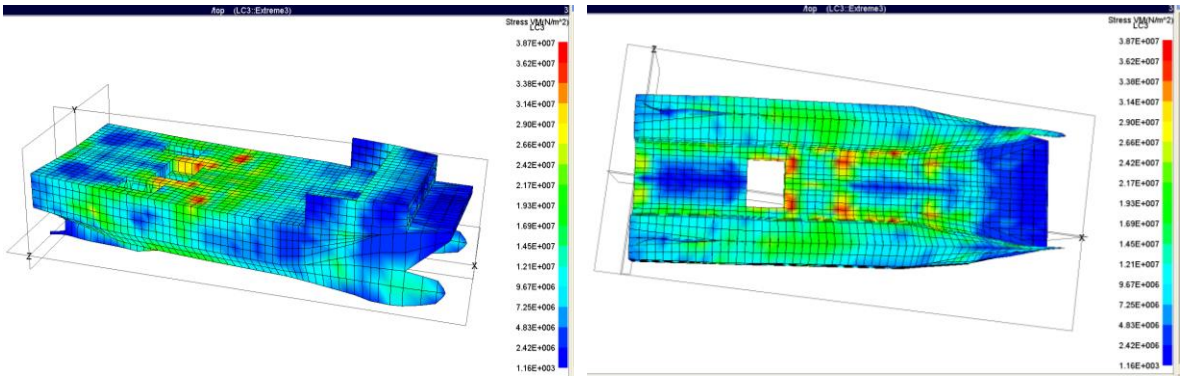

Figure A.0.11 XY in- plane shearing stress (LC 3 – VM)

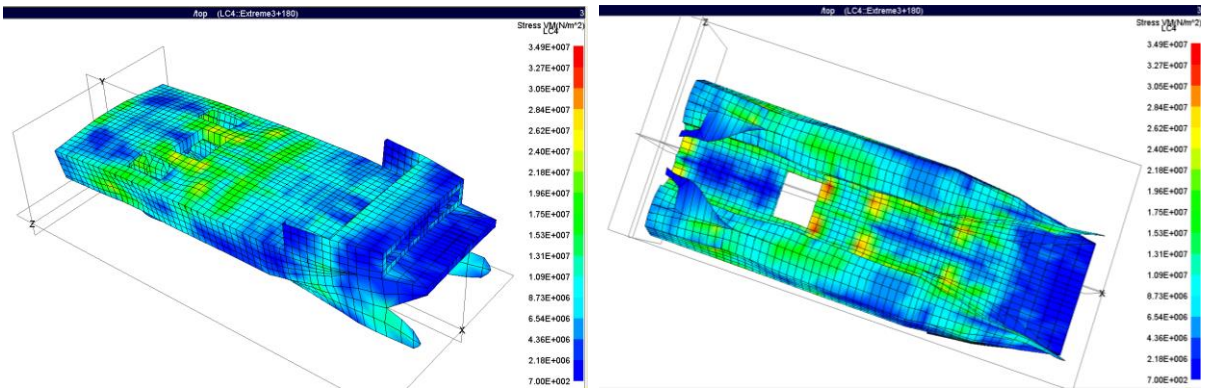

Figure A. 0.12 Figure 0.13 XY in- plane shearing stress (LC 4 – VM)